I.R.Iran

ISSN:2423-5547
e-ISSN:2423-7469

Journal of Renewable Energy and Environment

Volume 7, Number 3, Summer 2020

Materials and Energy Research Center

Iranian Association of Chemical Engineers

CONTENTS

Mohsen Fallah **Zahra Medghalchi**	Heat Transfer, Environmental Benefits, and Social Cost Analysis of Different Insulation Methods by Considering Insulation Disadvantages	1-13
Ghazanfar Shahgholian	An Overview of Hydroelectric Power Plant: Operation, Modeling, and Control	14-28
Nima Amani	Energy Simulation and Management of the Main Building Component Materials Using Comparative Analysis in a Mild Climate Zone	29-46
Roya Pashangpour **Faramarz Faghihi** **Soodabeh Soleymani** **Hassan Moradi CheshmehBeigi**	Cost and Environmental Pollution Reduction Based on Scheduling of Power Plants and Plug-in Hybrid Electric Vehicles	47-55
Mahdi Shakouri **Alireza Noorpoor** **Hossein Ghadamian**	Quantification of Thermal Energy Performance Improvement for Building Integrated Photovoltaic Double-Skin Façade Using Analytical Method	56-66
Hasan Hekmatnia **Ahmad Fatahi Ardakani** **Armin Mashayekhan** **Morteza Akbari**	Assessing Economic, Social, and Environmental Impacts of Wind Energy in Iran with Focus on Development of Wind Power Plants	67-79
Mahdi Shahmari **Payam Zarafshan** **Shahriar Kouravand** **Morteza Khashehchi**	Design and Analysis of a Combined Savonius-Darrieus Wind Turbine for Irrigation Application	80-86

AIMS AND SCOPE

Journal of Renewable Energy and Environment publishes original papers, review articles, short communications and technical notes in the field of science and technology of renewable energies and environmental-related issues including:

- Generation
- Storage
- Conversion
- Distribution
- Management (economics, policies and planning)
- Environmental Sustainability

INSTRUCTIONS FOR AUTHORS

Submission of manuscript represents that it had neither been published nor submitted for publication elsewhere and is result of research carried out by author(s). Only the extended and upgraded articles presented in a conference and/or appeared in a symposium proceedings could be evaluated for publication.

Authors are required to include a list describing all the symbols and abbreviations in the paper. Use of the international system of measurement units is mandatory.

- On-line submission of manuscripts results in faster publication process and is recommended. Instructions are given in the JREE web sites: www.jree.ir
- References should be numbered in brackets and appear in sequence through the text. List of references should be given at the end of the paper. All journal articles listed in the References section must follow with article doi.
- Figure captions are to be indicated under the illustrations. They should sufficiently explain the figures.
- Illustrations should appear in their appropriate places in the text.
- Tables and diagrams should be submitted in a form suitable for reproduction.
- Photographs should be of high quality saved as jpg files.
- Tables' illustrations, figures and diagrams will be normally printed in single column width (8 cm). Exceptionally large ones may be printed across two columns (17 cm).

JREE: Vol. 7, No. 3, (Summer 2020) 1-13

Journal of Renewable Energy and Environment

Research Article

Journal Homepage: www.jree.ir

Heat Transfer, Environmental Benefits, and Social Cost Analysis of Different Insulation Methods by Considering Insulation Disadvantages

Mohsen Fallah[a,b*], Zahra Medghalchi[b]

[a] *Department of Mechanical Engineering, Azarbaijan Shahid Madani University, Tabriz, Iran.*
[b] *Research Institute of Applied Power System Studies, Azarbaijan Shahid Madani University, Tabriz, Iran.*

PAPER INFO

Paper history:
Received 11 December 2019
Accepted in revised form 18 May 2020

Keywords:
Anti-Insulation
Wall Insulation Configuration
HVAC Operation Mode
Greenhouse Gas Emission
Social Cost

ABSTRACT

In this paper, the thermal performance of four common insulators in two internal and external insulation systems is investigated for the ASHRAE setpoint range by applying detailed numerical simulation and Anti-Insulation phenomenon. Anti-Insulation phenomenon and consequent extra load on the HVAC system can occur following the thermal insulation of a building if proper temperature setpoint is not selected. In the next step, the proper setpoint is analyzed under simulated building conditions, and all related criteria are studied for this temperature. Also, continuous and intermittent operations of the air conditioning system are investigated. Moreover, the assessment of the environmental benefit of wall insulation is performed by evaluating greenhouse gasses emission payback period and social cost saving. A residential building is simulated in the EnergyPlus software for the case study. Results show that Anti-Insulation occurs approximately at 22 ºC. Both external and internal insulations lead to a significant reduction in energy consumption. Nevertheless, the external insulation shows a bit more reduction. Intermittent operation outperforms the continuous operation by 8 % on average. The insulator's production phase is considered in the analysis of the insulation environmental benefits. Results show that, in this case, the prioritization of insulators would be different from that case in which this process is not considered. According to results, in terms of social costs, applying thermal insulation to residential buildings is necessary.

1. INTRODUCTION

The demand for energy is increasing due to the population growth and the improvement of thermal comfort along with the enhancement of life standards in Iran. According to statistics, about 40 % of the country's generated energy is used by domestic, commercial, and public building sectors [1, 2], and 70 % of this amount is allocated to the heating and cooling process [3]. In other words, approximately 28 % of the total energy is consumed by air-conditioning equipment. Because 60-80 % of heating and cooling loads relate to the heat transition through the building's envelops [4], it is necessary to improve the thermal characteristics of outer walls by thermal insulation for saveing energy.

Thermal insulation protects the indoor environment from outside temperature fluctuations to provide a high comfort level and reduce energy consumption when it is accompanied by a proper setpoint. Besides, an accurate insulation location could regulate the temperature changes using thermal inertia. Moreover, as a result of energy saving by wall insulation, there would be a remarkable reduction in greenhouse gas emissions, which adversely affect the environment.

In addition to this purpose, many studies have been performed to assess the effectiveness of thermal insulation and their suitable location in the wall by evaluating energy-saving, optimum thickness, emission reduction, and pay-back period of insulation investment as benchmarks. Tabel 1 involves the abstract concepts of these studies and their most important results.

*Corresponding Author's Email: mfallah@azaruniv.ac.ir (M. Fallah)

Some of these studies tend to evaluate the impact of HVAC system operation on the thermal performance of the building's envelope [5-9]. These studies consider two operations, continuous and intermittent, for the HVAC system and seek a proper insulation location on the wall under each operation. For this purpose, the wall's thermal mass should be considered; therefore, the simulation done by all of these studies has been dynamic. Overall, results show that, under intermittent operation, internal insulation outperforms external insulation [6-9]. However, under continuous operation, the external insulation indicates better performance. However, in some cases, the external insulation performs better than the internal insulation under intermittent operation [5]. The important result of these studies is that different intermittent operation schedules result in different energy-saving and wall configurations; therefore, the exact HVAC operation should be applied to the simulations. Other studies have investigated insulation location without taking HVAC operation type into account [10-14]. These studies have compared performances of different insulation methods (external, internal, or mid insulation) under solely continuous or intermittent operation.

Other types of studies investigate building insulation regarding economical aspects [11, 12, 15-21]. Some of these studies evaluate optimal thickness of different insulators by considering different criteria such as climatic condition [20], wall orientation [19], wall and insulation material [21], glazing area percentage [17, 20], fuel type [20, 21], and life cycle [15]. Other studies that regard economical issues determine the insulation investment payback period by considering different insulator types and insulation methods [12, 16, 22]. It should be emphasized that, in this type of

studies, economical indexes such as inflation rate, building lifespan, etc. are considered too.

Environmental issues represent another kind of researches that falls into the scope of building insulation studies. These studies evaluate greenhouse gas emission reduction due to the building insulation [16, 18-20, 22]. In this type of studies, mostly, building fuel type and insulation material are considered as criteria. Another school of studies tends to investigate different insulator's material and climatic conditions solely or compare insulation with other thermal enhancement techniques such as shading, natural ventilation, etc. [23-30]. All of them remark thermal insulation as the most important approach for energy-saving. The key information of the above-mentioned references is categorized in Table 1 for more clarification.

In all of the aforementioned studies, building insulation is introduced as a guaranteed method for energy saving, and none of these studies investigates the disadvantages of insulation. In these studies, a condition that the building insulation imposes extra load on the HVAC system (rather than saves the energy) is not taken into account, except in [16] and [25], which are merely noted in a few sentences. In this paper, to highlight those cases where building insulation could increase energy consumption, the thermal performance of a building is simulated by EnergyPlus software. Then, the reasons that cause this increment are investigated and, after resolving this problem, the thermal analysis of building insulation is conducted. In the second part of the paper, the environmental benefits of building insulation are evaluated by determining the greenhouse gas emissions conservation. The aforementioned references exclude the insulator's production phase in environmental analysis. In this paper, by regarding released emission in the insulator's production and transportation phase, greenhouse gas emission payback period is determined.

2. METHODOLOGY

In this work, 4 common insulators in Iran including Polystyrene, Polyurethane, Glass wool, and Rock wool are applied to the internal and external insulation of a residential building's walls. Figure 1 shows the study plan and its steps. As Figure 1 indicates, the first step relates to the thermal analysis in both of the cooling and heating parts for the ASHRAE setpoint. However, because we face disadvantages of thermal insulation (imposing extra cooling load to the HVAC system) in the cooling part, the second step is dedicated to assess the insulation reverse function in this part and resolve it by investigating the proper cooling setpoint. In the next step, thermal analysis is conducted for a new setpoint, and the building's cooling and heating is evaluated by determining energy saving, wall's heat flux, etc. Finally, insulation environmental issues are investigated by calculating greenhouse gas emissions regarding the production and transportation phase. In addition, social cost saving due to greenhouse gas conservation is evaluated to express insulation environmental benefits economically.

Table 1. References abstract & main results.

Ref. number	Static/Dynamic	Experimental	Insulator type	Insulation location in the wall	HVAC system type	Energy-saving	Optimum thickness	GHG*	Payback period	LCA	Results
5	D	No	XPS	External/Internal /Mid	Continuous/ Intermittent	*					Under intermittent operation, it is a better insulation layer placed in exterior side. For selecting the wall's layers' configuration, the real HVAC system operation must be considered.
6	D	Yes	Foamed concrete	External/Internal /Mid	Continuous/ Intermittent	*					Under intermittent operation, the inner surface of wall has the most impact on the thermal response of the wall. Internal insulation has the lowest heat flow among all other wall configurations.
7	D	No	XPS	External/Internal	Continuous/ Semi-continues	*					In climates in which the cooling system operates during part of a day, internal insulation performs better than external insulation. However, in climates with free cooling periods, external insulation outperforms the internal system.
8	D	No	EPS/Light weight self-insulation brick/Heavy weight self-insulation brick	External/Internal /Mid/self-insulation wall	Continuous/ Intermittent	*					Internal insulation outperforms external insulation under intermittent operation. Intermittent operation is more appropriate for occupant than continuous operation.
9	D	Yes	Foamed concrete	External/Internal /Mid	Continuous/ Intermittent	*					Under continuous operation, external insulation performs better than internal insulation. However, under intermittent operation, internal insulation outperforms the external insulation.
10	D	No	Insulation foam	6 Different location in the	Continuous	*					The optimum thermal performance is achievable in the condition that insulator

				wall							is located on the outer side of the wall and massive materials are exposed to the interior space.
11	D	No	EPS	External/Internal	Continuous/ Semi-continues	*			*		External insulation saves more energy (8 %) than internal insulation. Investment cost for internal insulation is about 50 % less than external insulation.
12	D	No	XPS	External/Internal	Intermittent	*					Internal insulation outperforms the external insulation by 18 %.
13	D	No	EPS	Filled into the hollow brick (External/ Internal)	Intermittent	*					The optimal location of filling insulation materials in brick's hollows depends on filling ratio.
14	S	No	XPS	External/Internal	Intermittent	*					External insulation has better performance than internal insulation.
15	D	No	Mineralwool/Rockwool/Corck/ Fiberglass/ Polystyrene/ Polyurethane	External	Semi-continuous	*	*			*	The best insulator for energy saving is Mineralwool, the optimum thickness of which varies by different life cycle assumptions.
16	S	No	EPS	Mid	-	*	*	*			By optimum thickness utilization, energy consumption reduces up to 46.6 % and Co_2 and So_2 emission decreases 41.53 %.
17	D	No	Insulators with R=0.88 m^2 ˚k/W	-	Semi-continuous	*		*	*		The envelop insulation, airtightness, and the windows replacement result in 45 % energy saving and 70 tons Co_2 reduction annually. The upgrading investment return year is 7.7 years.
18	S	No	XPS/Rockwool	-	-	*	*	*	*		Insulation optimum thickness and payback period vary according to glazing area percentage, climate, and fuel type. Greenhouse gas emission could be reduced up to 54 % by the utilization of optimum thickness.
19	D	Yes	EPS	External	Continuous	*	*				70 % energy saving could be obtained by good insulation associated with thermal inertia. Optimum thickness for cooling energy varies between 1cm and 7 cm.
20	D	No	XPS/EPS	External	Continuous	*	*	*			The least heating energy consumption is related to brick wall with XPS insulation. Optimum thickness changes according to wall's orientation. 85 % saving in greenhouse gas emission is achievable by 9 cm insulation.
21	S	No	Fumed silica/Glass fiber/EPS	-	-	*		*	*		10.2 %, 41.3 %, and 26.7 % reductions in annual heating and carbon dioxide emission are achievable in three different buildings by implementing vacuum insulators in buildings. Fumed Silica has the shortest payback period among the evaluated insulation.
22	S	No	Foam polyvinylchloride /Polyurethane/ EPS/Rockwool glasswool/5 wall structure	-	-	*	*		*		Optimum thickness, investment return year, and energy cost-saving vary between 0.2 cm- 14 cm, 0.66 year- 11.6 year and 3$ -155$, respectively. These parameters depend on wall and insulation material and fuel typ.
23	D	No	EPS	External	Intermittent	*					Necessary measure (among external insulation, shading technology, and natural ventilation) that contributes to energy saving in all climates is external insulation.
24	D	No	Composite insulated block (mid-plane EPS)	Mid	-	*					Wall insulation with 16 cm EPS makes 30 % energy saving and thermal bridge insulation with 5cm EPS makes 23 % energy saving.

25	-	Review		-	-						One of the most important techniques to improve the performance of the NZEB buildings is envelope insulation by considering climatic condition, heat sources, and the comfort temperature.
26	D	No	-	-	-	*					This paper introduces ROBESim software, a retrofit-oriented building energy simulator, which uses Energy Plus engine. Part of the simulation is allocated to evaluating insulation efficiency on energy reduction. Results show that 7.5-15 cm insulation of wall could lead to 4-10 % energy savings.
27	D	No	Insulation with k=0.03 $W/m^2{}^\circ k$	Internal	-	*					34-56 % energy saving is achievable by using just a 2.5 cm insulation under Tehran's climate condition.
28	-	Yes	Polyurethane/ Polystyrene/ Mineral wool	Mid	-	*					More than 65 % cooling energy saving is achievable by insulation. It equals 37 % about heating energy.
29	-	Yes	XPS	External	-	*					Insulation makes 23.5 % energy saving in the summer.
30	S	No	Nano vacuum panel/Polystyrene	Mid	-	*					Utilization of nano-vacuum insulators associated with Nano gel glazing outperforms polystyrene insulation-associated double glazing by 18 %.

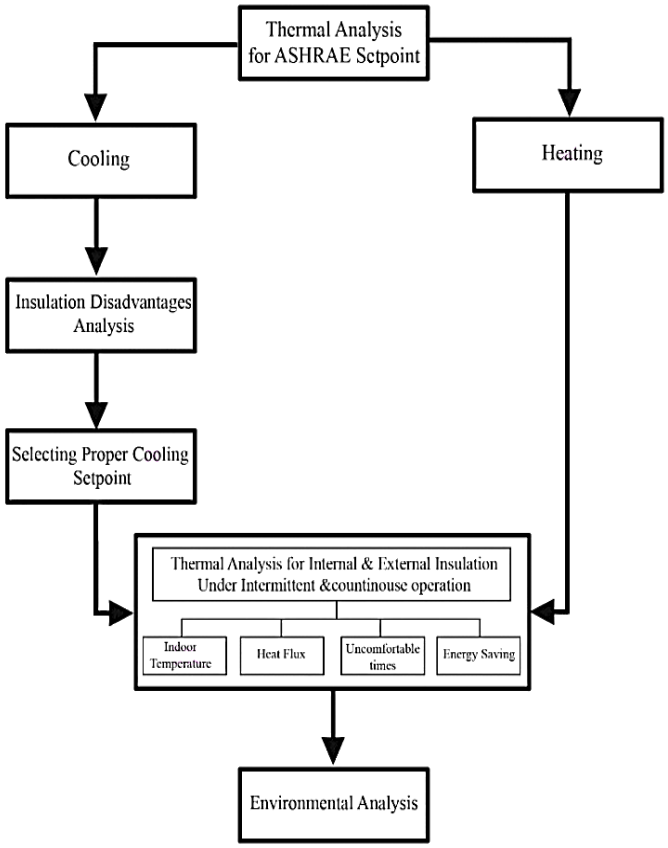

Figure 1. Flowchart of simulation steps.

2.1. Physical model description

Figure 2 shows the simulated building that is a unit in the mid-floor of the 7-story block and located in the metropolitan and industrial city of Tabriz with 38.05°N and 46.17°E coordinates. Each unit consists of one bedroom, one living room, a kitchen, and a bathroom. The bedroom and bathroom are assumed as an individual zone, but the living room and kitchen are considered as a unit zone. Except bathroom, other zones are equipped with the HVAC system.

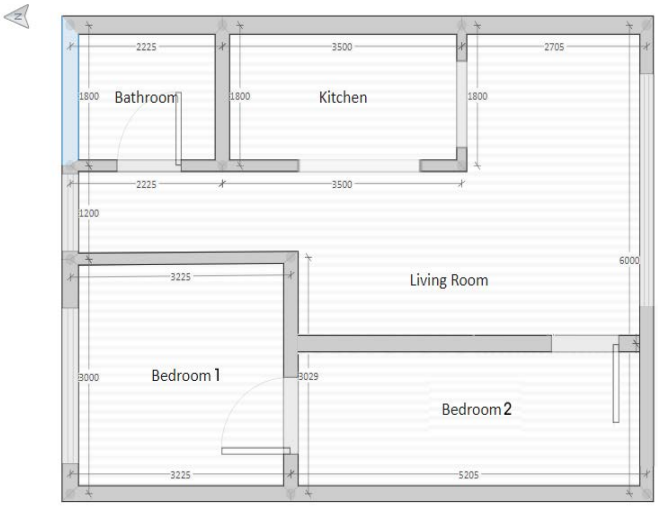

Figure 2. Floor plan of case study.

The composition and properties of the materials used in the walls are presented in Table 2 [31]. Moreover, the internal and external insulation configurations are shown in Figure 3.

Table 2. Wall materials' characteristics.

Material	**Density (kg/m^3)**	**Conduction heat transfer Coe. (W/K.m)**	**Heat capacity Coe. (J/kg.K)**
Facing rock	2590	2.9	860
Concrete	1300	1.75	750
Brick	1900	1.34	900
Cement plaster	1860	0.72	800
Gypsum plaster	1200	0.5	1090
Glass wool	80	0.038	670
Rock wool	70	0.042	840
Polystyrene	40	0.038	1210
Polyurethane	33	0.035	1400

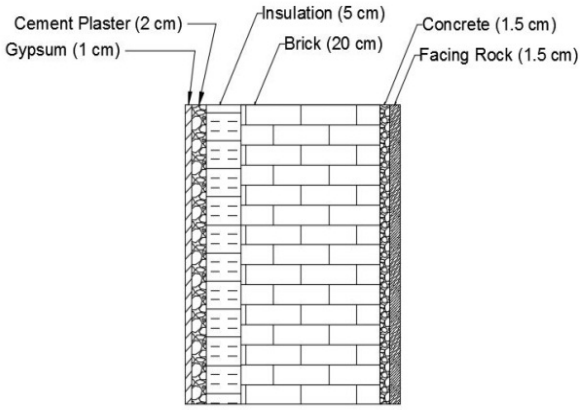

(a)

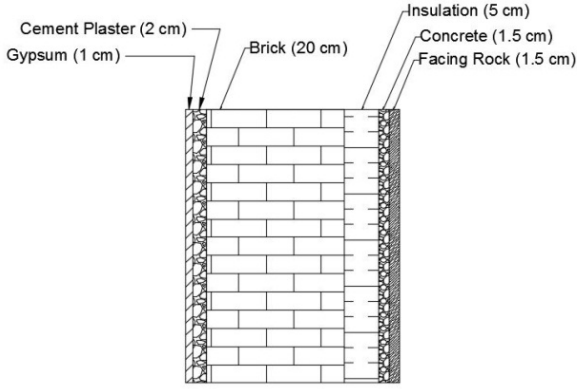

(b)

Figure 3. Wall's layer's configurations: a) internal insulation and b) external insulation.

2.2. Simulation parameters

Annual heating and cooling loads of the building are simulated by EnergyPlus software. An Ideal Load System is established to investigate the building performance. Simulation time-step equals one minute. HVAC system operation schedule is presented in Table 3 for continuous and intermittent cases. Four inhabitants (parents and two children) with average sensible and latent cooling load are assumed. Furthermore, all internal thermal sources such as the lighting of spaces and electrical equipment are included in the calculations. Table 4 shows internal gain of occupancy presence, lighting, and equipment operation [32]. Natural gas and electricity grid are used for heating and cooling demand, respectively. The averaged typical meteorological year (TMY) [33] data was used for simulating the weather conditions with a 1-minute time step that makes the calculations precise.

2.3. Environmental parameters

Building insulation causes energy conservation and consequent greenhouse gas emission reduction. For calculating the saving of these emissions, it is assumed that the heating energy is supplied by natural gas in the site and cooling energy is supplied by electricity through electric power distribution. To evaluate the pollution caused by the building's cooling, the energy consumption of electricity is converted to the base energy by a conversion factor of 0.33 (the average conversion factor for natural gas-fueled power plants in Iran) [34]. These gas emissions are calculated for both insulated and non-insulated buildings and, by this approach, the saving amount is determined.

Although wall insulation diminishes environmental costs, insulation producing processes and transportation to the building location release emission to the environment. Therefore, for evaluating the actual effect of insulation on the environment, the amount of released greenhouse gas emission during the producing process and transportation is determined. In the production phase, different steps including raw materials transportation, fabrication, and packing are considered, as shown in Figure 4. Emissions of production and transportation phases are extracted by Simapro software. It is assumed that the insulation factors are placed in the Tehran (distance= 630 km), and insulators are transported to the Tabriz by road transportation.

Greenhouse gases have many social and environmental costs for people, government, and business. This emission causes climate change and, consequently, inflicts damages including changes in agricultural production, human health, property damages, and change in energy system cost (such as cooling energy cost increment). The imposed cost of these changes is called emission social cost. Although the current social cost does not include all physical, ecological, and economic damages, it could express how much emissions may impose the economical cost.

Table 3. HVAC operation schedule.

HVAC Operation cases	Operation mode	Time	Working status		
			Living room	Bedroom 1	Bedroom 2
Case 1	Continuous	Whole days	On	On	On
Case 2	Intermittent	00:00 – 06:30	Off	On	On
		06:30 – 08:00	On	Off	Off
		08:00 – 14:00	Off	Off	Off
		14:00 – 15:00	Off	On	Off
		15:00 – 17:00	On	Off	Off
		17:00 -19:00	Off	On	On
		19:00 – 22:00	On	Off	Off
		22:00 – 24:00	Off	On	On

Table 4. Internal gains schedule.

Time	Living room			Bedroom 1			Bedroom 2		
	Occupancy (W)	Equipment (W/m^2)	Lighting (W/m^2)	Occupancy (W)	Equipment (W/m^2)	Lighting (W/m^2)	Occupancy (W)	Equipment (W/m^2)	Lighting (W/m^2)
00.00-6:30	0	249.1	0	72	0	0.25	72	0	0.25
6:30-8:00	108	249.1	2.5	0	0	0.625	0	0	0.625
8:00-14:00	0	249.1	0	0	0	0	0	0	0
14:00-15:00	0	249.1	0	108	50	1.25	108	0	0
15:00-16:00	128.5	249.1	2.5	0	0	0	0	0	0
16:00-17:00	126	530	2.5	0	0	0	0	0	0
17:00-19:00	0	249.1	0	108	50	1.25	108	50	1.25
19:00-20:00	142	530	2.5	0	0	0	0	0	0
20:00-22:00	108	530	2.5	0	0	0	0	0	0
22:00-24:00	0	249.1	0	72	0	0	72	0	0

As mentioned before, the heating and cooling of residential buildings constitute a significant portion of the country's energy consumption and subsequently great amount of social cost. Therefore, social cost conservation owing to building insulation is determined in this study. The social cost of different greenhouse gases is reported in Table 5. These amounts are extracted from Balance IE. Deputy for Electricity and Energy, Ministry of Energy [3].

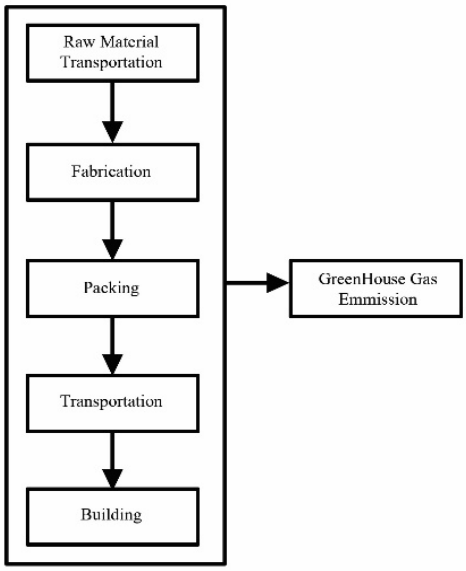

Figure 4. Insulation producing phase's steps.

Table 5. Different emission social costs.

Emission social cost in Iran (¢/kg)				
CO_2	CO	NO_x	SO_2	PM
0.238	4.3	14.5	43.2	102.5

3. RESULTS AND DISCUSSION

Building insulation simulation results are shown in this section. At first, simulation results for the ASHRAE setpoint range are mentioned. Then, the reverse function of insulation in cooling part for this range is discussed, and a proper setpoint is determined. After that, desired factors are studied at an optimum setpoint temperature. First, indoor temperature and heat flux distribution factors are discussed. Then, deliberation about energy consumption, saving percentage, etc. are considered. Finally, environmental discussion and social expenses are represented.

3.1. Simulation results for ASHRAE range

The weather condition has a profound impact on energy consumption and saving potential. Figure 5 shows the annual temperature and solar radiation distribution for Tabriz. The range of temperature varies from -10 °C to 30 °C, and the daily (24 hours) average solar radiation ranges from 50 to 166 W/m^2. Although the maximum direct solar radiation occurs in June, the maximum dry bulb temperature is recorded in mid of July. Based on these data, Iran Metrological Organization categorizes Tabriz city as a cold climate region in its official climate classification [35]. Therefore, more heating demand is needed for 205 days, from 1 October to 20 May, whereas the cooling system operates in the remaining days.

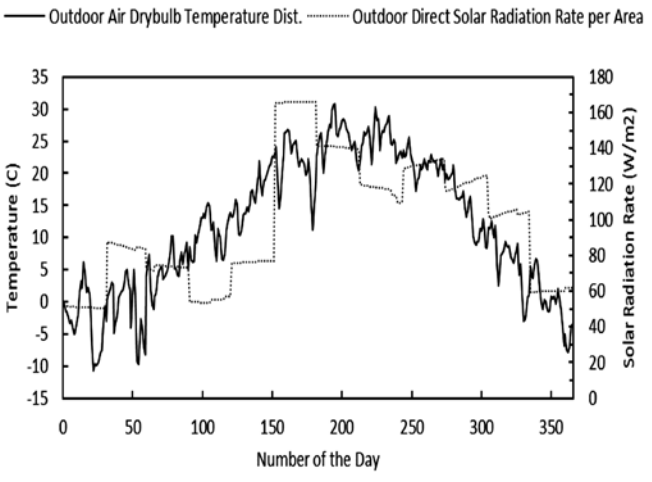

Figure 5. Outdoor air dry-bulb temperature distribution and daily average direct solar radiation rate for Tabriz.

Figure 6 shows the psychometric diagram and the temperature and moisture range for the resident's comfort for the ASHRAE organization [35]. According to this index, in this section, the temperatures of 20 °C and 24 °C are selected as comfort setpoints for cold and warm days, respectively. The operation schedule for the intermittent HVAC system is indicated in Table 3.

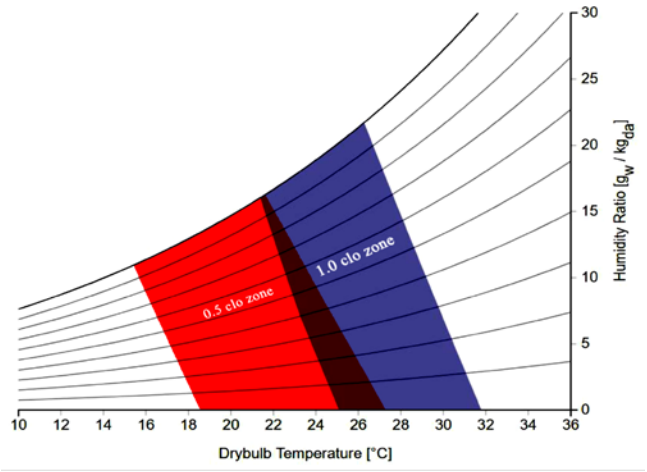

Figure 6. AHRAE comfort condition range.

Indoor temperature distribution for Polyurethane in both inside and outside insulations is shown in Figure 7 due to survey the comfort condition in the intermittent mode. As a result of off times, the temperature fluctuates out of the selected setpoint range. Under continuous operation, indoor temperature fluctuation would be 20 °C and 24 °C.

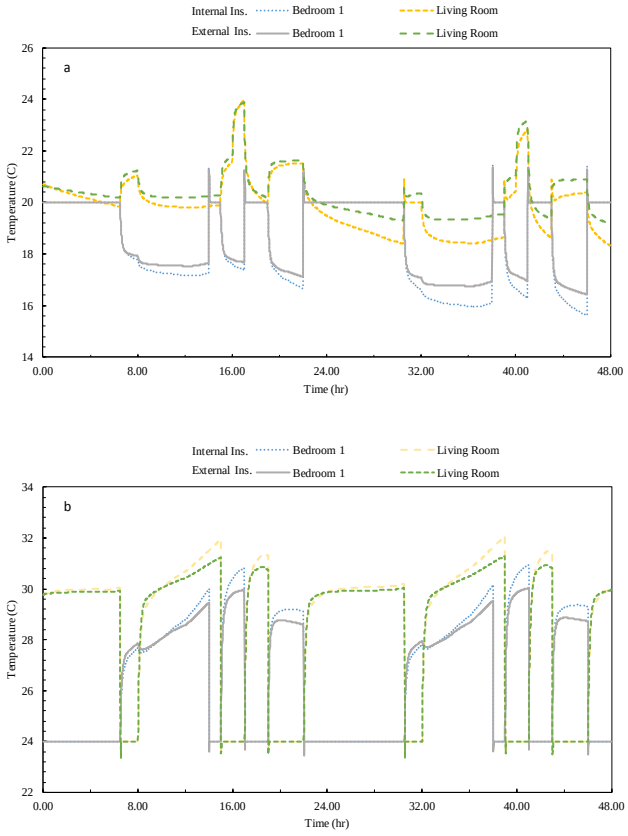

Figure 7. Indoor air temperature distribution for polyurethane insulation under intermittent HVAC operation mode for ASHRAE range, a) 21 and 22 January, b) 21 and 22 August.

Annual heating and cooling energy consumption rates are illustrated in Figure 8 for different insulation configurations and non-insulated building under intermittent and continuous modes. Envelope insulation reduces heating energy consumption that equals 81-92 % for different configurations on average. External insulation has better performance than the internal one in the heating sector. However, as Figure 8 shows, building insulation increases the cooling load. Different insulations impose -2 % to -16.38 % extra load on average on the HVAC system. The reason for this reverse function of insulation is investigated in the next section.

3.2. Insulation reverse function and optimum setpoint

If the building is assumed as a control volume, there are two internal and external sources for heating and cooling load. External sources include envelope heat transition, air infiltration, and solar radiation from transparent surfaces. Internal sources contain occupancy, lighting and equipment heat gain, warm water pipe, etc. Wall insulation reduces heat flux in the wall. If internal gain increases significantly, insulation creates thermal accumulation inside the building. This phenomenon has both positive and negative effects on energy conservation. During cold seasons, heat accumulation reduces HVAC system heating load and benefits from building energy conservation. Concerning warm seasons, however, it imposes extra loads on the system and increases energy consumption. For diminishing this negative effect, there are several solutions:

a) Reducing wall thermal resistance
b) Reducing internal gain
c) Changing operation setpoint

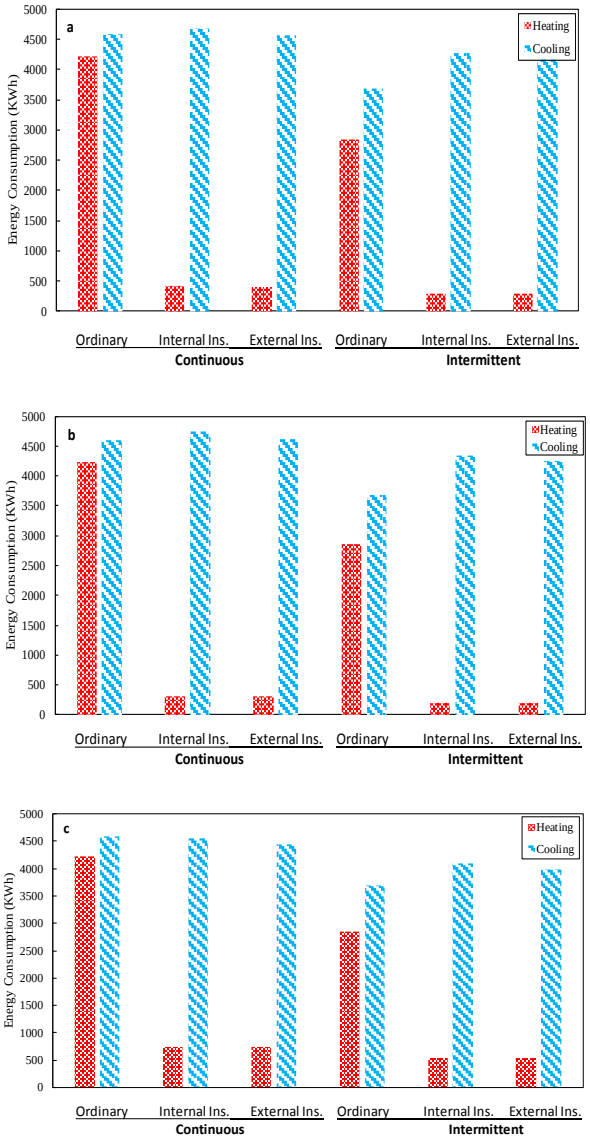

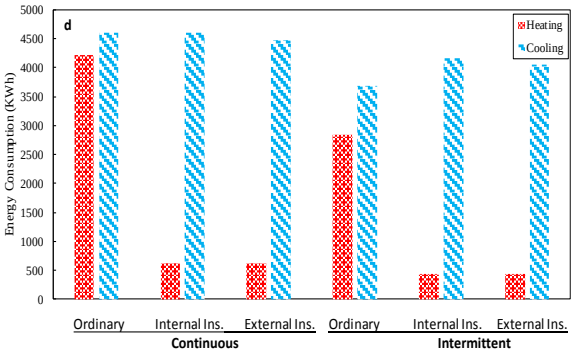

Figure 8. Yearly heating and cooling energy consumption: a) Polystyrene, b) Polyurethane, c) Glasswool and d) Rockwool.

Solution (a) can not be applied because it affects heating load negatively. Solution (b) is not as practical as expected because we can not change or remove equipment capacity. Therefore, changing the operation setpoint is the only alternative. Energy consumption profiles are shown in Figure 9 for non-insulated and insulated buildings against temperature setpoint variation. As can be seen, the reduction rate in the non-insulated building's cooling energy consumption is higher than the insulated one with the increasing setpoint temperature. The crossing point of insulated and non-insulated profiles (about 22 ºC) illustrates the temperature at which the Anti-Insulation phenomenon appears after that. In other words, wall insulation makes increments in the building's cooling load. Therefore, for diminishing the negative effect and prohibiting Anti-Insulation phenomenon upon results and ASHRAE standard comfort condition, temperatures of 20 ºC and 21 ºC are assumed for heating and cooling setpoints in this study.

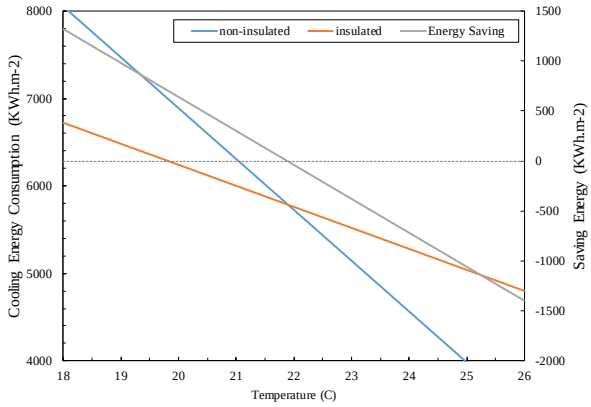

Figure 9. Energy consumption profile at different set point temperature.

3.3. Indoor temperature and heat flux distribution

For comparing different insulation modes in detail, indoor temperature and heat flux distribution for different zones are presented in this part.

3.3.1. Indoor temperature

In the continuous mode, the indoor temperature of zones varies in the comfort range (20 ºC to 21ºC). However, to check the quality of comfort condition in the intermittent operation, the internal temperature distribution of different zones is illustrated in Figure 10 for insulated buildings with polyurethane for instance. Under intermittent operation, the indoor temperature fluctuates out of the selected temperature range. During off intervals, gradients of temperature diagrams are smoother in the external insulation than the internal insulation. It is implied that temperature fluctuation in external insulation is low. Therefore, it provides a more comfortable condition for occupancy. Moreover, there is a more extreme deviation from the comfort range in the internal insulation. It is stated in the continuous operation, too.

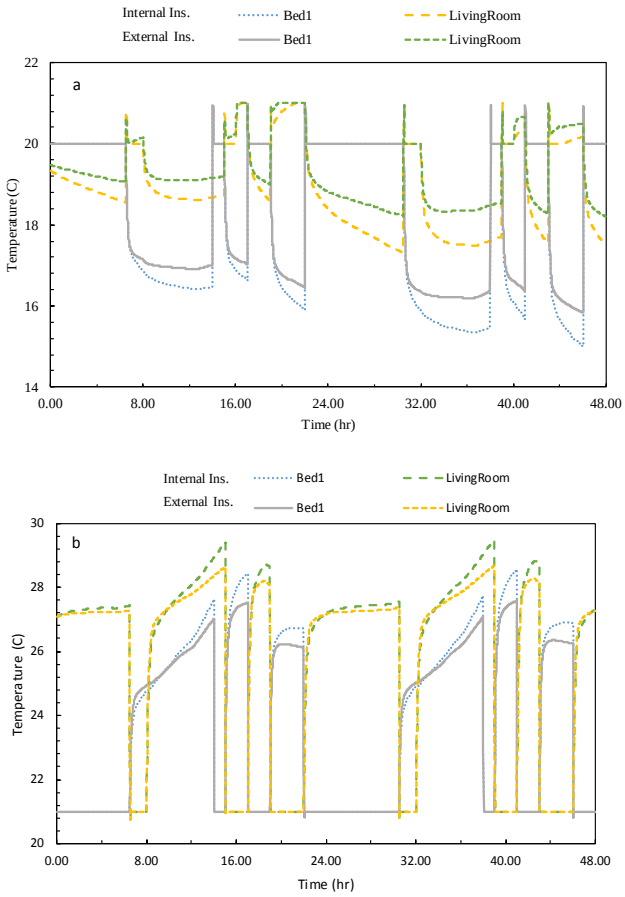

Figure 10. Indoor air temperature distribution for polyurethane insulation under intermittent HVAC operation mode: a) 21 and 22 January, b) 21 and 22 August.

3.3.2. Heat flux

Average heat flux in external walls for different zones in both non-insulated and insulated buildings with Polyurethane is shown in Figures 11,12, and 13. Considering these figures, it could be understood that heat flux partially grows with internal gains increment. As expected, wall insulation decreases heat flux in the insulated building compared with non-insulated buildings. Similarly, there is a heat flux reduction when the HVAC operation mode turns from the continuous to intermittent operation mode. In general, external insulation heat flux is lower than the internal one in both operation modes. However, during the working time of intermittent operation, the internal insulated building owns fewer heat flux values than external configuration.

As a result of intermittent operation, there are intervals at which the zone does not meet the comfortable setpoint (because of the delay for achieving the desired temperature after the HVAC system starts to work). Table 6 shows these uncomfortable times for each month; as can be seen, these time durations are very short, about 25 hours in a year. Therefore, the implementation of intermittent operation could be justified.

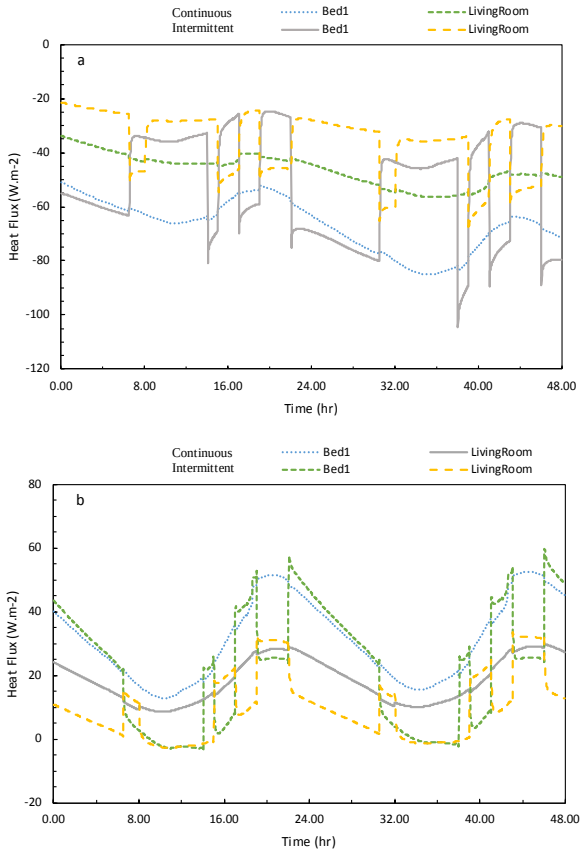

Figure 11. Building external walls heat flux for non-insulated building under continuous and intermittent mode: a) 21 and 22 January, b) 21 and 22 August.

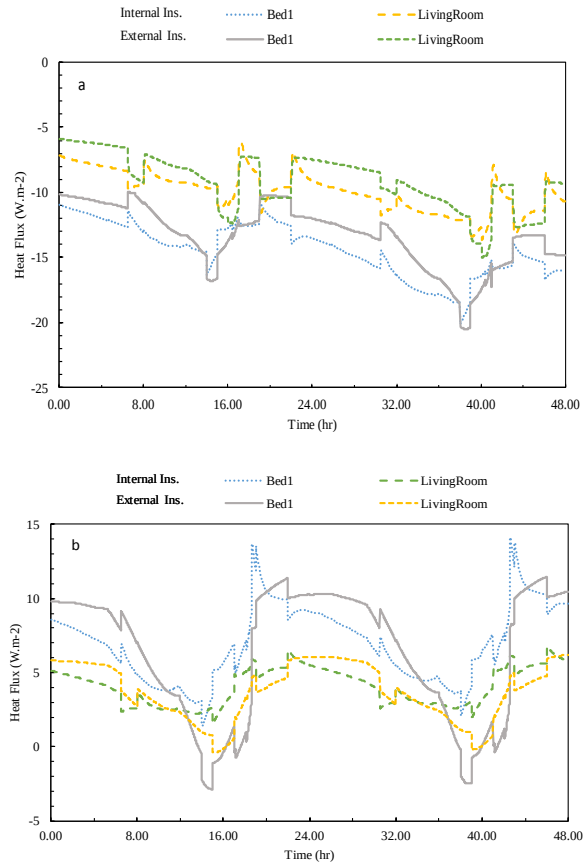

Figure 12. Building external walls heat flux for polyurethane insulation under hvac continuous operation mode: a) 21 and 22 January, b) 21 and 22 August.

3.4. Energy conservation

Annual heating and cooling energy conservation of building for each insulator under two operations of the HVAC system are calculated regarding non-insulated building with continuous operation, shown in Figure 14. As depicted in the diagram, heating energy saving is achieved by applying insulation to both continuous and intermittent HVAC operation modes and external insulation results in a relatively greater heating energy reduction due to the utilization of thermal mass.

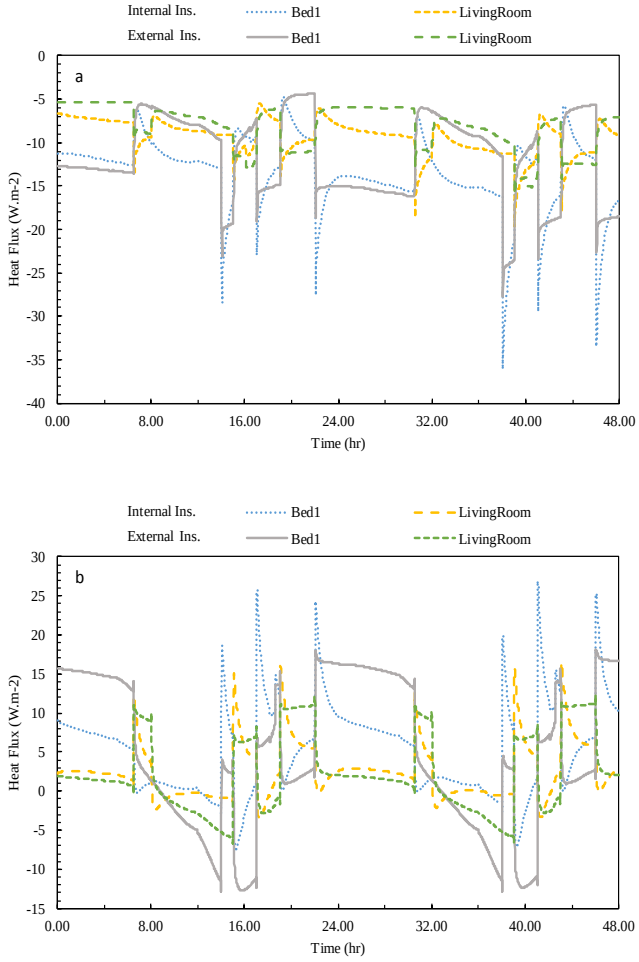

Figure 13. Building external walls heat flux for polyurethane insulation under hvac intermittent operation mode: a) 21 and 22 January b) 21 and 22 August.

According to Figure 14, cooling energy conservation is less than heating energy because of high internal gains that play a positive role in zone heating and a negative one in the cooling part. In other words, this high internal gain is trapped in the building by insulation, which compensates for a large portion of building heating demand, but imposes additional cooling load.

Tables 7 and 8 present energy-saving percentages in various cases of insulation and HVAC system operation. According to Table 7, 80-90 % heating and 8-11 % cooling energy-saving arise from the implementation of insulation in the continuous operation mode. As mentioned before, one of the reasons for high heating energy conservation is the trapped internal gains.

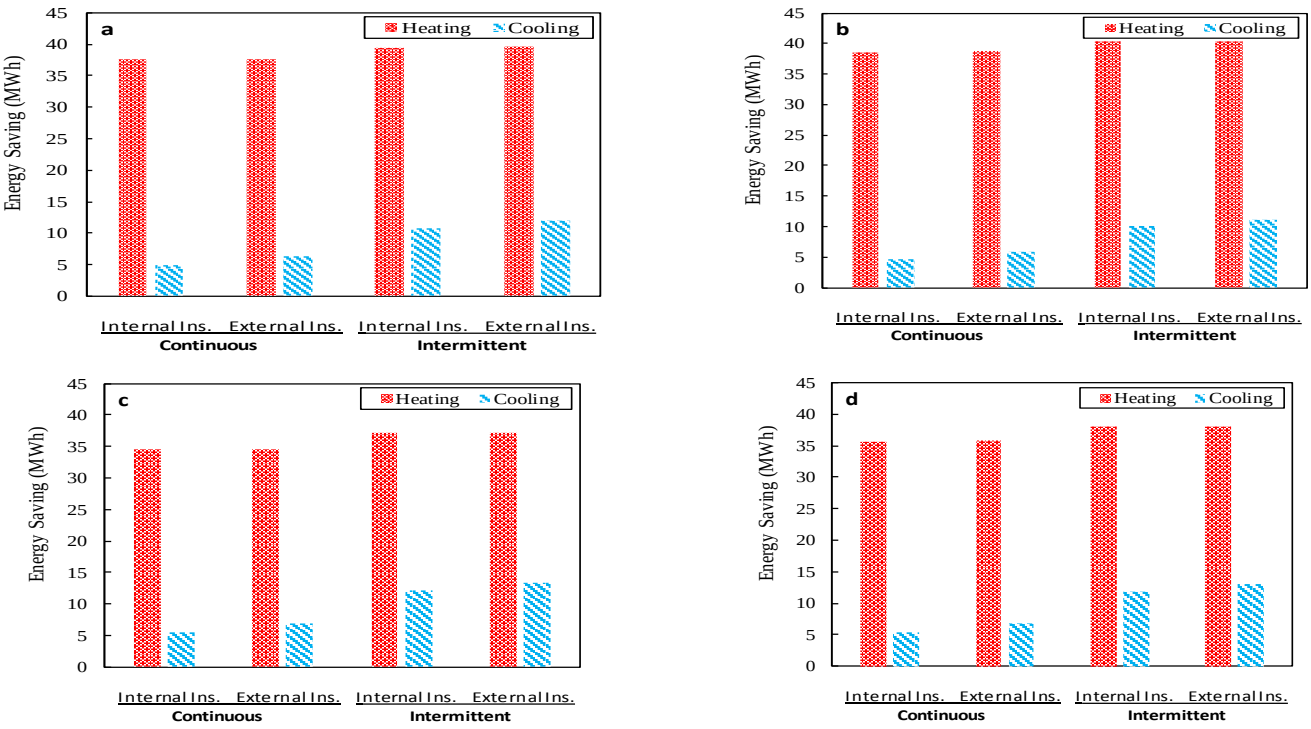

Figure 14. Yearly heating and cooling energy consumption: a) polystyrene, b) polyurethane, c) glasswool and d) rockwool.

Table 6. Zone heating and cooling setpoint not met time [hr].

	Month	Jan.	Feb.	Mar.	Apr.	May	Jun.	Jul.	Aug.	Sept.	Oct.	Nov.	Dec.	Ann.
Internal Ins.	Polystyrene	1.73	0.65	0.48	2.00	3.07	3.00	3.10	3.10	3.00	2.82	0.85	1.18	24.98
	Polyurethane	1.53	0.45	0.60	2.07	3.07	3.00	3.10	3.10	3.00	2.88	1.00	0.78	24.58
	Glasswool	2.43	1.23	0.32	1.58	3.05	3.00	3.10	3.10	3.00	2.68	0.63	1.65	25.78
	Rockwool	2.10	1.00	0.37	1.67	3.07	3.00	3.10	3.10	3.00	2.70	0.68	1.50	25.28
External Ins.	Polystyrene	1.60	0.57	0.37	1.75	3.05	3.00	3.10	3.10	3.00	2.80	0.68	0.90	23.92
	Polyurethane	1.22	0.30	0.47	1.93	3.07	3.00	3.10	3.10	3.00	2.85	0.95	0.52	23.50
	Glasswool	2.30	1.07	0.15	1.30	3.00	3.00	3.10	3.10	3.00	2.62	0.50	1.52	24.65
	Rockwool	1.97	0.92	0.13	1.48	3.02	3.00	3.10	3.10	3.00	2.70	0.47	1.35	24.23

Table 8 shows the energy saving values under the intermittent operation mode, which is 8 % higher than continuous mode values on average. In this case, there is more heating energy saving the same as the continuous operation. In both operations, external insulation makes more conservation than internal insulation due to the usage of the wall's thermal inertia. Regarding the heating and total energy, Polyurethane, Polystyrene, Rockwool, and Glasswool have the most to the least energy-saving, respectively. However, this sort stands in contrast to the cooling part. Because Polyurethane has higher thermal resistance, it is highly able to trap the internal gains and impose extra cooling load. Moreover, Glasswool's thermal conductivity is lower than Rockwool, and Rockwool total energy conservation is a bit higher than Glasswool's due to its greater heat capacity. The comparison of energy-saving of Glasswool and Polystyrene with the same conductivity, yet different heat capacitie, authenticates this principle too; greater heat capacity of Polystyrene facilitates greater energy saving.

3.5. Environmental and social expenses

Table 9 shows the yearly amount of reduction in greenhouse emission gained by wall insulation in terms of mass per unit of insulation area. Results indicate that employing wall insulation could reduce CO_2 emission at least 14 kg/m^2 insulator under continuous operation mode in comparison with non-insulated building in a year. Moreover, the intermittent operation decreases 18 kg/m^2 insulator CO_2 gas emission. Other greenhouse gas emission reduction amounts are shown in Table 9.

Table 10 represents amounts of CO_2 and CO greenhouse gas emissions that are released during producing process and transportation.

According to the values of Tables 9 and 10, a greenhouse gas emission reduction due to wall insulation compensates emission, released into the environment during insulator production and transportation processes just in few months, as shown in Table. 11. Therefore, the environmental benefit caused by wall insulation is justified entirely by this view. Moreover, the comparison of the payback period of greenhouse gas emissions shows that deciding about the insulator's environmental benefit based only on the emission reduction cannot be correct or efficient. Comparing two insulators Glasswool and Polyurethane could illustrate this point. As mentioned in Table 9, Polyurethane makes a greater gas emission reduction than Glasswool, but its payback period

is longer. This is the process of releasing much more pollution to the air by the Polyurethane Production process than Glasswool. It is worth mentioning that emission payback periods of insulation are negligible compared to a building lifespan. However, if water pollution, soil pollution, energy usage for production, and wastes during production and after building lifespan be considered too, the environmental impact would be an important criterion in choosing the insulation. This subject would be investigated in future studies.

The amounts of social costs saving are presented in Table. 12. On average, there would be 5.15 ¢ social cost savings per unit of insulation area annually. This amount is 4 $ for the sample building. This may initially be small for a building, but at the macro level, like the 3.6 million houses of Iran's last great construction project, it will be over 14,500,000 $, which is a substantial amount. Therefore, in terms of social costs, thermal insulation in residential buildings is necessary.

Table 7. Energy saving percentage-continuous operation.

	Polystyrene		Polyurethane		Glasswool		Rockwool	
	Inter. Ins.	**Exter. Ins.**	**Inter. Ins.**	**Exter. Ins.**	**Inter. Ins.**	**Exter. Ins.**	**Inter. Ins.**	**Exter. Ins.**
Heating	87.80	88.16	90.32	90.74	80.63	80.82	83.50	83.76
Cooling	8.01	10.08	7.42	9.41	8.97	11.30	8.68	10.91
Total	40.56	41.94	41.24	42.59	38.20	39.66	39.20	40.63

Table 8. Energy saving percentage-intermittent operation.

	Polystyrene		Polyurethane		Glasswool		Rockwool	
	Inter. Ins.	**Exter. Ins.**	**Inter. Ins.**	**Exter. Ins.**	**Inter. Ins.**	**Exter. Ins.**	**Inter. Ins.**	**Exter. Ins.**
Heating	92.41	92.54	94.23	94.39	86.00	86.85	89.00	89.14
Cooling	17.44	19.35	16.23	17.96	19.65	21.64	18.96	20.91
Total	48.03	49.21	48.06	49.14	47.13	48.24	47.61	48.75

Table 9. Greenhouse gas emission reduction per square of insulated area in one year (gr/m^2).

			CO_2	CO	CH_4	NO_x	N_2O	SO_2	PM
Continuous	**Polystyrene**	**Inter. Ins.**	18033.54	13.64	0.37	26.33	0.27	14.79	1.58
		Exter. Ins.	16340.81	11.96	0.32	19.42	0.27	7.62	1.26
	Polyurethane	**Inter. Ins.**	16169.77	11.70	0.32	17.75	0.28	5.63	1.19
		Exter. Ins.	16627.90	12.13	0.33	19.27	0.28	7.12	1.26
	Glasswool	**Inter. Ins.**	14895.22	10.89	0.29	17.57	0.25	6.78	1.15
		Exter. Ins.	15385.81	11.35	0.31	19.32	0.25	8.53	1.23
	Rockwool	**Inter. Ins.**	15306.27	11.16	0.30	17.75	0.26	6.57	1.16
		Exter. Ins.	15787.86	11.62	0.31	19.44	0.26	8.24	1.25
Intermittent	**Polystyrene**	**Inter. Ins.**	18480.71	13.84	0.37	25.44	0.29	13.14	1.56
		Exter. Ins.	18877.29	14.21	0.38	26.87	0.29	14.57	1.63
	Polyurethane	**Inter. Ins.**	18540.19	13.82	0.37	24.79	0.29	12.24	1.54
		Exter. Ins.	18905.20	14.16	0.38	26.09	0.29	13.53	1.60
	Glasswool	**Inter. Ins.**	18033.54	13.64	0.37	26.33	0.27	14.79	1.58
		Exter. Ins.	18400.24	14.00	0.37	27.78	0.27	16.28	1.65
	Rockwool	**Inter. Ins.**	18254.69	13.76	0.37	26.12	0.28	14.27	1.58
		Exter. Ins.	18631.17	14.12	0.38	27.56	0.28	15.74	1.65

Table 10. Greenhouse gas emissions in the process of insulator production and transportation.

	Polystyrene	**Polyurethane**	**Glasswool**	**Rockwool**
CO_2 (kg/m^2)	2.584	6.03	0.714	1.407
CO (g/m^2)	1.48	4.05	0.6405	1.239

Table 11. Greenhouse gas emissions payback period (month).

		Polystyrene		Polyurethane		Glasswool		Rockwool	
		Inter. Ins.	**Exter. Ins.**	**Inter. Ins.**	**Exter. Ins.**	**Inter. Ins.**	**Exter. Ins.**	**Inter. Ins.**	**Exter. Ins.**
Continuous	CO_2	1.72	1.90	4.47	4.35	0.58	0.56	1.10	1.07
	CO	1.30	1.48	4.15	4.01	0.71	0.68	1.33	1.28
Intermittent	CO_2	1.68	1.64	3.90	3.83	0.47	0.47	0.92	0.91
	CO	1.28	1.25	0.00	0.00	0.00	0.00	0.00	0.00

Table 12. Saving social cost due emission reduction (¢/m^2.year).

			CO_2	CO	No_x	SO_2	PM
Continuous	Polystyrene	Inter. Ins.	4.29	0.06	0.38	0.64	0.16
		Exter. Ins.	3.89	0.05	0.28	0.33	0.13
	Polyurethane	Inter. Ins.	3.85	0.05	0.25	0.24	0.12
		Exter. Ins.	3.96	0.05	0.28	0.31	0.13
	Glasswool	Inter. Ins.	3.55	0.05	0.25	0.29	0.12
		Exter. Ins.	3.66	0.05	0.28	0.37	0.13
	Rockwool	Inter. Ins.	3.64	0.05	0.25	0.29	0.12
		Exter. Ins.	3.76	0.05	0.28	0.36	0.13
Intermittent	Polystyrene	Inter. Ins.	4.40	0.06	0.36	0.57	0.16
		Exter. Ins.	4.49	0.06	0.38	0.63	0.17
	Polyurethane	Inter. Ins.	4.41	0.06	0.35	0.53	0.16
		Exter. Ins.	4.50	0.06	0.37	0.59	0.16
	Glasswool	Inter. Ins.	4.29	0.06	0.38	0.64	0.16
		Exter. Ins.	4.38	0.06	0.40	0.71	0.17
	Rockwool	Inter. Ins.	4.35	0.06	0.37	0.62	0.16
		Exter. Ins.	4.44	0.06	0.39	0.68	0.17

4. CONCLUSIONS

The present study assessed the insulation reverse function (Anti-Insulation phenomenon) and investigated proper setpoint temperature for insulated building. The thermal performances of four typical insulators including Polystyrene, Polyurethane, Glasswool, and Rockwool in both external and internal configurations were studied. Moreover, the continuous and intermittent operation modes of the air-conditioning system were investigated in this study. In addition, environmental benefits were evaluated by calculating the payback period of greenhouse gas emissions and social cost conservation. The case study is a unit in mid-floor of 7-story block in the cold region of Tabriz. EnergyPlus software was used for evaluating the envelope thermal performance. The main results of this study are given below.

- Considering temperature setpoint range in the insulated building is essential, and comfortable setpoint could not be selected just based on the standards range, because simulation indicates that choosing wrong setpoints in the insulated building could lead to the Anti-Insulation phenomenon and impose extra load on HVAC system.
- Anti-Insulation phenomenon occurs at 22 ºC for simulated building.
- Implementation of insulators enhances 38-42 % energy saving. Insulators Polyurethane, Polystyrene, Rock wool, and Glasswool have the most to the least energy saving, respectively, regarding heating and total energy. But, this sort stands in contrast to the cooling energy.
- Insulator Rockwool thermal conductivity coefficient is 9.5 % larger than Glasswool. However, its energy saving is 1 % more than Glasswool, because the heat capacity of Rockwool is 20 % more than Glasswool. This phenomenon states about Glasswool and Polystyrene compared with their saving percentage.
- External insulation results in a relatively more energy reduction due to the utilization of thermal mass. Moreover, the amplitude of indoor temperature fluctuation is smaller in external insulation.
- Intermittent operation of the air-conditioning system outperforms the continuous operation by 8 % on average. The uncomfortable times as a result of the intermittent operation in the building are just 24 hours in the year.
- The payback period of greenhouse gas emissions is about a few months. The significant result is that the insulator selection based on the payback period of the emissions is different from an emission reduction base.
- Based on the result, over 14,500,000 $ is the annual social cost saving due to the insulation of 3.6 million houses of Iran's last great construction project, which is a significant amount.

5. ACKNOWLEDGEMENT

The authors would like to thank the journal editor and anonymous referees for valuable comments and suggestions and all organizations that provided data for this research.

REFERENCES

1. Ameri, M. and Gerami, A., "A multi-scenario zero-energy building techno-economic case study analysis for a renovation of a residential building", ***Journal of Renewable Energy and Environment (JREE)***, Vol. 5, No. 3, (2018), 10-26. (https://doi.org/10.30501/jree.2018.88708).
2. Maftouni, N. and Askari, M., "Building energy optimization: Implementing green roof and rainwater harvester system for a residential building", ***Journal of Renewable Energy and Environment (JREE)***, Vol. 6, No. 2, (2019), 38-45. (https://doi.org/10.30501/jree.2019.96023).
3. Idris, Y.M. and Mae, M., "Anti-insulation mitigation by altering the envelope layers' configuration", ***Energy and Buildings***, Vol. 141, (2017), 186-204. (https://doi.org/10.1016/j.enbuild.2017.02.025).
4. I.M.o.E. Review of 29 Yearly Iran Energy Statistical Data, (2018-2019).
5. Barrios, G., Huelsz, G. and Rojas, J., "Thermal performance of envelope wall/roofs of intermittent air-conditioned rooms", ***Applied Thermal Engineering***, Vol. 40, (2012), 1-7. (https://doi.org/10.1016/j.applthermaleng.2012.01.051).
6. Huang, Y., Niu, J.-L. and Chung, T.-M., "Study on performance of energy-efficient retrofitting measures on commercial building external walls in cooling-dominant cities", ***Applied Energy***, Vol. 103, (2013), 97-108. (https://doi.org/10.1016/j.apenergy.2012.09.003).
7. Meng, X., Luo, T., Gao, Y., Zhang, L., Huang, X., Hou, C., Shen, Q. and Long, E., "Comparative analysis on thermal performance of different wall insulation forms under the air-conditioning intermittent operation in summer", ***Applied Thermal Engineering***, Vol. 130, (2018), 429-438. (https://doi.org/10.1016/j.applthermaleng.2017.11.042).
8. Zhang, L., Luo, T., Meng, X., Wang, Y., Hou, C. and Long, E., "Effect of the thermal insulation layer location on wall dynamic thermal response rate under the air-conditioning intermittent operation", ***Case***

Studies in Thermal Engineering, Vol. 10, (2017), 79-85. (https://doi.org/10.1016/j.csite.2017.04.001).

9. Zhou, J., Li, Y., Xiao, X. and Long, E., "Experimental research on thermal performance differences of building envelopes in multiple heating operation conditions", ***Procedia Engineering***, Vol. 205, (2017), 628-635. (https://doi.org/10.1016/j.proeng.2017.10.409).
10. Cheng, F., Zhang, X. and Su, X., "Comparative assessment of external and internal insulation for intermittent air-conditioned bedrooms in Shanghai", ***Procedia Engineering***, Vol. 205, (2017), 50-55. (https://doi.org/10.1016/j.proeng.2017.09.933).
11. Hou, C., Meng, X., Gao, Y., Mao, W. and Long, E., "Effect of the insulation materials filling on the thermal performance of sintered hollow bricks under the air-conditioning intermittent operation", ***Case Studies in Construction Materials***, Vol. 8, (2018), 217-225. (https://doi.org/10.1016/j.cscm.2018.02.007).
12. Kolaitis, D.I., Malliotakis, E., Kontogeorgos, D.A., Mandilaras, I., Katsourinis, D.I. and Founti, M.A., "Comparative assessment of internal and external thermal insulation systems for energy efficient retrofitting of residential buildings", ***Energy and Buildings***, Vol. 64, (2013), 123-131. (https://doi.org/10.1016/j.enbuild.2013.04.004).
13. Kossecka, E. and Kosny, J., "Influence of insulation configuration on heating and cooling loads in a continuously used building", ***Energy and Buildings***, Vol. 34, No. 4, (2002), 321-331. (https://doi.org/10.1016/S0378-7788(01)00121-9).
14. Yuan, L., Kang, Y., Wang, S. and Zhong, K., "Effects of thermal insulation characteristics on energy consumption of buildings with intermittently operated air-conditioning systems under real time varying climate conditions", ***Energy and Buildings***, Vol. 155, (2017), 559-570. (https://doi.org/10.1016/j.enbuild.2017.09.012).
15. Bojić, M., Miletić, M. and Bojić, L., "Optimization of thermal insulation to achieve energy savings in low energy house (refurbishment)", ***Energy Conversion and Management***, Vol. 84, (2014), 681-690. (https://doi.org/10.1016/j.enconman.2014.04.095).
16. Charles, A., Maref, W. and Ouellet-Plamondon, C.M., "Case study of the upgrade of an existing office building for low energy consumption and low carbon emissions", ***Energy and Buildings***, Vol. 183, (2019), 151-160. (https://doi.org/10.1016/j.enbuild.2018.10.008).
17. Derradji, L., Imessad, K., Amara, M. and Errebai, F.B., "A study on residential energy requirement and the effect of the glazing on the optimum insulation thickness", ***Applied Thermal Engineering***, Vol. 112, (2017), 975-985. (https://doi.org/10.1016/j.applthermaleng.2016.10.116).
18. Dombaycı, Ö.A., "The environmental impact of optimum insulation thickness for external walls of buildings", ***Building and Environment***, Vol. 42, No. 11, (2007), 3855-3859. (https://doi.org/10.1016/j.buildenv.2006.10.054).
19. Ozel, M., "Thermal, economical and environmental analysis of insulated building walls in a cold climate", ***Energy Conversion and Management***, Vol. 76, (2013), 674-684. (https://doi.org/10.1016/j.enconman.2013.08.013).
20. Özkan, D.B. and Onan, C., "Optimization of insulation thickness for different glazing areas in buildings for various climatic regions in Turkey", ***Applied Energy***, Vol. 88, No. 4, (2011), 1331-1342. (https://doi.org/10.1016/j.apenergy.2010.10.025).
21. Vincelas, F.F.C., Ghislain, T. and Robert, T., "Influence of the types of fuel and building material on energy savings into building in tropical region of Cameroon", ***Applied Thermal Engineering***, Vol. 122, (2017), 806-819. (https://doi.org/10.1016/j.applthermaleng.2017.04.028).
22. Alam, M., Singh, H., Suresh, S. and Redpath, D., "Energy and economic analysis of Vacuum Insulation Panels (VIPs) used in non-domestic buildings", ***Applied Energy***, Vol. 188, (2017), 1-8. (https://doi.org/10.1016/j.apenergy.2016.11.115).
23. Friess, W.A., Rakhshan, K., Hendawi, T.A. and Tajerzadeh, S., "Wall insulation measures for residential villas in Dubai: A case study in energy efficiency", ***Energy and Buildings***, Vol. 44, (2012), 26-32. (https://doi.org/10.1016/j.enbuild.2011.10.005).
24. Huo, H., Shao, J. and Huo, H., "Contributions of energy-saving technologies to building energy saving in different climatic regions of China", ***Applied Thermal Engineering***, Vol. 124, (2017), 1159-1168. (https://doi.org/10.1016/j.applthermaleng.2017.06.065).
25. Liu, Z., Liu, Y., He, B.-J., Xu, W., Jin, G. and Zhang, X., "Application and suitability analysis of the key technologies in nearly zero energy buildings in China", ***Renewable and Sustainable Energy Reviews***, Vol. 101, (2019), 329-345. (https://doi.org/10.1016/j.rser.2018.11.023).
26 Cabeza, L.F., Castell, A., Medrano, M., Martorell, I., Pérez, G. and Fernández, I., "Experimental study on the performance of insulation materials in Mediterranean construction", ***Energy and Buildings***, Vol. 42, No. 5, (2010), 630-636. (https://doi.org/10.1016/j.enbuild.2009.10.033).
27. Chuah, J.W., Raghunathan, A. and Jha, N.K., "ROBESim: A retrofit-oriented building energy simulator based on EnergyPlus", ***Energy and Buildings***, Vol. 66, (2013), 88-103. (https://doi.org/10.1016/j.enbuild.2013.07.020).
28. Fang, Z., Li, N., Li, B., Luo, G. and Huang, Y., "The effect of building envelope insulation on cooling energy consumption in summer", ***Energy and Buildings***, Vol. 77, (2014), 197-205. (https://doi.org/10.1016/j.enbuild.2014.03.030).
29. Farhanieh, B. and Sattari, S., "Simulation of energy saving in Iranian buildings using integrative modelling for insulation", ***Renewable Energy***, Vol. 31, No. 4, (2006), 417-425. (https://doi.org/10.1016/j.renene.2005.04.004).
30. Mujeebu, M.A., Ashraf, N. and Alsuwayigh, A.H., "Effect of nano vacuum insulation panel and nanogel glazing on the energy performance of office building", ***Applied Energy***, Vol. 173, (2016), 141-151. (https://doi.org/10.1016/j.apenergy.2016.04.014).
31. Raynham, P., Book review: The lighting handbook 10th edition, Reference and application, Sage Publications, Sage UK, London, England, (2012). (https://doi.org/10.1177/1477153512461896).
32. DiLaura, D.L., Houser, K., Mistrick, R. and Steffy, G.R., The lighting handbook: Reference and application, (2011).
33. Sierra-Pérez, J., Boschmonart-Rives, J., Dias, A.C. and Gabarrell, X., "Environmental implications of the use of agglomerated cork as thermal insulation in buildings", ***Journal of Cleaner Production***, Vol. 126, (2016), 97-107. (https://doi.org/10.1016/j.jclepro.2016.02.146).
34. Ucar, A., "The environmental impact of optimum insulation thickness for external walls and flat roofs of building in Turkey's different degree-day regions", ***Energy Education Science and Technology Part A-Energy Science and Research***, Vol. 24, No. 1, (2009), 49-69.
35. R. American Society of Heating, A.-C. Engineers, Thermal Environmental Conditions for Human Occupancy: ANSI/ASHRAE Standard 55-2017 (Supersedes ANSI/ASHRAE Standard 55-2013) Includes ANSI/ASHRAE Addenda Listed in Appendix N, ASHRAE, (2017).

JREE: Vol. 7, No. 3, (Summer 2020) 14-28

Journal of Renewable Energy and Environment

Review Article

Journal Homepage: www.jree.ir

An Overview of Hydroelectric Power Plant: Operation, Modeling, and Control

Ghazanfar Shahgholian[a,b]

[a] *Smart Microgrid Research Center, Najafabad Branch, Islamic Azad University, Najafabad, Iran.*
[b] *Department of Electrical Engineering, Najafabad Branch, Islamic Azad University, Najafabad, Iran.*

PAPER INFO

Paper history:
Received 01 March 2020
Accepted in revised form 14 June 2020

Keywords:
Operation
Control
Renewable Energy
Hydropower
Hydraulic Turbine
Governing System

ABSTRACT

Renewable energy provides twenty percent of electricity generation worldwide. Hydroelectric power is the cheapest way to generate electricity today. It is a renewable source of energy and provides almost one-fifth of electricity in the world. Also, it generates electricity using a renewable natural resource and accounting for six percent of worldwide energy supply or about fifteen percent of the world's electricity. Hydropower is produced in more than 150 countries. Hydropower plant producers provide energy due to moving or falling water. This paper presents and discusses studies on hydroelectric power plant fields, which have been carried out by different investigators. This work aims to study and provide an overview of hydroelectric power plants such as applications, control, operation, modeling and environmental impacts. Also, the hybrid power and efficiency of the hydroelectric power plants has been investigated. The applications of a flexible AC transmission system (FACTS) controller in the power system with the hydroelectric power plants are presented.

1. INTRODUCTION

Sustainability is one of the most important benefits of using renewable energy and, therefore, never disappears [1,2]. Vital renewable energies are one of the most interesting fields in engineering for numerous reasons [3,4]. Renewable energies such as wind energy [5,6], solar energy [7,8], and water power [9,10] vary widely in their cost effectiveness and are important in the world [11,12]. Even more importantly, renewable energy produces little or no waste products, hence minimal impact on the environment [13,14]. The nominal capacity of Iranian power plants by type of power plant in 2013-2014 and 2017-2018 is shown in Table 1.

Renewable energies have been widely adopted as alternatives to fossil fuels [15,16]. Instead of fossil fuels, renewable energies are used widely [17,18]. There is a world-wide requirement of hydropower turbines for peak load operation at increasing heads and for low head turbines operating with large head variations [19, 20].

Nowadays, hydropower has become the best source of electricity, which is widely utilized all over the world [21,22]. An installed capacity of supplied hydroelectric power is approximately 20 % of the world's electricity and accounts for about 80 % of electricity from renewable energy sources. Hydroelectricity, a clean and renewable energy source, has many economic, technical, and environmental benefits [23,24]. Basically, hydroelectric power generation is performed in compliance with the law of conservation of energy, where kinetic energy that results from the movement of the mass of water from the river is translated into electricity [25,26].

The main applications of a typical hydroelectric power plant include the generation of electric power, controlling of water flow in the rivers to create pondage, and storage of drinking water supply. Hydropower plants have essentially five major components: storage reservoir, intake tunnel, surge tank, penstock, and hydro turbine. A hydropower plant scheme is shown in Fig. 1 [27,28].

Many papers have been published in the field of applications and operation of hydroelectric power plants [29,30]. These are classified as (a) load frequency control in hydropower systems [31,32], (b) mathematical modeling of hydro turbine [33,34], (c) applications of FACTS devices in power system with hydropower plant [35], (d) hydropower plant control [36,37], (e) hydraulic turbine governing system [38], (f) coordination between the water energy and else renewable energy [39,40], and (g) impact on the environment [41,42].

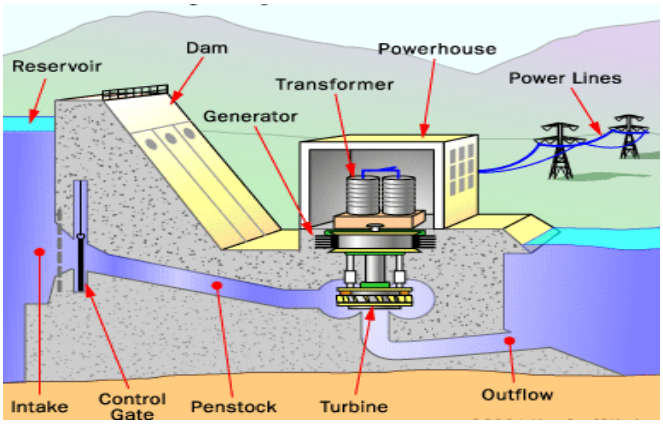

Figure 1. Components of a hydropower plant.

This paper reviews the operation and control of hydroelectric power plants. The present paper is organized in thirteen sections. Section 1 briefly reviews hydropower plants. Steps in the production of electricity in the hydropower plant are shown in Section 2. Section 3 briefly discusses the basic operating principles of the hydraulic turbine. Section 4 shows the model of the turbine. In hydro plants where the distance

*Corresponding Author's Email: shahgholian@iaun.ac.ir (Gh. Shahgholian)

between the reservoir and the turbine is quite large, a surge tank is usually utilized, as described in Section 5. One of the most important components of hydropower plant is hydraulic turbine regulating system (HTRS), which is explained in Section 6. Environmental impacts of hydroelectric power plants are shown in Section 7. Hydropower installations can have many environmental impacts by changing the environment and affecting land use, as described in Section 8. The differences between water and conventional power generations are given in Section 9. The efficiency of hydroelectric power plants is investigated in Section 10.

Table 1. Nominal capacity of Iranian power plants.

Plants	2013-2014		2017-2018	
	Manufacturing (MW)	Total percentage	Manufacturing (MW)	Total percentage
Steam	15830	22 %	15829	20.1 %
Combined cycle	17850	25 %	23166	29.4 %
Hydropower	10265	15 %	11942	15.1 %
Gas	24715	35 %	26200	33.2 %
Diesel - nuclear and renewable	1620	3 %	1761	2.2 %
Total	70280	100 %	78899	100 %

Hybrid power (combination of different technologies to produce power) is provided in Section 11. The applications of FACTS controller in power system with hydroelectric power plant are present in Section 12. The response of the hydraulic generating unit to a small change in load demand is shown in Section 13. The impact of the hydropower plant on the microgrid is shown in Section 14. Finally, concluding remarks are given in Section 15.

2. HYDROPOWER PLANTS CLASSIFICATION

In order to respond to the increasing demand for electricity, most countries give priority to its development and, accordingly, build many hydropower plants [43,44].

Hydropower plants based on quantity are classified as reservoir plants, pumped storage plants [45,46], and run-of-river plants.

According to the extent of water flow regulation, such plants may be classified into three categories: runoff river power plants without pondage, runoff river power plants with pondage, and reservoir power plants. The available head is an important determinant, and the head and capacity together largely determine the type of plant and installation. As per height of water or water head hydroelectric power plant can be divided into three categories: low head (Fig. 2), medium head (Fig. 3), and high head (Fig. 4) [47].

Generally, the grouping of hydroelectric power plants is shown in Fig. 5 [48,49].

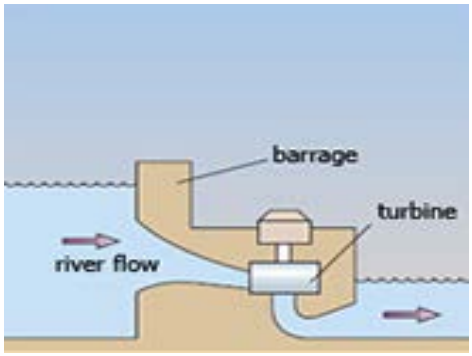

Figure 2. Low head power plant.

2.1. Based on head

There are three types of hydroelectric power plants based on the height of water available in the reservoir: low-head, medium-head, and high-head. The available water head in the low head is less than 30 m and in the medium head is more than 30 m, but is less than 300 m. However, the head of water available for producing electricity in high head is more than 300 m and can extend even up to 1000 m.

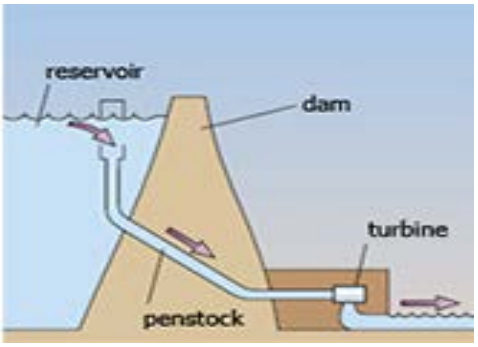

Figure 3. Medium head power plant.

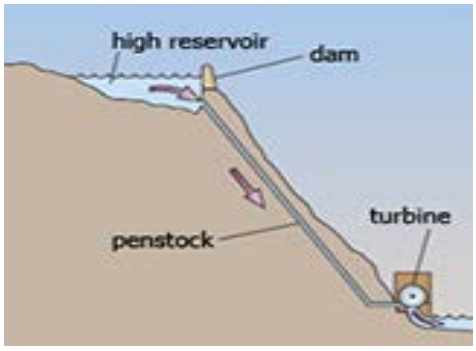

Figure 4. High head power plant.

A design technique based on optimal pole shift theory to control a low-head hydropower plant connected as a single machine to an infinite bus (SMIB) system was presented in [50], in which a state-space model with two-input and two-output variables was considered. The dynamic stability analysis of an islanded power system regarding the installation of a reversible hydropower plant for increasing renewable energy integration was shown in [51], in which these simulation results showed that the high-head hydropower installation provided a marginal contribution to system frequency regulation when explored in turbine operation mode, leading to a reversible power station with a single penstock.

2.2. Based on nature load

According to the nature of load, there are three types of hydroelectric power plants: base load plants, peak load plants, and pumped storage plant.

Base load plants are required to supply constant power to the grid. They are remotely controlled mostly and run continuously without any interruptions.

The supply of power during peak load is done through the peak load plant. They only work during certain hours of the day when the load is more than the average.

Pumped storage hydroelectric power plants are one of the most applicable energy storage technologies on large-scale capacity generation due to many technical considerations, thus maintaining the following loads in case of high penetration of renewables in the electrical grid [52].

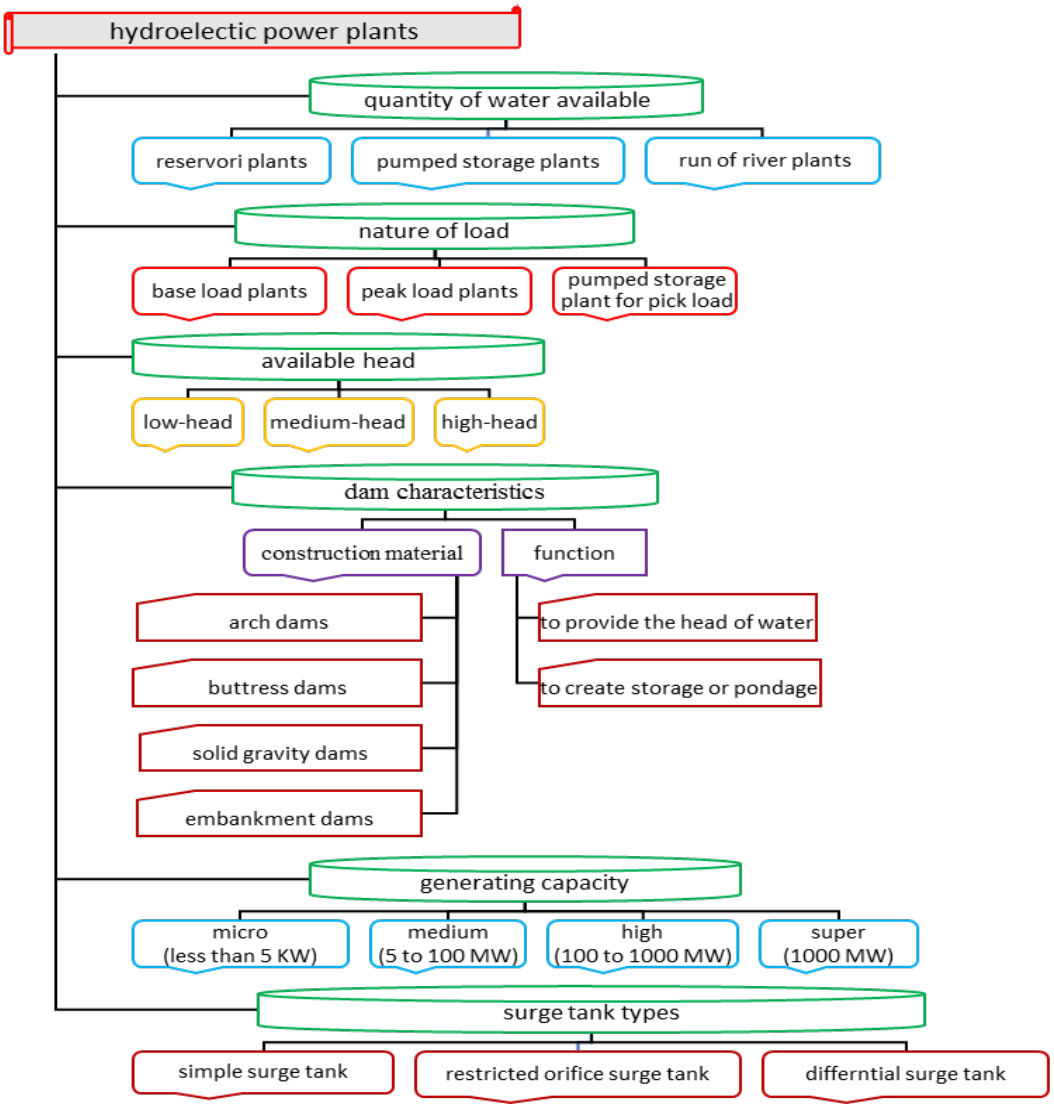

Figure 5. Showing the classification overview of hydroelectric power plants.

2.3. Based on surge tank types

Various types of surge tanks used in the hydropower water conveyance system are given as follows: simple surge tank, restricted orifice surge tank, differential surge tank, gallery type surge tank, and inclined surge tank [53,54].

The setting condition of the downstream surge tank of hydropower station with sloping ceiling tailrace tunnel was studied in [55], in which the flow inertia of penstock corresponding to the endpoint of inequality interval is the allowable value of flow inertia where the downstream surge tank is not necessary to set. By using the second version of non-dominated sorting genetic algorithm, the closing law of wicket-gates and the surge tank position at a pumped storage power plant were optimized in [56], showing that the maximum rise and fall in the water level of surge tank decreased by 5.2 % and 7 %, respectively.

3. POWER PRODUCTION STEPS

Figure 6 shows the main energy transformation at the hydroelectric power plant.

At a hydroelectric power plant, water turns into electricity, which is carried to consumers along a transportation and distribution network. The power generation steps are illustrated in Fig. 7 [57].

1. HYDRAULIC TURBINE

A hydraulic turbine is the prime mover of hydropower development. It is a mechanical device that converts the potential energy of water into rotational mechanical energy. Hydro turbine plants exhibit complex dynamics, having parameters that vary significantly with changes in operating conditions. Classification of hydraulic turbines is shown in Fig. 8 [58].

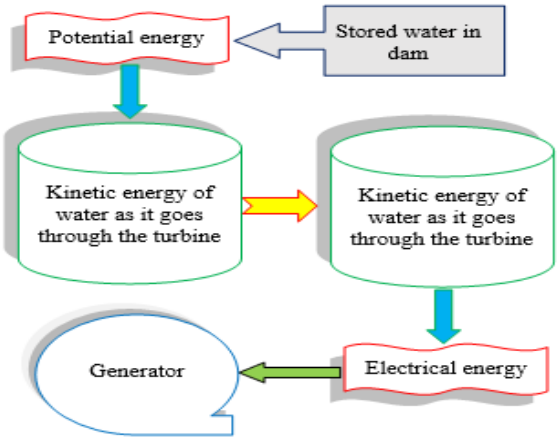

Figure 6. Main energy transformation.

4.1. Based on pressure change

Another common classification of hydro turbines is based on pressure change: impulse or reaction type that describes how the turbine transforms potential water energy into rotational mechanical energy [59,60].

The two main types of reaction turbine are the propeller (with Kaplan variant) and Francis turbines. Three main types of impulse turbine are in use: the Pelton, the Turgo, and the Crossflow.

4.2. Based on inelt head

Head is the height difference between where the water enters into the hydro system and where the former leaves the latter. Based on the head at the inlet of turbine, the hydraulic turbine is divided into low-head [61,62], medium head, and high-head [63]. Generally, for high heads, Pelton turbines are used, whereas Francis turbines are used to exploit medium heads [64,65]. For low heads, common Kaplan [66,67] and bulb turbines are applied [68]. The comparative results of the turbine performance based on head are summarized in Table 2.

4.3. Based on specific speed

The specific speed value of a turbine is the speed of a geometrically similar turbine, which would produce unit power (1 KW) under unit head (1 m).

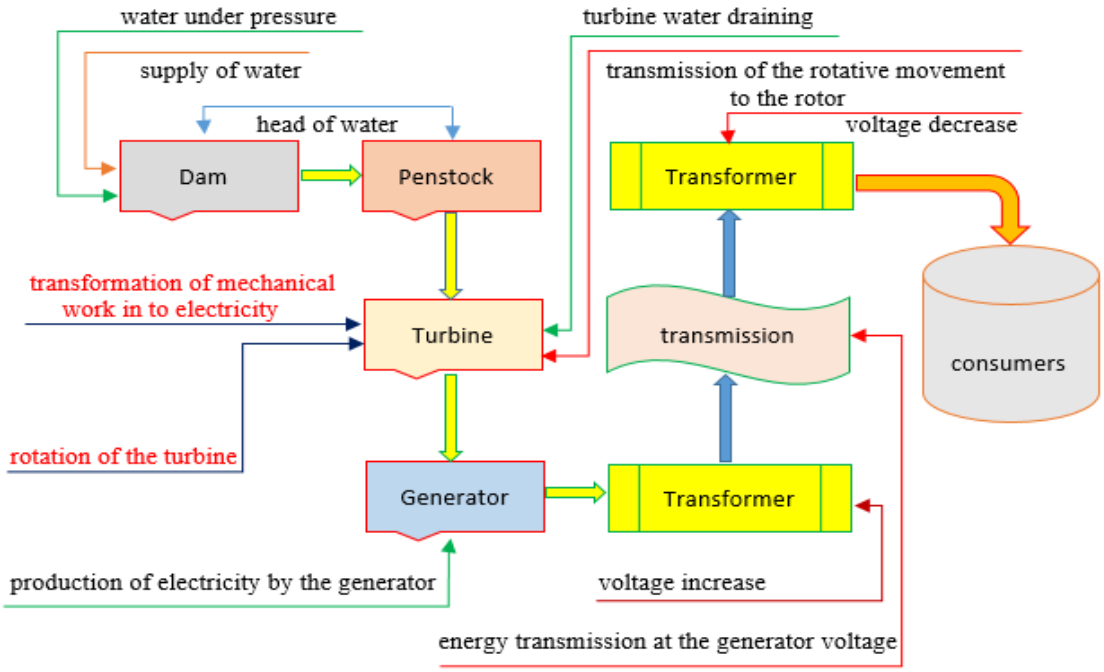

Figure 7. Steps in production of electricity at hydropower plant.

Turbine types can be classified by their specific speed, which always applies at the point of maximum efficiency. In the range of 1 to 20, impulse turbines are appropriate. In the range of 10 and 90, Francis-type runners should be selected. For up to 110, Deriaz turbines may be suitable. If speed ranges from 70 to the maximum of 260, propeller or Kaplan turbines are appropriate.

2. TURBINE MODEL

Several models of hydropower generation were investigated by scientists. Due to increasing the size and complexity of interconnected systems, hydraulic turbine generator units are applied increasingly to grant the control system needs. The block diagram of Fig. 9 shows the basic elements of a hydro turbine within the power system environment [69]. A number of different models for hydraulic turbines and their speed controllers were presented in [70].

Figure 10 shows the relationship between parameters in a hydropower plant.

The turbine and water channel characteristic is determined by assuming the rigidity of the gutter and the incompressible water flow regardless of the impact of the bump tank or the existence of a large bump tank based on the blocks shown in Figs. 11, 12, and 13.

The turbine gain relating ideal gate opening (G) to real gate opening (g) is given by:

$$A_t = \frac{\overline{G}}{\overline{g}} = \frac{1}{G_{FL} - G_{NL}} \quad (1)$$

where G_{FL} and G_{NL} are the gate opening at rated load and no load, respectively. q_{NL} is no-load flow.

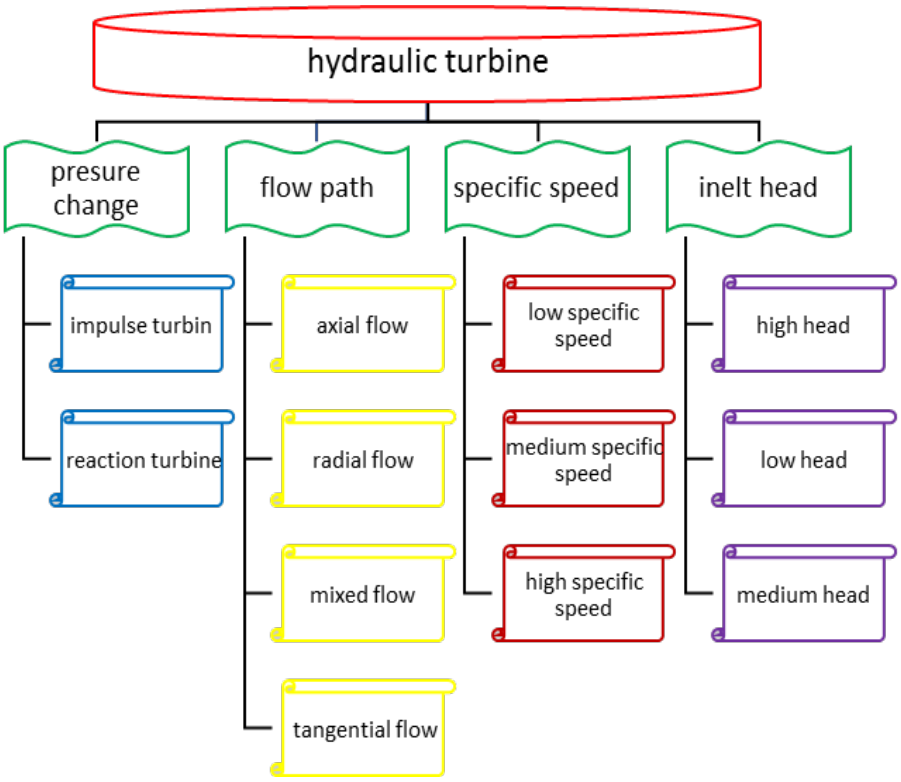

Figure 8. Classifications of hydraulic turbines.

Table 2. Characteristics of the turbine base on head.

Head	**High head (more than 50 m)**	**Medium head (between 15 m and 50 m)**	**Low head (less than 15 m)**
Turbines	Low-speed Francis, Pelton	Normal-speed Francis, Kaplan, fixed-blade propeller tubular turbine	Kaplan or fixed-blade propeller tubular turbine
Topographical conditions	Mountainous region	Hilly country (mountainous region)	Flat land
Character of storage	Seasonal annual or over-year storage	Daily or weekly poundage (storage)	No or daily pondage
Characterization of economies	Production cost being relatively low	Production cost being relatively moderate	Production cost being relatively high

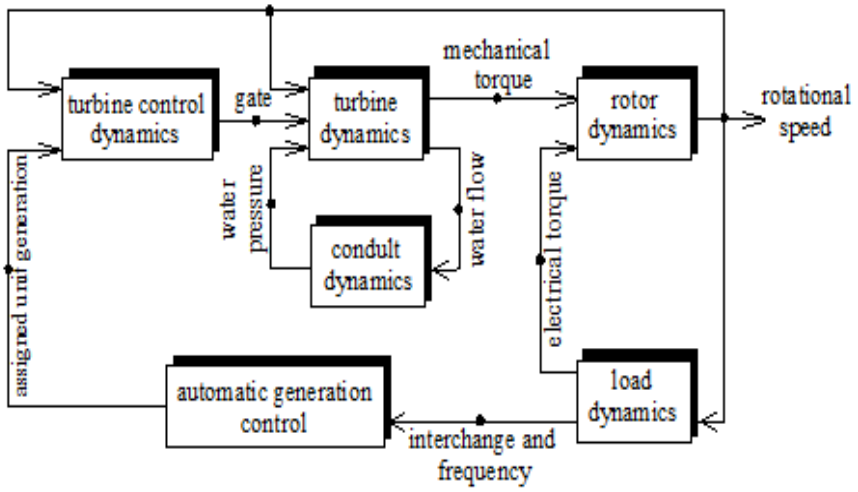

Figure 9. Functional block diagram showing the relationship between hydro prime mover system and controls to complete system.

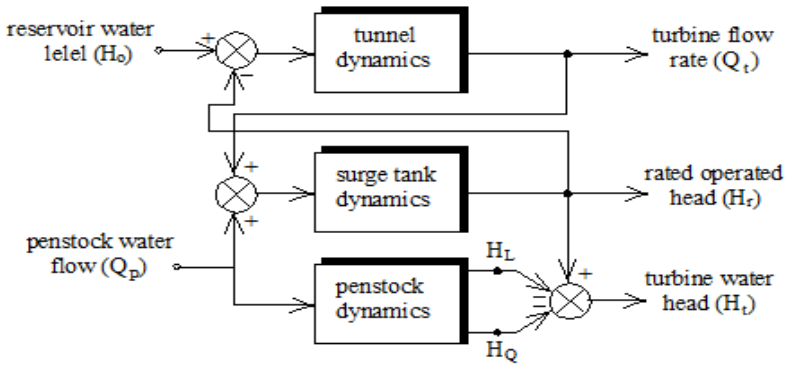

Figure 10. Relationship between parameters in hydropower plant.

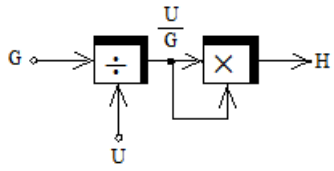

Figure 11. Block diagram based on water velocity equation.

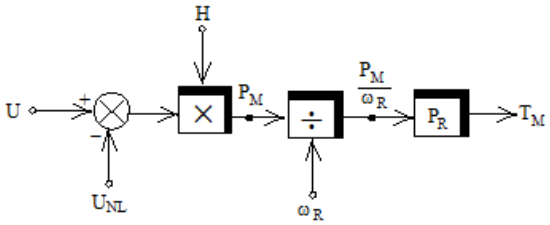

Figure 12. Block diagram based on blue turbine power equation.

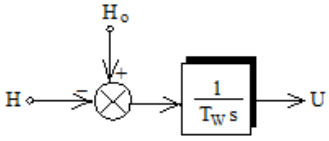

Figure 13. Block diagram based on water column acceleration equation.

Figure 14 shows the block diagram of the hydraulic turbine. Transfer function F(s) that represents the hydraulic system is the water velocity to head at turbine. F(s) represents a distributed parameter system. The complete hydraulic system conversion function that determines the relationship between water speed and turbine height is:

$$F(s)=\frac{U_t(s)}{H_t(s)}=-\frac{1+\frac{F_1(s)\,F_2(s)}{Z_P^2}}{\phi_p+F_1(s)+F_2(s)} \tag{2}$$

where ϕ_p is the channel friction coefficient, and Z_p is the channel hydraulic impedance.

The conversion function of the tunnel and bump tank shows the ratio of the bump tank height (H_S) to the water velocity of the upper channel (U_P):

$$F_1(s)=-\frac{H_S(s)}{U_P(s)}=\frac{\phi_C+T_{WC}s}{1+T_S\varphi_C s+T_{WC}T_S s^2} \tag{3}$$

where T_S is the bump tank lift time, T_{WC} is the tunnel start time, and ϕ_C is tunnel friction coefficient. If there is no bump tank, the function $F_1(s)$ is zero.

The $F_2(s)$ in terms of channel elastic stretching time (T_{ep}) and channel hydraulic impedance is given by:

$$F_2(s)=Z_P\tanh(T_{ep}s) \tag{4}$$

The application of a nonlinear controller based on a feedback linearization scheme to the multi-input multi-output model of a system consisting of a synchronous generator and a hydraulic turbine was described in [71].

3. SURGE TANK

A surge tank is a stand pipe or storage reservoir at the dam to absorb sudden rises of pressure and to quickly provide extra water during a brief drop in pressure [72]. The surge tank mitigates pressure variations due to rapid changes in the velocity of water. Surge tanks are usually provided at high or medium-head plants when there is a considerable distance between the water source and the power unit, necessitating a long penstock [73,74].

The main functions of a surge tank are given below: (a) it reduces the amplitude of pressure fluctuations by reflecting the incoming pressure waves and (b) it improves the regulation characteristic of a hydraulic turbine. Some of the most common different types of surge tanks that are possible to be installed are simple surge tank, restricted orifice surge tank, and differential surge tank.

The surge tank model is shown in Fig. 15, in which T_W is water starting time, C_S is the storage constant of the surge tank, h_S is surge tank head, q_S is flow into the surge tank, q_T is flow down the upper tunnel, and q_P is flow to turbine [75].

A model of a hydro-turbine system with the effect of surge tank based on state-space equations to study the nonlinear dynamical behaviors of the hydro-turbine system was presented in [76], in which both theoretical analysis and numerical simulations show chaotic oscillations. The simulation of a hydroelectric power plant equipped with a Francis turbine, which has a high-water head and a long penstock with upstream and downstream surge tanks, was given in [77].

4. HYDRAULIC TURBINE GOVERNING SYSTEM

A crucial control system of hydropower plant is the hydraulic turbine governing system (HTGS) [78,79]. It plays a key role in maintaining safety, stability, and economic operation of hydropower generating units [80,81].

The HTGS is a complex nonlinear, multivariable, time-variant system in nature, and non-minimum phase system that involves the interactions among hydraulic system, mechanical system, and electrical system [82,83]. The modeling of HTGS is an important and difficult task [84,85].

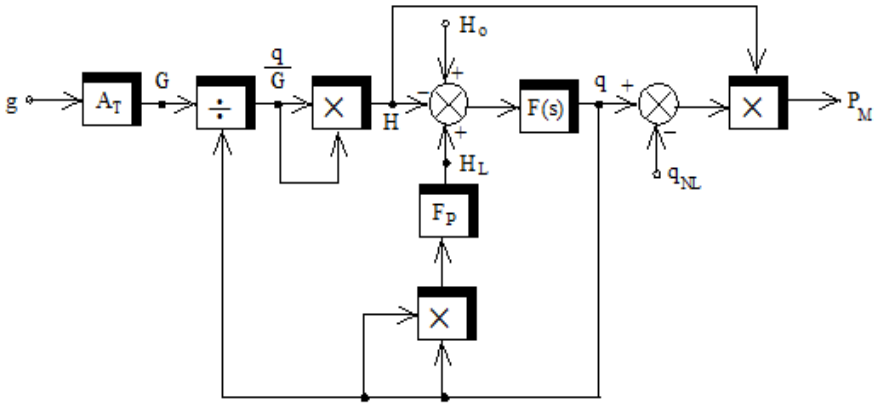

Figure 14. Hydraulic turbine block diagram.

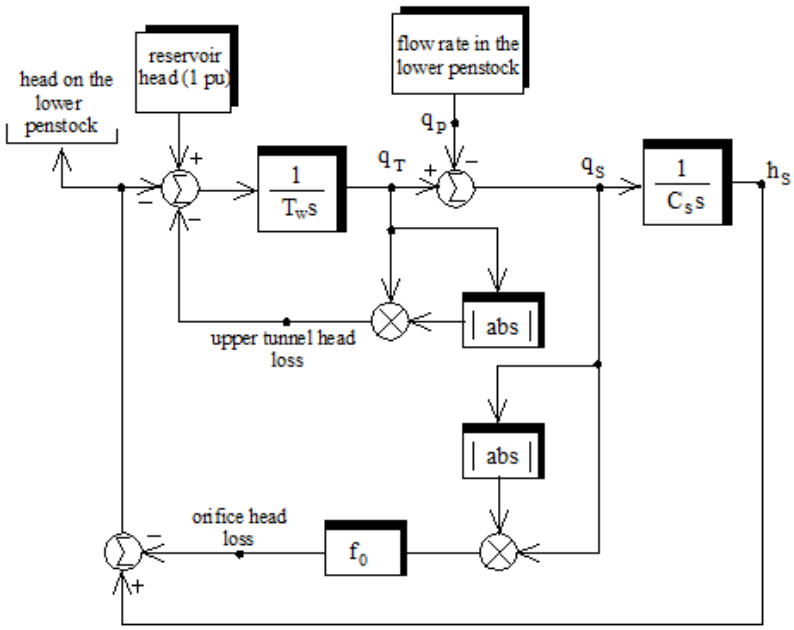

Figure 15. Surge tank model.

The main task of the HTGS system is to adjust the power output to the grid and track the frequency of the grid in general [86,87]. It consists of five parts, that is, conduit system, hydro-turbine, governor, electrohydraulic servo system, and power generator [88,89]. In this system, turbine governor is the controller and hydroelectric generating unit is the controlled object [90,91]. The main difference between the hydroturbine governing system and the gas and steam turbine governing systems is that a higher force is required to move the control gate, since the water pressure and the frictional forces are high. To provide this force, two servomotors are used. A functional diagram of the HTGS is shown in Fig. 16 [92,93].

A number of papers have improved the behavior of the HTGS. In [94], the design and analysis of a robust PID controller for a hydraulic turbine generator governor using a frequency response technique was presented. In [95], an improved gravitational search algorithm was proposed and applied to solve the identification problem for HTGS under load and no-load running conditions, in which HTGS is modeled by considering the impact of turbine speed on water flow and torque. The Hamiltonian mathematical modeling and dynamic characteristics of multi-hydro-turbine governing systems with sharing common penstock under the excitation of stochastic and shock load were presented in [96] for improving the stability of hydropower stations. A gravitational search algorithm was introduced and applied in parameter identification of an HTGS in [97], where the developed optimization algorithm GSA was improved by a compound search strategy of particle swarm optimization. A fractional order mathematical model of an HTGS to analyze the nonlinear dynamic behaviors of the HTGS in the process of operation was presented in [98]. A grey prediction control method for turbine speed control system to solve the stability problem of power system in various perturbations was presented in [99]. The stability for the primary frequency regulation of the hydro-turbine governing system with surge tank was given in [100], where the nonlinear dynamic performance of the system under opening control mode and power control mode was investigated. A mathematical model of an HTGS was presented in [101], and the nonlinear dynamical behaviors of the system considering the process of load rejection transient were studied.

When the water valve opens to compensate for the increase in load by initially reducing the turbine pressure, a short initial change in the turbine occurs, which is opposite to changing the valve position. However, by accelerating the water and increasing its velocity in the water-conducting pipe, the water

pressure increases, increasing the generator's output power and ultimately the active power balance. Therefore, blue turbine governors must have significant transient loss, and to ensure optimal and sustained speed control performance, the blue unit governor needs a transient compensator.

Figure 17 shows a block diagram of the governor of the blue turbine system for sustainability study. Two limiters are considered for the position of the water valve and the magnitude of its variations.

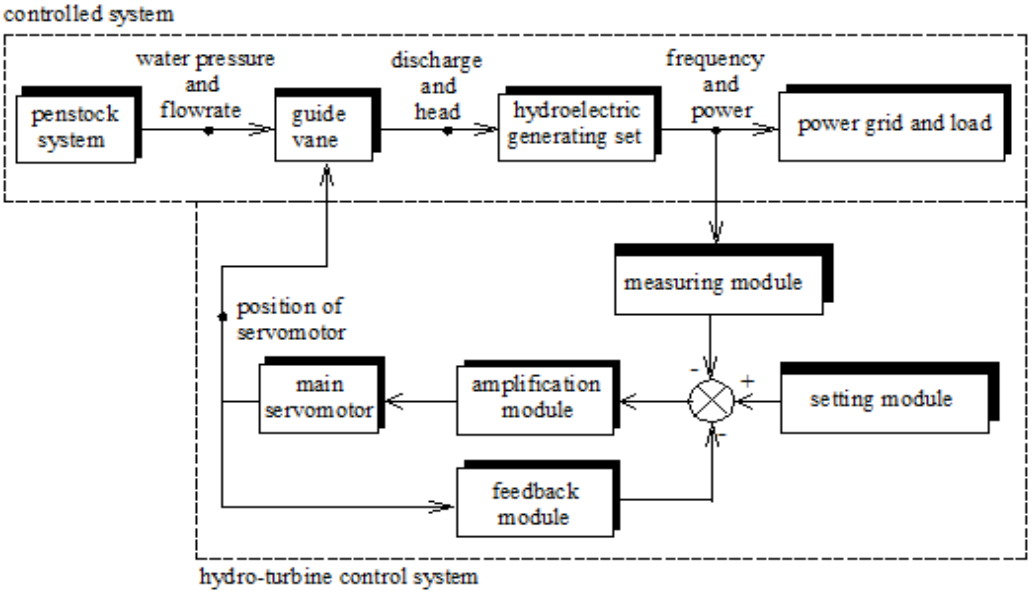

Figure 16. Block diagram of hydroelectric generating regulating system.

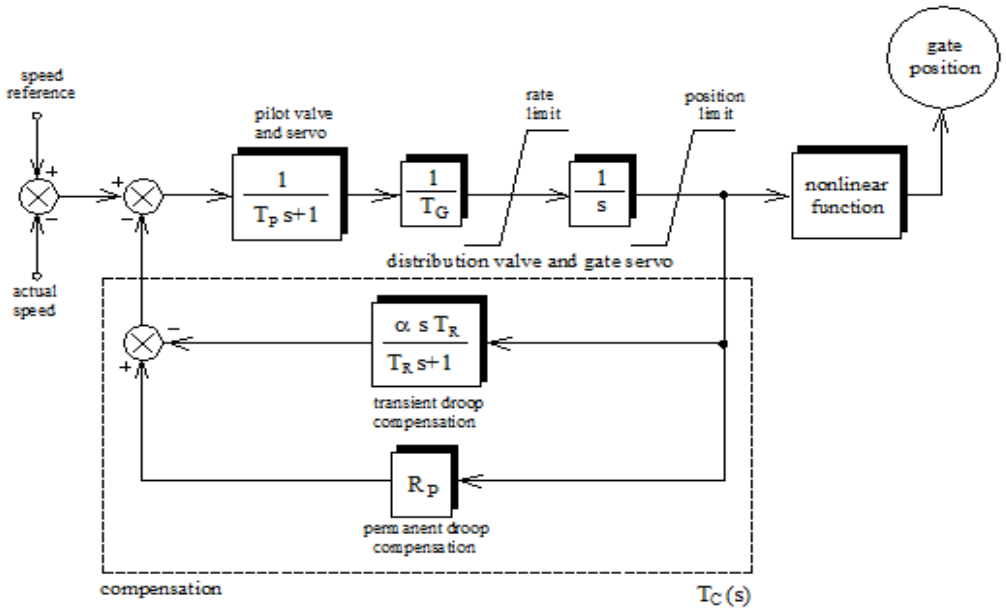

Figure 17. Block diagram Governor model of hydro turbine.

5. ENVIRONMENTAL IMPACTS

Hydropower does not pollute the water or the air. Water has a critical role in all environmental, social, and economic systems. Ecological impacts of hydroelectric power plants are large. They change natural watercourses and movement paths of wildlife around the plant and, thus, alter the ecosystem [102]. Hydropower plants can have positive and negative impacts on the socio-economic development of regions. Hydropower is clean. It prevents the burning of 22 billion gallons of oil or 120 million tons of coal each year. Hydropower does not produce greenhouse gasses or other air pollution. Hydropower leaves behind no waste. Reservoirs formed by hydropower projects in Wisconsin have expanded water-based recreation resources, and they support diverse, healthy, and productive fisheries. In fact, catch rates for game fish like walleye and smallmouth bass are substantially higher on hydropower reservoirs than natural lakes. Negative impact of dams are as follows: in flat basins, large dams cause flooding of large tracts of land, destroying local animals and habitats; people have to be displaced, causing a change in lifestyle and customs of -about 40 to 80 million people that have been displaced physically by dams worldwide; large amounts of plant life are submerged and decay anaerobically; the migratory patterns of river animals like salmon and trout are affected; dams restrict sediments that are responsible for the fertile lands downstream; saltwater intrusion into the deltas means that the saline water cannot be used for

irrigation; large dams are breeding grounds for mosquitoes and cause the spread of disease; dams serve as a heat sink, and the water is hotter than the normal river water. This warm water when released into the river downstream can affect animal life [103].

6. DIFFERENCES BETWEEN WATER AND CONVENTIONAL POWER GENERATIONS

A power plant can be of several types based mainly on the type of fuel used. Based on power generation, three major classifications of power production on a reasonably large scale include hydroelectric power generation, thermal power generation, and nuclear power generation. Hydropower produces electricity twenty-four hours a day and has little environmental impact not like solar and wind energy which is not functional twenty-four hours per day [104,105]. The primary disadvantage of solar power is that it obviously cannot be created during the night. The power generated is also reduced during times of cloud cover (although energy is still produced on a cloudy day).

At a hydropower plant, in the frequency control mode, it is possible to save power, which is not the case for a wind power plant [106,107]. Compared with steam turbines, hydro turbines are easier and cheaper to control. Hydropower enjoys high efficiency. Conventional hydropower efficiency is about 80 %. The thermal efficiency of thermal power plants is only 30 %-50 %.

7. HYDROPOWER PLANTS EFFICIENCY

The conversion efficiency of a hydroelectric power station depends mainly on the type of water turbine. In general terms, efficiency is the output of a process compared to the input [108].

In the context of a hydroelectric power plant, there are three types of efficiencies: operational efficiency, economic efficiency, and energy efficiency. The electricity is generated by moving water comes from large hydroelectric power plants and also from smaller ones such as mini-power and micropower plants. It is worth mentioning that more than 90 % of the total hydropower generated in the European Union comes from large hydro. The installed capacity of a small hydroelectric power plant is generally a few MW (<5 MW with an efficiency between 80 and 85 %). The conversion efficiency of a hydroelectric power plant depends mainly on the type of water turbine employed and can be as high as 95 % for large installations. Smaller plants with output powers less than 5 MW may have efficiencies between 80 and 85 % [109,110].

A method to calculate the cost of efficiency losses using a unit commitment dispatch in hydroelectric generators was presented in [111], demonstrating that costs can be comparable to the income of the generator in the short-term market.

8. HYBRID POWER SYSTEM

The output power of a renewable energy generator is highly affected by atmospheric conditions [112,113]. Therefore, a hybrid power system (including two or more input sources) has become the design trend for renewable energy processing, in which a constant output voltage and sustained power supply can be completed [114,115]. As mentioned earlier, hybrid systems can minimize the intermittency problem of renewable systems, which is important. Hybrid power system may or may not be in connection with the grid; therefore, they usually are not dependent on centralized grids and can be used in rural places [116,117].

The load frequency control of an interconnected two-area power system under deregulated environment was presented in [118], where Area 1 is a thermal system having two generating companies and Area 2 is the hydrothermal system. A coordination methodology for wind and pumped-storage hydro units in the day-ahead operation planning of power systems was proposed in [119], where the pumped-storage unit can offset intra-hour wind energy imbalances with coordination and minimize wind energy curtailments. The wind market value in power systems where hydroelectric stations with large reservoirs prevail was assessed in [120]; when moving from 0 % to 30 % wind penetration, hydropower mitigates the value drop by a third. The competitive interactions between an autonomous pumped-storage hydropower plant and a thermal power plant in order to optimize power generation and storage were studied in [121], where each type of the power plant individually tries to maximize its profit by adjusting its strategy.

9. FACTS EFFECTS ON HYDROELECTRIC POWER PLANT

FACTS controllers are static power-electronic devices installed in AC transmission networks to stability, increasing power transfer capability and controllability of the networks through series and/or shunt compensation [122,123]. They are used in the energy system [124].

The analysis of automatic generation control of a two-area interconnected power system under the open market scenario in the presence of thyristor controlled phase shifter-based hydrothermal system in the continuous mode using the fuzzy logic controller was presented in [125]. The LFC of the interconnected two-area system with one area as multi-unit of all-hydro power system and the other as all thermal/ thermal-hydro mixed were investigated in [126]. The authors presented a coordinated control between TCPS and SMES, with the gains of the integral controller in AGC loop and parameters of TCPS/ SMES being optimized by craziness-based PSO. A static synchronous compensator along with a variable frequency drive for voltage and frequency control of a small-hydro turbine-driven self-excited induction generator system was proposed in [127], where the FACTS devices were used to control the terminal voltage through variable reactive power injection.

10. RESPONSE GENERATING UNIT

The governors of hydraulic units require transient droop compensation for stable speed control performance. The nature of the responses of generating units with a hydraulic turbine with reheat steam turbine and without reheat steam turbine when subjected to a step change in load is shown in Figs. 18, 19, and 20.

The simulation results show that the steady state speed deviation is the same for all three units considered, and there are significant differences in their transient response.

11. HYDROPOWER PLANT IN MICROGRID

A microgrid is a localized grouping of distributed energy resources, loads, energy storage devices, inverters, and protection devices [128-131]. There are different approaches

in the operation of microgrids [132-134]. A simplified microgrid system with (a) controllable generation like the generation diesel generators and load bank, (b) not controllable generation (limited) like the photovoltaic cell and wind turbine, and (c) distributed energy storage like batteries and supercapacitors is shown in Fig. 21 [135,136].

A number of studies have investigated the application of the heyroplant power plant in the microgrid [137,138].

A microgrid topology with two generators, one of which is driven by a small-hydro turbine and other driven by a small-scale wind turbine, was studied in [139], demonstrating that the voltage and frequency of the system were regulated and the power-quality-related issues were also resolved in this microgrid. A control system to improve the parallel operation of two microhydro power plants, equipped with fix-speed turbines that drive induction generators, on an islanded microgrid was presented in [140], in which the proposed control method is a combination between active elements and passive ones. The modeling and control of a small hydro-power plant for a DC microgrid based on passivity theory was presented in [141], where the electrical, mechanical, and hydraulic dynamics in the mathematical model of the plant were considered.

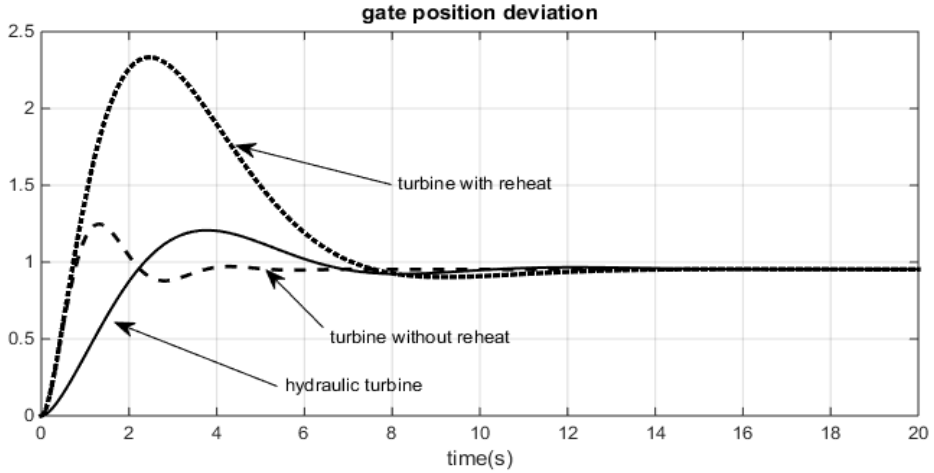

Figure 18. Turbine valve/gate position.

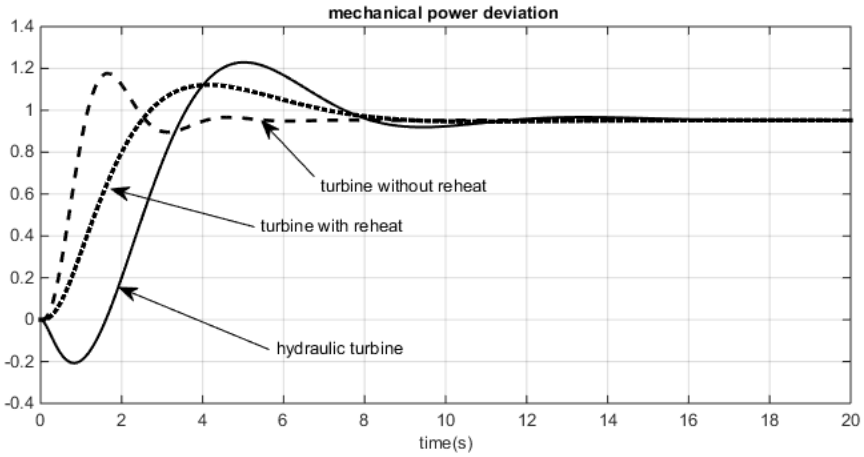

Figure 19. Mechanical power.

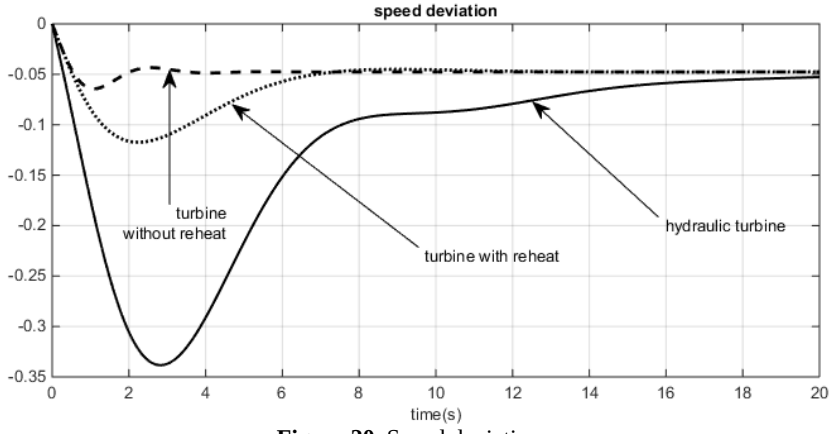

Figure 20. Speed deviation.

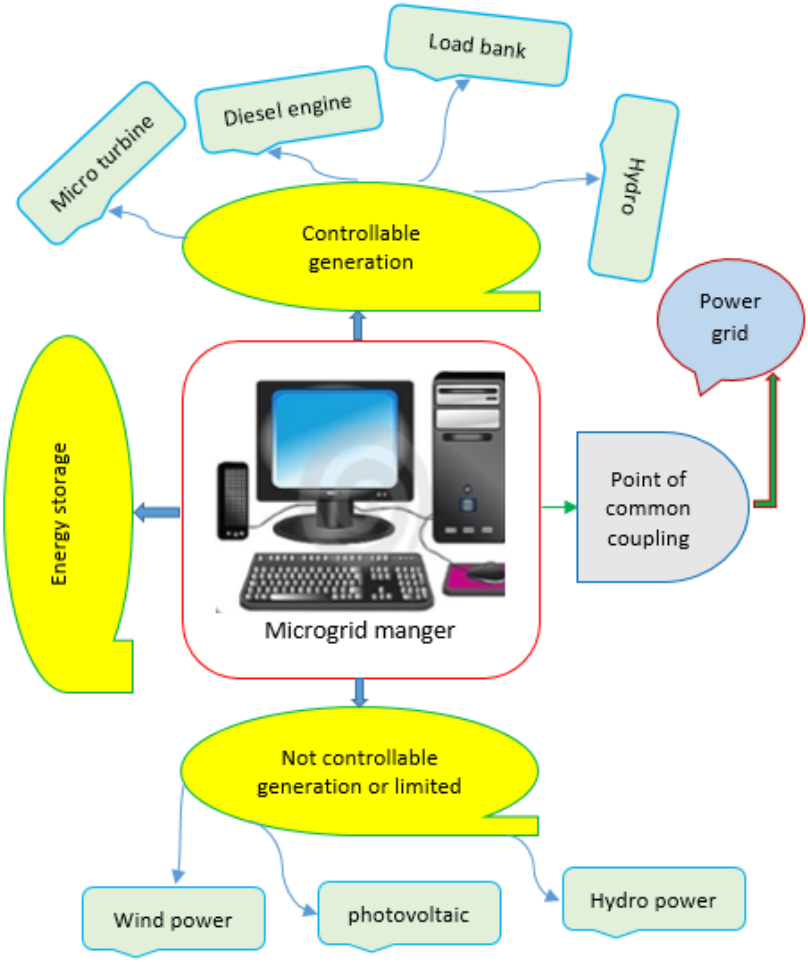

Figure 21. Schematic of a microgrid with different connected energy sources.

15. CONCLUSIONS

Hydropower is generally available in remote areas. It is a major energy source among the renewable energy sources. Worldwide, about 20 % of all electricity is generated by hydropower. Most of the countries now have hydropower as the source of major electricity producers. Hydropower schemes are classified according to installed capacity, how dependent energy production is on available flow, head conditions, and potential for the scheme to be multi-purpose.

In this paper, an extensive literature review of the research of hydroelectric power plants was carried out. Therefore, hydropower is a sustainable and long-lasting source of energy. It produces a great amount of electricity. Dams can also be used for other purposes such as fishing and sports. All these advantages show the importance of hydropower electricity, which gives us a solution to the problems of this boom and gloom economy.

12. ACKNOWLEDGMENT

The authors would like to thank the respected journal executive, journal editor, and referees for making suggestions to improve the quality of the paper. This research has been conducted in the Smart Microgrid Research Center, Najafabad Branch, Islamic Azad University, Najafabad, Iran.

REFERENCES

1. Hanmandlu, M. and Goyal, H., "Proposing a new advanced control technique for micro hydro power plants", ***Electrical Power and Energy Systems***, Vol. 30, (2008), 272-282.
2. Shahgholian, Gh. and Izadpanahi, N., "Improving the performance of wind turbine equipped with DFIG using STATCOM based on input-output feedback linearization controller", ***Energy Equipment and Systems***, Vol. 4, No. 1, (June 2016), 65-79.
3. Fang, H., Chen, L. and Shen, Z., "Application of an improved PSO algorithm to optimal tuning of PID gains for water turbine governor", ***Energy Conversion and Management***, Vol. 52, No. 4, (April 2011), 1763-1770. (https://doi.org/10.1016/j.enconman. 2010.11.005).
4. Shahgholian, Gh., "Analysis and simulation of dynamic performance for DFIG-based wind farm connected to a distrubition system", ***Energy Equipment and Systems***, Vol. 6, No. 2, (June 2018), 117-130. (https://doi.org/10.22059/EES.2018. 315 31).
5. Kumar, D. and Chatterjee, K., "A review of conventional and advanced MPPT algorithms for wind energy systems", ***Renewable and Sustainable Energy Reviews***, Vol. 55, (March 2016), 957-970. (https://doi.org/10.1016/j.rser.2015.11.013).
6. Fooladgar, M., Rok-Rok, E., Fani, B. and Shahgholian, Gh., "Evaluation of the trajectory sensitivity analysis of the DFIG control parameters in response to changes in wind speed and the line impedance connection to the grid DFIG", ***Journal of Intelligent Procedures in Electrical Technology***, Vol. 5, No. 20, (Winter 2015), 37-54.
7. Irvine, S.J.C. and Rowlands-Jones, R.L., "Potential for further reduction in the embodied carbon in PV solar energy systems", ***IET Renewable Power Generation***, Vol. 10, No. 4, (March 2016), 428-433. (https://doi.org/10.1049/iet-rpg.2015.0374).
8. Joselin Herbert, G.M., Iniyan, S., Sreevalsan, E. and Rajapandian, S., "A review of wind energy technologies", ***Renewable and Sustainable Energy Reviews***, Vol. 11, No. 6, (August 2007), 1117-1145. (https://doi.org/10.1016/j.rser.2005.08.004).
9. Vilanova, M.R.N. and Balestieri, J.A.P., "Modeling of hydraulic and energy efficiency indicators for water supply systems", ***Renewable and Sustainable Energy Reviews***, Vol. 48, (2015), 540-557. (https://doi.org/10.1016/j.rser.2015.04.024).
10. Shahgholian, Gh., "Power system stabilizer application for load frequency control in hydro-electric power plant", ***International Journal***

of Theoretical and Applied Mathematics, Vol. 2, No. 1, (Feb. 2017), 21-30. (https://doi.org/10.11648/j.engmath.20170 201.14).

11. Faiz, J., Hakimi-Tehrani, A. and Shahgholian, Gh., "Current control techniques for wind turbines: A review", ***Journal of Electromotion***, Vol. 19, No. 3-4, (July/Dec. 2012), 151-168.
12. Liu, Y., Xin, H., Wang, Z. and Gan, D., "Control of virtual power plant in microgrids: a coordinated approach based on photovoltaic systems and controllable loads", ***IET Generation, Transmission and Distribution***, Vol. 9, No. 10, (June 2015), 921-928. (https://doi.org/10.1049/iet-gtd.2015.0392).
13. Njiri, J.G. and Söffker, D., "State-of-the-art in wind turbine control: Trends and challenges", ***Renewable and Sustainable Energy Reviews***, Vol. 60, (July 2016), 377-393. (https://doi.org/10.1016/j.rser.2016.01.110).
14. Asadirad, V., Mozafari, B. and Soleymani-morcheh-khorti, S., "The application three-phase to single-phase z-source matrix converter in wind turbine", ***Journal of Intelligent Procedures in Electrical Technology***, Vol. 7, No. 28, (Winter 2017), 27-34.
15. Zhaohui, L. and Malik, O.P., "An orthogonal test approach based control parameter optimization and its application to a hydro-turbine governor", ***IEEE Transactions on Energy Conversion***, Vol. 12, No. 4, (December 1997), 388-393. (https://doi.org/10.1109/60.638956).
16. Aghajani, G., Mirabbasi, D., Alfi, B. and Seyyed-Hatami, H., "Demand side management in a smart micro-grid in the presence of renewable generation and demand response", ***Journal of Intelligent Procedures in Electrical Technology***, Vol. 8, No. 30, (Summer 2017), 55-70.
17. Shahgholian, Gh., Khani, K. and Moazzami, M., "Frequency control in autanamous microgrid in the presence of DFIG based wind turbine", ***Journal of Intelligent Procedures in Electrical Technology***, Vol. 6, No. 23, (Autumn 2015), 3-12.
18. Chatthaworn, R. and Chaitusaney, S., "Improving method of robust transmission network expansion planning considering intermittent renewable energy generation and loads", ***IET Generation, Transmission and Distribution***, Vol. 9, No. 13, (Sep. 2015), 1621-1627. (https://doi.org/10.1049/iet-gtd.2015.0363).
19. Garcia, F.J., Uemori, M.K.I., Rocha Echeverria, J.J. and Costa Bortoni, E.d., "Design requirements of generators applied to low-head hydro power plants", ***IEEE Transactions on Energy Conversion***, Vol. 30, No. 4, (June 2015), 1630-1638. (https://doi.org/10.1109/TEC.2015.2434617).
20. Yin, X., Lin, Y. and Li, W., "Operating modes and control strategy for megawatt-scale hydro-viscous transmission-based continuously variable speed wind turbines", ***IEEE Transactions on Sustainable Energy***, Vol. 6, No. 4, (October 2015), 1553-1564. (https://doi.org/10.1109/TSTE.2015.2455872).
21. Yu, X., Zhang, J., Fan, C. and Chen, S., "Stability analysis of governor-turbine-hydraulic system by state space method and graph theory", ***Energy***, Vol. 114, (Nov. 2016), 613-622. (https://doi.org/10.1016/j.energy. 2016.07.164).
22. Jafari, A. and Shahgholian, Gh., "Analysis and simulation of a sliding mode controller for mechanical part of a doubly-fed induction generator based wind turbine", ***IET Generation, Transmission and Distribution***, Vol. 11, No. 10, (July 2017), 2677-2688. (https://doi.org/10.1049/iet-gtd.2016.1969).
23. Chen, D., Ding, C., Ma, X., Yuan, P. and Ba, D., "Nonlinear dynamical analysis of hydro-turbine governing system with a surge tank", ***Appllied Mathematical Modelling***, Vol. 37, No. 14-15, (2013), 7611-7623. (https://doi.org/10.1016/j.apm.2013.01.047).
24. Shahgholian, Gh., "PID controller design for load-frequncy control in power system with hydro-turbine includes trinsient droop compensation", ***Dam and Hedroelectric Powerplant***, Vol. 2, No. 5, (2015), 50-64.
25. Ajibola, O.O.E., Ajala, O.S., Akanmu, J.O. and Balogun, O.J., "Improvement of hydroelectric power generation using pumped storage system", ***Nigerian Journal of Technology***, Vol. 37, No. 1, (Jan. 2018), 191-199. (https://doi.org/10.4314/njt.v37i1. 25).

26 Singh, R.R., Chelliah, T.R. and Agarwal, P., "Power electronics in hydro electric energy systems– A review", ***Renewable and Sustainable Energy Reviews***, Vol. 32, (April 2014), 944-959. (https://doi.org/10.1016/j.rser.2014.01.041).

27. Tenorio, L.A.L., "Hydro turbine and governor modelling electric-hydraulic interaction", Master Thesis, Norwegian University of Science and Technology, (June 2010).
28. Hedarpour, F. and Shahgholian, Gh., "Design and simulation of sliding and fuzzy sliding mode controller in hydro-turbine governing system", ***Journal of Iranian Dam and Hedroelectric Powerplant***, Vol. 4, No. 12, (Augest 2017), 10-20.
29. Souza, O.H., Barbieri, N. and Santos, A.H.M., "Study of hydraulic transients in hydropower plants through simulation of nonlinear model of penstock and hydraulic turbine model", ***IEEE Transactions on Power Systems***, Vol. 14, No. 4, (Nov. 1999), 1269-1272. (https://doi.org/10.1109/59.80 1883).
30. Martínez-Lucas, G., Sarasúa, J.I., Sánchez-Fernández, J.Á. and Wilhelmi, J.R., "Power-frequency control of hydropower plants with long penstocks in isolated systems with wind generation", ***Renewable Energy***, Vol. 83, (Nov. 2015), 245-255. (https://doi.org/10.1016/j.renene. 2015.04.032).
31. Oliveira, E.J., Honorio, L.M., Anzai, A.H., Oliveira, L.W. and Costa, E.B., "Optimal transient droop compensator and PID tuning for load frequency control in hydro power systems", ***International Journal of Electrical Power and Energy Systems***, Vol. 68, (June 2015), 345-355. (https://doi.org/10.1016/j.ijepes.2014.12.071).
32. Doolla, S. and Bhatti, T.S., "Automatic generation control of an isolated small-hydro power plant", ***Electric Power Systems Research***, Vol. 76, (2006), 889-896.
33. Liu, X. and Liu, C., "Eigenanalysis of oscillatory instability of a hydropower plant including water conduit dynamics", ***IEEE Transactions on Power Systems***, Vol. 22, No. 2, (May 2007), 675-681. (https://doi.org/10.1109/TPWRS.2007 .895156).
34. Brezovec, M., Kuzle, I. and Tomisa, T., "Nonlinear digital simulation model of hydroelectric power unit with Kaplan turbine", ***IEEE Transactions on Energy Conversion***, Vol. 21, No. 1, (March 2006), 235-241. (https://doi.org/10.1109/TEC.2005.847963).
35. Bhatt, P., Roy, R. and Ghoshal, S.P., "Comparative performance evaluation of SMES–SMES, TCPS–SMES and SSSC–SMES controllers in automatic generation control for a two-area hydro–hydro system", ***Electrical Power and Energy Systems***, Vol. 33, No. 10, (Dec. 2011), 1585-1597. (https://doi.org/10.1016/j.ijepes.2010.12.015).
36. Kishor, N., Saini, R.P. and Singh, S.P., "Optimal pole shift control in application to hydro power plant", ***Journal of Electrical Engineering***, Vol. 56, No. 11-12, (2005), 290-297.
37. Djukanovic, M.B., Dobrijevic, D.J., Calovic, M.S., Novicevic, M. and Sobajic, D.J., "Coordinated stabilizing control for the exciter and governor loops using fuzzy set theory and neural nets", ***International Journal of Electrical Power and Energy Systems***, Vol. 19, No. 8, (Nov. 1997), 489-499. (https://doi.org/10.1016/S0142-0615(97)00020-3).
38. Arnautović, D.B. and Džepčeski, D.D., "Suboptimal design of turbine governors for low head hydroturbines", ***Facta Universitatis-Series: Electronics and Energetics***, Vol. 23, No. 2, (2010), 191-198. (https://doi.org/10.2298/FUEE1002191A).
39. Karki, R., Hu, P. and Billinton, R., "Reliability evaluation considering wind and hydro power coordination", ***IEEE Transactions on Power Systems***, Vol. 25, No. 2, (May 2010), 685-693. (https://doi.org/10.1109/TPWRS. 2009.2032758).
40. Helseth, A., Gjelsvik, A., Mo, B. and Linnet, U., "A model for optimal scheduling of hydro thermal systems including pumped-storage and wind power", ***IET Generation, Transmission and Distribution***, Vol. 7, No. 12, (Dec. 2013), 1426-1434. (https://doi.org/10.1049/iet-gtd.2012.0639).
41. Andrade, A.L. and Santos, M.A., "Hydroelectric plants environmental viability: Strategic environmental assessment application in Brazil", ***Renewable and Sustainable Energy Reviews***, Vol. 52, (Dec. 2015), 1413-1423. (https://doi.org/10.1016/ j.rser.2015.07.152).
42. Moya, D., Paredes, J. and Kaparaju, P., "Technical, financial, economic and environmental pre-feasibility study of geothermal power plants by RETScreen–Ecuador's case study", ***Renewable and Sustainable Energy Reviews***, Vol. 92, (Sep. 2018), 628-637. (https://doi.org/10.1016/j.rser.2018.04.027).
43. Rajagopal, V., Singh, B. and Kasal, G.K., "Electronic load controller with power quality improvement of isolated induction generator for small hydro power generation", ***IET Renewable Power Generation***, Vol. 5, No. 2, (March 2011), 202-213. (https://doi.org/10.1049/iet-rpg.2010.0081).
44. Doolla, S. and Bhatti, T.S., "Load frequency control of an isolated small-hydro power plant with reduced dumped load", ***IEEE Transactions on Power Systems***, Vol. 21, No. 4, (Nov. 2006), 1912-1919. (https://doi.org/10.1109/TPWRS.2006.881157).

45. Hayes, B.P., Wilson, A., Webster, R. and Djokic, S.Z., "Comparison of two energy storage options for optimum balancing of wind farm power outputs", ***IET Generation, Transmission and Distribution***, Vol. 10, No. 3, (March 2016), 832-839. (https://doi.org/10.1049/iet-gtd.2015.0486).
46. Sarasúa, J.I., Pérez-Díaz, J.I., Wilhelmi, J.R. and Sánchez-Fernández, J.Á., "Dynamic response and governor tuning of a long penstock pumped-storage hydropower plant equipped with a pump-turbine and a doubly fed induction generator", ***Energy Conversion and Management***, Vol. 106, (Dec. 2015), 151-164. (https://doi.org/10.1016/j.enconman.2015.09.030).
47. Singh, V.K. and Singal, S.K., "Operation of hydro power plants-A review", ***Renewable and Sustainable Energy Reviews***, Vol. 69, (March 2017), 610-619. (https://doi.org/10.1016/j.rser.2016.11.169).
48. Mahdavian, M., Shahgholian, Gh., Janghorbani, M., Soltani, B. and Wattanapongsakorn, N., "Load frequency control in power system with hydro turbine under various conditions", ***Proceedings of the IEEE/ECTICON***, Hua Hin, Thailand, (June 2015), 1-5. (https://doi.org/10.1109/ECTICon.2015.7206938).
49. Elbatran, A.H., Yaakob, O.B., Ahmed, Y.M. and Shabara, H.M., "Operation, performance and economic analysis of low head micro-hydropower turbines for rural and remote areas: A review", ***Renewable and Sustainable Energy Reviews***, Vol. 43, (Nov. 2015), 1624-1635. (https://doi.org/10.1016/j.rser.2014.11. 045).
50. Mukherjee, V. and Ghoshal, S.P., "Comparison of intelligent fuzzy based AGC coordinated PID controlled and PSS controlled AVR system", ***International Journal of Electrical Power and Energy Systems***, Vol. 29, No. 9, (Nov. 2007), 679-689. (https://doi.org/10.1016/j.ijepes.2007.05.002).
51. Beires, P., Vasconcelos, M.H., Moreira, C.L. and Peças Lopes, J.A., "Stability of autonomous power systems with reversible hydro power plants: A study case for large scale renewables integration", ***Electric Power Systems Research***, Vol. 158, (May 2018), 1-14. (https://doi.org/10.1016/j.epsr.2017.12.028).
52. Abdellatif, D., AbdelHady, R., Ibrahim, A.M. and El-Zahab, E.A., "Conditions for economic competitiveness of pumped storage hydroelectric power plants in Egypt", ***Renewables: Wind, Water, and Solar***, Vol. 5, No. 2, (2018). (https://doi.org/10.1186/s40807-018-0048-1).
53. Zhou, J., Palikhe, S. and Bhattarai, K.P., "Hydraulic optimization of double chamber surge tank using NSGA-II resham dhakal", ***Water***, Vol. 12, No. 2, (Feb. 2020), 1-20. (https://doi.org/10.3390/w12020455).
54. Kishor, N., Saini, R.P. and Singh, S.P., "A review on hydropower plant models and control", ***Renewable and Sustainable Energy Reviews***, Vol. 11, No. 5, (June 2007), 776-796. (https://doi.org/10.1016/j.rser.2005.06.003).
55. Guo, W. and Zhu, D., "Setting condition of downstream surge tank of hydropower station with sloping ceiling tailrace tunnel", ***Chaos, Solitons and Fractals***, Vol. 134, Article 109698, (May 2020). (https://doi.org/10.1016/j.chaos.2020.109698).
56. Rezghi, A., Riasi, A. and Tazraei, P., "Multi-objective optimization of hydraulic transient condition in a pump-turbine hydropower considering the wicket-gates closing law and the surge tank position", ***Renewable Energy***, Vol. 148, (April 2020), 478-491. (https://doi.org/10.1016/j.renene. 2019.10.054).
57. https://www.visualdictionaryonline.com/energy/hydroelectricity/steps-in-production-electricity.php.
58. Grøtterud, M., "Analysis of the slow floating in grid frequency of the nordic power system impact of hydraulic system characteristics", Master Thesis, Norwegian University of Science and Technology, (June 2012).
59. Židonis, A. and Aggidis, G.A., "State of the art in numerical modelling of Pelton turbines", ***Renewable and Sustainable Energy Reviews***, Vol. 45, (May 2015), 135-144. (https://doi.org/10.1016/j.rser.2015.01.037).
60. Židonis, A., Benzon, D.S. and Aggidis, G.A., "Development of hydro impulse turbines and new opportunities", ***Renewable and Sustainable Energy Reviews***, Vol. 51, (Nov. 2015), 1624-1635. (https://doi.org/10.1016/j.rser.2015.07.007).
61. Fernandes, A.C. and Armandei, M., "Low-head hydropower extraction based on torsional galloping", ***Renewable Energy***, Vol. 69, (Sep. 2014), 447-452. (https://doi.org/10.1016/j.renene.2014.03.057).
62. Djukanovic, M., Novicevic, M., Dobrijevic, D., Babic, B., Sobajic, D.J. and Pao, Y.H., "Neural-net based coordinated stabilizing control for the exciter and governor loops of low head hydropower plants", ***IEEE Transactions on Energy Conversion***, Vol. 10, No. 4, (Dec. 1995), 760-767. (https://doi.org/10.1109/60.475850).
63. Zuo, Z., Liu, S., Sun, Y. and Wu, Y., "Pressure fluctuations in the vaneless space of high-head pump-turbines: A review", ***Renewable and Sustainable Energy Reviews***, Vol. 41, (Jan. 2015), 965-974. (https://doi.org/10.1016/j.rser.2014.09.011).
64. Thapa, B.S., Dahlhaug, O.G. and Thapa, B., "Sediment erosion in hydro turbines and its effect on the flow around guide vanes of Francis turbine", ***Renewable and Sustainable Energy Reviews***, Vol. 49, (Sep. 2015), 1100-1113. (https://doi.org/10.1016/ j.rser.2015.04.178).
65. Nagode, K. and Škrjanc, I., "Modelling and internal fuzzy model power control of a Francis water turbine", ***Energies***, Vol. 7, (2014), 874-889. (https://doi.org/10.3390/en7020874).
66. Kishor, N., Singh, S.P. and Raghuvanshi, A.S., "Dynamic simulations of hydro turbine and its state estimation based LQ control", ***Energy Conversion and Management***, Vol. 47, No. 18-19, (Nov. 2006), 3119-3137. (https://doi.org/10.1016/j.enconman.2006.03.020).
67. Schniter, P. and Wozniak, L., "Efficiency based optimal control of Kaplan Hydrogenertors", ***IEEE Transactions on Energy Conversion***, Vol. 10, No. 2, (June 1995), 348-353. (https://doi.org/10.1109/60.391902).
68. Kranjcic, D. and Stumberger, G., "Differential evolution-based identification of the nonlinear Kaplan turbine model", ***IEEE Transactions on Energy Conversion***, Vol. 29, No. 1, (March 2014), 178-187. (https://doi.org/10.1109/TEC.2013.2292927).
69. Zohbi, G.A., Hendrick, P., Renier, C. and Bouillard, P., "The contribution of wind-hydro pumped storage systems in meeting Lebanon's electricity demand", ***International Journal of Hydrogen Energy***, Vol. 41, No. 17, (May 2016), 6996-7004. (https://doi.org/10.1016/j.ijhydene.2016.01.028).
70. IEEE Committee Report, "Hydraulic turbine and turbine control models for system dynamic studies", ***IEEE Transactions on Power Systems***, Vol. 7, No. 1, (Feb. 1992), 167-179. (https://doi.org/10.1109/59.141700).
71. Akhrif, O., Okou, F.A., Dessaint, L.A. and Champagne, R., "Application of a multivariable feedback linearization scheme for rotor angle stability and voltage regulation of power systems", ***IEEE Transactions on Power Systems***, Vol. 14, No. 2, (May 1999). (https://doi.org/10.1109/59.761889).
72. Guo, W. and Yang, J., "Modeling and dynamic response control for primary frequency regulation of hydro-turbine governing system with surge tank", ***Renewable Energy***, Vol. 121, (June 2018), 173-187. (https://doi.org/10.1016/j.renene.2018.01.022).
73. Bao, H., Yang, J., Zhao, G., Zeng, W., Liu, Y. and Yang, W., "Condition of setting surge tanks in hydropower plants–A review", ***Renewable and Sustainable Energy Reviews***, Vol. 81, Part 2, (January 2018), 2059-2070. (https://doi.org/10.1016/j.rser.2017.06.012).
74. Peng, Z. and Guo, W., "Saturation characteristics for stability of hydro-turbine governing system with surge tank", ***Renewable Energy***, Vol. 131, (Feb. 2019), 318-332. (https://doi.org/10.1016/j.renene.2018.07.054).
75. Mansoor, S., "Behaviour and operation of pumped storage hydro plants", Ph.D. Thesis, University of Wales, Bangor, (April 2000). (ISNI: 0000 0001 2418 7904).
76. Chen, D., Ding, C., Do, Y., Ma, X., Zhao, H. and Wang, Y., "Nonlinear dynamic analysis for a Francis hydro-turbine governing system and its control", ***Journal of the Franklin Institute***, Vol. 351, No. 9, (Sep. 2014), 4596-4618. (https://doi.org/10.1016/j.jfranklin.2014.07.002).
77. Fang, H., Chen, L., Dlakavu, N. and Shen, Z., "Basic modeling and simulation tool for analysis of hydraulic transients in hydroelectric power plants", ***IEEE Transactions on Energy Conversion***, Vol. 23, No. 3, (June 2008), 834-841. (https://doi.org/10.1109/TEC.2008.921560).
78. Gil-González, W., Garces, A. and Escobar, A., "Passivity-based control and stability analysis for hydro-turbine governing systems", ***Applied Mathematical Modelling***, Vol. 68, (April 2019), 471-486. (https://doi.org/10.1016/j.apm.2018.11.045).
79. Luqing, Y., Weidong, L., Zhaohui, L., Malik, O.P. and Hope, G.S., "An integral criterion for appraising the overall quality of a computer-based hydroturbine governing system", ***IEEE Transactions on Energy Conversion***, Vol. 10, No. 2, (June 1995), 376-381. (https://doi.org/10.1109/60.391906).
80. Li, C., Chang, L., Huang, Z., Liu, Y. and Zhang, N., "Parameter identification of a nonlinear model of hydraulic turbine governing system with an elastic water hammer based on a modified gravitational search algorithm", ***Engineering Applications of Artificial Intelligence***,

Vol. 50, (April 2016), 177-191. (https://doi.org/10.1016/j.engappai.2015.12.016).

81. Chen, Z., Yuan, Y., Yuan, X., Huang, Y., Li, X. and Li, W., "Application of multi-objective controller to optimal tuning of PID gains for a hydraulic turbine regulating system using adaptive grid particle swam optimization", ***ISA Transactions***, Vol. 56, (May 2015), 173-187. (https://doi.org/10.1016/j.isatra. 2014.11.003).
82. Yang, J., Wang, M., Wang, C. and Guo, W., "Linear modeling and regulation quality analysis for hydro-turbine governing system with an open tailrace channel", ***Energies***, Vol. 8, (2015), 11702-11717. (https://doi.org/10.3390/en81011702).
83. Guo, W., Yang, J., Wang, M. and Lai, X., "Nonlinear modeling and stability analysis of hydro-turbine governing system with sloping ceiling tailrace tunnel under load disturbance", ***Energy Conversion and Management***, Vol. 106, (Dec. 2015), 127-138. (https://doi.org/10.1016/j.enconman.2015.09.026).
84. Li, C., Zhou, J., Xiao, J. and Xiao, H., "Hydraulic turbine governing system identification using T–S fuzzy model optimized by chaotic gravitational search algorithm", ***Engineering Applications of Artificial Intelligence***, Vol. 26, No. 9, (Oct. 2013), 2073-2082. (https://doi.org/10.1016/j.engappai.2013.04.002).
85. Jiang, C., Ma, Y. and Wang, C., "PID controller parameters optimization of hydro-turbine governing systems using deterministic-chaotic-mutation evolutionary programming (DCMEP)", ***Energy Conversion and Management***, Vol. 47, No. 9-10, (June 2006), 1222-1230. (https://doi.org/10.1016/j.enconman.2005.07.009).
86. Yuan, X., Chen, Z., Yuan, Y. and Huang, Y., "Design of fuzzy sliding mode controller for hydraulic turbine regulating system via input state feedback linearization method", ***Energy***, Vol. 93, Part 1, (Dec. 2015), 173-187. (https://doi.org/10.1016/j.energy.2015.09.025).
87. Malik, O.P. and Zeng, Y., "Design of a robust adaptive controller for a water turbine governing system", ***IEEE Transactions on Engrgy Conversion***, Vol. 10, No. 2, (June 1995), 354-359. (https://doi.org/10.1109/60.391903).
88. Li, J. and Chen, Q., "Nonlinear dynamical analysis of hydraulic turbine governing systems with nonelastic water hammer effect", ***Journal of Applied Mathematics***, Vol. 2014, (June 2014). (https://doi.org/10.1155/2014/412578).
89. Zhang, H., Chen, D., Wu, C. and Wang, X., "Dynamics analysis of the fast-slow hydro-turbine governing system with different time-scale coupling", ***Communications in Nonlinear Science and Numerical Simulation***, Vol. 54, (Jan. 2018), 136-147. (https://doi.org/10.1016/j.cnsns. 2017.05.020).
90. Chen, Z., Yuan, X., Ji, B., Wang, P. and Tian, H., "Design of a fractional order PID controller for hydraulic turbine regulating system using chaotic non-dominated sorting genetic algorithm II", ***Energy Conversion and Management***, Vol. 84, (August 2014), 390-404. (https://doi.org/10.1016/j.enconman. 2014.04.052).
91. Zhu, D. and Guo, W., "Setting condition of surge tank based on stability of hydro-turbine governing system considering nonlinear penstock head loss", ***International Journal of Electrical Power and Energy Systems***, Vol. 113, (Dec. 2019), 372-382. (https://doi.org/10.1016/j.ijepes.2019.05.061).
92. Yuan, X., Chen, Z., Yuan, Y., Huang, Y., Li, X. and Li, W., "Sliding mode controller of hydraulic generator regulating system based on the input/output feedback linearization method", ***Mathematics and Computers in Simulation***, Vol. 119, (Jan. 2016), 18-34. (https://doi.org/10.1016/j.matcom.2015.08.020).
93. Wang, F., Chen, D., Xu, B. and Zhang, H., "Nonlinear dynamics of a novel fractional-order Francis hydro-turbine governing system with time delay", ***Chaos, Solitons and Fractals***, Vol. 91, (Oct. 2016), 329-338. (https://doi.org/10.1016/j. chaos.2016.06.018).
94. Natarajan, K., "Robust PID controller design for hydro turbines", ***IEEE Transactions on Energy Conversion***, Vol. 20, No. 3, (Sep. 2005), 661-667. (https://doi.org/10.1109/TEC.2005.845448).
95. Chen, Z., Yuan, X., Tian, H. and Ji, B., "Improved gravitational search algorithm for parameter identification of water turbine regulation system", ***Energy Conversion and Manageement***, Vol. 78, (Feb. 2014), 306-315. (https://doi.org/10.1016/j.enconman.2013.10.060).
96. Xu, B., Wang, F., Chen, D. and Zhang, H., "Hamiltonian modeling of multi-hydro-turbine governing systems with sharing common penstock and dynamic analyses under shock load", ***Energy Conversion and Management***, Vol. 108, (Jan. 2016), 478-487. (https://doi.org/10.1016/j.enconman.2015.11.032).
97. Li, C. and Zhou, J., "Parameters identification of hydraulic turbine governing system using improved gravitational search algorithm", ***Energy Conversion and Management***, Vol. 52, No. 1, (Jan. 2011), 374-381. (https://doi.org/10.1016/j.enconman. 2010.07.012).
98. Xu, B., Chen, D., Zhang, H. and Wang, F., "Modeling and stability analysis of a fractional-order Francis hydro-turbine governing system", ***Chaos, Solitons and Fractals***, Vol. 75, (June 2015), 50-61. (https://doi.org/10.1016/j.chaos.2015.01.025).
99. Wang, M., Zhang, Y., Ji, T. and Wang, X., "Grey prediction control and extension assessment for turbine governing system", ***IET Generation, Transmission and Distribution***, Vol. 10, No. 11, (Aug. 2016), 2601-2605. (https://doi.org/10.1049/iet-gtd.2015.1028).
100. Wencheng, G. and Jiandong, Y., "Stability performance for primary frequency regulation of hydro-turbine governing system with surge tank", ***Applied Mathematical Modelling***, Vol. 54, (Feb. 2018), 446-466. (https://doi.org/10.1016/j.apm.2017.09.056).
101. Zhang, H., Chen, D., Xu, B. and Wang, F., "Nonlinear modeling and dynamic analysis of hydro-turbine governing system in the process of load rejection transient", ***Energy Conversion and Management***, Vol. 90, (Jan. 2015), 128-137. (https://doi.org/10.1016/j.enconman.2014.11.020).
102. Vezmar, S., Spajić, A., Topić, D., Šljivac, D. and Jozsa, L., "Positive and negative impacts of renewable energy sources", ***International Journal of Electrical and Computer Engineering Systems***, Vol. 5, No. 2, (2014).
103. Gupta, V., Khare, R. and Prasad, V., "Performance evaluation of pelton turbine: A review", ***Journal of Water, Energy and Environment***, No. 13, (July 2013), 28-35. (https://doi.org/10.3126/hn.v13i0.10042).
104. Hosseini, E. and Shahgholian, Gh., "Different types of pitch angle control strategies used in wind turbine system applications", ***Journal of Renewable Energy and Environment (JREE)***, Vol. 4, No. 1, (Winter 2017), 20-35. (https://doi.org/10.30501/jree.2017.70103).
105. Mozafarpoor-Khoshrodi, S.H. and Shahgholian, Gh., "Improvement of perturb and observe method for maximum power point tracking in wind energy conversion system using fuzzy controller", ***Energy Equipment and Systems***, Vol. 4, No. 2, (Autumn 2016), 111-122. (https://doi.org/10.22059/EES.2016.23031).
106. Hosseini, E. and Shahgholian, Gh., "Partial- or full-power production in WECS: A survey of control and structural strategies", ***European Power Electronics and Drives***, Vol. 27, No. 3, (Dec. 2017), 125-142. (https://doi.org/10.1080/09398368.2017.1413161).
107. Hosseini, E. and Shahgholian, Gh., "Output power levelling for DFIG wind turbine system using intelligent pitch angle control", ***Automatika***, Vol. 58, No. 4, (2017), 363-374. (https://doi.org/10.1080/00051144.2018.1455017).
108. Kaunda, C.S., Kimambo, C.Z. and Nielsen, T.K., "Hydropower in the context of sustainable energy supply: A review of technologies and challenges", ***ISRN Renewable Energy***, Vol. 2012, (2012), 1-15. (https://doi.org/10.5402/2012/730631).
109. Borkowski, D. and Wegiel, T., "Small hydropower plant with integrated turbine-generators working at variable speed", ***IEEE Transactions on Energy Conversion***, Vol. 28, No. 2, (June 2013), 452-459. (https://doi.org/10.1109/TEC.2013.2247605).
110. Ferreira, J.H.I., Camacho, J.R. and Malagoli, J.A., "A contribution to the study of the estimate hydroelectric potential for small hydropower plant", ***IEEE Latin America Transactions***, Vol. 14, No. 7, (July 2016), 3215-3224. (https://doi.org/10.1109/TLA.2016.7587623).
111. Galvis, J.C., Padilha-Feltrin, A. and Yusta Loyo, J.M., "Cost assessment of efficiency losses in hydroelectric plants", ***Electric Power System Research***, Vol. 81, No. 10, (October 2011), 1866-1873. (https://doi.org//10.1016/j.epsr.2011.05.006).
112. Kumar, K.R. and Kulgod, S.P., "Simulation and analysis of energy harvesting from Grey water and rain water in high rises", ***Proceedings of the IEEE/ICEETS***, Nagercoil, Tamil Nadu, India, (April 2016), 856-861. (https://doi.org/10.1109/ICEETS.2016.7583866).
113. Khankari, G. and Kamakar, S., "Combined thermal-hydro power generation: A novel approach of plant capacity addition", ***International Journal of Renewable Energy Research***, Vol. 6, No. 1, (2016), 255-262.
114. Shen, C.L. and Shen, Y.S., "Output filter design for a novel dual-input PV-wind power converter by energy balance principle", ***Applied Sciences***, Vol. 6, (2016), 1-15. (https://doi.org/10.3390/app 6090263).
115. Shahgholian, Gh., Khani, K. and Moazzami, M., "The Impact of DFIG based wind turbines in power system load frequency control with hydro

turbine", ***Dam and Hedroelectric Powerplant***, Vol. 1, No. 3, (Winter 2015), 38-51.

116. Heidarpour, F. and Shahgholian, Gh., "Stability improvement of hydraulic turbine regulating system using round-robin scheduling algorithm", ***Journal of Renewable Energy and Environment (JREE)***, Vol. 5, No. 1, (Winter 2018), 1-7. (https://doi.org/10.30501/jree.2018.88584).
117. Singh, V., Kumar, A. and Batish, N., "Simulation and analysis of integrated wind power with small hydroelectric hybrid power system for transient stability", ***Advanced Research in Electrical and Electronic Engineering***, Vol. 1, No. 1, (2014), 42-48.
118. Rahman, A., Saikia, L.C. and Sinha, N., "Load frequency control of a hydro-thermal system under deregulated environment using biogeography-based optimised three-degree-of-freedom integral-derivative controller", ***IET Generation, Transmission and Distribution***, Vol. 9, No. 15, (Nov. 2015), 2284-2293. (https://doi.org/10.1049/iet-gtd.2015.0317).
119. Khodayar, M.E., Abreu, L. and Shahidehpour, M., "Transmission-constrained intrahour coordination of wind and pumped-storage hydro units", ***IET Generation, Transmission and Distribution***, Vol. 7, No. 7, (July 2013), 755-765. (https://doi.org/10.1049/iet-gtd.2012.0272).
120. Hirth, L., "The benefits of flexibility: The value of wind energy with hydropower", ***Applied Energy***, Vol. 181, (Nov. 2016), 210-223. (https://doi.org/10.1016/j.apenergy.2016.07.039).
121. Forouzandehmehr, N., Han, Z. and Zheng, R., "Stochastic dynamic game between hydropower plant and thermal power plant in smart grid networks", ***IEEE System Journal***, Vol. 10, No. 1, (March 2016), 88-96. (https://doi.org/10.1109/JSYST.2014.2317555).
122. Motaghi, A., Alizadeh, M. and Abbasian, M., "Reactive power compensation and reducing network transmission losses by optimal placement of parallel and series FACTS devices with fuzzy-evolutionary method", ***Journal of Intelligent Procedures in Electrical Technology***, Vol. 9, No. 35, (Autumn 2019), 27-38.
123. Shahgholian, Gh., Hamidpour, H. and Movahedi, A., "Transient stability promotion by FACTS controller based on adaptive inertia weight particle swarm optimization method", ***Advances in Electrical and Electronic Engineering***, Vol. 16, No. 1, (March 2018), 57-70. (https://doi.org/10.15598/aeee.v16i1.2369).
124. Ghaedi, H., Shahgholian, Gh. and Hashemi, M., "Comparison of the effects of two flatness based control methods for STATCOM on improving stability in power systems including DFIG based wind farms", ***Iranian Electric Industry Journal of Quality and Productivity***, Vol. 8, No. 1, (2019), 72-81.
125. Rao, C.S., Nagaraju, S.S. and Raju, P.S., "Automatic generation control of TCPS based hydrothermal system under open market scenario: A fuzzy logic approach", ***International Journal of Electrical Power and Energy Systems***, Vol. 31, No. 7-8, (Sep. 2009), 315-322. (https://doi.org/10.1016/j.ijepes.2009. 03.007).
126. Bhatt, P., Ghoshal, S.P. and Roy, R., "Load frequency stabilization by coordinated control of thyristor controlled phase shifters and superconducting magnetic energy storage for three types of interconnected two-area power systems", ***International Journal of Electrical Power and Energy Systems***, Vol. 32, No. 10, (Dec. 2010), 1111-1124. (https://doi.org/10.1016/j.ijepes. 2010.06.009).
127. Singh, B., Murthy, S.S., Chilipi, R.R., Madishetti, S. and Bhuvaneswari, G., "Static synchronous compensator-variable frequency drive for voltage and frequency control of small-hydro driven self-excited induction generators system", ***IET Generation, Transmission and Distribution***, Vol. 8, No. 9, (Sep. 2014), 1528-1538. (https://doi.org/10.1049/iet-gtd.2013.0703).
128. Khani, K. and Shahgholian, Gh., "Analysis and optimization of frequency control in isolated microgrid with double-fed induction-generators based wind turbine", ***Journal of International Council on Electrical Engineering***, Vol. 9, No. 1, (Feb. 2019), 24-37. (https://doi.org/10.1080/22348972.2018.1564547).
129. Jafari, A., Shahgholian, Gh. and Zamanifar, M., "Stability analysis of doubly-fed induction generator wind turbine systems using modal analysis", ***Iranian Journal of Electrical and Computer Engineering***, Vol. 17, No. 3, (Autumn 2019), 173-189. (In Farsi).
130. Keyvani-Boroujeni, B., Shahgholian, Gh. and Fani, B., "A distributed secondary control approach for inverter-dominated microgrids with application to avoiding bifurcation-triggered Instabilities", ***IEEE Journal of Emerging and Selected Topics in Power Electronics***, Early Access Article, (February 2020), 1-8. (https://doi.org/10.1109/JESTPE.2020.2974756).
131. Bisheh, H., Moazzami, M., Fani, B. and Shahgholian, Gh., "A new method for controlling microgrids protection settings with the high penetration of distributed generation", ***Computational Intelligence in Electrical Engineering***, Vol. 10, No. 4, (Winter 2020), 71-90.
132. Carpintero-Renter, M., Santos-Martin, D. and Guerrero, J.M., "Microgrids literature review through a layers structure", ***Energies***, Vol. 12, No. 22, (2019), 1-22. (https://doi.org/10.3390/en12224381).
133. Shahgholian, Gh., Fani, B., Keyvani, B., Karimi, H. and Moazzami, M., "Improve the reactive power sharing by uses to modify droop characteristics in autonomous microgrids", ***Energy Engineering and Management***, Vol. 9, No. 3, (2019), 64-71. (In Farsi).
134. Karimi, H., Shahgholian, Gh., Fani, B., Sadeghkhani, I. and Moazzami, M., "A protection strategy for inverter interfaced islanded microgrids with looped configuration", ***Electrical Engineering***, Vol. 101, No. 3, (Sep. 2019), 1059-1073. (https://doi.org/10.1007/s00202-019-00841-6).
135. Pham, T.H., Prodan, I., Genon-Catalot, D. and Lefèvre, L., "Economic constrained optimization for power balancing in a dc microgrid: A multi-source elevator system application", ***International Journal of Electrical Power and Energy Systems***, Vol. 118, Article 105753, (June 2020), 1-15. (https://doi.org/10.1016/j.ijepes.2019.105753).
136. Sadegheian, M., Fani, B., Sadeghkhani, I. and Shahgholian, Gh., "A local power control scheme for electronically interfaced distributed generators in islanded microgrids", ***Iranian Electric Industry Journal of Quality and Productivity***, Vol. 8, No. 3, (2020), 47-58.
137. Tiomo, D. and Wamkeue, R., "Dynamic modeling and analysis of a micro-hydro power plant for microgrid applications", ***Proceedings of The IEEE/ CCECE***, Edmonton, AB, Canada, (May 2019), 1-6. (https://doi.org/10.1109/CCECE.2019.8861875).
138. Shojaeean, S. and Akrami, H., "Coordination between wind power, hydro storage facility and conventional generating units according to the annual growth load", ***Journal of Intelligent Procedures in Electrical Technology***, Vol. 4, No. 14, (Spring 2013), 31-40.
139. Singh, B. and Bhalla, K.K., "Reduced converter topology for integrated wind and small-hydro energy generation system", ***IET Renewable Power Generation***, Vol. 9, No. 5, (June 2015), 520-529. (https://doi.org/10.1049/iet-rpg.2014.0235).
140. Ion, C.P. and Marinescu, C., "Autonomous microgrid based on micro hydro power plants", ***Proceedings of The IEEE/OPTIM***, Brasov, Romania, (May 2012), 941-946. (https://doi.org/10.1109/OPTIM.2012.6231918).
141. Gil-González, W., DaniloMontoya, O. and Garces, A., "Modeling and control of a small hydro-power plant for a DC microgrid", ***Electric Power Systems Research***, Vol. 180, Article 106104, (March 2020), 1-6. (https://doi.org/10.1016/j.epsr.2019.106104).

JREE: Vol. 7, No. 3, (Summer 2020) 29-46

Journal of Renewable Energy and Environment

Research Article

Journal Homepage: www.jree.ir

Energy Simulation and Management of the Main Building Component Materials Using Comparative Analysis in a Mild Climate Zone

Nima Amani

Department of Civil Engineering, Chalous Branch, Islamic Azad University, Chalous, Iran.

PAPER INFO

Paper history:
Received 16 April 2020
Accepted in revised form 04 July 2020

Keywords:
Energy Conservation
Energy Management
Comparative Analysis
Residential Building
Materials
Case Study

ABSTRACT

Must limited energy resources and the need for energy saving make the design of buildings more efficient in terms of energy consumption. For this reason, proper orientation of buildings, use of sunlight, natural ventilation, application of consumable materials are factors that help reduce heat and cooling loads. The objective of this study is to evaluate the energy efficiency of residential buildings using natural energy and optimizing the choice of materials for heat and cold saving with the Ecotect simulation software. According to analysis and simulation, it was found that the optimum materials of the main building components in a mild climate zone of Rasht city include (a) the Brick Conc block Plaster for a wall with the total radiation incident of 340 W/m^2 and a radiation absorption of 240 W/m^2, (b) Double Glazed-Low E for windows with the total radiation incident of 340 W/m^2 and a radiation absorption of 100 W/m^2, (c) Foam Core Ply Wood for door with the total radiation incident of 340 W/m^2 and a radiation absorption of 200 W/m^2, (d) ConcSlab-OnGround for floor with the total radiation incident of 340 W/m^2 and a radiation absorption of 220 W/m^2, and (e) Conc Roof Asphalt for roof with the total radiation incident of 340 W/m^2 and a radiation absorption of 300 W/m^2. According to an hourly temperature analysis of all stories of the building on two hot and cold days of the year and as observed by the design and material selection requirements, the building will be conditioned in an almost thermal comfort zone (below 30 degrees) in the warm season.

1. INTRODUCTION

The issue of energy and access of the developed countries to low-cost energy sources has always been subject to many challenges [1]. This is one of the most important and common topics in today's world. These days, worldwide environmental changes have put human civilization in jeopardy [2]. An effective indoor condition relies upon a better comprehension of ecological components including building structure and setting. Indoor climatic conditions play a critical role in the sustainability of building construction [3]. The building sector is responsible for 40 % of energy consumption and 38 % of the CO_2 emissions in the U.S. [4]. About 27 % of the CO_2 emissions in the UK are attributed to buildings (heat loss at homes). Thermal analysis has the most important role in dealing with building energy consumption and is one of the key points of investigation [5, 6]. One of the main topics in the debate on the sustainable building plan is the balance between energy storage and distributed renewable energy consumption (solar and wind energies) [7]. A sustainable building is developed using environment-friendly materials and low energy consumption during the whole lifecycle of a building [8]. Buildings and their corresponding energy requirements significantly impact the environment, which is presently a matter of concern among the related research community [9]. Since worldwide interests are aligned with energy efficiency in buildings under the current environmental changes, thermal comfort studies are received considerable attention nowadays [10]. In this respect, ensuring ecological energy saving and constructing green buildings in many countries have become exceptionally fascinating [1]. Increase in building energy consumption can affect the world in negative terms [11]. The negative climatic effects on developing countries and their buildings result from the high intensity of solar radiation and high daily air temperature [12].

Limited energy resources and energy saving requirements make the design of buildings more efficient in terms of energy consumption [13]. For this reason, proper orientation of buildings, use of sunlight, natural ventilation, and the choice of consumable materials to reduce heat and cooling loads and prevent energy loss are important. A number of factors are conducive to the increase and decrease rates of energy consumption of buildings. Factors such as form, materials, pop-ups, and orientation of the building to sunlight and wind are the most important ones, among which the shape and orientation of the building usually receive more emphasis. Many studies have been done on the design of building materials, Phase Change Material (PCM), and simulation and optimization of heating and cooling system in order to achieve energy efficiency [14-30]; however, in terms of designing an optimum thermal form with favorable performance, studies have rather underestimated the parameter of using proper materials. The objective of this study is to evaluate the energy efficiency of residential buildings using natural energy and optimizing the choice of materials for heat and cold saving with the Ecotect simulation software. For this purpose, the design phase along with the choice of optimum materials can play a notable role in the energy management of a building. In this study, modeling is performed with Ecotect software according to the climate data (mean annual temperature) of the area, building orientations, sunlight angle, available natural ventilation, and optimum material selection analysis.

*Corresponding Author's Email: nimaamani@iauc.ac.ir (N. Amani)

Based on comparative results, the best conditions will be obtained for energy conservation in the early stages of design.

Autodesk Ecotect is a very powerful environmental design software product that examines the basic 3D model of solar, heat, lighting, acoustics, and cost [31]. As a result, based on the climatic conditions, initial architectural design can be done [32, 33]. Ecotect analysis offers a wide scope of simulation and building energy analysis, which can develop the performance of existing buildings as well as new building plans [34]. Ecotect analyzes the design of building materials and the best material and component choices for energy conservation [5]. This analysis includes a broad range of simulation and analysis practices required to study how a building materials design will be operationalized and performed [35]. For these reasons, Ecotect was selected as the analysis software of this study.

2. RESEARCH METHODOLOGY

The residential building of Mehr in Rasht, Iran is selected as a case study to estimate the impact of architectural design and building materials used on the amount of heating and cooling energy required. The amount of heat and cooling energy required is calculated through modeling in Ecotect software. In the case study, all the details used will be computed for the walls, roof (ceiling), floor, door, and window. Figure 1 illustrates the steps of the study method in the following flowchart format.

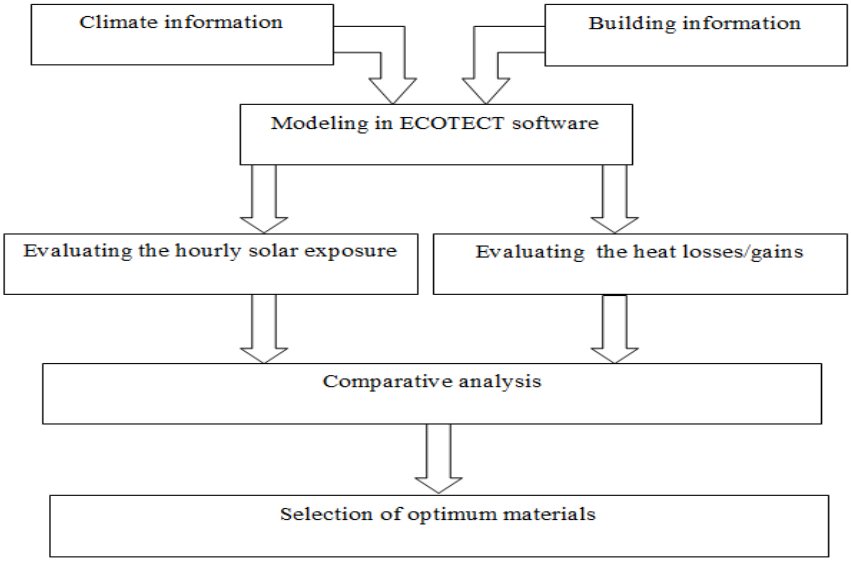

Figure 1. Research method flowchart.

2.1. Weather data

All The average annual temperature in Rasht, the capital of Guilan province, Iran, is 15.9 °C. The average annual maximum and minimum temperatures are 20.6 °C and 11.3 °C. The difference between the maximum and minimum annual temperatures is 9.3 degrees. The average temperature is 6.8 °C in the coldest month of winter (January) and 25.2 °C in the hottest month of summer (July). The mean seasonal temperatures are 18.8 °C in the spring, 24 °C in summer, 13 °C in autumn, and 7.6 °C in winter [36]. Figure 2 shows the maximum and minimum air temperatures according to the Climate Consultant software 6.0 output. Two months of the year (January and February) require the use of a heating system (the maximum temperature diagram is below the thermal comfort range). However, it takes about six months of the year (May to October) to use a cooling system to provide thermal comfort. Figure 3 depicts the solar radiation diagram for determining the warm and cold periods in Rasht.

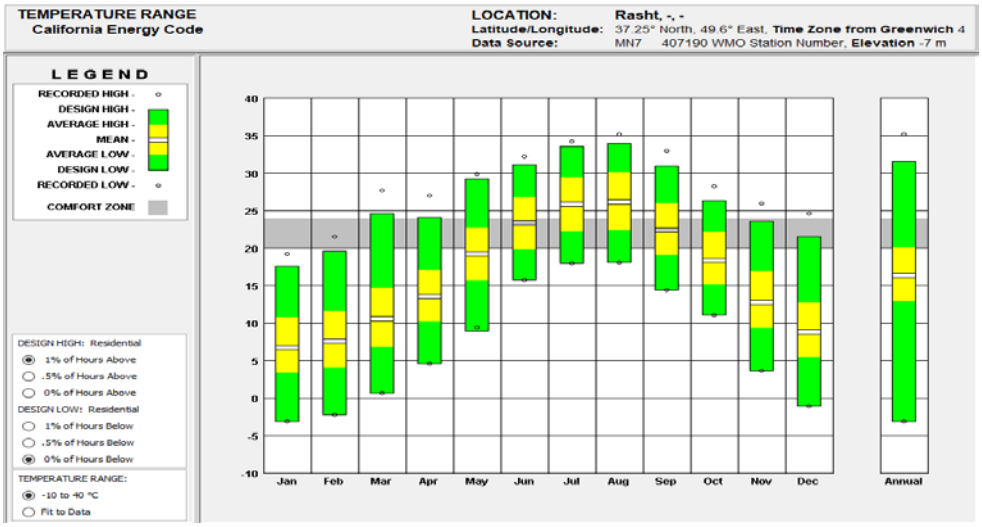

Figure 2. The maximum and minimum air temperatures in Rasht city [37].

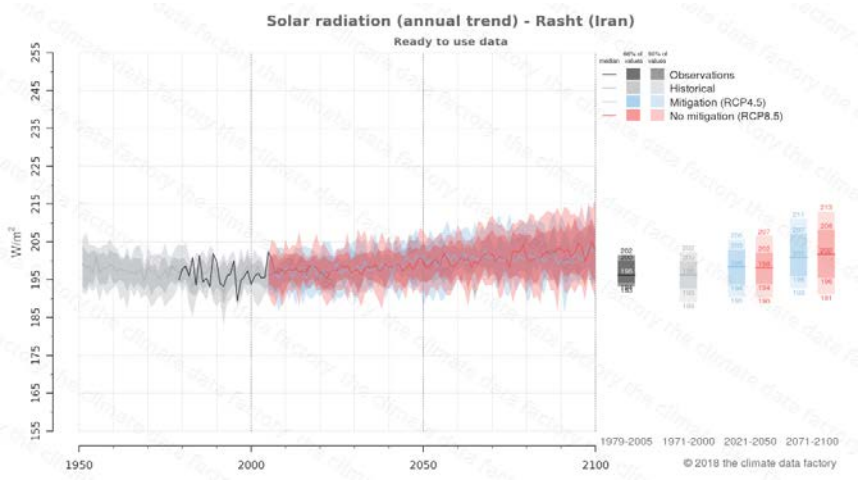

Figure 3. Solar radiation diagram for determining the warm and cold months in Rasht, Iran [38].

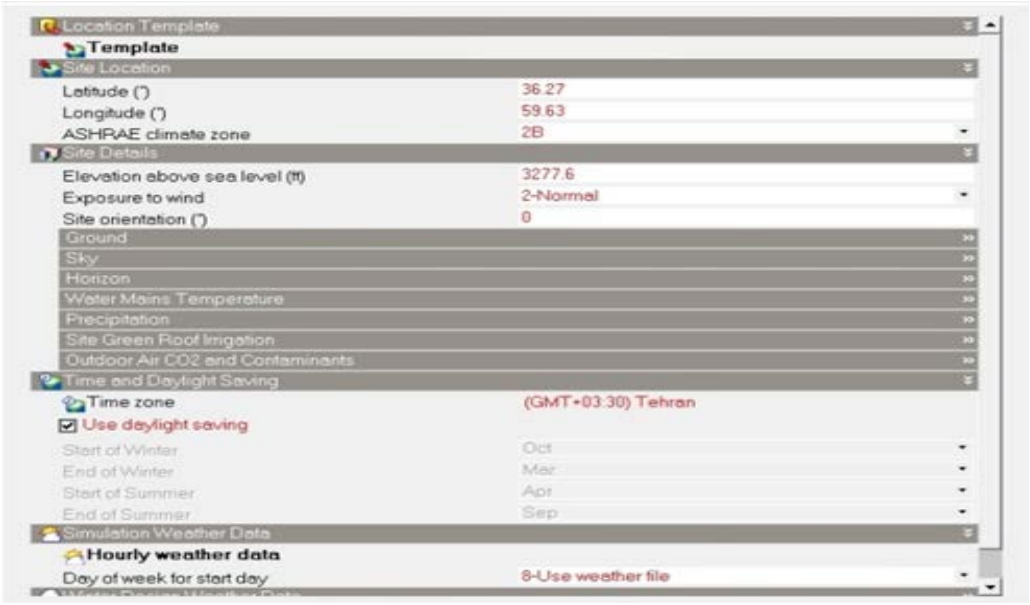

Figure 4. Weather data input in Ecotect.

2.2. Building description

This study analyzed a residential building that covers an area of 150 m^2 (each story) and a length of 3 m, two north and south windows with an area of 1.5 m^2, and the door with an area of 1.8 m^2 on the east side. Table 1 shows the technical specifications of the building.

Table 1. Technical specifications of the building.

Area	900 (m^2) (5 storey) (150 m^2 in each storey)
Construction	Structural concrete frame
Floor sizes	15×10 (m^2)
Floor heights	3 (m)
Window dimensions	1.5 m^2 (10 windows in each storey)
Door dimensions	1.8 m^2

Based on the residential consumption rate of each story, a number of 4 to 6 people were considered full time working all days of the year and each story enjoys natural lighting for all available space in the building which translates into profitability. Figure 5 shows the simulation of the proposed scheme in Ecotect software.

Table 2 presents the required materials for analysis and comparison.

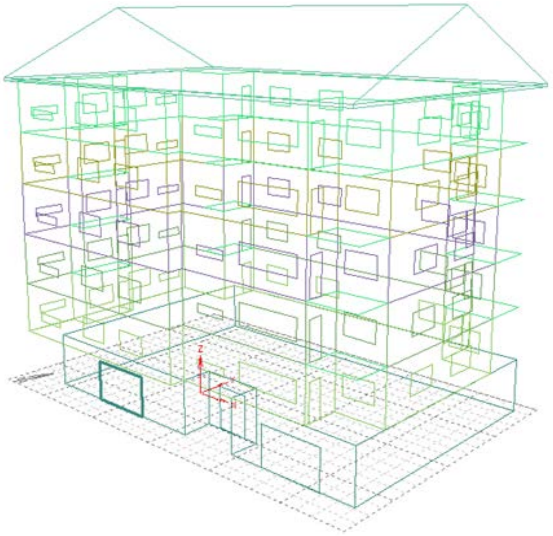

Figure 5. Building simulation design with Ecotect software.

Table 2. Building materials for modeling and simulation.

Five types of materials of the main building components for modeling and simulation																					
Wall					**Floor**					**Roof**					**Door**					**Window**				
Brick Cavity Conc Block Plaster	Brick Conc Block Plaster	Brick Timber Frame	Double Brick Solid Plaster	Timber Clad Masonery	ConcSlab-OnGround	ConcFlr-Carpeted-Suspended	ConcFlr-timber-Suspended	ConcFlr-tiles-Suspended	ConcSlab-tiles-OnGround	Clay-TiledRoof	Clay-TiledRoof-Ref_Foil_Gyproc	Concrete Roof_Asphalt	Plaster-Foil-Heat Retention-Ceramic tile	MetalDeck_Insulated	FoamCore_Plywood	GlassSliding_Door	HollowCore_Ply wood	Solid Core_Oaktimber	Solid Core_Pine timber	Double Glazed-LowE-AlumeFrame	Double Glazed-LowE-AlumeFrame	Double Glazed-LowE-AlumeFrame	Single Glazed-TimberFrame	Translucent_Sky light

The best orientation is a 15-degree rotation towards the east of the southern front for maximum use of natural light (Figure 6).

Figure 6. Building rotation in a mild climate area.

3. RESULTS

3.1. Simulation of the hourly solar exposure

The simulation of Ecotect software shows the output of hourly solar exposure of 5 groups of materials used in the residential building. The analysis was performed from 7 AM to 4 PM. The graphs show the amount of solar radiation in a single day zone per hour. The red curve shows the total amount of the radiation incident; the green curve shows the total amount of the radiation absorbed; the yellow curve shows the maximum intensity of indirect radiation. The numbers on the right, left, and down sections show the indicator percentage of the shading, the indicator values in W/m^2, and the working times/hours, respectively. Figures 7 to 11 show the results of the simulation analysis with five different types of materials used for each group of the main building components including walls, floors, roofs (ceilings), doors, and windows.

3.2. Simulation of the fabric gains

Figures 12 to 16 show the graph of heat losses and gains. In this graph, the numbers on the left and right show the working times and the values of heat losses and gains in Watts, respectively. Yellow and blue curves demonstrate absorption and thermal waste indicators, respectively. Comparisons are made through the fabric gains diagram between the highest absorption of radiative energy and the amount of shading on each of the selected materials in the building components. Finally, optimum materials are selected from the solar energy absorption and transmission, daytime shading in hot and cold seasons, and the best thermal comfort temperature for building occupants. The building's south-facing facade with a 15-degree turn to the east allows for maximum energy absorption only once in the morning. Therefore, the choice of high-thickness materials can delay the transfer of heat from the exterior wall to the interior wall and, over time, the sun angle changes and shadow will reduce the amount of energy absorbed. This subject can provide good thermal comfort and makes heating systems more efficient in winter due to reduced energy absorption. To this end, to minimize gas consumption, materials must be selected to maximize energy absorption (thickness and weight) resulting in savings in winter gas consumption. For all of the materials used in the main building components, the energy absorption of the various materials in each section is compared; finally, the best materials with the highest absorption rate are selected. Figures 12 to 16 show the results of the comparison of selected materials through the fabric gains diagram.

Wall_1	
Brick Cavity Conc Block Plaster	
U-value ($W/m^2.K$)	1/720
Admittance ($W/m^2.K$)	4/220
Solar absorption (0-1)	0/428
Visible transmittance (0-1)	0
Thermal decrement (0-1)	0/41
Thermal lag (hrs)	7/8
(SBEM) CM1	0
(SBEM) CM2	0
Thickness (m)	280
Weight (Kg)	408/565

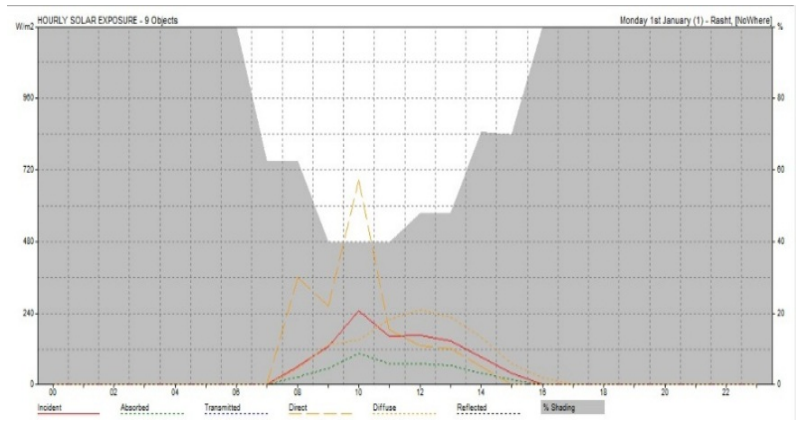

Wall_2	
Brick Conc Block Plaster	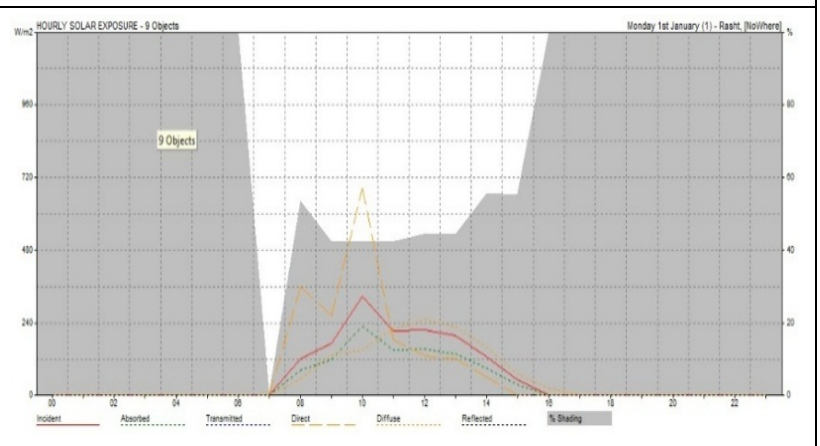
U-value (W/m^2.K)	1/88
Admittance (W/m^2.K)	4/4
Solar absorption (0-1)	0/7
Visible transmittance (0-1)	0
Thermal decrement (0-1)	0/44
Thermal lag (hrs)	7/7
(SBEM) CM1	0
(SBEM) CM2	0
Thickness (m)	340
Weight (Kg)	584/5
Wall_3	
Brick Timber Frame	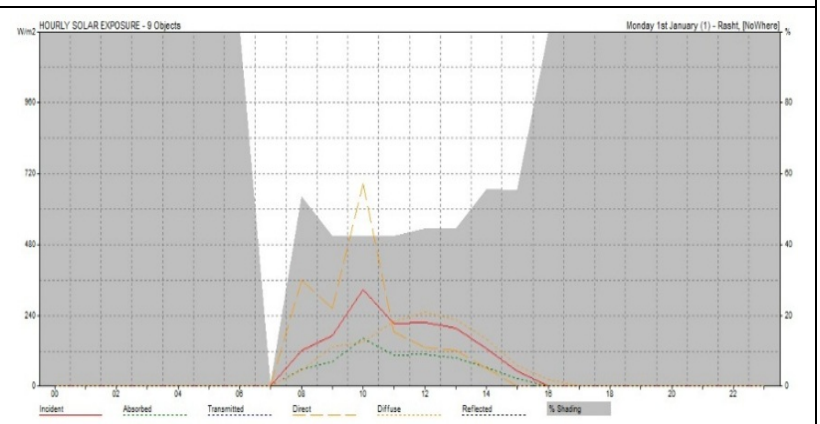
U-value (W/m^2.K)	1/77
Admittance (W/m^2.K)	2/2
Solar absorption (0-1)	0/495
Visible transmittance (0-1)	0
Thermal decrement (0-1)	0/77
Thermal lag (hrs)	4
(SBEM) CM1	0
(SBEM) CM2	0
Thickness (m)	195
Weight (Kg)	232/598
Wall_4	
Double Brick Solid Plaster	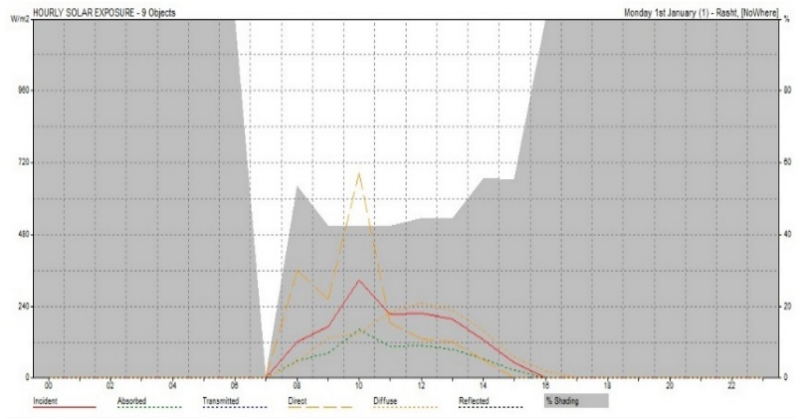
U-value (W/m^2.K)	1/95
Admittance (W/m^2.K)	4/55
Solar absorption (0-1)	0/495
Visible transmittance (0-1)	0
Thermal decrement (0-1)	0/39
Thermal lag (hrs)	7/8
(SBEM) CM1	0
(SBEM) CM2	0
Thickness (m)	230
Weight (Kg)	452/5
Wall_5	
Timber Clad Masonry	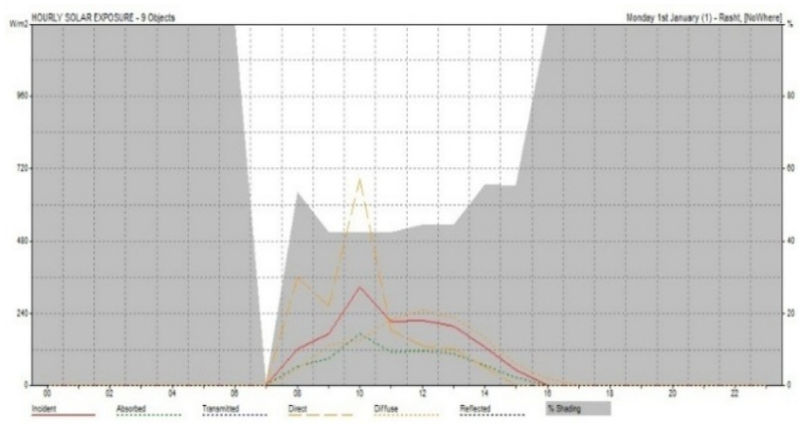
U-value (W/m^2.K)	0/3
Admittance (W/m^2.K)	4/96
Solar absorption (0-1)	0/531
Visible transmittance (0-1)	0
Thermal decrement (0-1)	0/35
Thermal lag (hrs)	5
(SBEM) CM1	0
(SBEM) CM2	0
Thickness (m)	210
Weight (Kg)	240/848

Figure 7. Hourly solar exposure of 5 groups of different materials used in the wall.

Floor_1

CocSlab-OnGround	
U-value (W/m^2.K)	0/88
Admittance (W/m^2.K)	6
Solar absorption (0-1)	0/467
Visible transmittance (0-1)	0
Thermal decrement (0-1)	0/3
Thermal lag (hrs)	4/6
(SBEM) CM1	0
(SBEM) CM2	0
Thickness (m)	0
Weight (Kg)	0

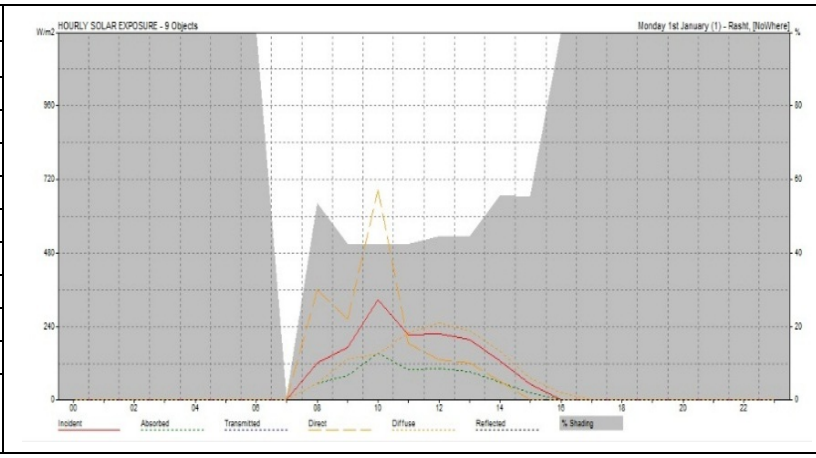

Floor_2

ConcFlr-Carpeted-Suspended	
U-value (W/m^2.K)	2/560
Admittance (W/m^2.K)	4/2
Solar absorption (0-1)	0/3244
Visible transmittance (0-1)	0
Thermal decrement (0-1)	0/7
Thermal lag (hrs)	4
(SBEM) CM1	0
(SBEM) CM2	0
Thickness (m)	0
Weight (Kg)	0

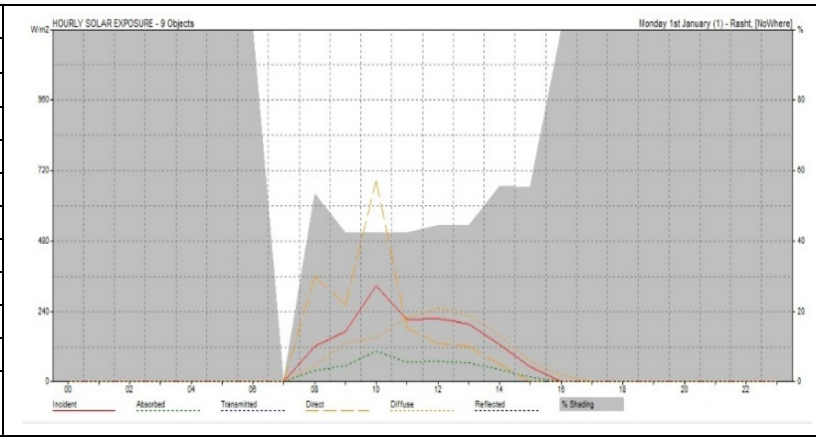

Floor_3

ConcFlr-timber-Suspended	
U-value (W/m^2.K)	2/160
Admittance (W/m^2.K)	2
Solar absorption (0-1)	0/333165
Visible transmittance (0-1)	0
Thermal decrement (0-1)	0/97
Thermal lag (hrs)	0/7
(SBEM) CM1	0
(SBEM) CM2	0
Thickness (m)	0
Weight (Kg)	0

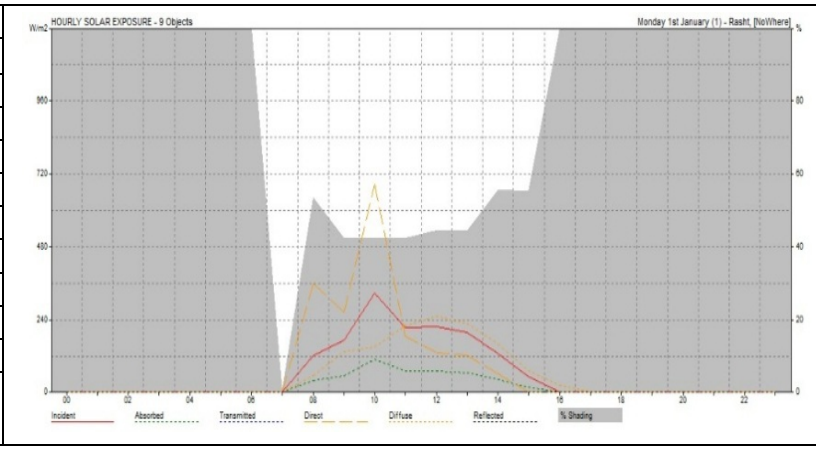

Floor_4

ConcFlr-tiles-Suspended	
U-value (W/m^2.K)	2/9
Admittance (W/m^2.K)	5/2
Solar absorption (0-1)	0/475208
Visible transmittance (0-1)	0
Thermal decrement (0-1)	0/69
Thermal lag (hrs)	4/1
(SBEM) CM1	0
(SBEM) CM2	0
Thickness (m)	0
Weight (Kg)	0

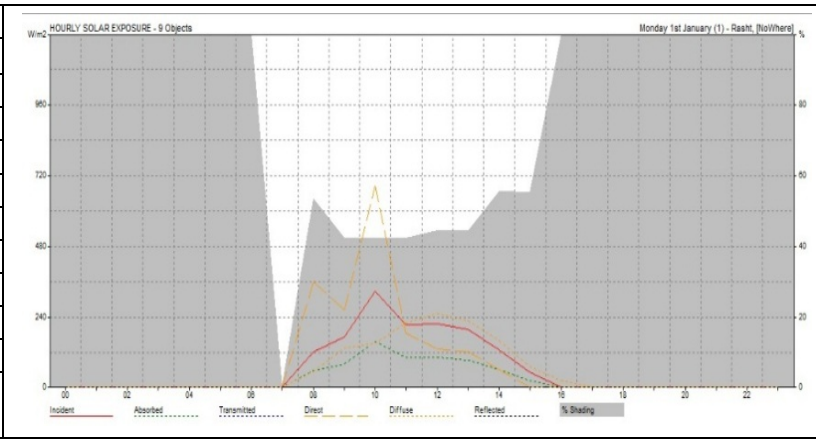

Floor_5	
ConcSlab-tiles-OnGround	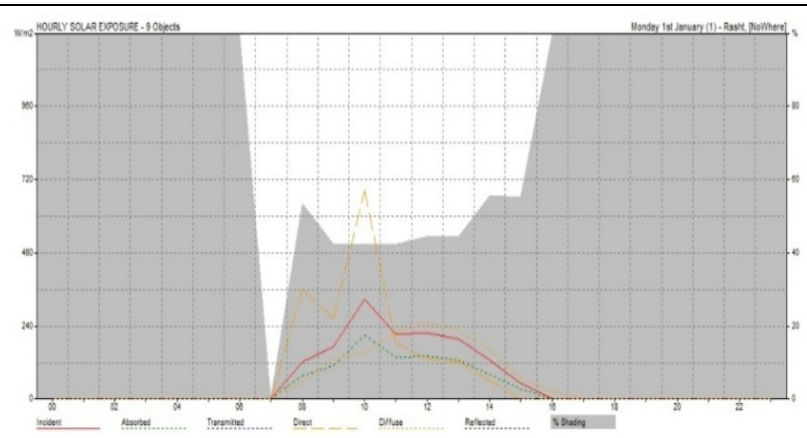
U-value (W/m^2.K)	3/418
Admittance (W/m^2.K)	5/8
Solar absorption (0-1)	0/642
Visible transmittance (0-1)	0
Thermal decrement (0-1)	0/02
Thermal lag (hrs)	9
(SBEM) CM1	0
(SBEM) CM2	0
Thickness (m)	0
Weight (Kg)	0

Figure 8. Hourly solar exposure of 5 groups of different materials used in the floor.

Roof_1	
Clay-TiledRoof	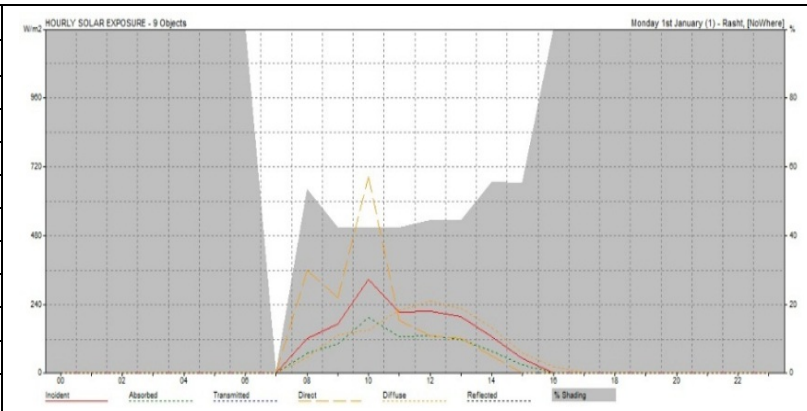
U-value (W/m^2.K)	0/896
Admittance (W/m^2.K)	2/3
Solar absorption (0-1)	0/9
Visible transmittance (0-1)	0
Thermal decrement (0-1)	0/58
Thermal lag (hrs)	7
(SBEM) CM1	0
(SBEM) CM2	0
Thickness (m)	175
Weight (Kg)	360/60
Roof_2	
Clay-TiledRoof-Ref_Foil_Gyproc	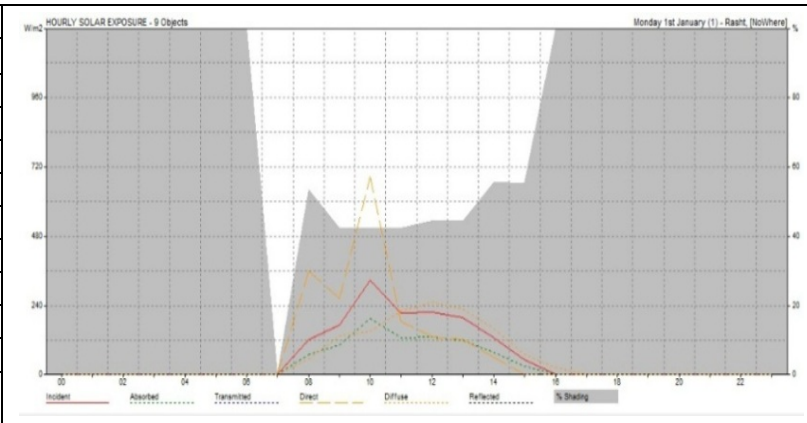
U-value (W/m^2.K)	1/82
Admittance (W/m^2.K)	2
Solar absorption (0-1)	0/6
Visible transmittance (0-1)	0
Thermal decrement (0-1)	0/95
Thermal lag (hrs)	0/5
(SBEM) CM1	0
(SBEM) CM2	0
Thickness (m)	132
Weight (Kg)	31/760
Roof_3	
Concrete Roof_Asphalt	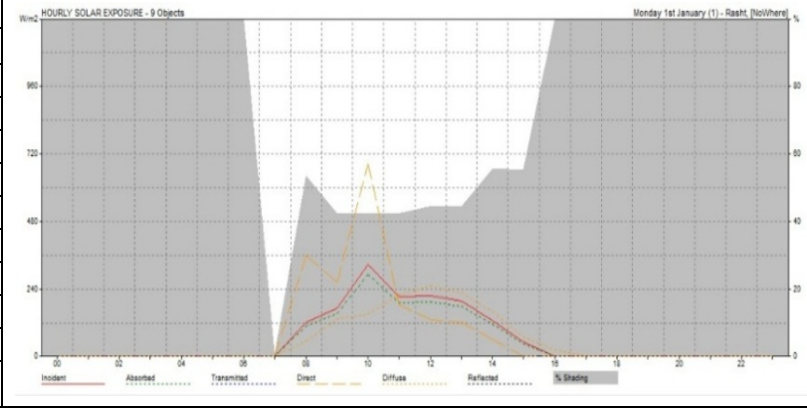
U-value (W/m^2.K)	3/1
Admittance (W/m^2.K)	3/1
Solar absorption (0-1)	0/6
Visible transmittance (0-1)	0
Thermal decrement (0-1)	1
Thermal lag (hrs)	0/2
(SBEM) CM1	0
(SBEM) CM2	0
Thickness (m)	1/32
Weight (Kg)	31/760

Roof_4	
Plaster-Foil-Heat Retention-Ceramic Tile	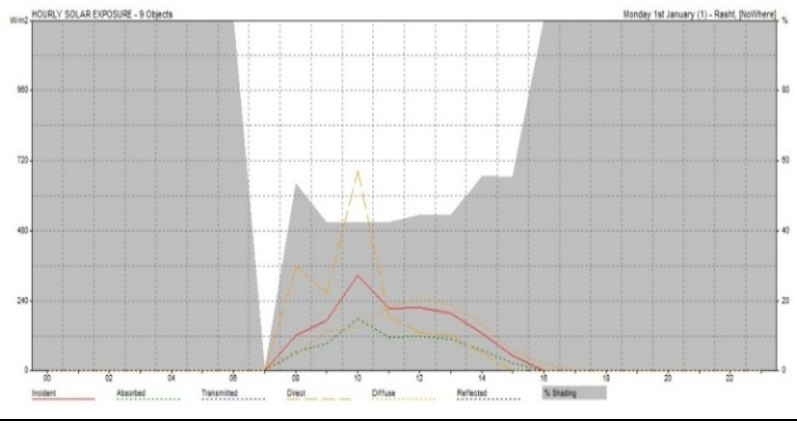
U-value (W/m^2.K)	0/61
Admittance (W/m^2.K)	1
Solar absorption (0-1)	0/548235
Visible transmittance (0-1)	0
Thermal decrement (0-1)	0/9
Thermal lag (hrs)	1/5
(SBEM) CM1	0
(SBEM) CM2	0
Thickness (m)	0
Weight (Kg)	0
Roof_5	
MetalDeck_Insulated	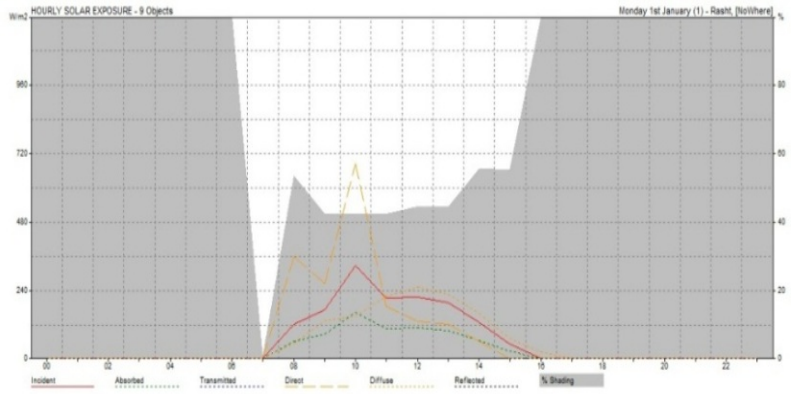
U-value (W/m^2.K)	0/55
Admittance (W/m^2.K)	1
Solar absorption (0-1)	0/5
Visible transmittance (0-1)	0
Thermal decrement (0-1)	0/96
Thermal lag (hrs)	0/7
(SBEM) CM1	0
(SBEM) CM2	0
Thickness (m)	75
Weight (Kg)	13

Figure 9. Hourly solar exposure of 5 groups of different materials used in the roof.

Door_1	
FoamCore_Plywood	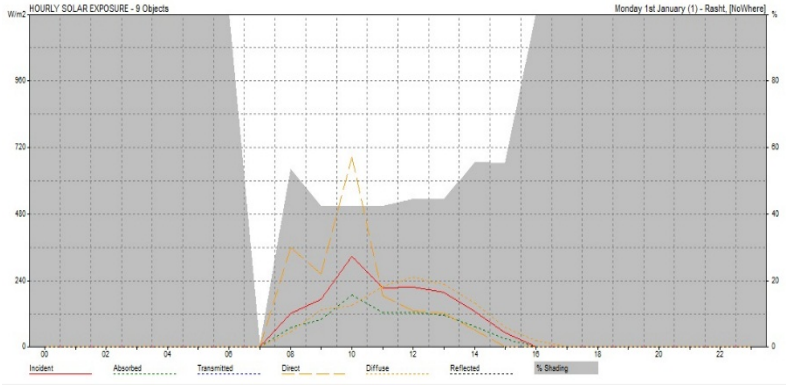
U-value (W/m^2.K)	2/310
Admittance (W/m^2.K)	3/540
Solar absorption (0-1)	0/404
Visible transmittance (0-1)	0
Thermal decrement (0-1)	0/98
Thermal lag (hrs)	0/4
(SBEM) CM1	0
(SBEM) CM2	0
Thickness (m)	40
Weight (Kg)	22
Door_2	
GlassSliding_Door	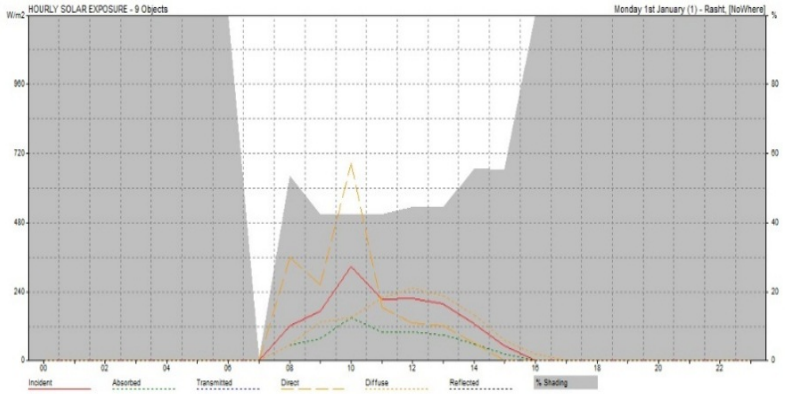
U-value (W/m^2.K)	5/356
Admittance (W/m^2.K)	5/360
Solar absorption (0-1)	0/1
Visible transmittance (0-1)	-1
Thermal decrement (0-1)	0/34
Thermal lag (hrs)	0/39
(SBEM) CM1	0
(SBEM) CM2	0
Thickness (m)	0
Weight (Kg)	25/1

Door_3	
HollowCore_Ply Wood	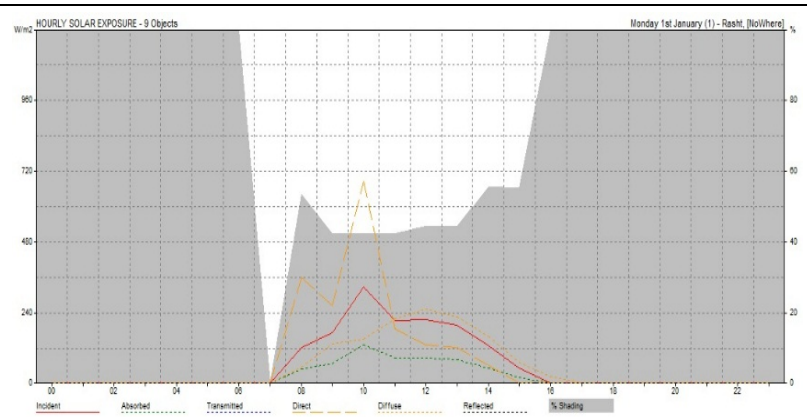
U-value (W/m^2.K)	3/31
Admittance (W/m^2.K)	0/870
Solar absorption (0-1)	0/578628
Visible transmittance (0-1)	0
Thermal decrement (0-1)	0/98
Thermal lag (hrs)	0/4
(SBEM) CM1	0
(SBEM) CM2	0
Thickness (m)	40
Weight (Kg)	4/744
Door_4	
Solid Core_Oaktimber	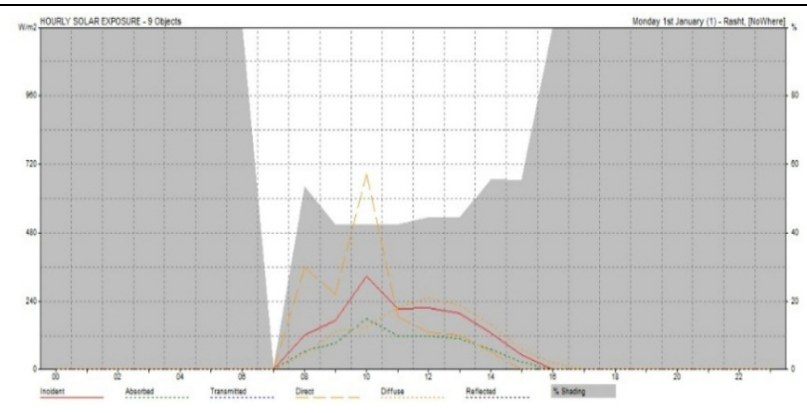
U-value (W/m^2.K)	2/260
Admittance (W/m^2.K)	3/190
Solar absorption (0-1)	0/46
Visible transmittance (0-1)	0
Thermal decrement (0-1)	0/95
Thermal lag (hrs)	0/4
(SBEM) CM1	0
(SBEM) CM2	0
Thickness (m)	40
Weight (Kg)	33
Door_5	
Solid Core_Pine Timber	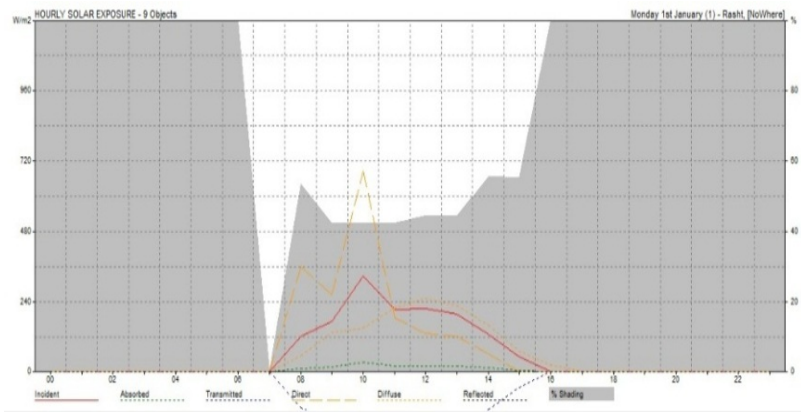
U-value (W/m^2.K)	2/980
Admittance (W/m^2.K)	0/650
Solar absorption (0-1)	0/55
Visible transmittance (0-1)	0
Thermal decrement (0-1)	0/98
Thermal lag (hrs)	0/4
(SBEM) CM1	0
(SBEM) CM2	0
Thickness (m)	40
Weight (Kg)	3/224

Figure 10. Hourly solar exposure of 5 groups of different materials used in the door.

Window_1	
Double Glazed-LowE-AlumeFrame	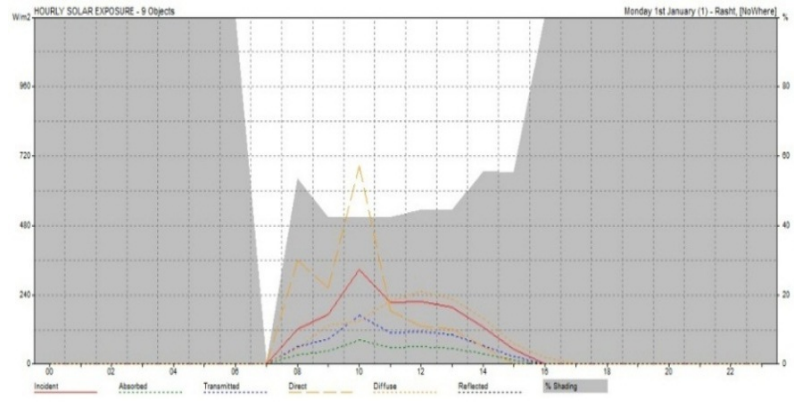
U-value (W/m^2.K)	2/7
Admittance (W/m^2.K)	2/8
Solar absorption (0-1)	0/81
Visible transmittance (0-1)	0/639
Thermal decrement (0-1)	1/74
Thermal lag (hrs)	0/42
(SBEM) CM1	0/56
(SBEM) CM2	-
Thickness (m)	0
Weight (Kg)	0

Window_2	
Double Glazed-LowE-AlumeFrame	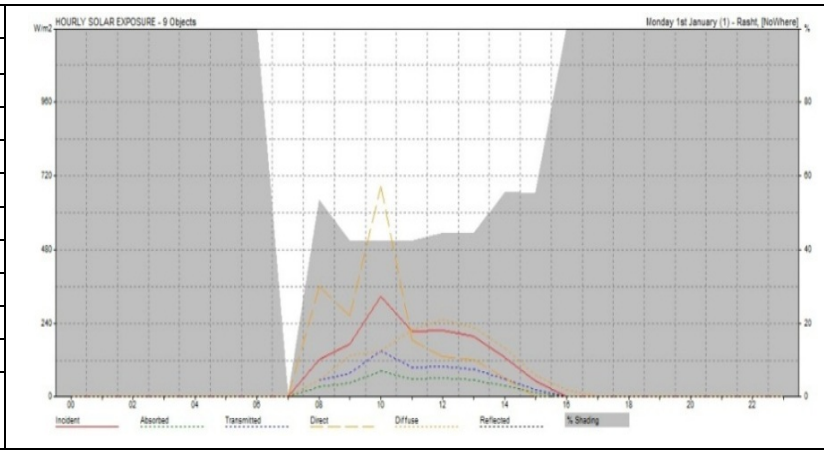
U-value (W/m^2.K)	2/41
Admittance (W/m^2.K)	2/380
Solar absorption (0-1)	0/75
Visible transmittance (0-1)	0/611
Thermal decrement (0-1)	1/74
Thermal lag (hrs)	0/21
(SBEM) CM1	0/29
(SBEM) CM2	-
Thickness (m)	0
Weight (Kg)	0
Window_3	
Double Glazed-LowE-AlumeFrame	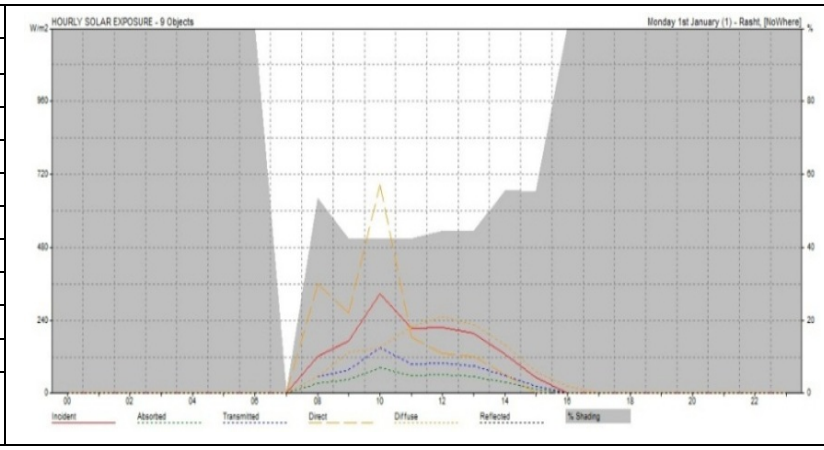
U-value (W/m^2.K)	2/26
Admittance (W/m^2.K)	2/2
Solar absorption (0-1)	0/75
Visible transmittance (0-1)	0/639
Thermal decrement (0-1)	1/74
Thermal lag (hrs)	0/21
(SBEM) CM1	0/29
(SBEM) CM2	-
Thickness (m)	0
Weight (Kg)	0
Window_4	
Single Glazed-TimberFrame	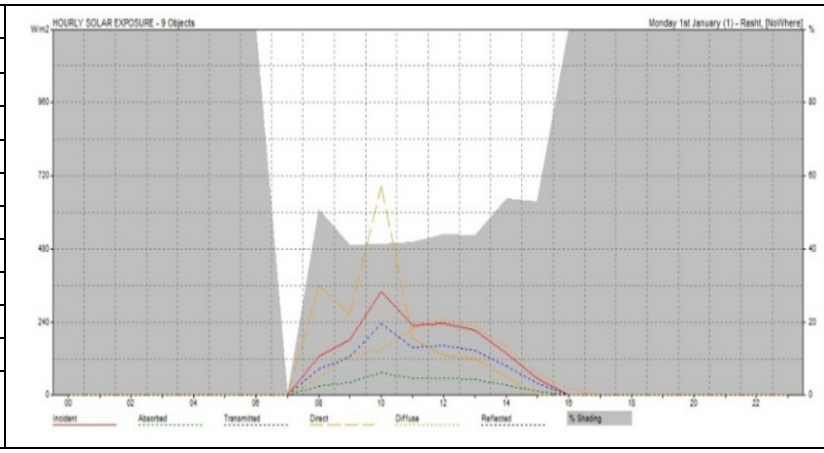
U-value (W/m^2.K)	5/1
Admittance (W/m^2.K)	5
Solar absorption (0-1)	0/94
Visible transmittance (0-1)	0/737
Thermal decrement (0-1)	1/74
Thermal lag (hrs)	0/47
(SBEM) CM1	0/64
(SBEM) CM2	0
Thickness (m)	0
Weight (Kg)	0
Window_5	
Translucent Sky Light	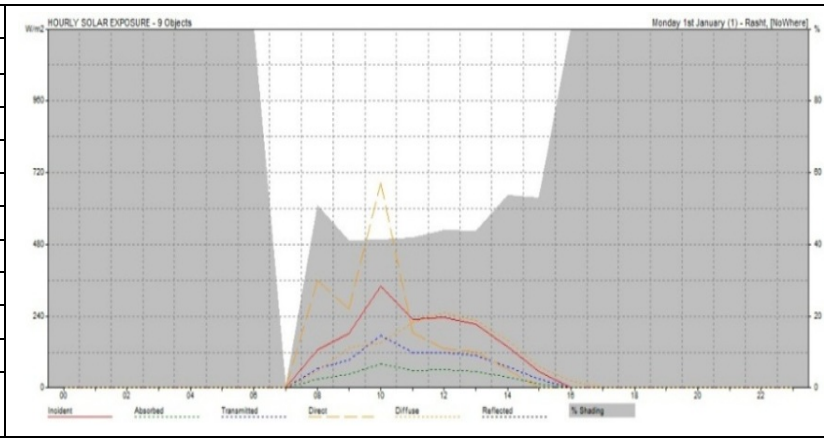
U-value (W/m^2.K)	5
Admittance (W/m^2.K)	5
Solar absorption (0-1)	0/78
Visible transmittance (0-1)	0/658
Thermal decrement (0-1)	1/74
Thermal lag (hrs)	0/38
(SBEM) CM1	0/47
(SBEM) CM2	-
Thickness (m)	0
Weight (Kg)	0

Figure 11. Hourly solar exposure of 5 groups of different materials used in the window.

Fabric Gains (heat losses and gains)	Incident (w/m^2)	Absorbed (w/m^2)	Transmitted (w/m^2)	Wall material
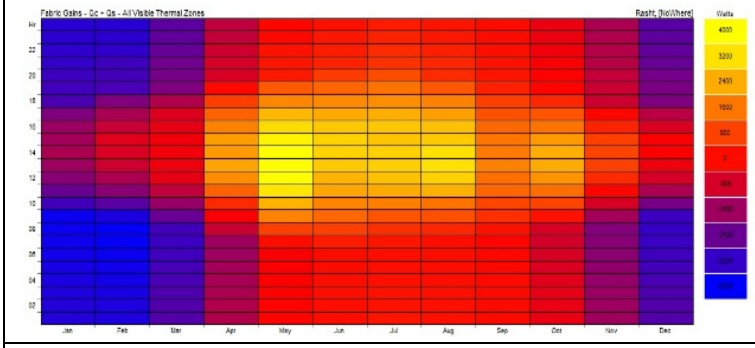	340	120	700	Brick Cavity Conc Block Plaster
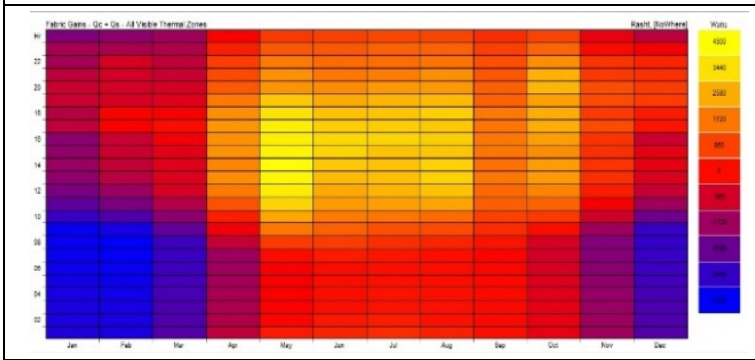	340	240	700	Brick Conc Block Plaster
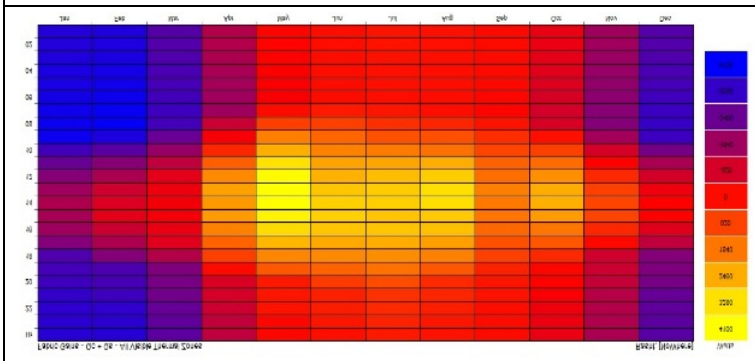	340	180	700	Brick Timber Frame
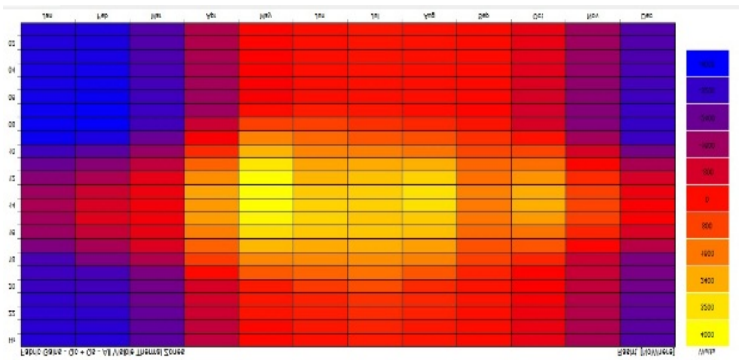	340	180	700	Double Brick Solid Plaster
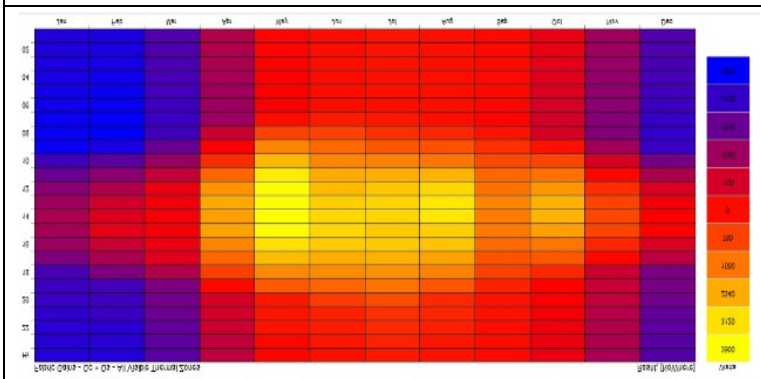	340	190	700	Timber Clad Masonery

Figure 12. Fabric gains analysis of the selected wall materials.

Fabric Gains (heat losses and gains)	Incident (w/m^2)	Absorbed (w/m^2)	Transmitted (w/m^2)	Floor material
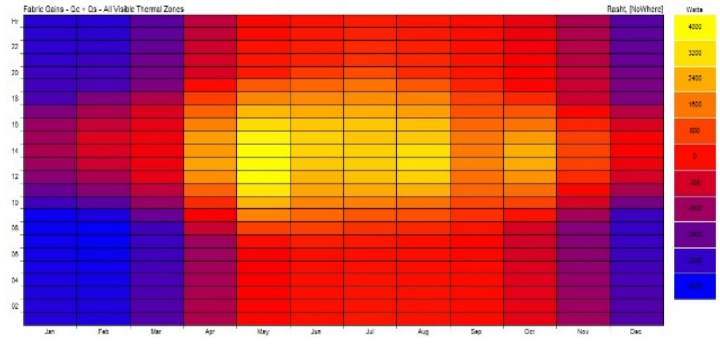	340	140	700	ConcSlab□OnGround
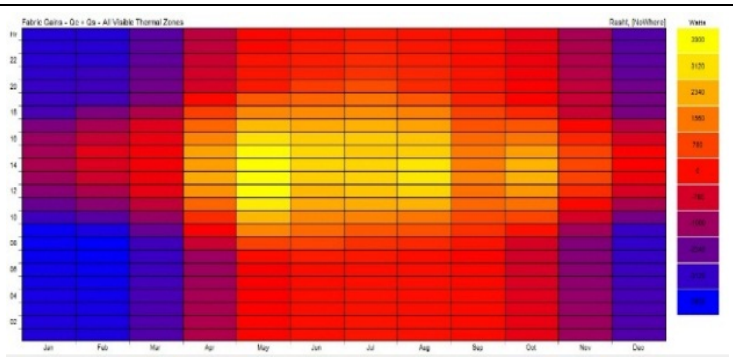	340	110	700	ConcFlr-Carpeted-Suspended
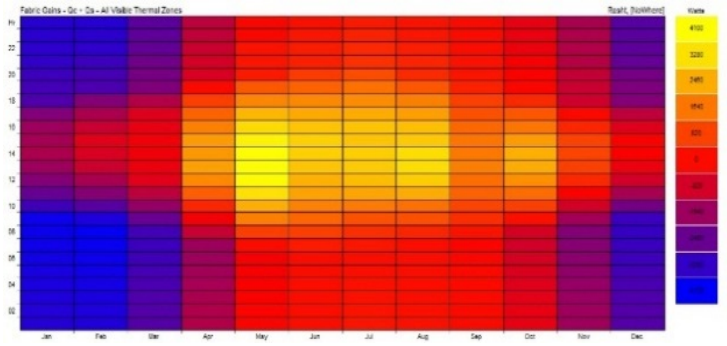	340	115	700	ConcFlr-timber-Suspended
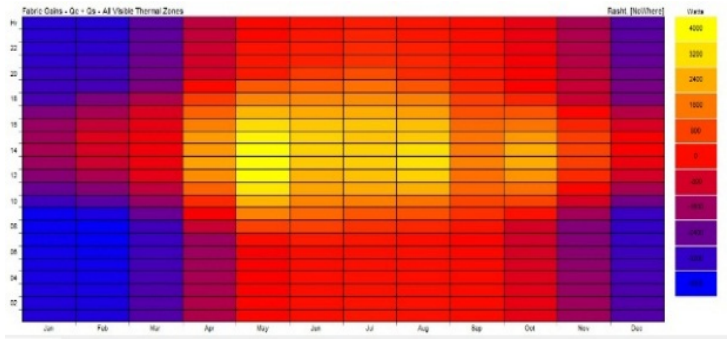	340	170	700	ConcFlr-tiles-Suspended
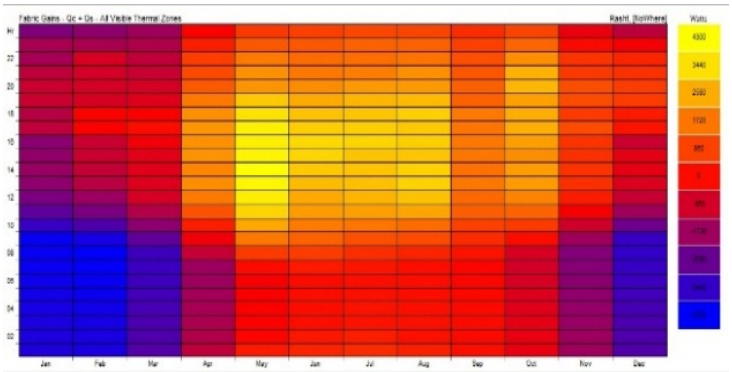	340	220	700	ConcSlab-tiles-OnGround

Figure 13. Fabric gains analysis of the selected floor materials.

Fabric Gains (heat losses and gains)	Incident (w/m^2)	Absorbed (w/m^2)	Transmitted (w/m^2)	Roof material
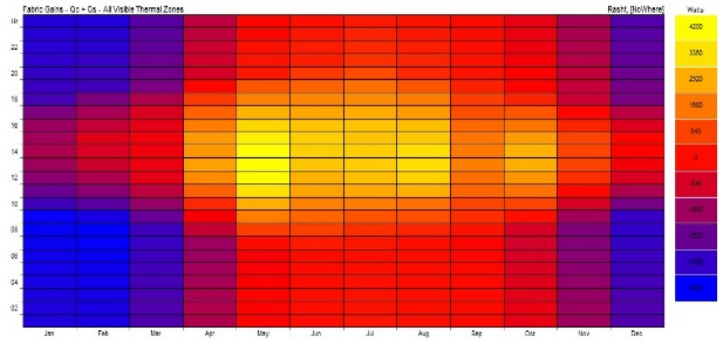	340	200	700	Clay-TiledRoof
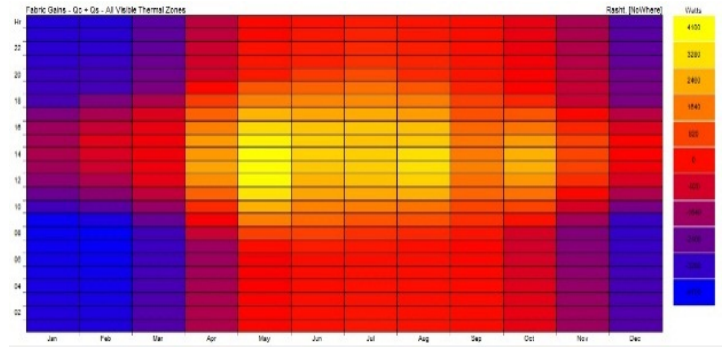	340	190	700	Clay-TiledRoof-Ref_Foil_Gyproc
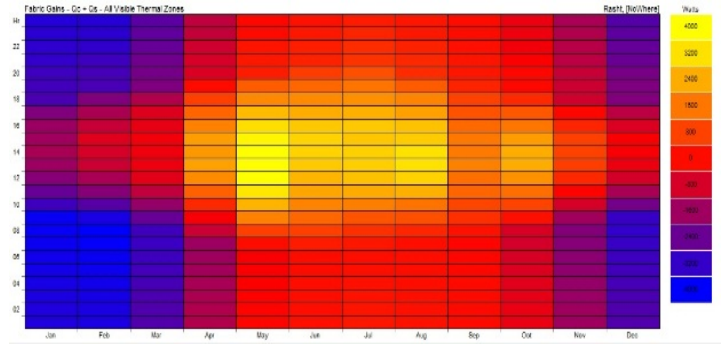	340	300	700	Concrete Roof_Asphalt
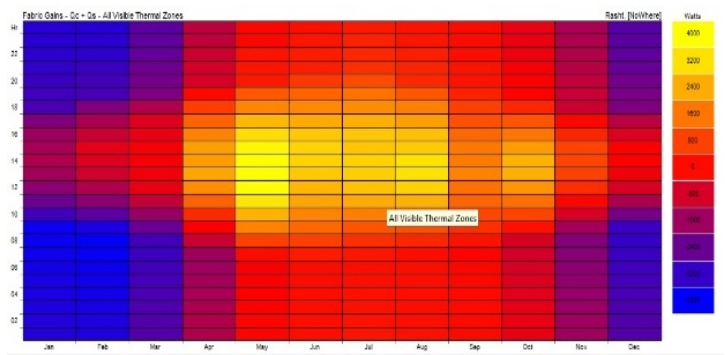	340	180	700	Plaster-Foil-Heat Retention-Ceramic tile
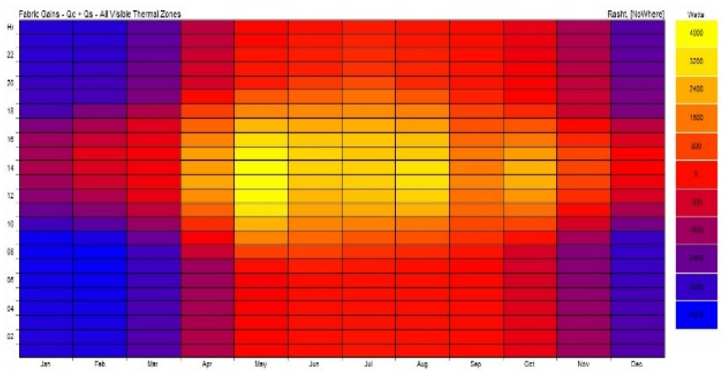	340	160	700	MetalDeck_Insulated

Figure 14. Fabric gains analysis of the selected roof materials.

Fabric Gains (heat losses and gains)	Incident (w/m^2)	Absorbed (w/m^2)	Transmitted (w/m^2)	Door material
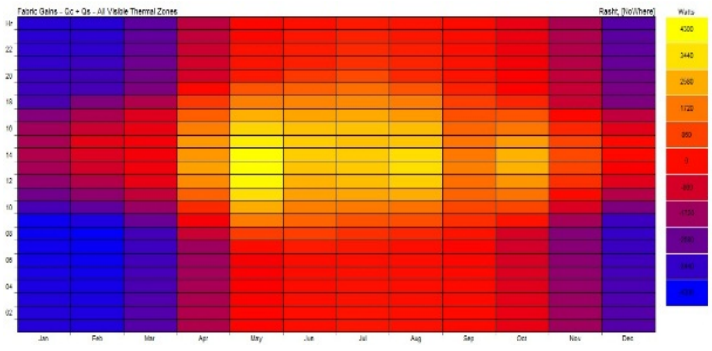	340	200	700	FoamCore_Plywood
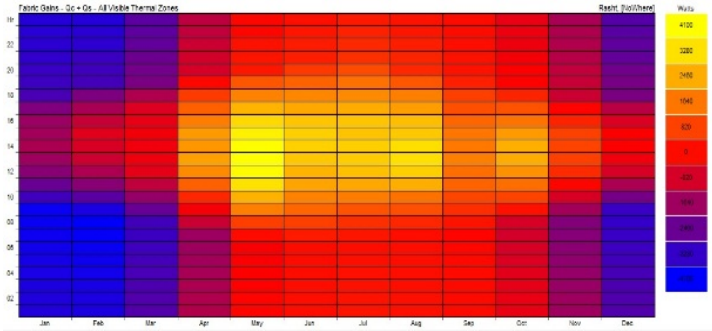	340	20	700	GlassSliding_Door
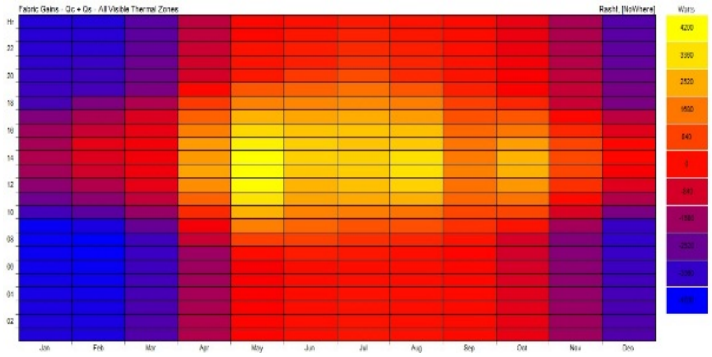	340	180	700	HollowCore_Plywood
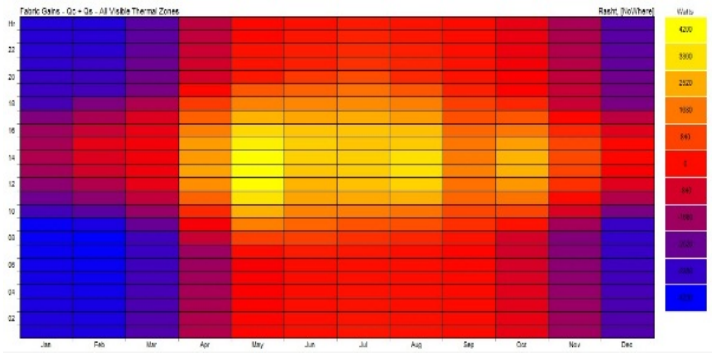	340	150	700	Solid Core_Oaktimber
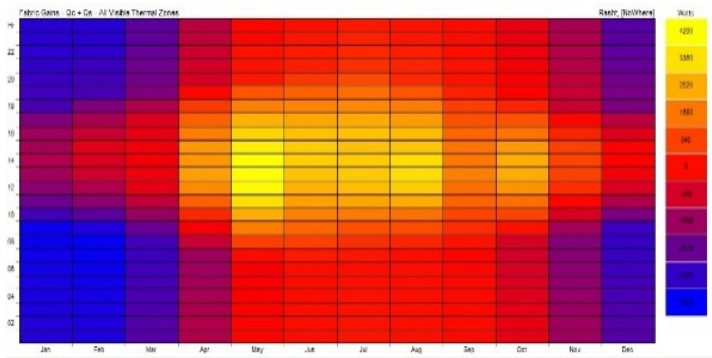	340	130	700	Solid Core_Pine timber

Figure 15. Fabric gains analysis of the selected door materials.

Fabric Gains (heat losses and gains)	Incident (w/m^2)	Absorbed (w/m^2)	Transmitted (w/m^2)	Windows material
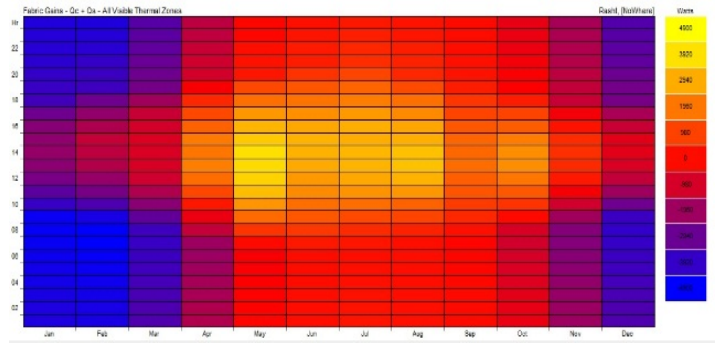	340	100	700	Double Glazed-LowE-AlumeFrame
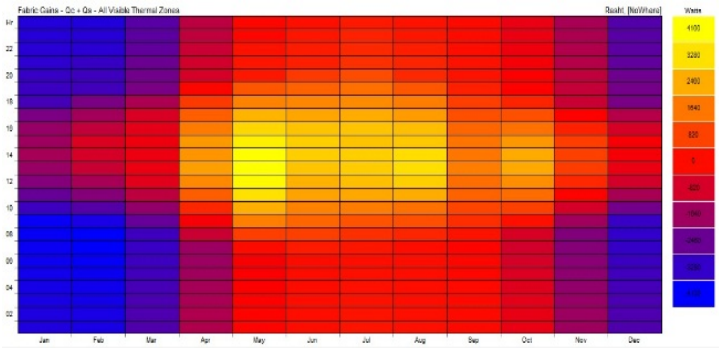	340	90	700	Double Glazed-LowE TimberFrame
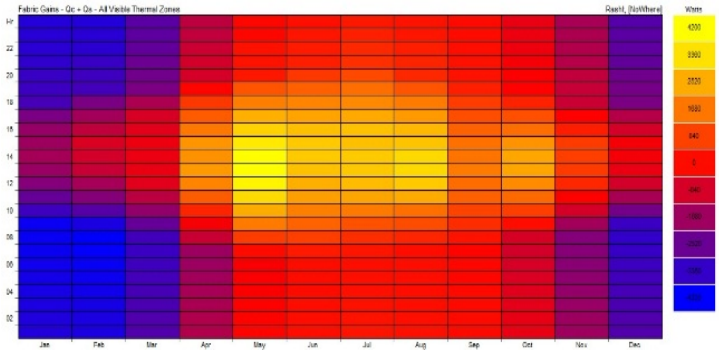	340	90	700	Double Glazed- TimberFrame
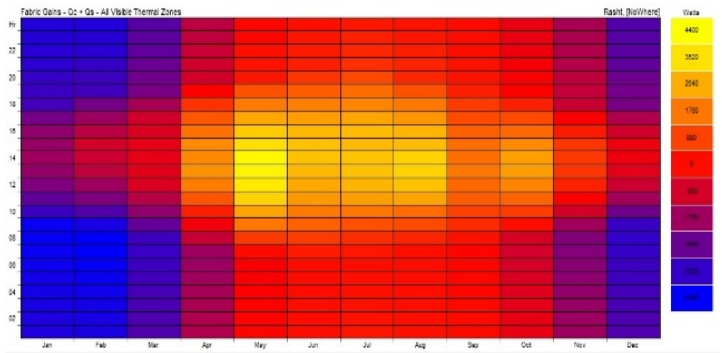	340	70	700	Single Glazed-TimberFrame
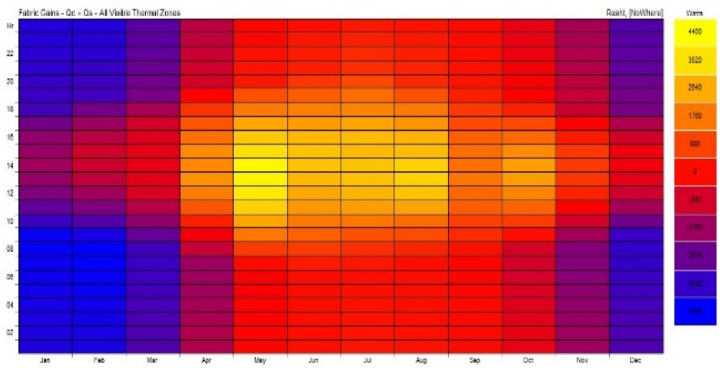	340	90	700	Translucent_Sky light

Figure 16. Fabric gains analysis of the selected window materials.

4. DISCUSSION

Figures 7 to 16 present the selection of optimum materials along with the comparative analysis of the results obtained from the simulation of hourly solar exposure and fabric gains. Table 3 shows the simulation and analysis results of selecting optimum materials in the main building components to find the best material based on the maximum transmission and absorption of solar energy in Rasht. These comparisons are made based on solar radiation analysis and heat losses/gains (Figures 12 to 16).

Table 3. Selection of optimum materials of residential building components for energy conservation in Rasht number for different geometric cases (must be typed).

Wall	
Brick Conc block Plaster	
U-value ($W/m^2.K$)	1/88
Admittance ($W/m^2.K$)	4/4
Solar absorption (0-1)	0/7
Visible transmittance (0-1)	0
Thermal decrement (0-1)	0/44
Thermal lag (hrs)	7/7
(SBEM) CM1	0
(SBEM) CM2	0
Thickness (m)	340
Weight (Kg)	584/5
Window	
Double Glazed-Low E	
U-value ($W/m^2.K$)	5/1
Admittance ($W/m^2.K$)	5
Solar absorption (0-1)	0/94
Visible transmittance (0-1)	0/737
Thermal decrement (0-1)	1/74
Thermal lag (hrs)	0/47
(SBEM) CM1	0/64
(SBEM) CM2	-
Thickness (m)	0
Weight (Kg)	0
Floor	
ConcSlab-OnGround	
U-value ($W/m^2.K$)	0/88
Admittance ($W/m^2.K$)	6
Solar absorption (0-1)	0/467
Visible transmittance (0-1)	0
Thermal decrement (0-1)	0/3
Thermal lag (hrs)	4/6
(SBEM) CM1	0
(SBEM) CM2	0
Thickness (m)	0/2
Weight (Kg)	2/439
Door	
Foam Core Ply Wood	
U-value ($W/m^2.K$)	2/31
Admittance ($W/m^2.K$)	3/54
Solar absorption (0-1)	0/404
Visible transmittance (0-1)	0
Thermal decrement (0-1)	0/98
Thermal lag (hrs)	0/4
(SBEM) CM1	0
(SBEM) CM2	0
Thickness (m)	0/4
Weight (Kg)	22
Roof	
Conc Roof Asphalt	
U-value ($W/m^2.K$)	3/1
Admittance ($W/m^2.K$)	3/1
Solar absorption (0-1)	0/6
Visible transmittance (0-1)	0
Thermal decrement (0-1)	1
Thermal lag (hrs)	0/2
(SBEM) CM1	0
(SBEM) CM2	0
Thickness (m)	0/132
Weight (Kg)	31/760
Partition	
Famed-Plastboard-Partition	
U-value ($W/m^2.K$)	2/2
Admittance ($W/m^2.K$)	2/
Solar absorption (0-1)	0/4
Visible transmittance (0-1)	0
Thermal decrement (0-1)	0/93
Thermal lag (hrs)	0/3
(SBEM) CM1	0
(SBEM) CM2	0
Thickness (m)	0/1
Weight (Kg)	25/104

According to Table 3, the optimum materials were selected based on the highest absorption using simulation software. The following findings based on comparative results are presented as follows:

- Brick Conc block Plaster with the total radiation incident of 340 W/m^2, a radiation absorption of 240 W/m^2, and a radiation transmission of 700 W/m^2 is the optimum material for walls.
- Double Glazed-Low E with the total radiation incident 340 W/m^2, a radiation absorption of 100 W/m^2, and a radiation transmission of 700 W/m^2 is the optimum material for windows.
- Foam Core Ply Wood with the total radiation incident of 340 W/m^2, a radiation absorption of 200 W/m^2, and a radiation transmission of 700 W/m^2 is the optimum material for doors.
- ConcSlab- OnGround with the total radiation incident of 340 W/m^2, a radiation absorption of 220 W/m^2, and a radiation transmission of 700 W/m^2 is the optimum material for floors.
- Conc Roof Asphalt with the total radiation incident of 340 W/m^2, a radiation absorption of 300 W/m^2, and a radiation transmission of 700 W/m^2 is the optimum material for roof.

5. CONCLUSIONS

This research analyzed and simulated the optimum materials in the residential buildings under study based on the different materials used in the mild climate zone. According to the analysis performed using simulation software, it was revealed that the optimum material of the main building components in the mild climate zone of Rasht city were (a) the Brick Conc block Plaster for walls with the total radiation absorption of 240 W/m^2, (b) Double Glazed-Low E for windows with the total radiation absorption of 100 W/m^2, (c) Foam Core Ply Wood for doors with the total radiation absorption of 200 W/m^2; (d) ConcSlab- OnGround for floors with the total radiation absorption of 220 W/m^2; (e) Conc Roof Asphalt for roofs with the total radiation absorption of 300 W/m^2; and (f) Famed-Plastboard-Partition for partition. According to the diagrams obtained for all stories of the building in the two hot and cold days of the year, as determined by the design and material selection requirements, the building will be in an

almost thermal comfort zone (below 30 degrees) in the warm season.

6. ACKNOWLEDGEMENT

The author would like to thank Mr. Kiyanifar for the simulation analysis.

REFERENCES

1. Singh, M.K., Mahapatra, S. and Atreya, S.K., "Thermal performance study and evaluation of comfort temperatures in vernacular buildings of North-East India", ***Building and Environment***, Vol. 45, (2010), 320-329. (https://doi.org/10.1016/j.buildenv.2009.06.009).
2. Hemsath, T.L. and Bandhosseini, A.K., "Sensitivity analysis evaluating basic building geometry's effect on energy use", ***Renewable Energy***, Vol. 76, (2015), 526-538. (https://doi.org/10.1016/j.renene.2014.11.044).
3. Jamaludin, N., Mohammed, N.I., Khamidi, M.F. and Abdul Wahab, S.N., "Thermal comfort of residential building in Malaysia at different micro-climates", ***Procedia - Social and Behavioral Sciences***, Vol. 170, (2015), 613-623. (https://doi.org/10.1016/j.sbspro.2015.01.063).
4. U.S. Energy Information Administration., "Emissions of greenhouse gases in the United States", (accessed 2020).
5. Valinejad Shoubi, M., Valinejad Shoubi, M., Bagchi, A. and Shakiba Barough, A., "Reducing the operational energy demand in buildings using building information modeling tools and sustainability approaches", ***Ain Shams Engineering Journal***, Vol. 6, (2014), 41-55. (https://doi.org/10.1016/j.asej.2014.09.006).
6. Berardi, U. and Wang, T., "Daylighting in an atrium-type high performance house", ***Building and Environment***, Vol. 76, (2014), 92-104. (https://doi.org/10.1016/j.buildenv.2014.02.008).
7. Embrechts, R. and Bellegen, C.V., "Increased energy savings by individual light control", ***Right Light 4: Proceedings of The 4th European Conference on Energy-Efficient Lighting***, Copenhagen, Denmark, (1997), 179-182.
8. Ihm, P., Nemri, A. and Krarti, M., "Estimation of lighting energy savings from daylighting", ***Building and Environment***, Vol. 44, (2009), 509-514. (https://doi.org/10.1016/j.buildenv.2008.04.016).
9. Al-Tamimi, N. and Fadzil, S.F.S., "Energy-efficient envelope design for high-rise residential buildings in Malaysia", ***Architectural Science Review***, Vol. 55, (2012), 119-127. (https://doi.org/10.1080/00038628.2012.667938).
10. Gupta, P.A.S. and Shashwat, S., "Improvement of outdoor thermal comfort for a residential development in Singapore", ***International Journal of Energy & Environment***, Vol. 6, (2015), 567-586.
11. Youngjib, H. and Golparvar-Fard, M., "EPAR: Energy Performance Augmented Reality models for identification of building energy performance deviations between actual measurements and simulation results", ***Energy and Buildings***, Vol. 63, (2013), 15-28. (https://doi.org/10.1016/j.enbuild.2013.02.054).
12. Malsh, A. and Al-Oraier, F., "A comparative analysis using multiple thermal analysis tools", ***Proceedings of International Conference on Passive and Low Energy Cooling for the Built Environment***, Santorini, Greece, (2005).
13. Sadra, A. and Yahya Abadi, R., "Building sustainable architecture design using solar renewable energy", ***Proceedings of 3rd Annual Conference on Architectural, Urban Development and Urban Management Research***, (2017). (In Farsi).
14. Gao, W., Ariyama, T., Ojima, T. and Meier, A., "Energy impacts of recycling disassembly material in residential buildings", ***Energy and Buildings***, Vol. 33, (2001), 553-562. (https://doi.org/10.1016/S0378-7788(00)00096-7).
15. Praseeda, K.I., Venkatarama Reddy, B.V. and Mani, M., "Embodied energy assessment of building materials in India using process and input–output analysis", ***Energy and Buildings***, Vol. 86, (2015), 677-686. (https://doi.org/10.1016/j.enbuild.2014.10.042).
16. Ouyang, X. and Lin, B., "Analyzing energy savings potential of the Chinese building materials industry under different economic growth scenarios", ***Energy and Building***, Vol. 10915, (2015), 316-327. (https://doi.org/10.1016/j.enbuild.2015.09.068).
17. Melo, M.O., da Silva, L.B., Coutinho, A.S., Sousa, V. and Perazzo, N., "Energy efficiency in building installations using thermal insulating materials in northeast Brazil", ***Energy and Buildings***, Vol. 47, (2012), 35-43. (https://doi.org/10.1016/j.enbuild.2011.11.021).
18. Tettey, U.Y.A., Dodoo, A. and Gustavsson, L., "Effects of different insulation materials on primary energy and CO_2 emission of a multi-storey residential building", ***Energy and Buildings***, Vol. 82, (2014), 369-377. (https://doi.org/10.1016/j.enbuild.2014.07.009).
19. Alam, M., Zou, P.X.W., Sanjayan, J. and Ramakrishnan, S., "Energy saving performance assessment and lessons learned from the operation of an active phase change materials system in a multi-storey building in Melbourne", ***Applied Energy***, Vol. 238, (2019), 1582-1595. (https://doi.org/10.1016/j.apenergy.2019.01.116).
20. Sovetova, M., Memon, S.A. and Kim, J., "Thermal performance and energy efficiency of building integrated with PCMs in hot desert climate region", ***Solar Energy***, Vol. 189, (2019), 357-371. (https://doi.org/10.1016/j.solener.2019.07.067).
21. Johra, H. and Heiselberg, P., "Influence of internal thermal mass on the indoor thermal dynamics and integration of phase change materials in furniture for building energy storage: A review", ***Renewable and Sustainable Energy Reviews***, Vol. 69, (2017), 19-32. (https://doi.org/10.1016/j.rser.2016.11.145).
22. Ascione, F., Bianco, N., De Masi, R.F., de' Rossi, F. and Vanoli, G.P., "Energy refurbishment of existing buildings through the use of phase change materials: Energy savings and indoor comfort in the cooling season", ***Applied Energy***, Vol. 113, (2014), 990-1007. (https://doi.org/10.1016/j.apenergy.2013.08.045).
23. Cabeza, L.F., Castell, A., Barreneche, C., de Gracia, A. and Fernández, A.I., "Materials used as PCM in thermal energy storage in buildings: A review", ***Renewable and Sustainable Energy Reviews***, Vol. 15, No. 3, (2011), 1675-1695. (https://doi.org/10.1016/j.rser.2010.11.018).
24. Cascone, Y., Capozzoli, A. and Perino, M., "Optimisation analysis of PCM-enhanced opaque building envelope components for the energy retrofitting of office buildings in Mediterranean climates", ***Applied Energy***, Vol. 211, (2018), 929-953. (https://doi.org/10.1016/j.apenergy.2017.11.081).
25. Saffari, M., de Gracia, A., Ushak, S. and Cabeza, L.F., "Passive cooling of buildings with phase change materials using whole-building energy simulation tools: A review", ***Renewable and Sustainable Energy Reviews***, Vol. 80, (2017), 1239-1255. (https://doi.org/10.1016/j.rser.2017.05.139).
26 Saafi, K. and Daouas, N., "Energy and cost efficiency of phase change materials integrated in building envelopes under Tunisia Mediterranean climate", ***Energy***, Vol. 187, (2019), 115987. (https://doi.org/10.1016/j.energy.2019.115987).
27. Akeiber, H., Nejat, P., Majid, M.Z.A., Wahid, M.A. and Zaki, S.A., "A review on phase change material (PCM) for sustainable passive cooling in building envelopes", ***Renewable and Sustainable Energy Reviews***, Vol. 60, (2016), 1470-1497. (https://doi.org/10.1016/j.rser.2016.03.036).
28. Zhou, Z., Zhang, Z., Zuo, J., Huang, K. and Zhang, L., "Phase change materials for solar thermal energy storage in residential buildings in cold climate", ***Renewable and Sustainable Energy Reviews***, Vol. 48, (2015), 692-703. (https://doi.org/10.1016/j.rser.2015.04.048).
29. Hoseinzadeh, S., Zakeri, M.H., Shirkhani, A. and Chamkha, A.J., "Analysis of energy consumption improvements of a zero-energy building in a humid mountainous area", ***Journal of Renewable and Sustainable Energy***, Vol. 11, No. 1, (2019), 015103, 1-12. (https://doi.org/10.1063/1.5046512).
30. Hoseinzadeh, S. and Azadi, R., "Simulation and optimization of a solar-assisted heating and cooling system for a house in Northern of Iran", ***Journal of Renewable and Sustainable Energy***, Vol. 9, No. 4, (2017), 045101, 1-14. (https://doi.org/10.1063/1.5000288).
31. Amani, N., "Building energy conservation in atrium spaces based on ECOTECT simulation software in hot summer and cold winter zone in Iran", ***International Journal of Energy Sector Management***, Vol. 12, No. 3, (2018), 98-313. (https://doi.org/10.1108/IJESM-05-2016-0003).
32. Peng, C., "Calculation of a building's life cycle carbon emissions based on Ecotect and building information modeling", ***Journal of Cleaner Production***, Vol. 112, Part 1, (2016), 453-465. (https://doi.org/10.1016/j.jclepro.2015.08.078).
33. Ibarra, D.I. and Reinhart, C.F., "Daylight factor simulations-how close do simulation beginners 'really' get?", ***Proceedings of Eleventh International IBPSA Conference***, Glasgow, Scotland, (2009), 196-203.
34. Amani, N., "Energy efficiency using the simulation software of atrium thermal environment in residential building: a case study", ***Advances in***

Building Energy Research, Vol. 13, No. 1, (2019), 65-79. (https://doi.org/10.1080/17512549.2017.1354781).

35. Rashwan, A., Farag, O. and Moustafa, W.S., "Energy performance analysis of integrating building envelopes with nano materials", ***International Journal of Sustainable Built Environment***, Vol. 2, No. 2, (2013), 209-223. (https://doi.org/10.1016/j.ijsbe.2013.12.001).
36. I.R. Iran of Meteorological Organization., (2019).
37. Climate Consultant 6.0.
38. The Climate Data Factory, "Solar radiation–Rasht (Iran)", (2020).

JREE: Vol. 7, No. 3, (Summer 2020) 47-55

Journal of Renewable Energy and Environment

Research Article

Journal Homepage: www.jree.ir

Cost and Environmental Pollution Reduction Based on Scheduling of Power Plants and Plug-in Hybrid Electric Vehicles

Roya Pashangpour[a], Faramarz Faghihi[a*], Soodabeh Soleymani[a], Hassan Moradi CheshmehBeigi[b]

[a] *Faculty of Mechanics, Electrical Power and Computer, Science and Research Branch, Islamic Azad University, Tehran, Iran.*
[b] *Department of Electrical Engineering, Razi University, Kermanshah, Iran.*

PAPER INFO

Paper history:
Received 02 February 2020
Accepted in revised form 05 July 2020

Keywords:
Scheduling of Power Plants
Plug-in Hybrid Electric Vehicles
GAMS
Uncertain Behavior

ABSTRACT

There has been a global effort to reduce the amount of greenhouse gas emissions. In an electric resource scheduling, emission dispatch and load economic dispatch problems should be considered. Using renewable energy resources (RESs), especially wind and solar, can be effective in cutting back emissions associated with power system. Further, the application of electric vehicles (EV) capable of being connected to power grid reduces the pollution level in the transportation sector. This paper investigates a resource scheduling with uncertain behavior of RESs and EVs by considering the penalty factors of emission for each conventional power plant in Hormozgan province of Iran for a 10-year period from 2016 to 2026. In this study, combined-cycle and thermal units are also taken into account. The CPLEX Solver is utilized for resource scheduling problem in GAMS. For combined-cycle power plants, ramp rate constraints are also included. To investigate the impact of uncertainties, different scenarios are considered. The obtained results demonstrate that Hormozgan province has a decent potential of utilizing RESs and EVs to achieve pollution reduction and optimal cost.

1. INTRODUCTION

In recent years, global warming and pollution have become one of the main environmental issues worldwide [1]. The power industry produces 40 % gas emission of global greenhouse per year, whereas the transportation industry is recognized to be responsible for 24 % of universal emission [2]. From the environmental approach, thermal units are the most polluting power plants, especially when their fuel is coal [3].

According to the rising concern over global climate change, Green House Gas (GHG) emission problem, policymakers are promoting the integration of renewable energy sources [5]. Further to that, as the worldwide energy reserves are rapidly depleted, renewable energy resources should be substituted for oil and gas, even for the transportation sector where the use of electric vehicles and electric vehicles (EVs) must be raised [6].

The use of EVs with vehicle-to-grid (VG) capability is another solution to decrease GHG emissions in the transportation sector [5]. Therefore, these EVs can be used as loads, energy resources, and energy storage units. An investigation conducted in the national renewable energy laboratory shows that the application of EVs can significantly reduce CO_2 emissions [7]. Although renewable energy resources (RESs) are cheap, they often exhibit uncertain behavior [5]. Therefore, resource scheduling in the grid with RESs and EVs is an important problem. In this new paradigm, the main objective should be not only to meet the power demand by operating power generators with the minimum cost while satisfying the constraints, but also to minimize their GHG emissions [8].

*Corresponding Author's Email: faramarz.faghihi@srbiau.ac.ir (F. Faghihi)

In several resource scheduling studies, the Particle Swarm Optimization (PSO) algorithms are employed to calculate the unit's emission contribution [1], [2], [5]. In [1], a combined economic emission dispatch was employed to investigate the effectiveness of using EVs and renewable energy sources from different aspects. Ref. [5] proposed scheduling for the smart grid with RESs and compared the emissions in different states. For minimizing the expected cost and emissions of the unit commitment schedule for the set of scenarios, an optimization algorithm was used. In [2], the study was the same as [5], but the emission rate was noticed more, and scheduling for charging and discharging of the EVs was described in more detail. The optimal energy scheduling for residential smart grid applied with centralized RESs was discussed in [9]. In [11], the role of RESs in environmental protection and CO_2 justification through solar cookers, dryer, improved cookstoves, biofuel, and water heaters was debated. In [12], an economical and environmental comparison study of conventional, hybrid, and EV was carried out. In [13], historic developments of urbanization, thermal power generation, and GHG emissions were investigated. Zhu Chuanyong and et al. [14] and K. Alrafea and et al. [15] studied the emissions of coal-fired power plants. There has not been any investigation on resource scheduling with EVs, RESs and combined-cycle power plants by considering penalty factor for emissions. Other recent related investigations about scheduling and emission were presented in [16-18]; however, there is no comprehensive scientific report for the effectiveness coefficient of solar-wind-EVs penetration according to traditional power plant on emission improvement in dual peak load curve.

According to the National Weather Service (NWS) report, the average ambient temperature of Iran in 2014 was one degree higher than the average ambient temperature in 2013.

Additionally, the pollution indicator was increased compared to the previous year [19]. Therefore, increasing pollution is one of the significant environmental issues in Iran, too.

The considered region for this research is Hormozgan province. Iran has significant reserves of natural gas and oil [20], [21]. Hence, naturally, almost total production of energy (99 %) comes from oil and gas [22]. On the other hand, Iran, particularly in its southern part, has a great potential for solar energy. Moreover, the south offshore has a suitable wind speed, which can be appropriate for applying energy convertor system wind turbines [23]. Wind energy harvesting is expected to rise in the future. The number of vehicles, which is used for this study, is logical according to Hormozgan's population. The solar farm size and the wind farm size are estimated. It is assumed that the wind farm and the solar farm are located on an energy convertor system and in Bandar-Abbas, respectively. The resource scheduling is presented under uncertainty to investigate the cycle of RESs and EVs.

In this paper, to take into account the uncertainty, a set of one thousand scenarios for load demand, solar radiation, wind speed, and EVs regime are considered and simulated in GAMS; finally, the probability of each scenario is estimated. One of the output parameters of the algorithm is the power of each unit on a random day. The charging and discharging modes of vehicles, which are placed in parking lots, are considered for different hours. The effect of increasing the penetration coefficient of EVs, solar and wind resources is discussed for a 10-year period from 2016 to 2026. Three penetration levels for solar, wind, and EVs including zero, low, and high are considered for Hormozgan province.

The main objective of this paper is to reduce cost and environmental pollution based on the scheduling of power plants and EVs. In this regard, three different cases are considered, and all results are analyzed for each case. This problem is solved in low penetration of EV and RES, high penetration of EV and RES, and absence of EV and RES.

In Section (2), the problem formulation is proposed, Section (3) describes the methodology of this research, Section (4) describes result and discussion, and the final section presents the concluding remarks.

2. PROBLEM FORMULATION

Due to the uncertain behavior of resources, EVs, and load demand, the normal probability distribution is estimated to present the nature of uncertainty. For proving the effect of conventional power plants on air pollution, RESs such as solar energy and wind sources with traditional power plants such as combined-cycle ones are proposed.

According to uncertain solar radiation, the output power of PV panels can be calculated as in (1) [24].

$$P_{PV} = F_{PV} P_{PV-r} \frac{G}{G_{STC}} [1 + \alpha_T (T - T_{STC})] \quad (1)$$

The output power of solar panels depends on the rated output power of PV (P_{PV-r}), de-rating factor considering wiring, shading, (F_{PV-r}), solar radiation in current time (G), and the solar radiation in the standard test condition (G_{STC}). To calculate the output power of solar radiation, α_{PV}, F_{PV}, and α_T are proposed to be 0.8, 0.8, and -0.48, respectively.

Wind turbines are more complex because of their mechanical nature. The wind power is related to the output power of wind turbine (P_{wt-r}), the cut-in and cut-out wind speeds (V_{ci} , V_{co}), the wind speed (V_w), and the rated wind speed (V_r) [23] and [26].

$$\begin{cases} P_{wind} = 0, & \text{if } v_w < v_{ci} \text{ or } v_w > v_{co} \\ P_{wind} = P_{wt-r} \dfrac{v_w - v_{ci}}{v_r - v_{ci}}, & \text{if } v_{ci} \le v_w \le v_r \\ P_{wind} = 0, & \text{if } v_r \le v_w \le v_{co} \end{cases} \quad (2)$$

The wind and solar energies exclusively may not meet all the load demand; therefore, the use of some conventional units is often required. The pollution rate of combined cycle power plants is lower than other types of traditional plants [11], [25].

In the transportation sector, current vehicles cause pollution. The amount of carbon dioxide released is proportional to the amount of carbon in the fuel. The quantity of the fuel burned is also pretty important [26]. As a practical point, the combined-cycle power plants must be included into the investigation as a critical source of pollution. However, some thermal power plants are discussed and formulated [1], [2], and [5].

A. Saber et al. [2], [5] and Yuan Wu et al. [9] did not consider the pollution factor, because resource scheduling according to cost reduction was more important than scheduling according to pollution level minimization for them. The emission penalty for each unit is indicated by ef_i and calculated as in (3) [23].

$$ef_i = \frac{a_i P_i^{max2} + b_i P_i^{max} + c_i}{\alpha_i P_i^{max2} + \beta_i P_i^{max} + \gamma_i} \quad (3)$$

Ramp rate constraints are not defined for thermal units; therefore, other papers did not investigate them. However, in this paper, for combined-cycle power plants, ramp rate up and down constraints are considered. These constraints are discussed in (8) and (9). All constraints and functions are defined as follows:

$$\text{emission}_i(P_i^s(t)) = \alpha_i + \beta_i (P_i^s(t)) + \gamma_i (P_i^s(t))^2 \quad (4)$$

$$\text{emission}_i(L_i, e_i) = L_i \times e_i \quad (5)$$

$$fc_i\left(P_i^s(t)\right) = a_i + b_i P_i^s(t) + c_i (P_i^s(t))^2 \quad (6)$$

$$\sum_{i=1}^{N} P_i^s(t) + P_{PV}^s(t) + P_{wind}^s(t) + \sum_{j=1}^{NV2G} P_{EV}^s(t) = D^s(t) \quad (7)$$

If EVs are in the charged mode,

$$\sum_{i=1}^{N} P_i^s(t) + P_{PV}^s(t) + P_{Wind}^s(t) = D^s(t) + \sum_{j=1}^{NV2G} P_{EV}^s(t) \quad (8)$$

EVs are in the discharged mode,

$$P_i^s(t) \le P_i^s(t-1) + RU_i \quad (9)$$

$$P_i^s(t) \ge P_i^S(t-1) - RD_i \quad (10)$$

$$P_i^{min} \le P_i^s(t) \le P_i^{max} \quad (11)$$

$$\Psi_{min} P_V \le P_V^s(t) \le \Psi_{max} P_V \quad (12)$$

$$n \times E_{min} \le E_t^s \le n \times E_{max} \quad (13)$$

$$E^s(t) = N \times E_0 + \left(R \times P^s_{ch}(t)\right) - \left({}^{P^s_{dch}(t)}/_{R}\right), \quad \text{if } t=t1 \tag{14}$$

$$E^s(t) = E^s(t-1) + \left(R \times P^s_{ch}(t)\right) - \left({}^{P^s_{dch}(t)}/_{R}\right), \quad \text{if } t>t1 \tag{15}$$

$$\psi_{min} \times E_{max} \times nv2g^s(t) \times i1_{ch}(t) \le P^s_{ch}(t) \le \psi_{max} \times E_{max} \times nv2g^s(t) \times i1_{ch}(t) \tag{16}$$

$$\psi_{min} \times E_{max} \times nv2g^s(t) \times i1_{dch}(t) \le P^s_{dch}(t) \le \psi_{max} \times E_{max} \times nv2g^s(t) \times i1_{dch}(t) \tag{17}$$

$$P^s_{dch}(t) - P^s_{ch}(t) = P^s_{EV}(t) \tag{18}$$

As mentioned before, the main purpose of such a resource scheduling problem is to minimize the GHG emission and generation costs simultaneously. This objective can be mathematically described by (19).

$$\text{Min}\left\{\sum_{s\in S}\sum_{i=1}^{N}\sum_{t=1}^{H}\left[w_c\left(fc_i(P_i^s(t))\right) + sc_i\left(1 - I_i(t-1)\right)\right] + \left[w_e\left(ef_i(\text{emission}_i(p_i^s(t)))\right)\right]\right\} \tag{19}$$

3. METHODOLOGY

The behavior of EVs, solar and wind resources, and the value of load demand are under uncertainty. For instance, both wind speed and solar radiation are uncontrollable. The load demand is also not constant during the day, and the number of EVs located in parking lots is not deterministic. This makes resource scheduling a complex problem. To investigate uncertainties, 1000 different scenarios for both solar-wind-EV resources and demand are observed. These scenarios are defined based on normal probability distribution of the estimated values for a random day. These scenarios are assumed with stated probabilities to analyze random behavior of demand, solar radiation, wind speed, and EVs. Normal distribution with suitable mean and standard deviation values based on estimated data and predictable data is used to investigate the uncertainties. By running the functions **(**For s: 1: 1000;) and (Psolar(s, :) = Psolar + randn × Psolar × 0.1**)** in MATLAB, different thousand scenarios for power of solar farm are established.

The proposed algorithm for scheduling is shown in Figure 1. To run the program by GAMS, the nonlinear functions should be broken into numerous linear functions. An iterative method is used for optimization. As is shown in Figure 1, in the first step, the equations, variables, and parameters should be defined in GAMS software. The nonlinear functions must be converted to linear ones to reduce the time of calculating the results. In the third step, λ value should be initialized. Next, according to the amount of λ, the power of all resources and EVs should be calculated. Then, the difference between load demand and sum of the produced power should be computed. If this value is smaller than the relation error and the iteration is more than one, the results are achieved. Otherwise, the value of λ should be changed or the iteration method must be done again.

In this analysis, the operation costs of resource scheduling, as well as a punishment factor for releasing GHG by conventional units, are considered. According to the multi-objective function, by considering penalty factor in emissions, the power of conventional power plants decreased to minimize the pollution and cost. The proposed case study is Hormozgan province with one and a half million inhabitants in an area of 70,697 km^2.

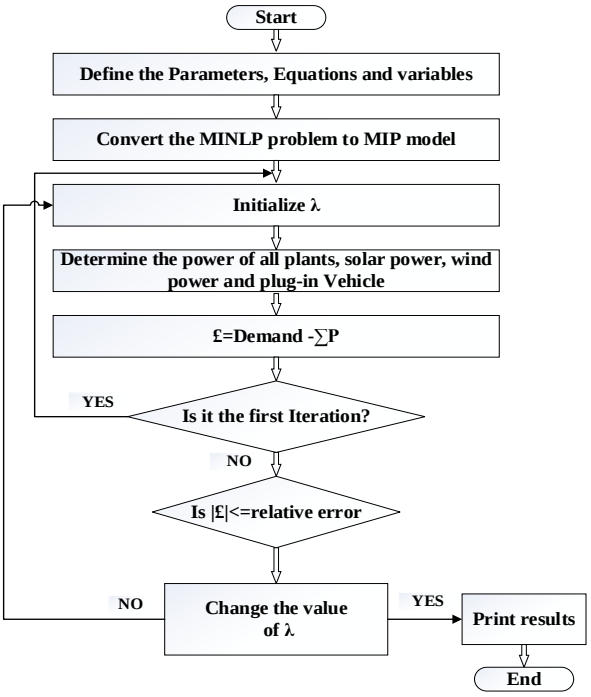

The GHG released by power plants and conventional vehicles includes several gases such as NO_X, SO_2, CH_4, and CO_2. The amount of released CO_2 is much more than the other gases; therefore, the amount of released dioxide carbon is illustrated as GHG emission. In Hormozgan, there are three power plants; two of them are combined cycle power plants, while another is thermal one. The size of plant and its capacity are given in Table 1. A summary of the generator emission coefficients is given in Table 2 [27]. In this investigation, the average solar radiation data and average wind speed on a random day, as shown in Figures 3 and 4, are used [28], [29]. Considering the uncertainties of wind and solar resources, 1000 scenarios are defined.

Table 1. Plant size and capacity of 3-Unit system.

	Termal unit	**Combined-cycle**	**Combined-cycle**
	Unit 1	Unit 2	Unit 3
P_{Max} (MW)	1200	990	660

Table 2. Generator emission coefficients.

	α_i **(Ton.h^{-1})**	β_i **(Ton.MWh^{-1})**	γ_i **(Ton.$MW^{-2}h$)**
Unit 1	30.039	-0.2444	0.00502
Unit 2	10.339	-0.40695	0.00312
Unit 3	20.039	-0.49695	0.00409

Since the total number of clients in the region is almost 485000, this is a logical assumption to consider the number of EVs which includes approximately 240000 units in 2026 [30]. Data of Figure 3, 4 are given based on real information. Each

EV includes a 15 kWh battery. The load demand curve on a random day is depicted in Figure 5. Data of Tables 1, 2 and Figure 5 are given based on real data of Hormozgan regional electric company, which were published through the 2015 annual report. It must be noted that Hormozgan load curve has two peaks. This is due to tropical weather of Hormozgan. Normally, people come back home at 12:00 am and rest for three or four hours while air condition is on. Then, the second working time starts at 4:00pm. In particular, nights continue up to 1:00am or 2:00am. This is the reason for the dual peak load curve.

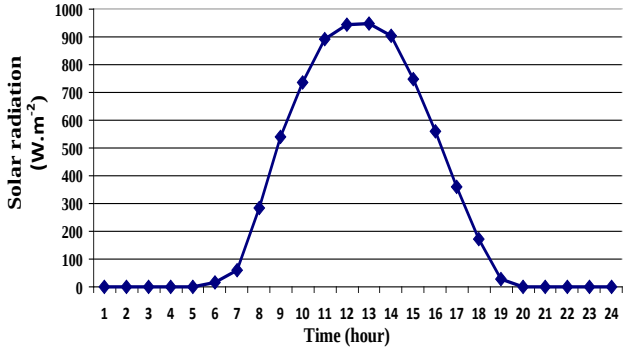

Figure 2. Average solar radiation for a random day of Hormozgan province.

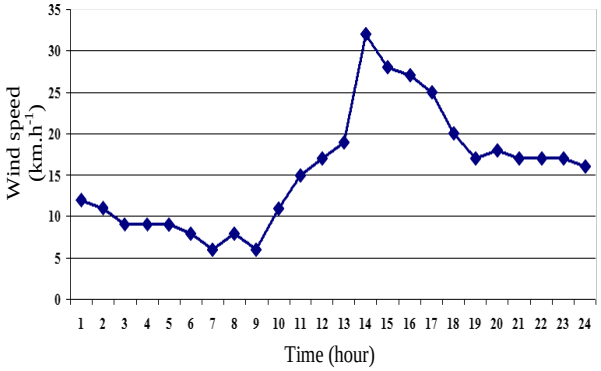

Figure 1. Average wind speed for a random day of Hormozgan province.

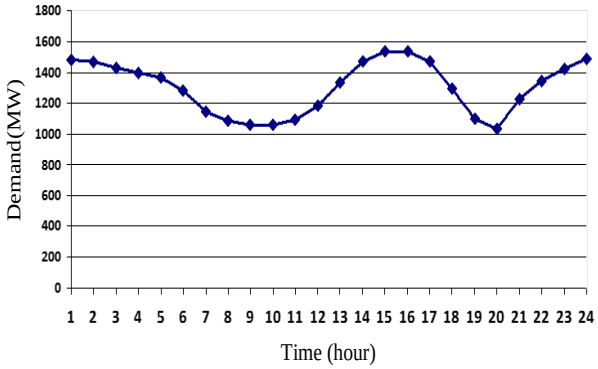

Figure 2. Load demand curve for a random day.

4. RESULTS AND DISCUSSION

Simulation of an independent system operator for the three-unit system with 240000 registered EVs is carried out in this investigation. They are conceptual scenarios; however, there are several logical reasons for the selection of the suggested scenarios:

1. These scenarios are designed based on actual specifications of Hormozgan province such as population, power plant capacity, customer power consumption, and so on.
2. There are some targets for Hormozgan province for the penetration of wind and solar energy. These targets are considered in suggested scenarios.
3. These scenarios introduce a logical approach to penetration of wind power, solar energy, and EVs.

Firstly, the simulation is performed without any EVs, solar and wind sources for 2016. Secondly, the solar farm, wind farm, and EVs are proposed. The solar farm and wind farm size are assumed to be 20 MW and 12 MW for 2020. In this case, just 120000 EVs, which can be connected to the grid as loads and sources, are analyzed. Finally, the penetration coefficient of renewable energy sources and EVs gets promoted. The solar farm size is increased to 40 MW. The wind farm size is estimated to be 25.5 MW for 2026. In this case, the EV's number is assumed to be 240,000. The results of each case are presented as follows:

Case 1: Scheduling without EVs and RESs

Resource scheduling problem is solved by only taking into account the three conventional units. In Hormozgan, there is no renewable source and EV. The obtained results for the best state are presented in Table 3.

The total emission and total running cost in the optimal state are 34,160.303 Tons and 62,668.760 $, respectively. In order to calculate the emission of the transportation system, the effect of conventional vehicles should be investigated. Based on an average distance of about 12000 miles driven by each vehicle in a year and an average emission from each vehicle being 1.2 l b/mile, the emissions from total 240,000 vehicles are 1,567,503 Tons.

Case 2: Resource scheduling with low penetration of RESs and EVs

In this case, 120,000 EVs are proposed for Hormozgan province for 2021. In addition, 240000-120000=120,000 mechanical vehicles are assumed. The charging regime of EVs is under uncertainty. These 120000 vehicles are not connected to the grid instantaneously. Some vehicles are in the charged or discharged mode, and the others may be in the ideal state. The number of vehicles, placed in parking lots for different hours, is estimated, and 1000 scenarios for the assumed numbers are defined. The solar farm size is proposed to be 20 MW. The wind farm size is considered to be 12 MW. The obtained results of optimal resource scheduling are presented in Table 4.

The total emission and cost are 41, 327.32 tons and 681, 250.6 $, respectively. The cost for a random day and the emission are 1, 792.9 $ and 1,015.5 tons, experiencing an reduction. This reduction was calculated without considering the emissions of mechanical vehicles. The emissions, which are released from 120,000 mechanical vehicles, are 783, 751.68 tons in a year. In comparison with the last case, by considering RESs and EVs, the decreased amount of emissions is 1, 154, 409.18 tons. In other words, the amount of cost and emissions in the optimal scenario decreased by 1.56 % and 9 %, respectively.

Case 3: Resource scheduling with high penetration of RESs and EVs

In this case, all the vehicles are considered as EVs and there is no conventional vehicle. The proposed wind farm size is 25.5 MW. It is assumed that the solar farm size increases to 40 MW. The obtained results of optimal resource scheduling are presented in Table 5. The total cost and emissions are 682465.06 $ and 40,297.7 per day, respectively. Both decreased more than the second case. Therefore, according to the results, it is obvious that if the penetration coefficients of renewable sources and EVs rise, it will be better for clients, suppliers, and even for the environment. In comparison with Case 2, the cost and emissions decreased by 2.30 % and 8.71 %; in addition, in comparison with Case 1, cost and emissions in the optimal scenario reduced by 3.79 % and 17 %, respectively.

According to the above table, the EVs at peak-load hours are in the discharged mode. They are charged at off-peak hours like 8, 9, 10, etc. They try to be beneficial for grid and reduce the cost and emissions. In this case, there are no mechanical vehicles and all vehicles are plug-in ones. Therefore, the emission rate is significantly lower than other cases. When comparing Cases 3 and 2, it is shown that if the solar farm size and wind farm size are less than the 20 MW rise and all of the vehicles are plug-in vehicles, the annual costs and emissions will be reduced to 359, 722.1 $ and 1, 157, 555.6 tons, respectively.

The emission value without considering the pollution of conventional vehicles for different cases is shown in Figure 5. At 1:00, which is the time for discharging, the emission amount is lower than other states. In comparison with the first case, a reduction in value is 883.9 tons. From 1:00 to 5:00, the difference between the second and third cases decreases and, at 6:00, the curves of these two cases converge to each other. In the second case, the 7:00 is the time for charging; therefore, the emission value grows and gets higher than the amount of the first case. Times 9:00, 10:00, and 11:00 are charging hours for the second and third cases. For the charge hours, the emission rates of the second and third cases are more than the emission values of the first case. For charging, more power should be generated by other resources; therefore, the emission seems to increase at charging hours. From 9:00 to 11:00, the emission curves of the second and third cases converge to each other. The solar and wind farm size in the second case is smaller than that in the third case; therefore, to supply the power, which corresponds to the demand, more hours for charging the batteries are needed. For instance, according to Figure 4, 1:00, 2:00, 4:00, 14:00, 15:00, 16:00, and 17:00 are the peak-load hours. From 13:00 to 17:00, all three curves diverge from each other.

According to Figures 6 and 7, at peak-load hours, EVs are in the discharged mode, which is the reason for a large difference among the cases. In the second case, 1:00, 14:00, 15:00, 16:00, 17:00, and 24:00 are the discharging hours. Therefore, before 16:00, the emission amount of the second case is smaller than others. However, from 17:00 to 18:00, the emission in the third case is the smallest one. 19:00 and 20:00 are the charging hours for charging more vehicles which require more power; thus, the plants supply more power and cause more emission. From 21:00 to 23:00, the curves of the second and third cases get close to each other; however, from 23:00 to 24:00, they differ from each other and the emission rate of the third case decreases significantly.

Table 3. Schedule and dispatch of 3-unit system without considering RESs and EVs in 2016.

Time (Hour)	Unit 1 (MW)	Unit 2 (MW)	Unit 3 (MW)	*P*solar (MW)	*P*wind (MW)	Demand (MW)	Summary of important points
H1	480	383.5	404	0	0	1,267.5	Expected cost=683,043.530 $
H2	480	373.24	404	0	0	1,257.24	
H3	480	340.24	404	0	0	1,224.468	
H4	480	318	397.89	0	0	1,195.899	
H5	480	318	369.12	0	0	1,167.125	
H6	480	318	299.310	0	0	1,097.32	
H7	377.724	318	286	0	0	981.724	Expected emission=42,342.87 Tons
H8	324.125	318	286	0	0	928.125	
H9	300.919	318	286	0	0	904.91	
H10	304.825	318	286	0	0	908.8	
H11	330.104	318	286	0	0	934.10	
H12	409.677	318	286	0	0	1,013.677	
H13	480	318	344.326	0	0	1,142.326	
H14	599.702	486	404	0	0	1,489.702	
H15	480	464.41	404	0	0	1,348.419	
H16	480	463.30	404	0	0	1,353.032	Emission for optimal scenario=34,160.303 Tons
H17	480	410.063	404	0	0	1,294.063	
H18	480	318	404	0	0	1,137.294	
H19	362.522	318	286	0	0	966.52	
H20	304.724	318	286	0	0	908.724	
H21	475.344	318	286	0	0	1,097.34	
H22	480	318	387.423	0	0	1,185.4	
H23	480	369.24	404	0	0	1,253.24	
H24	564.75	486	404	0	0	1,454.75	Number of scenarios=1000

Table 4. Schedule and dispatch of 3-unit system with RESs and EVs in 2026.

Time (Hour)	Unit1 (MW)	Unit 2 (MW)	Unit 3 (MW)	P_{solar} (MW)	P_{wind} (MW)	P_{EV} (MW)	Summary of important points
H1	300	424.7	404	0	9.31	129.4	Expected cost=681,250.6 $, expected Emission=41,327.32 tons Emission for optimal scenario=32,720.8 tons Cost for optimal scenario=61,715.06 $
H2	359.02	486	404	0	8.22	0	
H3	328.4	486	404	0	6.02	0	
H4	300	458.8	404	0	6.02	0	
H5	300	457	404	0	6.02	0	
H6	300	388.13	404	0.24	4.93	0	
H7	300	360.3	404	0.961	2.73	-86.11	
H8	300	319.6	404	4.61	4.93	-105.03	
H9	300	318.8	404	8.82	2.73	-129.46	
H10	300	318	335.3	11.99	8.22	-64.7	
H11	300	318	354.7	14.54	11.508	-64.11	
H12	300	369.05	404	15.42	11.508	-86.7	
H13	300	411.3	404	15.47	11.508	0	
H14	429.5	486.0	404	14.77	11.508	143.8	
H15	300	478.1	404	12.17	11.75	154.14	
H16	407.6	486.00	404	9.12	11.83	46.2	
H17	339.9	486	404	5.9	12	46.2	
H18	300	418.4	404	2.82	12	0	
H19	300	318	404	0.48	12	-67.967	
H20	300	318	404	0	12	-125.2	
H21	300	363.3	404	0	12	0	
H22	300	469.4	404	0	12	0	
H23	351.2	486	404	0	12	0	
H24	414.02	486	404	0	12	138.7	

Table 5. Schedule and dispatch with larger RESs and 240000 EVs in 2026.

Time (Hour)	Unit 1 (MW)	Unit 2 (MW)	Unit 3 (MW)	P_{solar} (MW)	P_{wind} (MW)	P_{EV} (MW)	Summary of important points
H1	300	318	365.2	0	23.80	260.4	Expected cost=680,265.06 $ Expected emissions=40,297.7 Tons Total cost for the optimal scenario=60,292.2 $ Total emission for optimal scenario=31,864.9 Tons
H2	346.2	486	404	0	21	0	
H3	319.06	486	404	0	15.4	0	
H4	300	476.4	404	0	15.4	0	
H5	300	447.7	404	0	15.4	0	
H6	300	380.1	404	0.52	12.6	0	
H7	300	318	354.6	2.061	7.001	0	
H8	300	318	404	9.88	12.6	-116.3	
H9	300	318	404	18.9	7.001	-142.9	
H10	300	318	374.3	25.7	21.004	-130.2	
H11	300	318	389.6	31.17	25.5	-130.2	
H12	300	318	337.1	33.51	25.5	0	
H13	300	379.6	404	33.15	25.5	0	
H14	480	486	466.5	31.65	25.5	0	
H15	432.3	486	404	26.09	25.5	0	
H16	339.4	486	404	19.56	25.5	104.04	
H17	300	465.2	404	12.64	25.5	86.7	
H18	300	401.7	404	6.04	25.5	0	
H19	300	374.7	404	1.048	25.5	-138.7	
H20	300	376.1	404	0	25.5	-196.8	
H21	300	349.8	404	0	25.5	0	
H22	300	455.9	404	0	25.5	0	
H23	337.7	486	411.4	0	25.5	0	
H24	300	404.4	404	0	25.5	320.8	

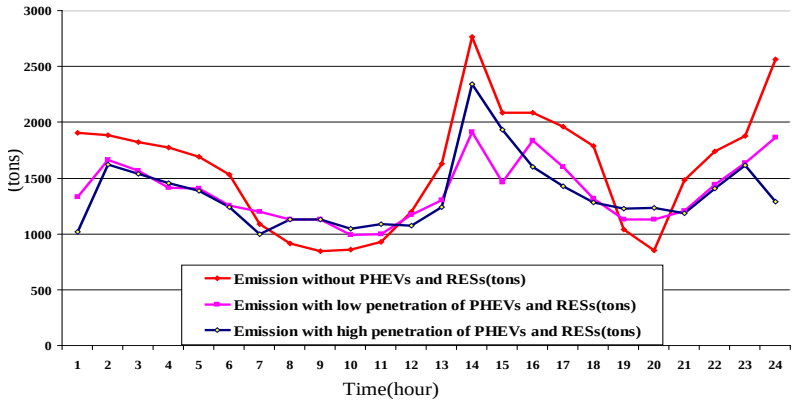

Figure 5. Emission rate in different cases for Hormozgan province.

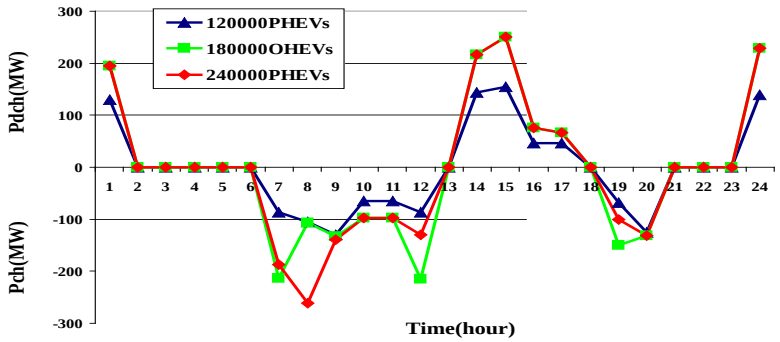

Figure 3. Values of charged and discharged power at different hours for different numbers of EVs.

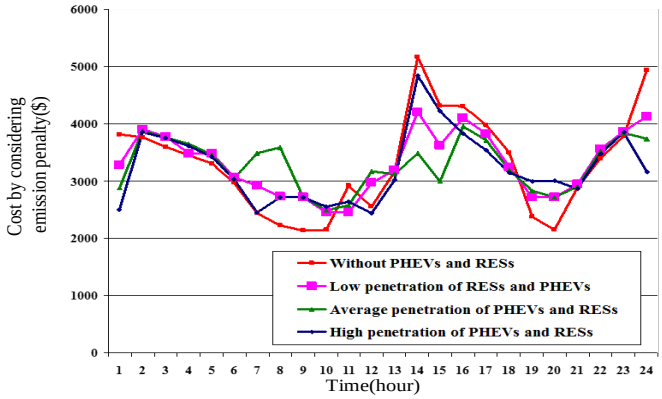

Figure 4. Cost by considering emission penalty for 4 different states.

In Figure 7, costs associated with the emission penalty factor are calculated. For three states including EVs, 120,000, 180,000, and 240,000 EVs are considered. The negative powers are for the discharged mode and the positive values are for the charged mode. The behaviors of all cases are similar to each other. To help suppliers and level the load demand curve, during peak-load hours, vehicles are discharged and, during off-peak load hours, EVs are charged. When the number of EVs grows, the values of discharged and charged power will increase.

In this paper, the objective is to minimize the cost and emissions simultaneously. Moreover, the penalty factor in polluting the weather is defined for each power plant. In Figure 8, costs are shown considering the pollution penalty factor. The worst case is the case without any PHEVs. Particularly at the peak load hours, the cost values are high. At charging hours such as 7:00 and 8:00, the value of the objective function rises. At discharging hours such as 1:00, 16:00, 17:00, and 24:00, the amounts of the objective are reduced. When the number of EVs grows, the expected amounts of emission and cost will decrease. However, the batteries of EVs should be charged at off-peak hours, and the cost considering the pollution penalty factors will rise and converge to the values of the first case. At the discharging hours like 1:00, 16:00, 17:00, and 24:00, the curves separate from each other. The third case which includes 240,000 EVs is the best and has the lowest cost.

5. CONCLUSIONS

In this research, increasing the penetration coefficients of using RESs and EVs to minimize the pollution level and costs in the southern part of Iran for a period of 10 years is studied. Resource scheduling for combined-cycle power plants, considering PV power and wind power, is performed. The

uncertainties of load, solar energy, and wind speed are derived from prior statistics, heuristics, and experiences. The mode of EVs is presented for each hour. The uncertain behavior of EVs, solar radiation, and wind speed are investigated in 1000 scenarios. According to the proposed model, the charge times for EVs are at off-peak hours and are discharged at peak hours to help the supplier. Using the high penetration of RESs and EVs in 2026 for Hormozgan province, which has not any RESs and EVs in 2016, the cost and emission, considering the penalty factors, will decrease 3.79 % and 17 % per day, respectively. In the past research by PSO for the same sizes of wind farm, solar farm and 50000 EVs, the value of cost and emissions decreased by nearly 2.5 %. Therefore, it is proved that our results are logical and even better because of considering GHGs penalty factor.

6. ACKNOWLEDGEMENT

The authors wish to thank the Islamic Azad University of Tehran, Science and Research Branch and Razi University.

NOMENCLATURE

Ψ_{min}/Ψ_{max}	Min/max state of charge
$I_i(t)$	Status of unit i at hour t
L_i	Length of travel in mile
RU_i, RD_i	Ramp rates of unit i
N_{EV}	Number of electric vehicles connected to the grid at time t
$\alpha_i, \beta_i, \gamma_i$	Emission coefficients
a_i, b_i, c_i	Fuel cost coefficients
H	Scheduling hours
S	Sets of scenario
N	Number of generators
R	Efficiency of the battery
$D^s(t)$	Load demand at time t considering scenarios
ef_i	Emission penalty factor of unit i
e_i	Per mile emission from vehicle
w_c, w_e	Weight factors for cost and emissions
$Sc_i()$	Start-up cost function of unit i
$Fc_i()$	Fuel cost function
emission $c_i()$	Emission function of unit i
$P_V(t)$	Capacity of the vehicle's battery at time t
$P^s_{solar}(t)$	Power from solar farm at time t considering scenario S
$P^s_{wind}(t)$	Power from wind farm at time t considering scenario S
$P^s_i(t)$	Power of unit i at time t considering scenario S
$P^s_{EV}(t)$	Power of the electric vehicle at time t considering scenario S
P_i^{max}/P_i^{min}	Max/Min output limit of unit i
$E^S(t)$	Total energy of all batteries at time t considering scenario s
E_F	Energy of battery at final hour of day
E_0	Primary energy of battery at starting time for scheduling
E_{min}, E_{max}	Maximum and minimum energy of battery
$P^s_{ch}(t)$	Charging power of all plug-in vehicles at time t considering scenario s
$P^s_{dch}(t)$	Discharging power of all plug-in vehicles at time t considering scenario s
P_{pv}	Output power of solar panel
P_{pv-r}	Rated output power of solar panel
G	Solar radiation in current time
G_{STC}	Solar radiation in standard test condition
v_w	Wind speed
v_r	Rated wind speed
v_{ci}	Cut-in wind speed
v_{co}	Cut-off wind speed
P_{wt-r}	Output power of wind turbine
Randn	A random number between 0 and 1 in normal probability distributed curve
N	Number of electric vehicles in each case
$n^s_{v2g}(t)$	Number of electric vehicles which are connected to the grid at time t considering scenario s
$i1_{ch}(t), i1_{dch}(t)$	Status of charging and discharging plug-in vehicles

REFERENCES

1. Gholami, A., Ansari, J., Jamei, M. and Kazemi, A., "Environmental/economic dispatch incorporating renewable energy sources and plug-in vehicles", ***IET Generation, Transmission & Distribution***, Vol. 8, No. 12, (2014), 2183-2198. (https://doi.org/10.1049/iet-gtd.2014.0235).
2. Saber, A.Y. and Venayagamoorthy, G.K., "Plug-in vehicles and renewable energy sources for cost and emission reductions", ***IEEE Transactions on Industrial Electronics***, Vol. 58, No. 4, (2010), 1229-1238. (https://doi.org/10.1109/TIE.2010.2047828).
3. Kargari, N. and Mosturi, R., "Comparing GHG emissions in different types of power places by using LCA approach", ***International Journal of Engineering***, Vol. 13, No. 2, (2010), 67-78.
4. Zhang, M. and Guo, Y., "Process simulations of large-scale CO_2 capture in coal-fired power plants using aqueous ammonia solution", ***International Journal of Greenhouse Gas Control***, Vol. 16, (2013), 61-71. (https://doi.org/10.1016/j.ijggc.2013.03.010).
5. Saber, A.Y. and Venayagamoorthy, G.K., "Resource scheduling under uncertainty in a smart grid with renewable and plug-in vehicles", ***IEEE Systems Journal***, Vol. 6, No. 1, (2011), 103-109. (https://doi.org/10.1109/JSYST.2011.2163012).
6. Madawala, U.K., Schweizer, P. and Haerri, V.V., "Living and mobility: A novel multipurpose in-house grid interface with plug-in hybrid blue Angle", ***IEEE International Conference on System Engineering and Technology***, (2008), 531-536. (https://doi.org/10.1109/ICSET.2008.4747065).
7. Parks, K., Denholm, P. and Markel, T., "Costs and emissions associated with plug-in hybrid electric vehicle charging in the Xcel Energy Colorado service territory", National Renewable Energy Lab, Golden, Colorado, Tech. NREL/TP 64041410, (2007).
8. Aydin, D., Ozyon, S., Yasar, C. and Liao, T., "Artificial bee colony algorithm with dynamic population size to combined economic and emission dispatch problem", ***International Journal of Electrical Power and Energy Systems***, Vol. 54, (2014), 144-153. (https://doi.org/10.1016/j.ijepes.2013.06.020).
9. Wu, Y., Lau, V.K.N., Tsang, D.H.K., Qian, L.P. and Meng, L.M., "Optimal energy scheduling for residential smart grid with centralized renewable energy source", ***IEEE Systems Journal***, Vol. 8, No. 2, (2014), 562-576. (https://doi.org/10.1109/JSYST.2013.2261001).
10. Vasudevan, S., Farooq, Sh., Karimi, I.A. and Agrawal, R., "Energy penalty estimates for CO_2 capture: Comparison between fuel types and capture-combustion modes", ***Energy***, Vol. 103, Issue C, (2016), 709-714. (https://doi.org/10.1016/j.energy.2016.02.154).
11. Panwar, N.L., Kaushik, S.C. and Kothari, S., "Role of renewable energy sources in environmental protection: A review", ***Journal of Renewable and Sustainable Energy Reviews***, Vol. 15, (2011), 1513-1524. (https://doi.org/10.1016/j.rser.2010.11.037).
12. Nanaki, E.A. and Koroneos, C.J., "Comparative economic and environmental analysis of conventional, hybrid and electric vehicles- the case study of Greece", ***Journal of Cleaner Production***, Vol. 53, (2013), 261-266. (https://doi.org/10.1016/j.jclepro.2013.04.010).
13. Sethi, M., "Location of greenhouse gases emissions from thermal power plants in India along the urban-rural continuum", ***Journal of Cleaner Production***, Vol. 103, (2015), 586-600. (https://doi.org/10.1016/j.jclepro.2014.10.067).
14. Zhu, C., Tian, H., Cheng, K., Liu, K., Wang, K., Hua, Sh., Gao, J. and Zhou, J., "Potentials of whole process control of heavy metals emissions from coal-fired power plants in China" ***Journal of Cleaner Production***, Vol. 114, (2016), 343-351. (https://doi.org/10.1016/j.jclepro.2015.05.008).

15. Alrafea, K., Elkamel, A. and Abdul-Wahab, S.A., "Cost-analysis of health impacts associated with emissions from combined-cycle power plants", ***Journal of Cleaner Production***, Vol. 139, (2016), 1408-1424. (https://doi.org/10.1016/j.jclepro.2016.09.001).

16. Konda, S.R., Panwar, L.K., Panigrahi, B.K. and Kumar, R., "A multiple emission constrained approach for self-scheduling of GENCO under renewable energy penetration", ***CSEE Journal of Power and Energy Systems***, Vol. 3, No. 1, (2017), 63-73. (https://doi.org/10.17775/CSEEJPES.2017.0009).

17. Elsakaan, A.A., El-Sehiemy, R.A., Kaddah, S.S. and Elsaid, M.I., "Optimal economic–emission power scheduling of RERs in MGs with uncertainty", ***IET Generation, Transmission & Distribution***, Vol. 14, No. 1, (2019), 37-52. (https://doi.org/10.1049/iet-gtd.2019.0739).

18. Ullah, Z., Mokryani, G., Campean, F. and Hu, Y.F., "Comprehensive review of VPPs planning, operation and scheduling considering the uncertainties related to renewable energy sources", ***IET Energy Systems Integration***, Vol. 1, No. 3, (2019), 147-157. (https://doi.org/10.1049/iet-esi.2018.0041).

19. National Weather Service (NWS) [Online].

20. Energy Information Administration (EIA).

21. Iran Renewable Energy Organization (SUNA).

22. Xu, L., Ruan, X. and Ma, Ch., "An improved optimal sizing method for wind-solar-battery hybrid power system", ***IEEE Transactions on Sustainable Energy***, Vol. 4, No. 3, (2013), 774-785. (https://doi.org/10.1109/TSTE.2012.2228509).

23. Mostafaeipour, A., "Feasibility study of offshore wind turbine installation in Iran compared with the world", ***Journal of Renewable and Sustainable Energy Reviews***, Vol. 14, No. 7, (2010), 1722-1743. (https://doi.org/10.1016/j.rser.2010.03.032).

24. Najafi, G., Ghobadian, B., Mamat, R., Yusaf, T. and Azmi, W.H., "Solar energy in Iran: Current state and outlook", ***Journal of Renewable and Sustainable Energy Reviews***, Vol. 49, (2015), 931-942. (https://doi.org/10.1016/j.rser.2015.04.056).

25. Amirante, R. and Tamburrano, P., "Novel, cost-effective configurations of combined power plants for small-scale cogeneration from biomass: Feasibility study and performance optimization", ***Journal of Energy Conversion and Management***, Vol. 97, (2015), 111-120. (https://doi.org/10.1016/j.enconman.2015.03.047).

26 Denny, E. and O'Malley, M., "Wind generation, power system operation, and emissions reduction", ***IEEE Transactions on Power Systems***, Vol. 21, No. 1, (2006), 341-347. (https://doi.org/10.1109/TPWRS.2005.857845).

27. Amini, A., Falaghi, H. and Ramezani, M., "Unit commitment in order to reduce cost and emissions simultaneously", ***Journal of Energy Management***, Vol. 1, No. 1, (2013), 2-15.

28. Solar Energy Services for Professionals, SODA, solar radiation data, [online].

29. Iran Winds [Online].

30. Saber, A.Y. and Venayagamoorthy, G.K., "Intelligent unit commitment with vehicle-to-grid: A cost-emission optimization", ***Journal of Power Sources***, Vol. 195, No. 3, (2010), 898-911. (https://doi.org/10.1016/j.jpowsour.2009.08.035).

JREE: Vol. 7, No. 3, (Summer 2020) 56-66

Journal of Renewable Energy and Environment

Research Article

Journal Homepage: www.jree.ir

Quantification of Thermal Energy Performance Improvement for Building Integrated Photovoltaic Double-Skin Façade Using Analytical Method

Mahdi Shakouri[a], Alireza Noorpoor[a*], Hossein Ghadamian[b]

[a] *Department of Environmental Engineering, School of Environment, College of Engineering, University of Tehran, P. O. Box: 11155-4563, Tehran, Iran.*
[b] *Department of Energy, Materials and Energy Research Center (MERC), MeshkinDasht, Alborz, Iran.*

PAPER INFO

Paper history:
Received 25 April 2020
Accepted in revised form 13 July 2020

Keywords:
Analytical Method
Building Integrated Photovoltaic Thermal
Double Skin Façade
Energy Saving
Thermal Performance

ABSTRACT

This study presents an analytical method for quantifying the improvement of thermal energy performance of a building integrated photovoltaic double-skin façade. The system was suggested as a retrofit measure for an existing building in Tehran. The effect of thermal performance was analyzed through computer-assisted developed codes using Engineering Equation Solver (EES) software. Three scenarios were defined and for each scenario, temperature and velocity profiles were provided through continuity, momentum, and energy equations. Given that the monocrystalline photovoltaic modules and the double-glazed windows are quite common in the current condition in Tehran, the authors considered them for analysis. A comparison of results is valuable for those cases that intend to select either glass or photovoltaic as the outer façade. The quantitative results illustrate that the proposed system would reduce the cooling demand in the summer case by 18.5 kilowatts, which is around 8.7 percent of the current cooling load. According to the results of the sensitivity analysis, both glass and photovoltaic façades were of greater efficiency in terms of energy saving in the summer. By increasing the ratio between the photovoltaic outer façade to the surface area of the glass section, the amount of energy saving due to the total cooling load reduction will increase. The results of the analysis showed that the application of the suggested system would reduce the thermal load by 2.1 percent in the winter season.

1. INTRODUCTION

New designs of façades should ensure a comfortable indoor climate, soundproof, use of daylighting, and reduced energy demand. Nowadays, Double-Skin Façades (DSFs) have become an increasing and important architectural element in buildings in combination with Photovoltaic (PV) panels.

Considering the need to use more renewable energy, investigation of Building Integrated Photovoltaic (BIPV) systems to improve their performance is of great importance [1]. Solar façades are designed to specifically reject or absorb and reutilize solar heat [2]. Because PV panels are heat sources in BIPV, such systems are often designed with the ability to provide ventilation through the solar chimney principle combined with a DSF design concept.

Thus, the self-ventilating and self-heat dissipation mechanisms of BIPV are realized through natural ventilation and buoyant force [3]. From the efficiency perspective of PV panel, typically 5-25 % of radiated solar energy on the PV panel front surface is transformed into electricity [4] and the remaining is transformed into heat [5].Because the solar cell temperature affects the generation efficiency of a PV module [6], PV modules have evolved with advances in BIPV from the units directly attached to a building envelope to the units detached from it. Therefore, appropriate cooling technologies must be used for enhancing the efficiency of panels. Recently, some researchers have attempted to develop thermal models to estimate the operating temperature of the PV system considering finer details of heat transfer. The methods of energy transfer from the PV module to the surroundings were theoretically modeled [7].

An investigation into the performance of a system that integrates a PV layer into a DSF using a simulated dynamic thermal behavior of the system leads to a reduction in the monthly cooling energy demand between 20-30 %. This result is particularly relevant to hot climates, where cooling loads are seen throughout the year [8]. Zogou and Stapountzis [9] installed a Double-Skin Façade Building Integrated Photovoltaic (DSF-BIPV) system on the south-facing façade of an office building and directed the channel flow heated by the DSF to indoor areas to warm and ventilate rooms. Rabani et al. [10] designed an air outlet in the form of DSF where the indoor air was drawn out of the building through a solar chimney effect and a water spraying system was installed in the air inlet to cool the air drawn from the outdoors. Corbin and Zhai [11] designed a Building Integrated Photovoltaic Thermal (BIPVT) system that was integrated with PV and a solar hot water heater, which increased the efficiency of the solar cell by 5.3 %. Shakouri et al. [12] reviewed the electrical and thermal performance of Photovoltaic Thermal (PVT) systems through optimization using a genetic algorithm in MATLAB software. Shakouri et al. [13] simulated a photovoltaic thermal system and thereafter, evaluated the overall performance of the system through parametric analysis. Pantic et al. [14] analyzed the energy performance of three different types of BIPVT systems. Outdoor air is directed through these systems, and heated air flows over the rock substrate where it is stored, whereas solar energy is stored through the sensible heat capacity of the rock. The energy performance of different types of glazing was compared to determine the best long-term comfort conditions

*Corresponding Author's Email: noorpoor@ut.ac.ir (A. Noorpoor)

in an open-space office with the climatic conditions of Paris, Milan, and Rome [15]. Serra et al. [16] directed air into the air-flow channel of a double-glazed facade through mechanical ventilation. Both clear glass and low emissivity glass were used as the transparent building materials, whereas Venetian blinds and polyvinyl chloride reflecting roller screens were used as the shading louvers. Ghadimi et al. [17] assessed the energy performance of multiple skin façade utilizing experiments and numerical simulations. Fuliotto et al. [18] developed the decoupling method for simulating the thermal properties of a ventilated double-glazed façade with a Venetian blind. Kuznik et al. [19] developed a simulation method using the zonal model approach and radiative/convective heat transfers, and they investigated the effects of airflow rates and blade angles on the heat transfer performance of a ventilated double-glazed façade with a Venetian blind. Mulyadi et al. [20] simulated the thermal performance of a ventilated double-glazed facade with a light-colored horizontal blind that extended over five stories of a building in Indonesia. Hoseinzadeh et al. [21-23] analyzed the energy consumption improvements of a zero-energy building in a humid mountainous area. They reviewed the thermal performance of electrochromic smart windows with nanocomposite structures under different climates in Iran. Thereafter, they have simulated and optimized a solar-assisted heating and cooling system for a house in the Northern part of Iran. Yousef Nezhad and Hoseinzadeh carried out their research on the mathematical modeling and simulation of a solar water heater for an aviculture unit using MATLAB [24]. According to the results, 80 % of the amount of electrical energy was used for air conditioning in the building and energy consumption decreased from 34 to 7 MW. In the case of Return on Investment (RoI), the electricity needs to be generated and the cost can be about $ 15,000 a year [21-24]. Multi-glazed façades can effectively cut off the conductive and convective heat transfer of the solar heat gain and radiative heat transfers are usually blocked through the reflective or absorptive characteristics of the coating material on the glass [16]. Thermal models developed so far require further modification and they could include heat loss from PV panel front and back surfaces into the environment, heat loss due to radiation, variable climatic conditions, and the effect of PV panel inclination angle on heat loss mechanisms [7].

Given that the research team has reviewed the researches done by other researchers, they found no appropriate and thorough analysis of the outer façade with a combined structure of both glass and photovoltaic modules. Thus, authors have focused on this research gap and tried to simulate the outer façade with the above-mentioned structure within the studied case, which is the existing office building in Tehran. The results of this study are interesting for both decision-makers and design engineers as the current cooling load peak in the summer case has become a concern for Iran. This type of suggested energy-saving measure can be considered as one of the proper solutions for the building sector to tackle the issue of cooling load peak in the summer case.

The present study provides one step further in Building Integrated Photovoltaic Thermal Double-Skin Façade (BIPVT-DSF) system and investigates the thermal performance through an analytical solution. The methods of solution applied to the current research and investigation are borrowed from a previous study on DSF [25]. However, this research provides a new approach to BIPVT-DSF as the application of both glass and PV façades has been considered as the outer layer of DSF and simulation results provide a wide range of possibilities for energy performance. The studied case is an office building located in Tehran, the capital city of Iran, with the latitude and the longitude of 35.76° and 51.45°. This building consists of five floors with ten units and a total controlled area in terms of heating, cooling, ventilation, and air conditioning and it is 1625 square meters. Cooling and thermal loads are calculated as 134 and 213 kilowatts (kW), respectively. According to the simulation, the total nominal installation capacity of photovoltaic modules of the suggested configuration is 10 kW. According to the direction of the buildings, it receives more radiation from the southern part. In this respect, much of the cooling loss depends on the southern side. To quantify the effect of different geometrical shapes of the southern façade, this surface is divided into five parts including sections A, B, C, D, and E, as shown in Figure 1, and it includes a front view of the existing façade, proposed outer façade as a retrofit solution, and a side view of the outer façade for summer and winter cases.

The research team aims to identify the impact of the system in both chimney and blanket modes. The system would have an impact in terms of energy saving both in the summer and winter cases. Accordingly, the research team intends to review the technical impact of the suggested structure in terms of energy efficiency and the outer façade has been simulated such that occupants in the building can see the outer side of the existing window through another window. Therefore, in the simulated outer façade, there are photovoltaic modules parallel to the wall for the inner façade and there are windows parallel to the windows. The geometry of sections A, C, and E provides proper ground for the application of both glass and PV modules as the outer façade. Glass can be used in parallel to glass windows of the existing façade and PV modules may be applied in parallel to the connecting small walls between levels. Due to the geometry of sections B and D for the existing façade which is a wall, the suggested outer façade is shaped by an integrated PV module wall. A detailed descriptive view of the existing façade with the proposed glass and photovoltaic outer façade is given in Figure 1.

2. MATERIALS AND METHODS

In this section, the theory of formulation behind the stated problem is clarified. Thereafter, considering the assumptions on the solution of the problem, the applied tool for this procedure was defined. Finally, all the relevant input parameters were defined. To achieve the objective of analysis, all required heat transfer equations were determined. By considering the Solar Heat Gain Coefficient (SHGC) of glass and solar total radiation on a vertical surface, the heat transfer rate of glass-based outer skin was calculated through Equation (1). The wall surface heat transfer rate was calculated using Equation (2). The mean temperature of the boundary layer and the temperature coefficient of thermal conductivity were calculated through Equations (3) and (4), respectively [26, 27].

$$q_w = SHGC \times G_{tV} = h_{conv_w} \times (T_w - T_{amb}) \quad (1)$$

$$q_{wall} = G_{tV} = h_{conv_{wall}} \times (T_{wall} - T_{amb}) \quad (2)$$

$$T_f = \frac{T_w + T_{amb}}{2} \text{ or } \frac{T_{Tedlar} + T_{amb}}{2} \quad (3)$$

$$\beta = \frac{1}{T_f + 273.15} \quad (4)$$

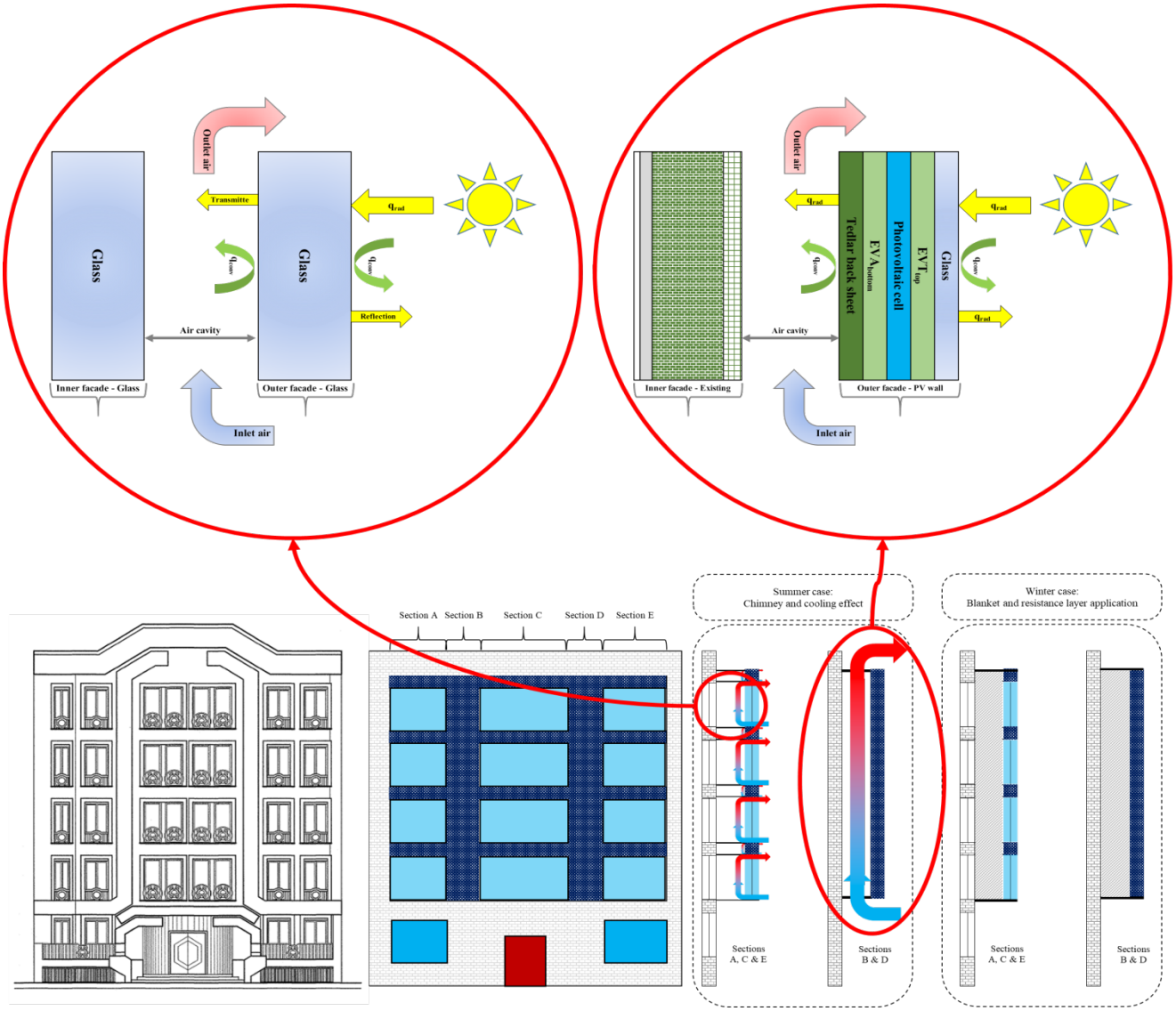

Figure 1. Front view of the existing facade (left bottom) and proposed outer facade as a retrofit solution (middle bottom); side view of outer façade for summer and winter cases (right bottom); side view of double façade with outer window wall (left top) and double façade with outer PV wall (right top).

Be keeping the amount of wind velocity and ambient temperature in mind, free convection heat transfer coefficient of outer skin outside and sky temperature were calculated through the experimental equations (5) and (6) [7, 28]. Temperatures of different photovoltaic layers were determined using energy balance equations by Equations (7) to (11) [29].

$$h_{conv_t} = 2.8+(3\times V_{wind}) \quad (5)$$

$$T_{sky} = \left(0.037536\times T_{amb}^{\,1.5}\right)+(0.32\times T_{amb}) \quad (6)$$

$$h_{conv_t}\left(T_{amb}-T_g\right)+\varepsilon_g F\sigma\left(T_{sky}^{\,4}-T_g^{\,4}\right) +\alpha_g G_{tV}-k_g\frac{T_g-T_{EVA_t}}{l_g}=0 \quad (7)$$

$$k_g\frac{T_g-T_{EVA_t}}{l_g}-k_{EVA_t}\frac{T_{EVA_t}-T_{cell}}{l_{EVA_t}}+\tau_g\alpha_{EVA}G_{tV}=0 \quad (8)$$

$$k_{EVA_t}\frac{T_{EVA_t}-T_{cell}}{l_{EVA_t}}-k_{EVA_b}\frac{T_{cell}-T_{EVA_b}}{l_{EVA_b}} +\tau_g\tau_{EVA}\left(\alpha_{cell}K+\alpha_{EVA}\left(1\text{-}K\right)\right)G_{tV}-\eta_{cell}G_{tV}=0 \quad (9)$$

$$k_{EVA_b}\frac{T_{cell}-T_{EVA_b}}{l_{EVA_b}}-k_{Tedlar}\frac{T_{EVA_b}-T_{Tedlar}}{l_{Tedlar}} +\tau_g\tau_{EVA}\tau_{EVA}\alpha_{Tedlar}\left(1\text{-}K\right)G_{tV}=0 \quad (10)$$

$$-h_{conv_{b\_PV}}\left(T_{Tedlar}-T_{amb}\right)+\varepsilon_{Tedlar}F\sigma\left(T_{Tedlar}^{\,4}-T_{amb}^{\,4}\right) +k_{Tedlar}\frac{T_{EVA_b}-T_{Tedlar}}{l_{Tedlar}}=0 \quad (11)$$

The selected photovoltaic (PV) module is of mono-crystalline type and it is characterized by better efficiency and greater popularity in Tehran for the integrated applications to buildings. The actual efficiency of the photovoltaic cell was calculated using the reference Equation (12) [30].

Heat transfer rate of PV module Tedlar surface was calculated through Equation (13). Properties of air including thermal conductivity, dynamic viscosity, density, kinematic viscosity, and Prandtl number for a cavity between two façades were determined using the corresponding tables. Modified Grashof number for constant heat flux was calculated through Equation (14) [26, 27].

$$\eta_{cell} = \eta_{ref}\left[1-\beta_{ref}\left(T_{cell}-T_{ref}\right)\right] \quad (12)$$

$$q_{Tedlar} = h_{conv_{b\_PV}} \times (T_{Tedlar} - T_{amb}) \quad (13)$$

$$Gr^* = \frac{\beta g q_w L^4}{k\gamma^2} \text{ or } Gr^* = \frac{\beta g q_{Tedlar} L^4}{k\gamma^2} \quad (14)$$

Finally, Nusselt number and natural convention heat transfer coefficient in the cavity boundary condition were calculated using Equations (15) and (16) for laminar flow and using Equations (17) and (18) for turbulent flow [26, 27].

$$10^5 < Gr^* Pr < 10^{11} \rightarrow Nu_x = 0.6 \times \left(Gr^* Pr\right)^{0.2} \quad (15)$$

$$h_m = 1.25 \times \frac{Nu_x k}{L} \quad (16)$$

$$2\times10^{13} < Gr^* Pr < 10^{16} \rightarrow Nu_x = 0.568 \times (Gr^* Pr)^{0.22} \quad (17)$$

$$h_m = 1.136 \times \frac{Nu_x k}{L} \quad (18)$$

Transport phenomenon was applied to thermal performance analysis of a studied building and to the development of a temperature and velocity profile for boundary conditions of the air cavity. Three main functions for the analysis including continuity, energy, and momentum equations are shown in Equations (19) to (21) [26, 27].

$$\frac{\partial u}{\partial x} + \frac{\partial \upsilon}{\partial y} = 0 \quad (19)$$

$$u\frac{\partial T}{\partial x} + \upsilon\frac{\partial T}{\partial y} = \frac{K}{\rho c_p}\frac{\partial^2 T}{\partial y^2} + \frac{\gamma}{c_p}\left(\frac{\partial u}{\partial y}\right)^2 \quad (20)$$

$$\rho\left(u\frac{\partial u}{\partial x} + \upsilon\frac{\partial u}{\partial y}\right) = \mu\frac{\partial^2 u}{\partial y^2} - \frac{\partial p}{\partial x} \quad (21)$$

The applied solution method for determining temperature and velocity profiles was the analytical method for both photovoltaic and glass as the external façade. Obtained temperature and velocity functions as well as rendered spacing and velocity functions for glass and PV outer skins were determined in Equations (22) to (25).

$$\frac{T_{(x,y)} - T_{amb}}{T_w \text{ or } T_{Tedlar} - T_{amb}} = \left(1-\frac{y}{\delta}\right)^2 \quad (22)$$

$$U_{(x,y)} = \left[U_0(x)\frac{\beta\delta^2 g}{4\gamma}\left(T_w \text{ or } T_{Tedlar} - T_{amb}\right)\right] \times \frac{y}{\delta}\left(1-\frac{y}{\delta}\right)^2 \quad (23)$$

$$\delta(x) = 3.93\left(0.952+Pr\right)^{0.25} \times \left[\frac{\beta g\left(T_w \text{ or } T_{Tedlar} - T_{amb}\right)}{\gamma^2}\right]^{-0.25} Pr^{-0.5} x^{0.25} \quad (24)$$

$$U_0(x) = 5.17\gamma\left(0.952+\frac{1}{Pr}\right)^{-0.5} \times \left[\frac{\beta g\left(T_w \text{ or } T_{Tedlar} - T_{amb}\right)}{\gamma^2}\right]^{0.5} x^{0.5} \quad (25)$$

Terms T_w and T_{Tedlar} must be used for glass-based and PV-based outer skins, respectively. Considering the geometry of the outer façade for different sections of the studied case, three situations need to be analyzed for developing temperature and velocity profiles below:

- Glass parts of sections A, C, and E: each section consists of four separate levels of glass façade with a height of 2.37 meters with different widths;
- PV parts of sections A, C, and E: each section consists of four separate levels of PV façade with a height of 0.53 meter with different widths;
- PV parts of sections B and D: each section consists of one integrated PV façade with a height of 12.5 meters with a similar width.

To compare the application of glass and PV façades and the existing inner façade in a critical condition, cooling and thermal losses were formulated. The effect of DSF in the summer case in a chimney was considered. In this situation, natural ventilation in the air cavity reduced the cooling load.

For calculation of this effect, Equations (26) to (29) were applied. By using Equations (26) and (27), the heat loss of the glass-based inner skin in the summer cases was obtained for single and double-façade modes, respectively. Through Equations (28) and (29), the heat loss of the wall-based inner skin in the summer cases was obtained for single and double-façade modes, respectively.

It should be noted that due to the complexity of the model, the impact of the windows frame was neglected within the analysis. Besides, the convective heat transfer in the air gap was disregarded in the winter case for simulation.

$$Q_{in_{w\_SS}} = SHGC \times G_{tV} A_{w_{in}} - h_{conv_w}\left(T_w - T_{in}\right)A_{w_{in}} - U_w\left(T_{amb} - T_{in}\right)A_{w_{in}} \quad (26)$$

$$Q_{in_{w\_DS}} = SHGC \times G_{tV} A_{w_{out}} - h_{conv_w}\left(T_w - T_{amb}\right)A_{w_{out}} - \bar{h}_m\left(\bar{T}_w - T_{in}\right)A_{w_{out}} - U_w\left(T_{critical} - T_{in}\right)A_{w_{in}} \quad (27)$$

$$Q_{in_{wall\_SS}} = G_{tV} A_{wall} - h_{conv_{wall}}\left(T_{wall} - T_{in}\right)A_{wall} - U_{wall}\left(T_{amb} - T_{in}\right)A_{wall} \quad (28)$$

$$Q_{in_{Pv\_DS}} = \varepsilon_{Tedlar} F\sigma\left(T_{Tedlar}^{\ 4} - T_{amb}^{\ 4}\right)A_{PV} - h_{conv_t}\left(T_g - T_{amb}\right)A_{PV} - \bar{h}_m\left(\bar{T}_{Tedlar} - T_{in}\right)A_{wall} - U_{wall}\left(T_{critical} - T_{in}\right)A_{wall} \quad (29)$$

On the other hand, for the winter case, the effect of DSF was considered as an extra thermal-resistant layer, which would reduce the heat loss from the inner side to the outside which is a so-called blanket mode. Using Equations (30) and (31), the heat loss of the glass-based inner skin in the winter cases was obtained in single and double-façade conditions, respectively. Using Equations (32) and (33), the heat loss of the wall-based inner skin in the winter case was obtained for single and double-façade modes, respectively.

$$Q_{out_{w\_SS}} = \frac{1}{R_{w\_SS}}\left(T_{in} - T_{amb}\right)A_{w_{in}} \quad (30)$$

$$Q_{out_{w\_SS}} = \frac{1}{R_{w\_SS}}\left(T_{in} - T_{amb}\right)A_{w_{in}} \quad (31)$$

$$Q_{out_{wall\_SS}} = \frac{1}{R_{wall\_SS}}\left(T_{in}\text{-}T_{amb}\right)A_{wall} \quad (32)$$

$$Q_{out_{PV\_DS}} = \frac{1}{R_{PV\_DS}}\left(T_{in}\text{-}T_{amb}\right)A_{PV} \quad (33)$$

Finally, Equations (34) and (35) were used for calculation of cooling and the thermal load reduction in critical seasonal conditions in the summer and winter cases, respectively.

$$Q_{in} = \left(Q_{in_{w\_SS}} - Q_{in_{w\_DS}}\right) + \left(Q_{in_{wall\_SS}} - Q_{in_{PV\_DS}}\right) \quad (34)$$

$$Q_{out} = \left(Q_{out_{w\_SS}}\text{-}Q_{out_{w\_DS}}\right) + \left(Q_{out_{wall\_SS}}\text{-}Q_{out_{PV\_DS}}\right) \quad (35)$$

To analyze the thermal energy performance of the proposed BIPVT-DSF, computerized code was developed using Engineering Equation Solver (EES) software. The procedure for running the mentioned code consists of five main steps as follows:

- Calculation of heat rate from outer to inner skin by analyzing input weather data and constant parameters;
- Assuming a convective heat transfer coefficient for the backside of the outer façade and calculation of all relevant heat transfer parameters including Nusselt and Grashof numbers for the boundary layer;
- Evaluation of convergence for calculated convective heat transfer coefficient and resulting temperature and velocity profiles for glass and photovoltaic outer façades;
- Providing the temperature and velocity profile following continuity, momentum, and energy equations;
- Calculation of cooling load and thermal load reductions as well as the amount of energy saving.

As the most benefits of DSF depend on the geographical positioning and the climatological condition of the building, it is necessary to review the application of DSF according to the critical seasonal conditions. All input parameters of critical condition for the summer case as well as constant parameters relevant to the geometry of outer façade and physical properties are shown in Table 1.

Input parameters are given in Table 2 that include surface areas, overall heat transfer coefficients, thermal resistance values, and ambient and seasonal comfort temperatures. Simulation outputs are presented in the results and discussion section.

Table 1. Input parameters and weather information in the critical condition.

Parameter (unit)	Value
Acceleration due to gravity: g (m/s^2)	9.81
Absorptivity of PV module ethylen vinyl asetat (EVA) layer: α_{EVA}	0.03
Absorptivity of PV module glass layer: α_g	0.02
Absorptivity of PV module photovoltaic cell layer: α_{cell}	1
Absorptivity of PV module Tedlar layer: α_{Tedlar}	1
Ambient temperature: T_{amb} (°C)	40.4
Cavity depth: Δ (m)	0.3
Efficiency of the PV module at the standard test condition: η_{ref}	0.1496
Emissivity of PV module glass layer: ε_g	0.91
Emissivity of PV module Tedlar layer: ε_{Tedlar}	0.85
Length of outer façade for photovoltaic sections A, C & E: L (m)	0.53
Length of outer façade for photovoltaic sections B & D: L (m)	12.5
Length of outer façade for windows sections A, C & E: L (m)	2.37
Packing factor of PV module: K	0.9
Solar heat gain coefficient: SGHC	0.42
Solar total radiation on a vertical surface: G_{tV} (W/m^2)	619.2
Stefan–Boltzmann constant: σ ($W/m^2.K^4$)	5.67×10^{-8}
Temperature coefficient of PV module: β_{ref}	0.0045
Temperature of PV module at standard test condition: T_{ref} (°C)	25
Thermal conductivity coefficient of PV module ethylene vinyl acetate (EVA) layer: k_{EVA} (W/m.K)	0.35
Thermal conductivity coefficient of PV module glass layer: k_g (W/m.K)	1.8
Thermal conductivity coefficient of PV module Tedlar layer: k_{Tedlar} (W/m.K)	0.3
Thickness of PV module ethylene vinyl acetate (EVA) layer: l_{EVA} (m)	0.0004
Thickness of PV module glass layer: l_g (m)	0.004
Thickness of PV module Tedlar layer: l_{Tedlar} (m)	0.0003
Transmission coefficient of PV module ethylen vinyl asetat (EVA) layer: τ_{EVA}	0.97
Transmission coefficient of PV module glass layer: τ_g	0.88
View factor: F	0.5
Wind velocity: V_{wind} (m/s)	3.8
Solar total radiation on a vertical surface: G_{tV} (W/m^2)	619.2

Table 2. Input parameters for calculation of cooling and thermal losses.

Parameter (unit)	Value
Ambient temperature in critical condition of a summer case: T_{amb} (°C)	40.4
Ambient temperature in critical condition of a winter case: T_{amb} (°C)	-4.6
Comfort temperature set for a summer case: T_{in} (°C)	21
Comfort temperature set for a winter case: T_{in} (°C)	18
Single-façade overall heat transfer coefficient for glass inner skin: U_w ($W/m^2.K$)	1.95
Single-façade overall heat transfer coefficient for wall inner skin: U_{wall} ($W/m^2.K$)	0.95

Surface area for glass inner façade: A_{w_in} (m^2)	102.38
Surface area for glass outer façade: A_{w_out} (m^2)	102.38
Surface area for PV outer façade for sections A, C & E: A_{PV_2} (m^2)	20.29
Surface area for PV outer façade for sections B & D: A_{PV_1} (m^2)	39.75
Surface area for wall inner façade: A_{wall} (m^2)	60.04
Thermal resistance for single-façade glass inner skin in winter case: R_{w_SS} (m^2.K/W)	0.512
Thermal resistance for double-façade glass outer skin in winter case: R_{w_DS} (m^2.K/W)	1.2
Thermal resistance for double-façade PV outer skin in winter case: R_{PV_DS} (m^2.K/W)	1.236
Thermal resistance for single-façade wall inner skin in winter case: R_{wall_SS} (m^2.K/W)	1.05

3. RESULTS AND DISCUSSION

Initial obtained results include thermal properties, Nusselt and Grashof numbers, natural convection heat transfer coefficients, rendered spacing for the boundary layer, and velocity in the initial condition for glass and PV façades, and they are tabulated in Table 3.

Results must be analyzed for both summer and winter case applications. Given the system description of the studied case, DSF was considered as a chimney in the summer case and as a blanket in the winter case.

A comparison of temperature values for the outer façade of glass and PV-based skins showed that the glass façade had higher values than the PV façade. The other important factor is the natural convection heat transfer coefficient which is lower in PV parts than glass parts. Therefore, it is expected that the glass façade will have a higher impact on cooling load reduction. Due to the geometrical difference of three parts, the spacing of the boundary layer varies between 2.08 to 4.59 centimeters.

Table 3. Simulation obtained results for three different status of outer façade.

Parameter (unit)	Window (sections A, C & E)	Photovoltaic (sections A, C & E)	Photovoltaic (sections B & D)
Cavity depth: Δ (m)	0.241	0.234	0.234
Free convection heat transfer coefficient: $h_{conv,t}$ (W/m^2.K)	-	14.2	14.2
Glass based outer skin heat transfer rate: q_w (W/m^2)	260	-	-
Kinematic viscosity of air: γ (m^2/s)	0.0000186	0.0000185	0.0000186
Mean temperature for boundary layer between inner surface and cavity: T_f (°C)	61.2	52.57	52.77
Modified Grashof number for constant heat flux: Gr*	2.4888×10^{13}	2.7153×10^{10}	7.9893×10^{15}
Natural convection heat transfer coefficient: h_x (W/m^2.K)	5.49	3.57	3.68
Natural convection heat transfer coefficient for laminar or turbulent flow: h_m (W/m^2.K)	6.24	4.45	4.18
Nusselt number for laminar or turbulent flow: Nu_x	539.04	68.65	1666.54
Photovoltaic cell efficiency: η_{cell}	-	0.1229	0.1226
Prandtl number of air: Pr	0.721	0.7223	0.722
PV module Tedlar surface hear transfer rate: q_{Tedlar} (W/m^2)	-	108.32	103.38
Rendered spacing function based on initial and boundary conditions: δ (m)	0.0278	0.0208	0.0459
Sky temperature: T_{sky} (°C)	-	22.57	22.57
Temperature coefficient of thermal conductivity: β (1/K)	0.002991	0.00307	0.003068
Temperature of PV module bottom EVA layer: $T_{EVA,\,b}$ (°C)	-	64.77	65.15
Temperature of PV module glass layer: T_g (°C)	-	63.25	63.61
Temperature of PV module photovoltaic cell layer: T_{cell} (°C)	-	64.73	65.11
Temperature of PV module top EVA layer: $T_{EVA,\,t}$ (°C)	-	64.24	64.61
Temperature of PV module Tedlar layer: T_{Tedlar} (°C)	-	64.74	65.13
Temperature on the wall outside surface: T_{wall} (°C)	-	84	84
Temperature on the windows outside surface: T_w (°C)	82	-	-
Thermal conductivity coefficient: k (W/m.K)	0.02782	0.02757	0.02758
Velocity function for boundary conditions: U_0 (m/s)	6.18	2.12	10.32

To investigate the shape of temperature and velocity profiles for three sections of the outer façade, three and two-dimensional graphs were illustrated using EES software considering the initial cavity depth of 0.3 meter. Following the identification of the appropriate cavity depth, comparative integrated temperature and velocity profiles were demonstrated for inlet and outlet positions of each of three parts. Temperature and velocity profiles for glass and PV-based different sections of the outer façade are shown in Figures 2 to 7.

By comparing temperature and velocity profiles, it is understandable that both material and geometrical characteristics of the outer façade will have an impact on the thermal performance of DSF. As a meaningful result of the analysis, the maximum temperature at the outlet of a cavity will be reduced in the case of larger heights. However, the maximum velocity at the outlet of a cavity reduced at smaller heights. Given that temperature profiles and cavity depth have a significant impact on the thermal performance of a cavity, sensitivity analysis of these parameters must be investigated for analyzing the thermal energy performance of the retrofit solution.

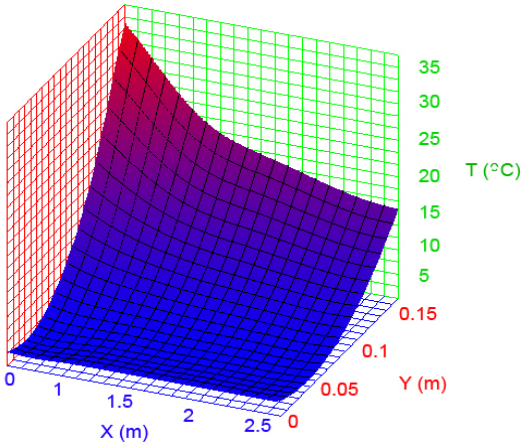

Figure 2. Temperature profile-sections A, C & E (glass).

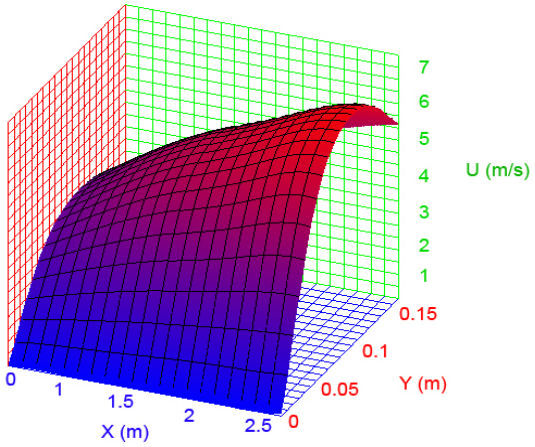

Figure 3. Velocity profile-sections A, C & E (glass).

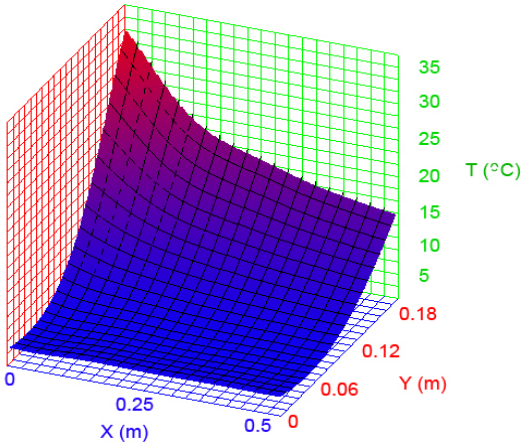

Figure 4. Temperature profile-sections A, C & E (PV).

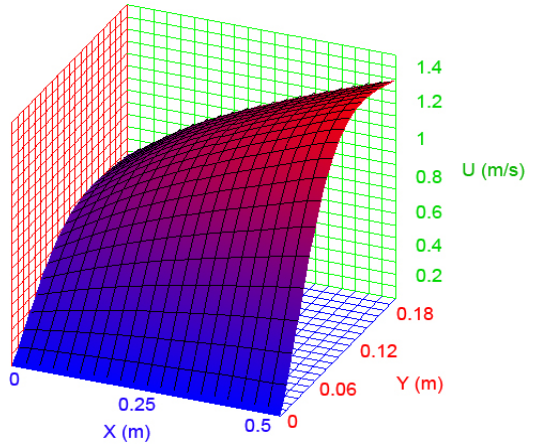

Figure 5. Velocity profile-sections A, C & E (PV).

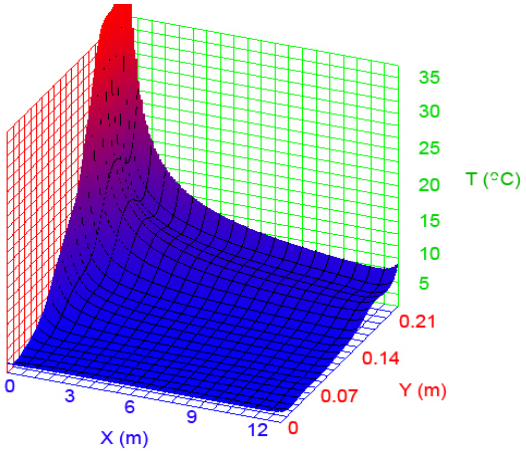

Figure 6. Temperature profile-sections B & D (PV).

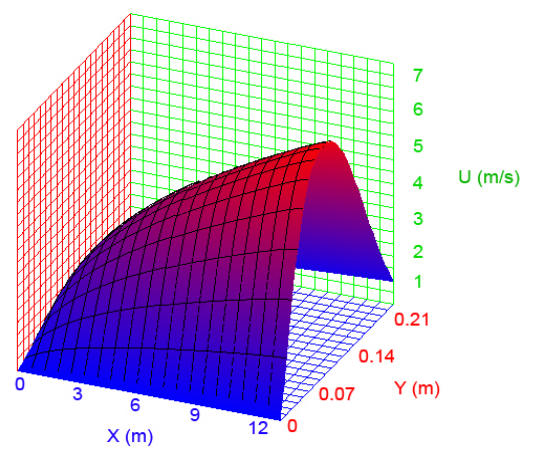

Figure 7. Velocity profile-sections B & D (PV).

According to the assumptions of this study, there are two temperature control strategies including:

- Temperature control on the inner side of the building as a comfort temperature protocol;
- Temperature control on the air gap between inner and outer façades.

For the first case strategy, it is assumed that the demand side will be responsible for keeping the comfort temperature as constant as possible. For the second case strategy, air temperature at skin spacing should be assumed to be at least 5 °C less than the ambient temperature for the summer case to prevent the crisis at the temperature profile through façades. Thus, it is required to investigate at what depth of the cavity will this crisis be averted for each of the outer façade modes. According to the simulation results, the temperature crisis occurs at a cavity depth of 8.35 centimeters at the inlet of the glass-based façade and at 9.37 centimeters, at the inlet of PV-based sections A, C, and E, and at 9.35 centimeters at the inlet of PV-based sections B and D. Simulation results show the appropriate cavity depth for glass-based and PV-based sections A, C, and E as well as the outer façades of sections B and D must be 21.65, 20.63 and 20.65 centimeters, respectively.

At the next step, comparative integrated temperature and velocity profiles were demonstrated for inlet and outlet positions in Figure 8.

A comparison of temperature and velocity profiles shows the proper application of DSF based on simulations. In accordance with the temperature profiles, outlet temperature reduced significantly in comparison to the inlet temperature in all cases, which led to less cooling load on mechanical or electrical devices due to natural cooling facilitated by the application of the outer façade. However, the effect of DSF was significant in sections B and D with the application of PV in terms of reduction in temperature, mainly due to the height of the outer wall. Although the results of the analysis for sections B and D are interesting, the effects of all elements on sections A, C, and E for glass-based and PV-based cases must be considered to properly conclude the results. This is because all the illustrated graphs are for one segment of each section.

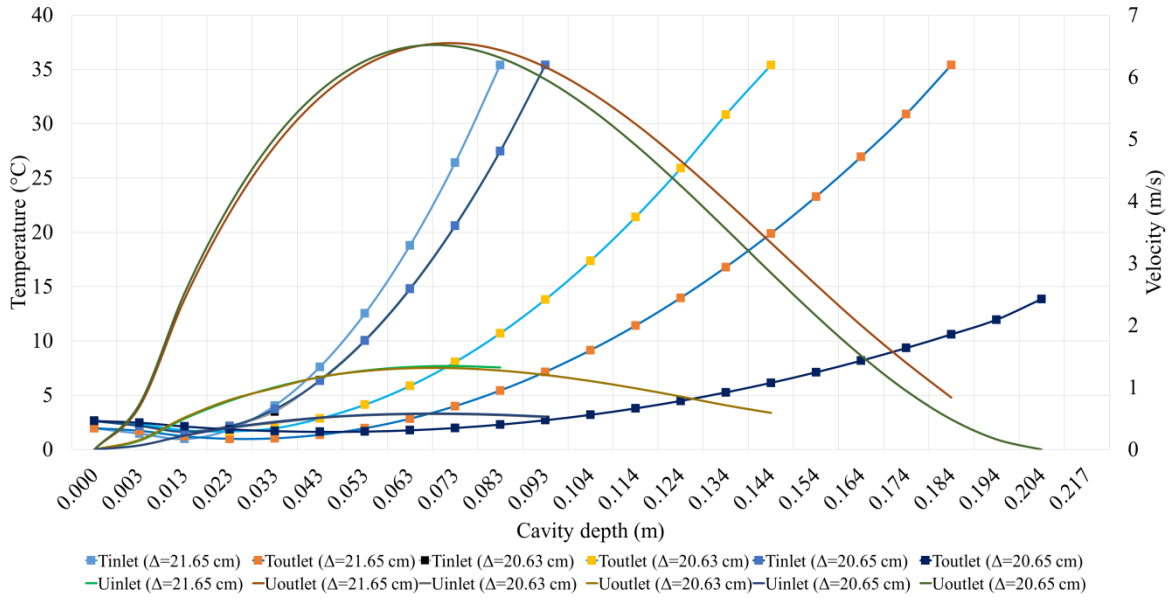

Figure 8. Temperature and velocity profiles for inlet and outlet of sections.

According to the results, DSF with the proposed configuration had a notable role in reducing the cooling demand and thermal load in the summer and winter cases by 18.5 kW and 2.79 kW, respectively, which were not considered in comparison to the summer case. In this respect, DSF had a significant effect on cooling load reduction by 8.7 percent and it managed to reduce the thermal load by 2.1 percent. All of the above results were provided with emphasis on the comfort temperatures of 21 and 18 °C for summer and winter, respectively.

In fact, there is a great potential for greater energy saving if comfort temperature set points would be adjusted as high as possible in the summer case and in reverse in the winter case. Table 4 shows the amount of cooling and thermal load reductions considering different comfort set points at a constant PV to glass façade surface ratio (58.6 %).

If the comfort indoor set point for summer cases varies between 18 and 24 °C, the total cooling load reduction will increase from 14.2 to 22.7 kW. In the winter case, if the comfort indoor set point varies between 15 and 21 °C, the total thermal load reduction will increase from 2.42 to 3.16 kW.

According to Table 4, the share of glass-based and PV-based façades on total cooling load reduction does not have a significant difference. However, the glass façade has by far greater impact on the reduction of the total thermal load than the PV façade. Besides, both glass and PV façades have a greater effect in summer cases compared to the winter case; however, the impact of the PV façade is more considerable in the summer case than that in the winter case.

The other important factor with a significant effect on cooling and thermal load reduction is the area ratio on the

outer façade which can be defined based on a variation of PV surface area divided by glass surface area. Table 5 demonstrates the effect of different area ratios on cooling and thermal load reduction.

Higher more area ratio results in a more significant reduction in the total cooling load and an insignificant decrease in the thermal load. However, slopes of cooling and thermal load reduction are significantly smaller than the area ratio. Of course, the application of more PV modules than a glass façade will result in a greater cooling load reduction at a constant comfort temperature (21 degrees Celsius). On the other hand, the application of more PV modules in comparison to the glass façade results in a lower thermal load reduction in the winter case.

Table 4. Cooling and thermal load reductions at different indoor temperature set points.

Inner side temperature (°C)	**15**	**18**	**21**	**24**
Cooling load reduction for windows section (kW)	-	7.36	9.81	12.3
Cooling load reduction for photovoltaic section (kW)	-	6.86	8.65	10.4
Total cooling load reduction (kW)	-	14.2	18.5	22.7
Thermal load reduction for windows section (kW)	2.25	2.6	2.94	-
Thermal load reduction for photovoltaic section (kW)	0.17	0.19	0.22	-
Total thermal load reduction (kW)	2.42	2.79	3.16	-
Inner side temperature (°C)	15	18	21	24
Cooling load reduction for windows section (kW)	-	7.36	9.81	12.3

Table 5. Cooling and thermal load reduction at different area ratios (photovoltaic to glass).

Photovoltaic area to windows area ratio (%)	**32.4**	**39.5**	**49.8**	**58.6**
Cooling load reduction for windows section (kW)	11.75	11.15	10.38	9.8
Cooling load reduction for photovoltaic section (kW)	5.73	6.63	7.78	8.65
Total cooling load reduction (kW)	17.47	17.78	18.16	18.46
Thermal load reduction for windows section (kW)	3.11	2.96	2.75	2.6
Thermal load reduction for photovoltaic section (kW)	0.13	0.15	0.17	0.19
Total thermal load reduction (kW)	3.24	3.1	2.93	2.79

4. CONCLUSIONS

The present study analyzed the thermal energy performance of the building integrated photovoltaic thermal double-skin façade (BIPVT-DSF) system using glass-based and photovoltaic-based façades as the outer façade for an existing building in Tehran city, located in the Middle East climate condition. To identify the amount of reduction in cooling and thermal loads through the suggested system, thermal performance analysis was conducted by using code development in EES software. The solution method was based on an analytical approach using heat transfer and thermodynamics phenomenon.

In accordance with the aim of this research study, a solution was provided using an analytical approach and the temperature and velocity profiles for different scenarios were investigated. The application of this approach led to analysis of the differences between glass-based and PV-based outer façades. Thus, the research team used the analysis results to compare the impact of glass-based and PV-based outer façades on cooling and thermal loads reduction and energy saving. According to the results, outlet temperature reduced significantly compared to the inlet temperatures in all of the reviewed cases.

Based on the quantitative results of the study, the proposed DSF had great impact on reducing cooling demand in the summer case by 18.5 kW reduction. However, the amount of thermal load reduction, i.e., 2.79 kW, in the winter case was not considerable. In doing so, DSF reduced cooling and thermal loads by 8.7 and 2.1 %, respectively.

Thereafter, the impact of variation of comfort indoor set points for the summer and winter cases with the application of BIPVT-DSF was reviewed. Finally, the effect of variation of PV to glass surface area on cooling and thermal load reduction was evaluated. Sensitivity analysis showed that both glass and PV façades had a greater impact in the summer case than those in the winter case. Additionally, the impact of the PV façade was more considerable in the summer case than that in the winter season. The building sector was considered as one of the key energy sectors in Iran with the Middle Eastern climate condition. Since Iran is facing a new challenge of the electricity demand peak load in the summer case, the suggested system can be considered within the process of building retrofit solution.

According to the results of this study, the proposed BIPVT-DSF system is an appropriate energy saving measure from the technical perspective mostly in the summer case. Therefore, if the government or the investors of the construction industry can consider the financial feasibility of this energy saving measure in their plans, it is worthwhile to apply this system to some parts of the existing buildings and some others for the new designs. Therefore, some part of the electricity demand in the summer case was reduced.

5. ACKNOWLEDGEMENT

This research was supported by the Iranian Fuel Conservation Company (IFCO). Authors appreciate colleagues of the research and development department as well as energy optimization at the building department who provided insight and expertise that assisted the research.

NOMENCLATURE

A_{PV}	Surface area for PV outer façade (m^2)
A_{w_in}	Surface area for glass inner façade (m^2)
A_{w_out}	Surface area for glass outer façade (m^2)
A_{wall}	Surface area for wall inner façade (m^2)
c_p	Specific heat at constant pressure (kJ/kg.K)
F	View factor
g	Acceleration due to gravity (m/s^2)
Gr*	Modified Grashof number for constant heat flux
G_{tV}	Solar total radiation on a vertical surface (W/m^2)
h_{conv}	Free convection heat transfer coefficient ($W/m^2.K$)
h_m	Natural convection heat transfer coefficient for laminar or turbulent flow ($W/m^2.K$)
$\bar{h}$	Average natural convection heat transfer coefficient ($W/m^2.K$)
k	Thermal conductivity coefficient (W/m.K)
K	Packing factor of PV module
L	Wall length for PV or windows as outer façade (m)
l	Thickness (m)
Nu_x	Nusselt number for laminar or turbulent flow
p	Pressure (kPa)
Pr	Prandtl number of air
Q_{in}	Cooling load reduction in critical temperature of summer case with the application of double façade (kW)
$Q_{in_{PV\_DS}}$	Double-façade heat loss for PV outer skin in summer case (W)
$Q_{in_{w\_DS}}$	Double-façade heat loss for glass outer skin in summer case (W)
$Q_{in_{w\_SS}}$	Single-façade heat loss for glass inner skin in summer case (W)
$Q_{in_{wall\_SS}}$	Single-façade heat loss for wall inner skin in summer case (W)
Q_{out}	Thermal load reduction in critical temperature of winter case with the application of double façade (kW)
$Q_{Out_{PV\_DS}}$	Double-façade heat loss for PV outer skin in winter case (W)
$Q_{Out_{w\_DS}}$	Double-façade heat loss for glass outer skin in winter case (W)
$Q_{Out_{w\_SS}}$	Single-façade heat loss for glass inner skin in winter case (W)
$Q_{Out_{wall\_SS}}$	Single-façade heat loss for wall inner skin in winter case (W)
q_{Tedlar}	PV module Tedlar surface hear transfer rate (W/m^2)
q_w	Glass-based outer skin heat transfer rate (W/m^2)
R_{PV_DS}	Thermal resistance for double-façade PV outer skin in winter case ($m^2.K/W$)
R_{w_DS}	Thermal resistance for double-façade glass outer skin in winter case ($m^2.K/W$)
R_{w_SS}	Thermal resistance for single-façade glass inner skin in winter case ($m^2.K/W$)
R_{wall_SS}	Thermal resistance for single-façade wall inner skin in winter case ($m^2.K/W$)
SHGC	Solar heat gain coefficient
T	Temperature (°C or K)
T (x, y)	Two-dimensional temperature profile (°C)
T_{amb}	Ambient temperature (°C)
T_f	Mean temperature for boundary layer between inner surface and cavity (°C or K)
T_{in}	Comfort temperature set for summer or winter case (°C)
T_{ref}	Temperature of PV module at standard test condition (°C)
T_{sky}	Sky temperature (°C or K)
u	velocity (x coordinate) (m/s)
U (x, y)	Two-dimensional velocity profile (m/s)
U_0	Velocity function for boundary conditions (m/s)
U_w	Single-façade overall heat transfer coefficient for glass inner skin ($W/m^2.K$)
U_{wall}	Single-façade overall heat transfer coefficient for wall inner skin ($W/m^2.K$)
V_{wind}	Wind velocity (m/s)
x, y	Coordinates in the Cartesian system (m)

Greek letters

α	Absorptivity
β	Temperature coefficient of thermal conductivity (1/K)
β_{ref}	Temperature coefficient of PV module
γ	Kinematic viscosity of air (m^2/s)
Δ	Cavity depth (m)
δ	Rendered spacing function based on initial and boundary conditions (m)
ε	Emissivity of PV module glass surface
η_{cell}	Photovoltaic cell efficiency
η_{ref}	Efficiency of the PV module in the standard test condition
μ	Dynamic viscosity of air (kg/m.s)
ρ	Density of air (kg/m^3)
σ	Stefan–Boltzmann constant ($W/m^2.K^4$)
τ	Transmission coefficient
ν	velocity (y coordinate) (m/s)

Subscripts

cell	PV module cell
DS	Double skin
EVA, b	PV module bottom EVA layer
EVA, t	PV module EVA top layer
g	PV module glass
PV	Photovoltaic panel
SS	Single-skin
Tedlar	PV module Tedlar back sheet
w	Building windows façade
wall	Building wall façade

REFERENCES

1. Lai, C. and Hokoi, S., "Solar façades: A review", ***Building and Environment***, Vol. 91, (2015), 152-165. (https://doi.org/10.1016/j.buildenv.2015.01.007).
2. Agathokleous, R.A. and Kalogirou, S.A., "Double skin facades (DSF) and building integrated photovoltaics (BIPV): A review of configurations and heat transfer characteristics", ***Renewable Energy***, Vol. 89, (2016), 743-756. (https://doi.org/10.1016/j.renene.2015.12.043).
3. Darkwa, J., Li, Y. and Chow, D.H.C., "Heat transfer and air movement behaviour in a double-skin façade", ***Sustainable Cities Society***, Vol. 10, (2014), 130-139. (https://doi.org/10.1016/j.scs.2013.07.002).
4. Kant, K., Shukla, A., Sharma, A. and Biwole, P.H., "Thermal response of poly-crystalline silicon photovoltaic panels: Numerical simulation and experimental study", ***Solar Energy***, Vol. 134, (2016), 147-155. (https://doi.org/10.1016/j.solener.2016.05.002).
5. Atkin, P. and Farid, M.M., "Improving the efficiency of photovoltaic cells using PCM infused graphite and aluminum fins", ***Solar Energy***, Vol. 114, (2015), 217-228. (https://doi.org/10.1016/j.solener.2015.01.037).
6. Lai, C. and Chen, R.H., "Novel heat dissipation design incorporating heat pipes for DC combiner boxes of a PV system", ***Solar Energy***, Vol. 85, No. 9, (2011), 2053-2060. (https://doi.org/10.1016/j.solener.2011.05.013).
7. Kant, K., Shukla, A., Sharma, A. and Biwole, P.H., "Heat transfer studies of photovoltaic panel coupled with phase change material", ***Solar Energy***, Vol. 140, (2016), 151-161. (https://doi.org/10.1016/j.solener.2016.11.006).
8. Elarga, H., Goia, F., Zarrella, A., Dal Monte, A. and Benini, E., "Thermal and electrical performance of an integrated PV-PCM system in double skin façades: A numerical study", ***Solar Energy***, Vol. 136, (2016), 112-124. (https://doi.org/10.1016/j.solener.2016.06.074).
9. Zogou, O. and Stapountzis, H., "Energy analysis of an improved concept of integrated PV panels in an office building in central Greece", ***Applied Energy***, Vol. 88, No. 3, (2011), 853-866. (https://doi.org/10.1016/j.apenergy.2010.08.023).
10. Rabani, R., Faghih, A.K., Rabani, M. and Rabani, M., "Numerical simulation of an innovated building cooling system with combination of solar chimney and water spraying system", ***Heat and Mass Transfer***,

Vol. 50, No. 11, (2014), 1609-1625. (https://doi.org/10.1007/s00231-014-1366-5).

11. Corbin, C.D. and Zhai, Z.J., "Experimental and numerical investigation on thermal and electrical performance of a building integrated photovoltaic-thermal collector system", ***Energy and Buildings***, Vol. 42, No. 1, (2010), 76-82. (https://doi.org/10.1016/j.enbuild.2009.07.013).
12. Shakouri, M., Golzari, S. and Zamen, M., "Energy and exergy optimization of water cooled thermal photovoltaic (PV/T) system using genetics algorithm", ***Journal of Solar Energy Research***, Vol. 1, No. 1, (2016), 45-51.
13. Shakouri, M., Noorpoor, A., Golzari, S. and Zamen, M., "Energy simulation and parametric analysis of water cooled photovoltaic/thermal system", ***Amirkabir Journal of Mechanical Engineering***, Vol. 50, No. 6, (2018), 435-438. (https://doi.org/10.22060/mej.2017.12703.5402).
14. Pantic, S., Candanedo, L. and Athienitis, A.K., "Modeling of energy performance of a house with three configurations of building-integrated photovoltaic/thermal systems", ***Energy and Buildings***, Vol. 42, No. 10, (2010), 1779-1789. (https://doi.org/10.1016/j.enbuild.2010.05.014).
15. Cappelletti, F., Prada, A., Romagnoni, P. and Gasparella, A., "Passive performance of glazed components in heating and cooling of an open-space office under controlled indoor thermal comfort", ***Building and Environment***, Vol. 72, (2014), 131-144. (https://doi.org/10.1016/j.buildenv.2013.10.022).
16. Serra, V., Zanghirella, F. and Perino, M., "Experimental evaluation of a climate facade: energy efficiency and thermal comfort performance", ***Energy and Buildings***, Vol. 42, No. 1, (2010), 50-62. (https://doi.org/10.1016/j.enbuild.2009.07.010).
17. Ghadimi, M., Ghadamian, H., Hamidi, A.A., Shakouri, M. and Ghahremanian, S., "Numerical analysis and parametric study of the thermal behavior in multiple-skin façades", ***Energy and Buildings***, Vol. 67, (2013), 44-55. (https://doi.org/10.1016/j.enbuild.2013.08.014).
18. Fuliotto, R., Cambuli, F., Mandas, N., Bacchin, N., Manara, G. and Chen, Q., "Experimental and numerical analysis of heat transfer and airflow on an interactive building façade", ***Energy and Buildings***, Vol. 42, No. 1, (2010), 23-28. (https://doi.org/10.1016/j.enbuild.2009.07.006).
19. Kuznik, F., Catalina, T., Gauzere, L., Woloszyn, M. and Roux, J., "Numerical modelling of combined heat transfers in a double skin façade full-scale laboratory experiment validation", ***Applied Thermal Engineering***, Vol. 31, No. 14-15, (2011), 3043-3054. (https://doi.org/10.1016/j.applthermaleng.2011.05.038).
20. Mulyadi, R., Yoon, G. and Okumiya, M., "Study on solar heat gain and thermal transmittance of east and west-facing double-skin façade in hot and humid climate", ***AIJ Journal of Technology and Design***, Vol. 18, No. 40, (2012), 989-994. (https://doi.org/10.3130/aijt.18.989).
21. Hoseinzadeh, S., Zakeri, M.H., Shirkhani, A. and Chamkha, A.J., "Analysis of energy consumption improvements of a zero-energy building in a humid mountainous area", ***Journal of Renewable and Sustainable Energy***, Vol. 11, No. 1, (2019). (https://doi.org/10.1063/1.5046512).
22. Hoseinzadeh, S., "Thermal performance of electrochromic smart window with nanocomposite structure under different climates in Iran", ***Micro and Nanosystems***, Vol. 11, No. 2, (2019), 154-164. (https://doi.org/10.2174/1876402911666190218145433).
23. Hoseinzadeh, S. and Azadi, R., "Simulation and optimization of a solar-assisted heating and cooling system for a house in Northern of Iran". ***Journal of Renewable and Sustainable Energy***, Vol. 9, No. 4, (2017). (https://doi.org/10.1063/1.5000288).
24. Yousef Nezhad, M.E. and Hoseinzadeh, S., "Mathematical modelling and simulation of a solar water heater for an aviculture unit using MATLAB/SIMULINK", ***Journal of Renewable and Sustainable Energy***, Vol. 9, No. 6, (2017). (https://doi.org/10.1063/1.5010828).
25. Ghadamian, H., Ghadimi, M., Shakouri, M., Moghadasi, M. and Moghadasi, M., "Analytical solution for energy modeling of double skin façades building", ***Energy and Buildings***, Vol. 50, (2012), 158-165. (https://doi.org/10.1016/j.enbuild.2012.03.034).
26 Holman, J.P. and White, P.R.S., Heat transfer, 7th Ed., McGraw-Hill, UK, (1992).
27. Incoropera, F.P. and DeWitt, D.P., Fundamentals of heat and mass transfer, 3rd Ed., New York, John Wiley & Sons, (1990).
28. Abdel-Khalik, S.I., "Heat removal factor for a flat-plate solar collector with a serpentine tube", ***Solar Energy***, Vol. 18, No. 1, (1976), 59-64. (https://doi.org/10.1016/0038-092X(76)90036-0).
29. Hammami, M., Torretti, S., Grimaccia, F. and Grandi, G., "Thermal and performance analysis of a photovoltaic module with an integrated energy storage system", ***Applied Sciences***, Vol. 7, No. 11, (2017). (https://doi.org/10.3390/app7111107).
30. Santbergen, R., Rindt, C.C.M., Zondag, H.A. and Van Zolingen, R.J.Ch., "Detailed analysis of the energy yield of systems with covered sheet and tube PVT collectors", ***Solar Energy***, Vol. 84, No. 5, (2010). 867-878. (https://doi.org/10.1016/j.solener.2010.02.014).

JREE: Vol. 7, No. 3, (Summer 2020) 67-79

Journal of Renewable Energy and Environment

Review Article

Journal Homepage: www.jree.ir

Assessing Economic, Social, and Environmental Impacts of Wind Energy in Iran with Focus on Development of Wind Power Plants

Hasan Hekmatnia[a], Ahmad Fatahi Ardakani[b*], Armin Mashayekhan[c], Morteza Akbari[d]

[a] *Department of Geography & Urban Planning, Payam Noor University, Iran.*
[b] *Department of Agricultural Economics, Faculty of Agriculture & Natural Resources, Ardakan University, P. O. Box: 184, Ardakan, Iran.*
[c] *Shirvan Higher Education Complex, Ferdowsi University of Mashhad (FUM), Mashhad, Iran.*
[d] *Department of Desert Area Management, Faculty of Natural Resources and Environment, Ferdowsi University of Mashhad (FUM), Mashhad, Iran.*

PAPER INFO

Paper history:
Received 15 March 2020
Accepted in revised form 18 July 2020

Keywords:
Renewable Energy,
Environmental Pollution
Wind Power Plant
Global Warming
Iran

ABSTRACT

As a key economic element, energy plays an important role in the development of societies. Economic growth and its urgent need for energy highlight the need for optimal energy use. Wind energy is an energy source that has become an increasingly common source of electricity. In this study, socio-economic impacts of the cost of electricity generated by wind power plants were assessed with Iran as the focus of this study. The environmental impacts of wind energy were also considered by reviewing and analyzing research papers. Studies showed that although the use of wind energy in Iran began in Manjil in northern Iran, no significant progress has been made in this field despite all the efforts over the past years. The results indicated that the initial cost of launching wind turbines was the most important factor in the failure of this technology. The costs of purchasing turbines, construction of roads, provision of electrical infrastructure, project management, installation of turbines, insurance premiums, grid connections, and power lines were shown to affect costs of energy production. Furthermore, operation and maintenance costs, the choice of installation location, increasing production capacity, expansion of the energy market, and policies in the country can play an essential role in determining the cost of wind energy production. Given that power generation using wind turbines are economical, it is recommended that turbines be installed in suitable windy locations. In addition, considering that one of the crises facing the world and especially Iran is environmental pollution, utilizing energies such as wind energy for generating electricity is advised due to their lower pollutant emissions and lower economic and social costs.

1. INTRODUCTION

Globally, the wind power industry has been growing at a staggering rate of nearly 30 % per year for the last 10 years. The major portion of this development is occurring in European, North American, and Asian markets. Such worldwide success has put exceptional pressure on the manufacturers of wind turbine components such as towers, rotor blades, gearboxes, bearings, and generators. In general, wind turbine components are large and heavy and their production process is complex and has long production cycles. These attributes are reflected clearly in the supply chain processes [1].

Even though wind power is more expensive than other forms of renewable power generation, using wind energy reduces the exposure of countries' economies to fuel price volatility. This risk reduction is presently not accounted for by the standard methods used by experts when calculating the costs of energy production. However, wind power is shown to be a long-term investment if public authorities calculate energy costs while taking risk reduction costs into account [2].

Today, issues such as climate change, rising fuel costs, security of energy supply, conflicts over oil and water, pollution, and other environmental crises are very common [3]. Annually, there are numerous conventions and agreements on energy use. In recent decades, increasing population and the rising demand for energy as well as fear of fossil fuel depletion have underlined the importance of paying attention to new and renewable energies. As a result, application of renewable energies is hailed as one of the most important methods of demand reduction and crisis management in the field of energy [4, 5, 6].

Energy and environment are highly interconnected [7] because energy is generated through the environment and can have a negative effect on it. Raising awareness of the impact of human activities on the natural environment leads to the sustainable use and conservation of energy [8]. Energy sources can be divided into three main groups including fossil fuels (oil, gas and coal), nuclear energy, and renewable energies (wind, solar, geothermal, hydroelectric, and biogas) [9, 10]. Studies show that fossil fuel reserves are limited; globally, more than 11 billion tons of fossil fuels are consumed every year [11, 12, 13]. Meanwhile, oil reserves are consumed at a rate of 4 billion tons per year. The exhaustion of fossil fuels in the near future has necessitated the use of renewable energies [14, 15, 16]. Renewable energies do not cause pollution and environmental degradation associated with fossil fuels, and nuclear energy is unlimited [17, 18].

Since ancient times, people have used wind energy. More than 5,000 years ago, ancient Egyptians used the wind to navigate their ships the Nile. Later, people used wind energy to grind wheat. The first windmills were built in Iran. Several centuries later, the people of the Netherlands improved the initial design of this windmill. The wind energy market is a

*Corresponding Author's Email: fatahi@ardakan.ac.ir (A. Fatahi Ardakani)

more competitive market than fossil fuel plants. Electricity produced by wind power offers new benefits to nearby people and industries. In addition, efforts have been made by various countries to generate electricity using wind energy [19, 20, 21, 22, 23].

Due to its geographical and climatic variety, Iran has undertaken the Five-Year Plan for Economic, Social and Cultural Development at the national level. In the energy sector the use of new and renewable energies is emphasized [24, 25] through 10,598 MW of renewable power plants (hydro, wind, solar, and biogas) to generate electricity as well as photovoltaic systems with a capacity of 584 KW and production of 40 MWh. Renewable energy has a rich potential for creating jobs in many parts of Iran through construction, installation, and repair of large and small turbines and plants. Further, the rising global concerns about energy insecurity and climate change have created a strong export potential for renewable energy technologies.

Being diverse in geography, Iran is a suitable country for extensive use of renewable energy sources [26]. The use of new energies in Iran and others, which have the potential to be the pioneers of utilizing new energy technologies, can be highly advantageous [27]. In this regard, identification of suitable areas and potential evaluation of wind energy production in the country have become unavoidable necessities for policymakers and planners [28, 29]. Various studies on this issue have been carried out or are under consideration, investigating the development of wind power plants, cost-effectiveness wind energy, its environmental and social impacts, etc. [30].

New Energy Deputy of Ministry of Energy and the Office of Wind and Wave of Iran's New Energy Organization are responsible for the development and implementation wind energy initiatives. The activities of organizations include potential assessment, preparation of the country's wind atlas, promoting and planning the implementation of plans to harvest wind energy, installing wind monitoring stations to study feasibility of building wind farms, and design management. The organizations also installed wind turbines in Manjil, Dizbad (Khorasan Razavi Province in eastern Iran) and Bojnourd (North Khorasan Province in northeastern Iran) and cooperate with the Global Environmental Facility Fund to develop wind power plants and identify the associated challenges [30, 31, 32].

Recently, there has been a dramatic increase in the investment of governments and the private sector in research and development of renewable energies. A variety of new technologies are also available for use in renewable energies, which has reduced the cost of generating electricity using renewable sources and has made renewable energies more competitive than traditional power generation systems [33, 34]. At present, the cost of generating electricity using some renewable sources, such as wind energy, is competitively better than that of fossil fuels [35]. Therefore, it is necessary for Iran to make further progress in this regard.

The growing economies of Asian countries, including Iran, have increased electricity demand of these countries and encouraged them to start generating electricity from non-fossil sources. The lack of a nationwide power network in many Asian countries has also increased the use of wind power systems for power generation in villages. Using wind energy in Iran has conserved oil products, helped preserve the environment, and reduced environmental pollution, along with providing sustainable social and economic development. Wind energy is essential to increasing household income in Iran. Also, access to electricity generated by wind energy is one of the key services with the largest poverty-reducing potential. While the annual electricity consumption per capita in EU27 countries averages 6,000 KWh, it is only 3,000 KWh in Iran [36].

In this study, reliable sources have been consulted on the important factors influencing the process of power generation using wind energy and its environmental impacts. In addition, experts' opinions have been also consulted. Valid scientific websites and scholarly references were included in the research, as well.

2. END OF FOSSIL FUELS

Currently, the major portion of the world's energy comes from fossil fuels [37, 38]. Therefore, due to the depletion of fossil fuels in the near future and increased energy consumption, concerns have been raised for its replacements [39]. Supplying energy for the next generations will be a major challenge [40, 41]. In 2030, global energy consumption will have doubled. Global demand for energy between 2000 and 2030 will increase by 1.8 % annually [42]. Currently, the question is whether fossil fuels will meet the global energy needs for survival and development in the next century.

Studies show that the expected life span of underground energy sources will not last for more than a hundred years on average, hence paying attention to alternative sources is necessary [43]. An increase in per capita demand and population growth have led to more pressure on natural resources. These resources include surface and underground water, clean air, and natural landscapes. According to the World Health Organization, 2.4 million people die each year due to air pollution. Demand for energy will affect the quality and quantity of non-renewable natural resources through the environmental damage caused by mining, depletion of underground aquifers due to excessive use, and degradation of surface soil which can lower crop yields and impact public health. Many environmental issues related to energy are associated with climate change, which is mainly the result of fossil fuel consumption and its direct impact on greenhouse gas emissions. In recent years, there has been an increasing trend in various commercial sources of renewable energy [44, 45, 46].

3. THE NEED TO DIVERSITY THE ENERGY SECTOR

Supplying energy in a country like Iran requires accurate and scientific planning. However, what has happened in practice is provision of energy as mainly oil and natural gas. In the past, more than 95 percent of the country's energy sector consisted of these two sources [47]. Change in energy sector of the country in recent years and the replacement of oil with gas have led to the ongoing development of the country's natural gas transmission network. In 2011, natural gas consumption in Iran increased by 6 % compared to 2010 [48]. The diversification of the energy sector with a move towards renewable energies has been the target in developed countries [49, 50]. Disturbances in the natural gas production system will affect the entire energy supply system, in turn causing political and social crises, even in the short term [51].

In the global energy basket, the role of renewable energies has been expanding, leading the global energy sector to move towards diversification and use of indigenous energy sources

[52]. In this regard, the European Union adopted a plan on January 23, 2008 whereby the share of renewable energies will reach 20 % in the average basket of member states by 2020 [53, 54, 55].

The use of energy is strongly linked to various social issues such as poverty reduction, population growth, urbanization, and opportunities for women. Poverty is the most important social concern for developing countries and one of the main threats to political stability in many countries. About 1.3 billion people in developing countries live on less than $1 a day. Although income is the only indicator used to measure the inferior social conditions of poor people, their energy use patterns, i.e., their dependence on traditional fuels, have also contributed to their poverty. Consequently, increasing income through energy production, employment, access to safe drinking water, and diminished need to collect fuel are the social benefits of generating energy from renewable sources [56].

Although it is generally accepted that population growth contributes to increasing energy demand, broadly speaking, access to appropriate energy services can reduce birth rates. Energy services can change the relative costs and benefits of childbearing toward the reduction of the desired number children in a family. Achieving low mortality and fertility (as is the case in industrialized countries) depends on realizing the vital goals of development including improving the local environment, training women, and decreasing extreme poverty [56, 57, 58].

4. STATUS OF RENEWABLE WIND ENERGY IN THE WORLD

In recent years, the global average annual growth of wind energy has been reported to be around 30 %, which is the highest growth rate among energy sources [59]. At present, the global wind energy market is dominated by China, United States, Germany, Spain, and India, which all have a production capacity of over 1 GW per year. The following table shows the capacity of wind farms in some of the leading countries in this industry (see Tables 1 and 2).

Table 1. Capacity of wind turbines during 2002-2018 (GW) [59].

Year / Country	2002	2004	2006	2008	2010	2018	Percent of total 2018
China	0.46	0.76	2.59	12.21	42.28	216.87	40.67
United States	4.68	6.72	11.60	25.17	40.18	96.36	18.07
Germany	12	16.62	20.62	239.02	27.21	59.31	11.12
Spain	4.83	8.26	11.63	16.74	20.67	23.41	10.64
India	1.70	3	6.27	9.58	13.06	35.01	6.56
Iran	0.02	0.04	0.06	0.08	0.21	0.70	0.13
World	31.18	47.69	74.12	120.02	194.39	533.12	100

Table 2. Power generated using wind by the top countries in 2017 (TWh) [82].

No.	Country	Wind power generation (TWh)
1	China	305
2	United States	257
3	Germany	106
4	United Kingdom	50
5	Spain	49.1
6	India	47.7
7	Brazil	42.3
8	Canada	28.8
9	France	24.7
10	Turkey	17.9
11	Iran	16

5. INSTALLATION CAPACITY AND CAPACITY FACTOR FOR WIND TURBINE PRODUCTION IN THE WORLD

A report released by World Wind Energy Association in February 2010 which includes wind energy development figures in more than 91 countries shows that the global installation rate reached 19.919 GW in 2010, which means the total installation capacity increased from 1207 GW in 2008 to 1585 GW in 2010. Since wind speed is not constant, the actual annual energy output of a wind generator is not equal to the value of the generator's generating capacity multiplied by the hours [60]. The ratio of actual production in one year to the theoretical maximum is called the capacity factor [61, 62]. A

generator located in a very favorable area will have a capacity ratio of about 35 % due to the changing nature of the wind [63].

The capacity factor of other types of power generation sources is dependent on parameters such as fuel cost and the time required for maintaining and supplying the system [64, 65]. Nuclear fuel plants have low fuel costs; in most cases, they work at their maximum capacity and, therefore, have a capacity factor of over 90 % [66]. Fuel-fired power plants are controlled by a steam valve to estimate and keep track of the required load. According to a report released by Stanford University in 2007, connecting 10 or more wind farms in a wide geographic area hardly allows for one-third of the total produced energy to be calculated as a base load [67].

Using storage systems such as pump storage or other types of storage will result in a 25 % increase in wind farm costs, but seem to be necessary to ensure reliable load [68]. Storage of electrical energy effectively balances the lower cost of electricity at times of high production and low demand with the higher cost at times of high demand and low production. The potential income from this compromise should balance the costs of installing and operating storage systems.

Electric power consumption can be coordinated with production changes using tools such as energy management and smart metering tools. This creates a variable electric energy pricing system at different hours of the day. For example, urban water pumps that feed water towers do not need to work continuously and at all hours; therefore, their operation hours can be limited to when electrical energy is abundantly available at low cost. Consumers can also choose the right time to use electrical tools.

Currently, the use of wind pumps in the US is increasing. Many lands in arid and semi-arid areas are irrigated using such pumps. At a wind speed of 24 km/h, a wind pump with a diameter of 3.6 m can produce 0.16 horsepower. This amount of energy can easily raise 159 L of water per minute to a height of 8.7 m. Research by UNESCO has shown that in arid areas, mills with a diameter of 15 m can produce 100,000 KWh of electricity per year at a wind speed of 20 km/h, which can be used for water heaters, pumps, and other uses in a unit of 100,000 people. In Denmark, wind turbines with a diameter of 54 m installed on 53-meter towers can generate 2 MW of electricity at a wind speed of 15 m/s [69, 70].

6. FUTURE PERSPECTIVES AND GLOBAL APPROACH TOWARD USING WIND POWER PLANTS TO GENERATE ELECTRICITY

The objectives and policies of different countries to provide electricity using wind energy in the coming years are as follows: Germany plans to generate 30 % of its electricity through constructing 54 GW worth of wind farms by 2030. The United States plans to meet 6 % of its electricity demand in 2020 by installing 100 GW worth of wind farms. The United Kingdom will supply 20 % of the country's electricity by generating additional 15 GW of energy by 2020. Japan plans to install 11.8 GW of wind power plants by 2030. Australia will generate 20 % of its electricity by wind farms in 2040. Brazil will supply 10 % of its electricity by constructing wind farms by 2022. China will build a 20 GW power plant by 2020 [71, 72, 73, 74].

7. HISTORY OF WIND ENERGY TECHNOLOGY RESEARCH IN IRAN

Iran was the first country to use wind energy for agriculture 2,500-3,000 years ago. The use of wind energy then spreads to other Islamic countries and Europe. The Americas and other parts of the world also used wind energy for various purposes such as water pumping and irrigation, milling of cereals, electricity generation, and mechanical applications such as sawing wood and making handicrafts. In the 14th century, the Netherlands was the most advanced country in this field and used wind energy for irrigation, but in 1890 Denmark was the first country to use wind energy for electricity generation using a wind turbine. Currently, Iran is well positioned in the region to build wind turbines. The 28.3 MW wind power plant in Binalood Heights in Dizbad area is one of the operational wind farms in Iran. In addition, the 120-day winds of Sistan in eastern Iran and the wind in Manjil and Kahak in Qazvin can be harnessed to generate electricity [75, 76].

Due to the existence of windy areas, design and manufacturing of windmills have been common in Iran since 2000 BC. Similarly, there is a good potential for expanding the use of wind turbines at present. Wind power generators can be a good alternative to gas and steam generators. Studies and calculations to estimate the potential of wind energy in Iran show that in 26 regions of the country, spanning more than 45 sites, the nominal capacity of sites with a total efficiency of 33 % is about 6,500 MW.

Iran has diverse climates and this diversity can be seen when comparing different parts of the country [77]. Iran is surrounded by high mountains on every side and is located between warm regions in the south and temperate regions in the north at the junction of atmospheric streams between Asia, Europe, Africa, the Indian Ocean, and the Atlantic Ocean. The effects of various factors on a given region determine the climate of that region, each factor making a unique contribution to climatic conditions. These factors include latitude (i.e., the distance from the equator and the north and south poles), elevation, topography, the presence of large bodies of water, air pressure and circulation, winds, and precipitation.

Mountainous terrain, the presence of large bodies of water in the north and south, the distance of central regions from open seas, distance from the vast plains of Asia, and the presence of high mountains around and within the country have made Iran a unique country where different climates can be seen. In winter, Iran is exposed to winds that blow from the Atlantic Ocean and Central Asia. In summer, winds originating from Iceland and Scandinavia enter Iran from the northwest and winds rising from the Indian Ocean blow from the south [78, 79, 80].

7.1. Capacity of installed wind turbines

Wind energy can be a suitable source of power generation in eastern Iran. In a new study on wind potential, 45 experimental areas were investigated. The future potential capacity was estimated at 6,500 MW. The installed capacity is currently only 11 MW, compared to 69 MW in Egypt and 54 MW in Morocco [81]. Wind farms have been established in several provinces in Iran to record data on wind potential and determine the true potential of wind energy in Iran. A total of 16 stations can be found in Gilan, West Azarbaijan, East Azarbaijan, and Ardabil.

A 600 KW wind turbine was built in Babian village, Gilan province. This area has a wind potential of 100 MW. The region's average wind speed at 40 m above ground is about 10

m/s. A total of 1250 KW/m^2. y of energy is produced in this area. Considering its potential and its efficient wind patterns, this area is one of the most suitable areas for installing wind turbines. The experimental wind turbine is a 40 m horizontally mounted turbine with an axle to gearbox configuration. A 20-KW electric power transmission line and a power station is installed to transfer the power generated by the wind turbines. The total capacity of the 1723 wind turbines (660-KW turbines) in Manjil, Herzowil, and Siahpush sites in Gilan province in northern Iran was about 46.24 MW from 2003 to 2007. The capacity of the wind farm installed in the Binalood site in Khorasan province with twenty-three 660-KW turbines was about 28.4 MW from 2006 to 2007 [82].

At the end of 2011, Iran's total installed wind capacity was 93 KW. Over the last two years, only 3 MW has been added to the country's installed capacity, which is considerably behind the government's target of 500 MW by 2009. According to the Iranian ministry of energy, wind power generated around 220 GWh of electricity in 2010. In addition, the Iranian government set a new target of 1.5 GW by the end of 2013, which is much higher than the current statistics. The following table illustrates the total installed capacity in Iran between 2002 and the end of 2011 (Table 3) [83].

Table 3. Potential of wind energy in Iran [83].

Description	Value
Average wind power density (w/m^2)	150
Total wind potential (MW)	152000
Covered area (km^2)	145138
Potential for wind power development (MW)	142000
Available technical potential (MW)	30000-40000

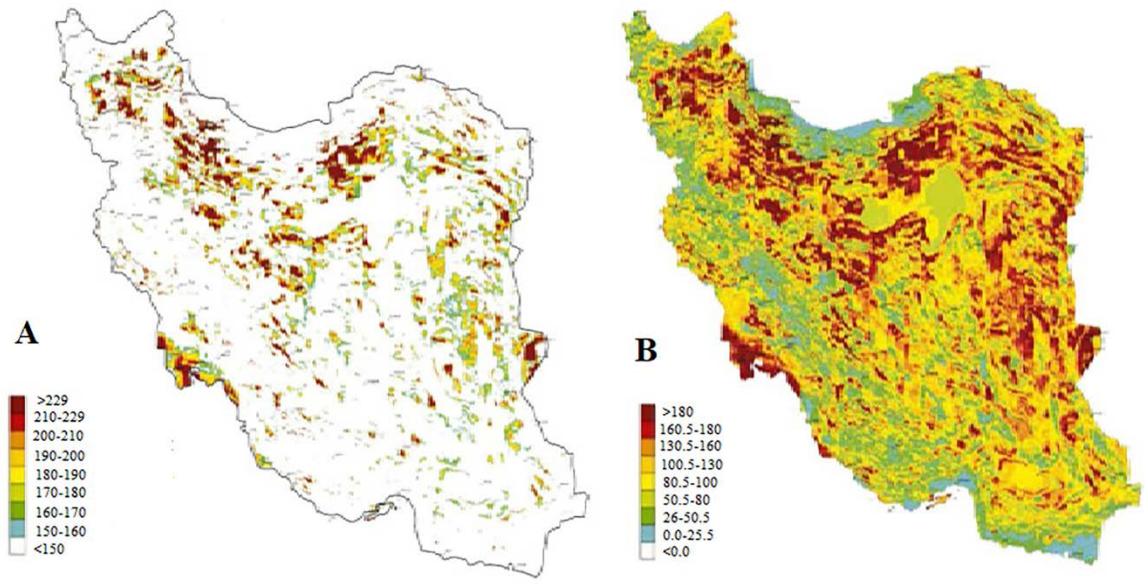

Figure 1. Regions with wind energy greater than 150 W/m^2 at 60 m above ground (A) and wind energy density at 60 m (B) [83].
Note that Figures 1A and 1B show regions with wind energy greater than 150 W/m^2 at 60 m above ground and wind energy density at 60 m, respectively.

Based on the current research and the existing technology of wind turbines, it is estimated that wind energy potential of Iran is more than 15,000 MW for power generation. Since swamps are commonly found in Iran, using wind energy is not only possible but also economically feasible [83, 84].

7.1.1. Optimal location of wind turbines

As a general rule, the use of wind turbines is practical where the average wind speed is 5.4 m/s (16 km per hour) or more. Location of wind power plants is usually pre-selected using a wind atlas and is confirmed by wind measurements. Meteorology plays an important role in determining possible locations for installing wind power plants, but meteorological data on wind alone are not adequate for accurate placement of large wind farms [85]. Meteorological data of an area are important for determining its potential. The ideal location to install wind turbines is a site with almost constant wind circulation throughout the year and the smallest possible change of wind. An important factor in locating wind turbines is access to local load or transmission capacity (i.e., access to transmission lines with empty capacity). A very critical stage in the development of a high potential location is collecting accurate and verifiable data on the speed and direction of wind, along with other parameters [86].

7.2. Small-scale wind power

Small-scale wind power equipment (100 KW or less) is usually used to provide electricity for houses, agricultural

lands, or small businesses. In remote locations that depend on diesel generators, people might prefer to use wind turbines to reduce fuel dependency [87]. In some cases, wind turbines are also used to reduce the cost of purchasing electricity or to generate clean electricity. Providing electricity for remote houses is achieved by connecting wind turbines to batteries. In the United States, the use of wind turbines in the 1-10 KW range is becoming increasingly common for houses that are connected to the network as well. Network-connected turbines eliminate the need for network power when the turbine is active. In systems that are not connected to the network, power should be used periodically or a battery should be used to store the energy. In urban areas where wind cannot be used on a large scale, wind energy can be used for applications such as parking meters or wireless internet hotspots by using a battery or a solar battery to eliminate the need for network connectivity.

7.3. Trends in cost and growth

Figures from the Global Wind Energy Council (GWEC) show that the global installed capacity increased to 51.3 GW by 2018. Total installed wind energy capacity was 591 GW in 2018, a growth of 9.6 % compared to the end of 2017. Despite the limitations of wind turbines, the wind energy market continued to grow at 32 % after 2005 and reached 41 % growth in 2019. In terms of economic value, the wind energy sector was valued at about 18 billion euros or 23 billion dollars in 2006, including the value of newly installed equipment, which makes wind energy one of the most important players in the energy market [88, 89]. Based on installed capacity in 2019, the China had the highest capacity (237029 MW) followed by United States, Germany, India, Spain, United Kingdom, and France with capacities of 105433, 61357, 37529, 25808, 23515, and 16646 MW, respectively.

In 2004, the cost of wind energy was one-fifth of its cost in the 1980s. Some experts expect further decline in cost as larger turbines with higher capacities are put in to service. However, the cost of facilities increased in 2005 and 2006. According to the American Wind Energy Industries Business Group, the average cost of wind energy per kilowatt is $1,600, which is comparable to $1,200 per kilowatt a few years ago.

The main methods of generating electricity are expensive, meaning that they need large investments at the beginning of the project and less investment later on (e.g., fuel and maintenance costs). These conditions are true for both wind power and hydroelectricity. However, fuel costs are close to zero for these two methods and the maintenance cost is negligible [90]. According to the Iranian Wind Energy Industries, the average cost of wind energy per kilowatt is $0.6, with a five-year return on investment. So far, 135 MW worth of wind turbines has been installed, of which 95 MW is installed in government projects. The private sector has not invested heavily in wind energy [91].

8. POSITIVE ENVIRONMENTAL EFFECT OF WIND ENERGY

The most important advantage of wind energy is that it does not release chemicals and pollutants into the environment. In contrast, power plants using fossil fuels release carbon dioxide, sulfur dioxide, and nitrogen oxides into the atmosphere. Toxic heavy metals and suspended particles are also produced by these power plants. Combustion gases of coal-fired power plants are desulphurized using limestone/gypsum. In this process, 90 % of the sulfur dioxide is captured, but the remaining 10 % is still above the standards.

The emission of pollutants from fossil fuels depends on the type of fuel and its quality. For example, in a gas-fired power station, the emission of sulfur oxides is relatively low. In these power plants, the problem is the release of nitrogen oxide, carbon dioxide, and other nitrogen oxides. Ten ppm of sulfur dioxide and nitrogen oxide can cause acid rain, subsequently causing environmental damage.

Seventy-five percent of the global carbon dioxide emission is due to combustion of fossil fuels. The release and accumulation of this gas in the atmosphere and the resulting intensification of the greenhouse effect are the main cause of global warming. Global warming causes changes in meteorological patterns and land use as well as rising sea levels.

Another problem caused by combustion of fossil fuels is the formation of smog. Similarly, suspended particles and toxic heavy metals in the atmosphere cause asthma and lung cancer. Fossil fuel plants consume a large amount of water in the thermodynamic cycle. Moreover, a large volume of water is used to wash coal. This is a serious problem when there is a shortage of water. The need for water in wind power plants is insignificant and only a small amount of water is needed to clean the blades. Nuclear power plants pose environmental hazards, as well. Wind energy does not produce pollutant gases or suspended particles and does not have the problem of radiation and waste management [92,93].

Natural gas is Iran's primary fuel source for electricity generation, accounting for 70 % of total generation. In 2016, Iran generated almost 276 billion KWh of electricity, of which 93 % was from fossil-fuel sources. Wind power does depend on gas or oil; therefore, wind power conserves fossil fuels [94].

Iran is a dry country and the average water consumption in Iranian power plants is 1.05 m^3/mWh. These power plants generate 262,000 GWh/year of electricity, requiring 275 million m^3 of water annually. Wind turbines do not need water for power generation and could save 275 million m^3 of water annually [95,96].

9. NEGATIVE ENVIRONMENTAL IMPACT OF WIND ENERGY

Human intervention in every natural environment will have environmental consequences and wind energy is no exception in this regard. Although wind is one of the cleanest sources of energy, it is associated with several environmental issues. These issues include death of birds as a result of collision with wind turbines, noise, and undesirable visual effects [97].

9.1. Death of birds due to collision with wind turbines

A report in 1980 on the death of birds due to collision with wind turbines at a wind farm 90 km from San Francisco, California, brought attention to this issue [97]. The most commonly used method for investigating this problem is to study the mortality of birds before and after the installation of wind turbines [97]. Some of the most important precautions that can be considered to reduce the risk of bird-turbine collisions include [98, 99]:

A- Turbine blades narrow than 60 cm

B- A distance of 1000 m between turbines
C- Painting the blades if possible (this is especially useful in the direction of birds' migration)
D- Using sound to drive birds away from turbines

In general, the risk of death due to collision with wind turbines is not severe enough to merit several projects. For example, 1250000 birds die from collision with tall buildings, skyscrapers, and telecommunication towers around the world. Similarly, nearly 98 million birds die every year as a result of collision with windows. In addition, 57 million birds are killed in collisions with cars. A four-year study showed that 54 % of deaths were due to collisions with power generation systems and transmission lines, while 38 % were caused by wind turbines. While discussing death of birds due to collision with wind turbines, the effects of other energy generation technologies on the environment should also be considered such as emission of greenhouse gases and acid rain, which have more destructive effects on the environment. Although the death toll of wind turbines is relatively small, organizations around the world have to try to minimize the losses. For this purpose, activities are ongoing in the United States and the United Kingdom [99].

9.2. Noise pollution

Noise is defined as any unwanted sound. In the past, due to the small number of turbines, the problem of noise was not an issue. Nowadays, however, due to the increasing development of these systems in industrialized and developing countries, it has become an important concern. Hence, researchers seek to design and construct turbines with the lowest noise level [63]. The easiest way to determine the level of noise pollution is to visit the turbine installation site. To measure it more precisely, a sound meter can be used. The American Wind Energy Association [63] has defined standards to minimize the error in sound measurements. According to this standard, the sound intensity of a wind turbine with a speed of 8 m/s should be measured at 8 m from the ground.

The two types of sound created by a wind turbine are mechanical and aerodynamic. Mechanical sound is created by relative movement of parts such as the gearbox, generator, right-to-left motors, cooling fans, hydraulic pumps, and other accessories. For example, intensity of the noise from the gearbox, generator, and other accessories in a wind turbine is 97.2 dB, 87.2 dB, and 76.7 dB, respectively. Therefore, a change in the design of these three parts can reduce noise pollution. Assessing the effects of the noise emitted by the wind farm in Manjil, Iran on the general health of the staff showed that low frequency sound (60 dBA) can cause harmful effects on the health of workers [78].

10. ECONOMIC IMPACT OF WIND ENERGY

Since the Industrial Revolution, humankind has achieved remarkable economic growth and attained more prosperity and comfort. Total energy consumption has increased in tandem with economic and population growth and in the meantime, environmental problems associated with human activities have become more intense [99].

The economy plays an important role in choosing the right option for energy production by the market. One of the major constraints on the use of renewable energy is the high cost of the technology [99, 64, 77]. However, technological developments in the field of wind turbines have made the use of wind energy a more viable option than other sources such as solar energy, thermal energy, biomass, and hydroelectricity. Figure 2 shows the cost of wind energy in a 40-year period.

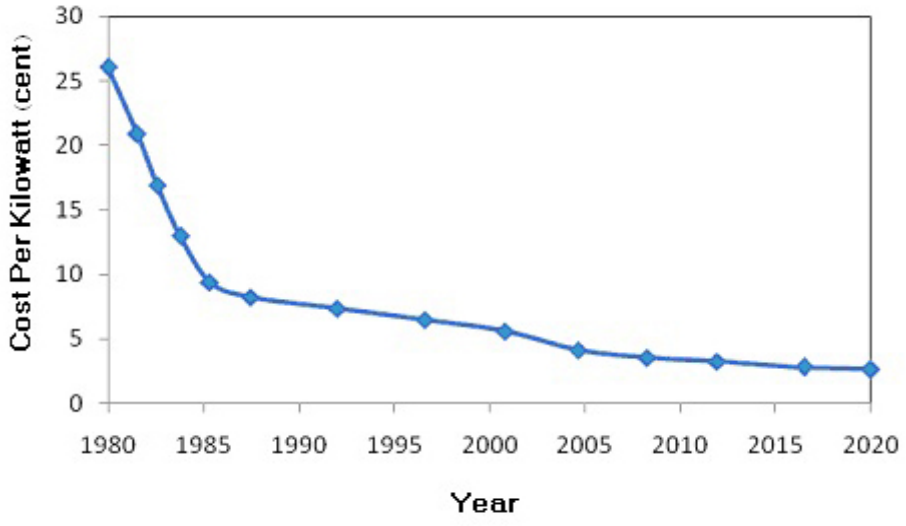

Figure 2. Changes in the cost of wind energy generation between 1980 and 2020 [25].

As is shown in Figure 2, the per-kilowatt cost of energy was 26.5 cents in 1980 and 5 cents in 2005. This means that expenses have decreased by 84 % over 23 years. There is hope that this decline will continue further with advances in our knowledge about wind turbines.

10.1. Factors affecting the cost of energy

Studies show that small wind turbines with a capacity of less than 100 KW used in residential areas are estimated to cost approximately $3,000 to $8,000 per kilowatt. The cost of a 10-KW wind turbine (suitable for use in a large residential building) varies between $50,000 and $80,000, depending on the type and height of the tower, among other variables [99]. It should be noted that the primary costs include the cost of turbines, construction of roads, electrical infrastructure, project management, installation, insurance premiums, access to turbines, and the cost of network connections and power lines, while the operational and maintenance costs include the annual costs of repair and maintenance.

Recent studies have shown that there is a relationship between a country's gross domestic product (GDP) and its use of renewable energy. This suggests that investing in renewable energies will have a positive impact on GDP [78]. Similarly, business growth depends on energy; some studies have shown that renewable energy projects are likely to create jobs [34]. In general, factors such as the location of installation, increased production capacity, and countries' markets and policies can contribute to the cost of energy generated by wind, which will be discussed in the following sections.

10.2. Location of installation

For wind turbines to work best, wind speeds should usually be higher than 12 to 14 mph. The energy in the wind flow is determined by the third power of its speed. For example, if speed increase by 2 m/s, its energy will increase 8 times. The cost is reduced by about 50 % as wind speed increases from 7 to 9.5 m/s. Such speeds are needed to spin turbines fast enough to generate electricity. Usually, each wind turbine generates about 50 to 300 KW. With 1,000 W of electricity, one hundred 10-watt lamps can be turned on. Thus, a 300-KW wind turbine can light up to three thousand 100-watt lamps. Therefore, a small wind turbine in a desert can be used to power a house or a school.

The coordination of wind-driven machines with wind speed plays an important role in keeping costs down. Costs of land, equipment transfer, and workers' wages vary from site to site. Also, the cost of constructing the foundation depends on soil resistance. When turbines are connected to a network system, the cost of the transfer will also be added. As wind speed increases with altitude, taller towers should be used. Construction of towers is one of the main costs of installing wind turbines. The presence of corrosive substances and other harmful factors will shorten a turbine's life, which increases maintenance costs [61, 51, 97, 98, 73, 99].

10.3. Increasing production capacity

The cost of wind turbines is significantly reduced by increasing their scale. As capacity increases from 20 to 50 KW, the cost is reduced by 18 %. Another factor is the lifespan of turbines. The average lifespan of a turbine is between 20 and 30 years [46]. With a lifespan of more than 25 years, cost will fall by 20 %.

10.4. Financial analysis of a 100-MW power plant with 50 wind turbines

In accordance with the provisions of Article 139 of the Five-Year Development Plan, the Iranian government is required to provide special support for wind energy with the help of private and cooperative sectors. In order to examine the role of government's support in this regard, it is first necessary to conduct financial analysis of the construction of wind power plants to determine the state of investment without government support [83, 94]. In other words, how attractive is the construction of a wind power plant without using and applying for government support and subsidies?

Financial evaluation of the plan includes calculating fixed investment costs and financing sources. In addition, the income from sales and all operating costs (fixed and variable) are calculated. Subsequently, the indices of internal rate of return, net present value associated with investment, and return period of investment are calculated. All of the above steps are taken using COMFAR (Computer Model of Feasibility Analysis and Reporting).

After identifying incomes and costs during construction and operation, cash flows of the project were extracted and financial indices were calculated and analyzed. Finally, the sensitivity of the model was analyzed by changing the independent variables to achieve the expected return rate.

Project schedule: The construction phase of the wind power plant and its operating life were estimated to be 2 and 20 years, respectively.

Estimated nominal capacity and anticipated production: The plant is capable of generating electricity with an annual nominal capacity of 337260 MW. Due to the reduction of carbon dioxide emissions, the project can benefit from the advantages of a clean development plan.

Utilization phase: Nominal capacity is assumed to be 337,260,000 KW and carbon dioxide reduction is assumed to be 0.0006 tonne per KWh. For estimation of incomes, the income from the sale of generated electricity and the dollar value of greenhouse gas reduction are calculated. Based on the guaranteed purchase tariffs, the sales price of electricity is estimated at 1300 rials per KWh (roughly $0.04 at the time of writing) on average and the price of carbon dioxide per tonne is taken to be 80000 rials (roughly $0.24 at the time of writing). In this paper, the annual growth rate of electricity sales is assumed to be 13 % and the average annual growth rate of energy prices and the annual growth rate of wages are assumed to be 10 %.

By applying a 25 % discount rate, net present value is set at $ 63251205, which indicates that the project is not justifiable and should not be selected.

The return period represents the number of years after investment within which the original cash flows invested in the project will return to the company. In other words, it is the number of years needed to reach positive cash flow. The smaller this index is, the faster the output cash flow is replaced by the inflow cash. Calculations for this project indicate that the return period of investment under normal conditions is more than 10 years and longer than the life of the project under a moving condition (considering the time value of money). According to these results, the project is not justified and thus will be unattractive to investors.

10.5. Potential benefits of using wind energy for electricity generation

10.5.1. Existence of deserts

Iran has 34 million ha of deserts (one-fifth of the total area of Iran) which are generally windy and flat. The desert areas of Iran are endless resources of clean energies such as wind energy and can function as strong infrastructure for socio-economic development. Deserts have the required conditions for installation of wind turbines [73]. Regarding Iran's potential for wind power, 1.3 % of the country's land area (2.1 million ha) has a mean annual wind speed of 8 m/s or higher, which is suitable for harnessing wind energy [76]. The studies show that the nominal estimated capacity of only 28 areas of Iran is almost higher than 6500 MW (compared to total nominal capacity of Iranian power plants). Capacity of 163 wind turbines embedded in Iran is higher than 92MW [76].

11. SOCIO-ECONOMIC BENEFITS AND ENERGY SUPPLY SECURITY

Using the right policies to introduce wind energy will create an extensive market for the export of electricity. National and international investments in local production will employ local residents. Easy access, high security, and affordable sources of energy will stimulate the economy in desert areas. It should to be noted that current and future increases in energy demand will result in conflicts over fossil resources such as political conflicts and tensions over common oil reserves in western and southern Iran. Therefore, the use of wind energy can promote regional peace as well as economic interactions [95].

In addition, due to intense mechanization, surface mines may require fewer workers than underground mines with similar production. Therefore, the impact of human populations on surface mines will be less significant than their impact on underground mines. However, the local population cannot provide the required labor in less populated areas and migration due to new jobs in the mine is likely [88, 99].

11.1. Energy market

If wind-generated electricity is completely utilized, the economic benefits of wind energy are achievable. Utility companies can encourage customers to use electric power by removing tariffs on electric power generated by wind. Current renewable energy markets face limitations. These limitations include lack of access to an affordable electricity network, higher initial cost than conventional energy sources, lack of awareness about the scale of available resources, the speed of development in renewable technologies, and the potential economic benefits of renewable energy [92, 93, 94].

11.2. Adoption of government's supportive policies

By studying the environmental benefits of wind energy, governments can develop policies to support this clean and environmentally-friendly industry. Given the environmental pollution caused by the use of fossil fuels and the associated diseases, governments should provide special support for this industry. Otherwise, large sums should be spent to promote the health and well-being of communities. Unfortunately, in many countries, energy policies focus on the use of common sources of energy such as fossil fuels. Recently, however, some developed countries have imposed taxes on polluting industries. This will make renewable technologies more competitive than conventional sources of energy production. Due to the size of initial investment and high risk at the outset, cooperation with financial institutions is essential, which may include partnerships with investors such as the World Bank, investment banks, development banks, and commercial banks [83, 94].

Iran is rich in oil and natural gas reserves and the income from fossil fuels dominates the economy and affects the country's energy policy. In 2010, Iran adopted a new strategy by shifting towards diversifying its energy sector by eliminating energy subsidies. The new strategy helps to free up over 60 billion USD of public funds, some of which can be invested in the renewables sector. In addition, the Iranian government has a clear vision of developing the country's wind energy industry to become a wind energy hub in the Middle East.

So far, there is no clear policy for wind energy in Iran, but the Iranian ministry of energy has made considerable efforts for developing a legal frame work. A new law aims for 20 GW of thermal power capacity and floating the two major wind farms in the country (Manjil and Binalood) on the stock market. The Foreign Investment Promotion and Protection Act, protecting investors against political risks, covers all foreign investments in Iran. However, international sanctions against Iran have negatively impacted the development of the renewable energy sector due to prohibition of any technical or financial foreign investments [89, 90, 93].

12. RECOMMENDATIONS

The presence of 120-day winds and scarcity of water resources encouraged people to make efficient use of windmills (As-bads) in Iran. As-bads are historical examples of the potential of wind energy to improve local livelihoods and prevent migration [94].

This study offers specific suggestions for overcoming the many limitations of developing wind power plants. In order to accelerate the use of wind energy, a positive approach and a strong political strategy at all levels are needed. Policies to promote the deployment of wind energy technologies are divided into four categories: financial incentives (tax credit), government investment (loans, feed-in tariffs, research and development), regulatory arrangements (determining the share of renewable energy in the country's energy basket, tender offers, guaranteed purchase tariffs), and access policies (bidding policy) [39, 85].

12.1. Tax credit

In this method, an investor receives an annual income-tax credit. Credit is calculated on the basis of the amount of investment in the project or the amount of energy generated during a year. This tool will enable investors to reduce part of their financial obligations. Tax credit has been factored into the state budget in many EU countries including Belgium, France, Italy and the Netherlands and is very sensitive to political conditions [73]. In EU countries, there are several direct and indirect taxes such as income tax, asset tax, company tax, and value-added tax to promote the use of renewable energy [85, 99].

12.2. Low-interest loans

In developing countries such as Iran, low-interest loans are essential for the purchase of wind energy systems. Many financial institutions provide low-interest loans to their customers to buy wind energy systems. In developing countries, low-interest loans should be provided to motivate residents to install wind energy systems [85, 73].

12.3. Feed-in tariffs

In developing countries, the government must specify tariffs on purchasing electricity from suppliers of wind energy. A feed-in tariff is the primary policy mechanism for supporting the development of renewable energies in industrialized countries such as Germany, Italy, France, Japan, China, and the United States [71, 73]. In Iran, the guaranteed-purchase tariff rates are 0.11-0.13 US dollars per KWh [86].

12.4. Research and development

Skilled labor is one of the most important factors in the development of wind energy technology. Skilled labor is

needed at all stages, from research to the installation of wind energy systems. For this purpose, educational institutions and training programs should provide education for specific groups such as planners, managers, and engineers [75]. Training programs on the installation and maintenance of wind technology are very important. To address this issue, locals are trained and skilled workers are employed to install and maintain wind energy systems. As research and development increases the efficiency of renewable energies and reduces production costs, developing countries need to allocate more funding to renewable energy research [80, 85].

12.5. Determining the share of renewable energy in the country's energy basket

This is a form of mandatory and predetermined development, in which a certain share of production is allocated to renewable energies within a specific timeframe. This share can be reflected in the National Energy Strategy of Iran, macro policies in development plans, and the proposed comprehensive renewable energy law.

12.6. Tender offers

Among the most important benefits of bidding are the discovery of real prices, reduction of electricity generation cost and, as a result, creation of a competitive space. At the same time, the price and capacity required for installation are controlled [79].

12.7. Guaranteed purchase

In this method, the purchase of electricity generated using renewable resources is guaranteed according to pre-set tariffs over a specified period of time. The tariff can be different for different plants according to plant size, and policymakers can adjust tariffs as technology develops. This method is an important policy tool for attracting private investors in the field of renewable energy and, consequently, increasing production.

12.8. Bidding policy for wind energy development

Tender offers are a popular policy tool. In 2015, more than 60 countries used this method to develop their renewable energy industry [85]. Turkey used bidding for construction of 2000 MW turbines in 2016, which will be operational in 2020. The United States has held tenders in five steps for the construction of 1,419 MW of renewable energy plants in 2011-2015. The goal is the reduction of prices in the bidding process. The policy ensures the average price per MWh $90 in the first tender and $80 in the third [94, 95].

13. CONCLUSIONS

Economic growth and its urgent need for energy show the necessity of optimal energy use. Wind energy is a new and renewable source of electricity with an increasing growth trend. In recent years, the use of this energy has begun in Iran, especially in Manjil, but little has been done in other parts of the country. Economic development will be possible if sufficient wind energy is available in a timely manner.

Among countries, Iran has a special place with its diverse energy resources. Nevertheless, energy consumption in the country is much higher than other developing countries and has led to environmental problems, which have alarmed economic planners. It should also be noted that the security of the country's energy supply increases with the diversification of its energy basket, which itself promotes national security. However, diversification of the energy sector requires accurate knowledge of the country's potential for different sources of energy and analysis of the effects of diversification. Some basic issues that should be considered in the design of a large energy sector include the ability to meet the needs of the economy, energy security, characteristics and potentials of the region, resources utilization technology, sustainability, and environmental issues.

In areas with low wind potential, hybrid systems have recently become common. For example, the advantage of a photovoltaic-wind-diesel system is that when wind speed is appropriate at times, energy production is carried out by wind turbines and the solar photovoltaic system is used when solar energy is preferred to wind power. When neither of the desired sources (wind and solar) has good potential, the diesel system can be used. Of course, the use of diesel systems alone can pollute the environment, but their use in a hybrid system releases less pollutants.

With a population of 80 million, the annual energy consumption of Iran will increase by about 7 %. According to expert estimates, the needed generation capacity will be about 90 GW by 2020. Currently, almost three-quarters of Iran's electricity is generated by gas-fired power plants and the rest is supplied using hydroelectric or diesel turbines.

Given that power generation using wind turbines is economical, it is recommended to install wind turbines in suitable locations. In addition, as one of the crises facing the world is environmental pollution and given that electricity generation by wind turbines lowers social costs, clean energies are recommended for electricity generation. The wind energy industry offers long-term advantages; therefore, it is advised to develop and expand the infrastructure needed for the development of wind turbines and wind power plants. Providing energy services can solve several social needs in developing countries, especially Iran, since Iran is subject to major changes in energy systems and their sustainable use.

14. ACKNOWLEDGEMENT

The authors would like to thank all those who have contributed to and collaborated on the current research by providing scientific advice or original data.

REFERENCES

1. Shahsavari, A. and Akbari, M., "Potential of solar energy in developing countries for reducing energy-related emissions", ***Renewable and Sustainable Energy Reviews***, Vol. 90, (2018), 275-291. (https://doi.org/10.1016/j.rser.2018.03.065).
2. Azau, S., "Annual Report", Brussels, Belgium: The European Wind Energy Association (EWEA), (2010).
3. Davy, R., Gnatiuk, N., Pettersson, L. and Bobylev, L., "Climate change impacts on wind energy potential in the European domain with a focus on the Black Sea", ***Renewable and Sustainable Energy Reviews***, Vol. 81, Part 2, (2018), 1652-1659. (https://doi.org/10.1016/j.rser.2017.05.253).
4. Benitez, L., "The economics of wind power with energy storage", ***Energy Economics***, Vol. 30, No. 4, (2008), 1973-1989. (https://doi.org/10.1016/j.eneco.2007.01.017).
5. Leonard, M.D., Michael ides, E.E. and Michael ides, D.N., "Substitution of coal power plants with renewable energy sources–Shift of the power demand and energy storage", ***Energy Conversion and Management***, Vol. 164, (2018), 27-35. (https://doi.org/10.1016/j.enconman.2018.02.083).

6. Liu, G., Li, M., Zhou, B., Chen, Y. and Liao, S., "General indicator for techno-economic assessment of renewable energy resources", ***Energy Conversion and Management***, Vol. 156, (2018), 416-426. (https://doi.org/10.1016/j.enconman.2017.11.054).
7. Oyedepo, S.O., "On energy for sustainable development in Nigeria", ***Renewable and Sustainable Energy Reviews***, Vol. 16, No. 5, (2012), 2583-2598. (https://doi.org/10.1016/j.rser.2012.02.010).
8. Pulliam, N., Energy and the environment, Published by the English Press, (2011), 1-111.
9. Business Monitor International (BMI) research, Iran power report, (2018).
10. Cambron, P., Masson, C., Tahan, A. and Pelletier, F., "Control chart monitoring of wind turbine generators using the statistical inertia of a wind farm average", ***Renewable Energy***, Vol. 116,Part B, (2018), 88-98. (https://doi.org/10.1016/j.renene.2016.09.029).
11. Bergey Wind Power Company, Vol. 10, (Accessed January 2013).
12. Komoto, K., Lto, M., Van der Vleuten, P., Faiman, D. and Kurokawa, K., Energy from the desert, Very large scale photovoltaic systems: Socio-economic, financial, technical and environmental aspect, Routledge, Taylor & Francis Group, London and New York, (2013).
13. Duran, S.A., "Progress and recent trends in wind energy", ***Progress in Energy and Combustion Science***, Vol. 30, No. 5, (2004), 501-543. (https://doi.org/10.1016/j.pecs.2004.04.001).
14. Gholizadeh, A., Rabiee, R. and Fadaeinedjad, A., "Scenario-based voltage stability constrained planning model for integration of large-scale wind farms", ***International Journal of Electrical Power & Energy Systems***, Vol. 105, (2019), 564-580. (https://doi.org/10.1016/j.ijepes.2018.09.002).
15. Richardson, D.B., "Electric vehicles and the electric grid: A review of modeling approaches, impacts, and renewable energy integration", ***Renewable and Sustainable Energy Reviews***, Vol. 19, (2013), 247-254. (https://doi.org/10.1016/j.rser.2012.11.042).
16. Hamouda, Y.A., "Wind energy in Egypt: Economic feasibility for Cairo", ***Renewable and Sustainable Energy Reviews***, Vol. 16, No. 5, (2012), 3312-3319. (https://doi.org/10.1016/j.rser.2012.02.058).
17. Najafi, G. and Ghobadian, B., "LLK1694-Wind energy resources and development in Iran", ***Renewable and Sustainable Energy Reviews***, Vol. 15, No. 5, (2011), 2719-2728. (https://doi.org/10.1016/j.rser.2011.03.002).
18. Sharifi, A., "Estimated energy available from the wind flow of the Ghazvin Kahk Plain in order to construct a wind power plant", ***Proceedings of 11th International Conference on Mechanical Engineering***, Isfahan University of Technology, Isfahan, (2006).
19. Wang, W.C., Wang, J.J. and Chong, W.T., "The effects of unsteady wind on the performances of a newly developed cross-axis wind turbine: A wind tunnel study", ***Renewable Energy***, Vol. 131, (2019), 644-659. (https://doi.org/10.1016/j.renene.2018.07.061).
20. Rosário, M., "Future challenges for transport infrastructure pricing in PPP arrangements", ***Research in Transportation Economics***, Vol. 30, No. 1, (2010), 145-154. (https://doi.org/10.1016/j.retrec.2010.10.015).
21. Abdullah, M.A., Yatim, A.H.M., Tan, C.W. and Saidur, R., "A review of maximum power point tracking algorithms for wind energy systems", ***Renewable and Sustainable Energy Reviews***, Vol. 16, No. 5, (2012), 3220-3227. (https://doi.org/10.1016/j.rser.2012.02.016).
22. Duan, H., "Emissions and temperature benefits: The role of wind power in China", ***Environmental Research***, Vol. 152, (2017), 342-350. (https://doi.org/10.1016/j.envres.2016.07.016).
23. Sedaghat, A., Hassanzadeh, A., Jamali, J., Mostafaeipour, A. and, Chen, W.H., "Determination of rated wind speed for maximum annual energy production of variable speed wind turbines", ***Applied Energy***, Vol. 205, (2017), 781-789. (https://doi.org/10.1016/j.apenergy.2017.08.079).
24. Keyhani, M., Ghasemi-Varnamkhasti, M. and Khanali, R., "An assessment of wind energy potential as a power generation source in the capital of Iran, Tehran", ***Energy***, Vol. 35, No. 1, (2010), 188-201. (https://doi.org/10.1016/j.energy.2009.09.009).
25. Fathabadi, H., "Novel high-efficient large-scale stand-alone solar/wind hybrid power source equipped with battery bank used as storage device", ***Journal of Energy Storage***, Vol. 17, (2018), 485-495. (https://doi.org/10.1016/j.est.2018.04.008).
26 Naeeni, N. and Yaghoubi, M., "Analysis of wind flow around a parabolic collector (1) fluid flow", ***Renewable Energy***, Vol. 32, No. 11, (2007), 1898-1916. (https://doi.org/10.1016/j.renene.2006.10.004).
27. Jafari, M. and Tavili, A., Reclamation of arid lands, University of Tehran Press, (2020).
28. Hooshmand, M. and Hosseini, S.H., "Economic evaluation of electricity generation using wind energy by the private sectoring Iran", ***Financial Monetary Economy***, Vol. 21, No. 8, (2013), 87-106. (In Farsi). (https://doi.org/10.22067/pm.v21i8.45858).
29. Mostafaeipour, H., "Harnessing wind energy at Manjil area located in north of Iran", ***Renewable and Sustainable Energy Reviews***, Vol. 12, No. 6, (2008), 1758-1766. (https://doi.org/10.1016/j.rser.2007.01.029).
30. Jensen, C.U., Panduro, T.E., Lundhede, T.H., Nielsen, A.S.E., Dalsgaard, M. and Thorsen, B.J., "The impact of on-shore and off-shore wind turbine farms on property prices", ***Energy Policy***, Vol. 116, (2018), 50-59. (https://doi.org/10.1016/j.enpol.2018.01.046).
31. Nasiri, J., "Wind energy potential in Iran", New Energy Articles, Ministry of Energy, (1997).
32. Nedaei, M., "Wind resource assessment in Hormozgan province in Iran", ***International Journal of Sustainable Energy***, Vol. 33, No. 3, (2014), 650-694. (https://doi.org/10.1080/14786451.2013.784319).
33. National Renewable Energy Laboratory, Vol. 10, (Accessed January 2013).
34. Henckes, P., Knaut, A., Obermüller, F. and Frank, C., "The benefit of long-term high resolution wind data for electricity system analysis", ***Energy***, Vol. 143, (2018), 934-942. (https://doi.org/10.1016/j.energy.2017.10.049).
35. Himpler, S. and Madlener, R., "Repowering of wind turbines: Economics and optimal timing", Institute for Future Energy Consumer Needs and Behavior (FCN), FCN Working Paper No. 19/2011, (2011).
36. World Bank, "Middle East and North Africa: Recovering from the crisis, economic developments and prospects report", World Bank, Washington D.C., (April 2010).
37. Abanda, F.H., "Renewable energy sources in Cameroon: Potentials, benefits and enabling environment", ***Renewable and Sustainable Energy Reviews***, Vol. 16, No. 7, (2012), 4557-4562. (https://doi.org/10.1016/j.rser.2012.04.011).
38. Murcia, J.P., Réthoré, P.E., Dimitrov, N., Natarajan, A., Sørensen, J.D., Graf, P. and Kim, T., "Uncertainty propagation through an aeroelastic wind turbine model using polynomial surrogates", ***Renewable Energy***, Vol. 119, (2018), 910-922. (https://doi.org/10.1016/j.renene.2017.07.070).
39. Howell, J.A., "Bird mortality at rotor swept area equivalents, Altamont Pass and Montezuma Hills, California", ***Transactions of the Western Section of the Wildlife Society***, Vol. 33, (1997), 24-29.
40. Chaianong, C.H., "Outlook and challenges for promoting solar photovoltaic rooftops in Thailand", ***Renewable and Sustainable Energy Reviews***, Vol. 48, (2015), 356-372. (https://doi.org/10.1016/j.rser.2015.04.042).
41. Ishaq, H., Dincer, I. and Naterer, G.F., "Performance investigation of an integrated wind energy system for co-generation of power and hydrogen", ***International Journal of Hydrogen Energy***, Vol. 43, No. 19, (2018), 9153-9164. (https://doi.org/10.1016/j.ijhydene.2018.03.139).
42. Burton, T., Sharpe, D., Jenkins, N. and Bossanyi, E., Wind energy handbook, John Willey & Sons, (2001).
43. Scherhaufer, P., Höltinger, S., Salak, B., Schauppenlehner, T. and Schmidt, J., "Patterns of acceptance and non-acceptance within energy landscapes: A case study on wind energy expansion in Austria", ***Energy Policy***, Vol. 109, (2017), 863-870. (https://doi.org/10.1016/j.enpol.2017.05.057).
44. Renewables Global Status Report, REN21, Paris, (2016).
45. Kordvani, A., Hassan, M., Dalton, L. and Berenjforoush, P., "Renewable energy in Iran", CMS Cameron McKenna LLP, (2016).
46. Barnett, D., "Kansas from 2007 to 2017: A decade of renewable energy development", ***The Electricity Journal***, Vol. 30, No. 6, (2017), 72-79. (http://doi.org/10.1016/j.tej.2017.06.006).
47. Hui, B.E. and Cain, J.O., "Public receptiveness of vertical axis wind turbines", ***Energy Policy***, Vol. 112, (2018), 258-271. (https://doi.org/10.1016/j.enpol.2017.10.028).
48. IFC (International Finance Corporation), Senven sisters: Accelerating solar power investments, (2016).
49. Gupta, R. and Biswas, A., "Wind data analysis of Silchar (Assam, India) by Rayleigh's and Weibull methods", ***Journal of Mechanical Engineering Research***, Vol. 2, (2010), 10-24. (https://doi.org/10.5897/JMER.9000051).

50. Best, R. and Burke, P.J., "Adoption of solar and wind energy: The roles of carbon pricing and aggregate policy support", ***Energy Policy***, Vol. 118, (2018), 404-417. (https://doi.org/10.1016/j.enpol.2018.03.050).
51. Mohammadzadeh, P., Zare, K. and Pourfarzin, Z., "Economic assessment of electricity production of wind turbines", ***Quarterly Journal of Energy Economics***, Vol. 12, No. 49, (2016), 181-200. (In Farsi).
52. Van Dijk, M.T., Van Wingerden, J.W., Ashuri, T. and Li, Y., "Wind farm multi-objective wake redirection for optimizing power production and loads", ***Energy***, Vol. 121, (2017), 561-569. (https://doi.org/10.1016/j.energy.2017.01.051).
53. Nie, J. and Jiachun, L., "Technical potential assessment of offshore wind energy over shallow continent shelf along China coast", ***Renewable Energy***, Vol. 128, Part A, (2018), 391-399. (https://doi.org/10.1016/j.renene.2018.05.081).
54. Santos-Alamillos, F.J., Thomaidis, N.S., Usaola-García, J., Ruiz-Arias, J.A. and Pozo-Vázquez, D., "Exploring the mean-variance portfolio optimization approach for planning wind repowering actions in Spain", ***Renewable Energy***, Vol. 106, (2017), 335-342. (https://doi.org/10.1016/j.renene.2017.01.041).
55. Martínez, E., Latorre-Biel, J.I., Jiménez, E., Sanz, F. and Blanco, J., "Life cycle assessment of a wind farm repowering process", ***Renewable and Sustainable Energy Reviews***, Vol. 93, (2018), 260-271. (https://doi.org/10.1016/j.rser.2018.05.044).
56. UNDP, Energy for sustainable development, A policy agenda, Edited by Johansson, T.B. and Goldemberg, J., (2002).
57. Prata, R., Carvalho, P.M. and Azevedo, I.L., "Distributional costs of wind energy production in Portugal under the liberalized Iberian market regime", ***Energy Policy***, Vol. 113, (2018), 500-512. (https://doi.org/10.1016/j.enpol.2017.11.030).
58. Williams, E., Hittinger, E., Carvalho, R. and Williams, R., "Wind power costs expected to decrease due to technological progress", ***Energy Policy***, Vol. 106, (2017), 427-435. (https://doi.org/10.1016/j.enpol.2017.03.032).
59. Pullen, A. and Sawyer, S., "Global wind report, Annual market update", Brussels, Belgium: Global Wind Energy Council (GWEC), (2011).
60. Akdağ, S.A. and Güler, O., "Alternative Moment Method for wind energy potential and turbine energy output estimation", ***Renewable Energy***, Vol. 120, (2018), 69-77. (https://doi.org/10.1016/j.renene.2017.12.072).
61. Elosegui, U. and Ulazia, A., "Novel on-field method for pitch error correction in wind turbines", ***Energy Procedia***, Vol. 142, (2017), 9-16. (https://doi.org/10.1016/j.egypro.2017.12.003).
62. Lupton, R.C. and Langley, R.S., "Scaling of slow-drift motion with platform size and its importance for floating wind turbines", ***Renewable Energy***, Vol. 101, (2017), 1013-1020. (https://doi.org/10.1016/j.renene.2016.09.052).
63. Ayodele, T.R., Ogunjuyigbe, A.S.O. and Amusan, T.O., "Techno-economic analysis of utilizing wind energy for water pumping in some selected communities of Oyo State, Nigeria", ***Renewable and Sustainable Energy Reviews***, Vol. 91, (2018), 335-343. (https://doi.org/10.1016/j.rser.2018.03.026).
64. Jorgenson, P., Denholm, T. and Mai, T., "Analyzing storage for wind integration in a transmission-constrained power system", ***Applied Energy***, Vol. 228, (2018), 122-129. (https://doi.org/10.1016/j.apenergy.2018.06.046).
65. Kumar, R., Raahemifar, K. and Fung, A.S., "A critical review of vertical axis wind turbines for urban applications", ***Renewable and Sustainable Energy Reviews***, Vol. 89, (2018), 281-291. (https://doi.org/10.1016/j.rser.2018.03.033).
66. Long, H., Zhang, Z., Sun, M.X. and Li, Y.F., "The data-driven schedule of wind farm power generations and required reserves", ***Energy***, Vol. 149, (2018), 485-495. (https://doi.org/10.1016/j.energy.2018.02.058).
67. Souza, R.R., Moreira, A.B., Barros, T.A. and Rupert, E., "A proposal for a wind system equipped with a doubly fed induction generator using the Conservative Power Theory for active filtering of harmonics currents", ***Electric Power Systems Research***, Vol. 164, (2018), 167-177. (https://doi.org/10.1016/j.epsr.2018.07.027).
68. Sadeghi, M. and Karimi, M., "GIS-based solar and wind turbine site selection using multi-criteria analysis: Case study: Tehran, Iran", ***The International Archive of the Photogrammetry, Remote Sensing and Spatial Information Sciences***, Vol. XLII-4/W4, (2017), 469-476. (https://doi.org/10.5194/isprs-archives-XLII-4-W4-469-2017).
69. Serri, E., Lembo, D., Airoldi, C. and Gelli, M., "Wind energy plants repowering potential in Italy: Technical-economic assessment", ***Renewable Energy***, Vol. 115, (2018), 382-390. (https://doi.org/10.1016/j.renene.2017.08.031).
70. Grau, T., "Comparison of feed-in tariffs and tenders to remunerate solar power generation", German Institute for Economic Research, (2014).
71. Sur, J.R., Belthoff, E.R., Bjerre, B.A. and Millsap, T.K., "The utility of point count surveys to predict wildlife interactions with wind energy facilities: An example focused on golden eagles", ***Ecological Indicators***, Vol. 88, (2018), 126-133. (https://doi.org/10.1016/j.ecolind.2018.01.024).
72. Mostafaeipour, A., "Feasibility study of harnessing wind energy for turbine installation in province of Yazd in Iran", ***Renewable and Sustainable Energy Reviews***, Vol. 14, No. 1, (2010), 93-111. (https://doi.org/10.1016/j.rser.2009.05.009).
73. Technical support document, "Technical update of the social cost of carbon for regulatory impact analysis under executive order 12866", Interagency Working Group on Social Cost of Carbon, United States Government, (2013).
74. Mirzahosseini, H. and Taheri, T., "Environmental, technical and financial feasibility study of solar power plants by RET Screen, according to the targeting of energy subsidies in Iran", ***Renewable and Sustainable Energy Reviews***, Vol. 16, No. 5, (2012), 2806-2811. (https://doi.org/10.1016/j.rser.2012.01.066).
75 Green, R.H., Sampling designs and statistical methods for environmental biologists, Wiley, New York, NY, (1979).
76. Akbari, M., Neamatollahi, E. and Neamatollahi, P., "Evaluating land suitability for spatial planning in arid regions of eastern Iran using fuzzy logic and multi-criteria analysis", ***Ecological Indicators***, Vol. 98, (2019), 587-598. (https://doi.org/10.1016/j.ecolind.2018.11.035).
77. Martino, T., Christian, B. and Banister, D., "Modelling diffusion feedbacks between technology performance, cost and consumer behavior for future energy-transport systems", ***Journal of Power Sources***, Vol. 251, (2014), 130-136. (https://doi.org/10.1016/j.jpowsour.2013.11.028).
78. Cansino, J.M., Pablo-Romero, M.P., Roma, R. and Yn˜iguez, R., "Tax incentives to promote green electricity: an overview of EU-27 countries", ***Energy Policy***, Vol. 38, No. 10, (2010), 6000-6008. (https://doi.org/10.1016/j.enpol.2010.05.055).
79. Lowther, S.M. and Tyler S., "A review of impacts of wind turbines on birds in the UK- Report No. W/13/00426/REP3", Energy Technology Support Unit (ETSU), (1996).
80. Łopucki, R., Klich, D., Ścibior, A., Gołębiowska, D. and Perzanowski, K., "Living in habitats affected by wind turbines may result in an increase in corticosterone levels in ground dwelling animals", ***Ecological Indicators***, Vol. 84, (2018), 165-171. (http://doi.org/10.1016/j.ecolind.2017.08.052).
81. Dusonchet, E.T., "Comparative economic analysis of support policies for solar PV in the most representative EU countries", ***Renewable and Sustainable Energy Reviews***, Vol. 42, (2015), 986-998. (https://doi.org/10.1016/j.rser.2014.10.054).
82. Gandomkar, M.R. and Kaviani, S.A., "Investigation of wind energy in Sistan and Baluchestan province in order to produce wind power", ***Research Journal of Isfahan University***, Vol. 27, (2009), 1-19.
83. Fortunato, G. and Mummolo, G., "Economic optimization of wind power plants for isolated locations", ***Solar Energy***, Vol. 60, No. 6, (1997), 347-358. (https://doi.org/10.1016/S0038-092X(97)00027-3).
84. Fornarelli, R., Shahnia, F., Anda, M., Bahri, P.A. and Ho, G., "Selecting an economically suitable and sustainable solution for a renewable energy-powered water desalination system: A rural Australian case study", ***Desalination***, Vol. 435, (2018), 128-139. (https://doi.org/10.1016/j.desal.2017.11.008).
85. Renewable energy in Iran, Watson Farley & Williams, (2016), 1-6.
86. Damodaran, A., "Country default spreads and risk premiums", Stern School of Business, New York University, (2017).
87. Dahlke, S., "Effects of wholesale electricity markets on wind generation in the midwestern United States", ***Energy Policy***, Vol. 122, (2018), 358-368. (https://doi.org/10.1016/j.enpol.2018.07.026).
88. Barré, K., Le Viol, I., Bas, Y. and Julliard, R.C., "Estimating habitat loss due to wind turbine avoidance by bats: Implications for European siting guidance", ***Biological Conservation***, Vol. 226, (2018), 205-214. (https://doi.org/10.1016/j.biocon.2018.07.011).

89. Azadi, P., Nezam-Sarmadi, A., Mahmoudzadeh, A. and Shirvani, T., "The outlook for natural gas, electricity and renewable energy in Iran", Stanford Iran 2040 project, An Academic Platform for Research on Iran's Long-Term Sustainable Development, (2017), 1-28.

90. AWEA, "The most frequently asked questions about wind energy", American Wind Energy Association, Washington D.C., (2002).

91. Arnold, B., Lutz, T. and Krämer, E., "Design of a boundary-layer suction system for turbulent trailing-edge noise reduction of wind turbines", ***Renewable Energy***, Vol. 123, (2018), 249-262. (https://doi.org/10.1016/j.renene.2018.02.050).

92. Anonymous Iran and World Energy Facts and Figures, (2014), 1-131.

93. Aman, M.M., Solangi, K.H., Hossain, M.S., Badarudin, A., Jasmon, G.B., Mokhlis, H., Bakar, A.H.A. and Kazi, S.N., "A review of safety, health and environmental (SHE) issues of solar energy system", ***Renewable and Sustainable Energy Reviews***, Vol. 41, (2015), 190-204. (https://doi.org/10.1016/j.rser.2014.08.086).

94. Alford, J., "Guarantee structure that launched Argentina's successful renewable energy auctions", King & Spalding, (2017).

95. Alamdari, P., Nematollahi, O. and Mirhosseini, M., "Assessment of wind energy in Iran: A review", ***Renewable and Sustainable Energy Reviews***, Vol. 16, No. 1, (2012), 836-860. (https://doi.org/10.1016/j.rser.2011.09.007).

96. Ahmed, A.S., "Wind energy characteristics and wind park installation in Shark El-Ouinat, Egypt", ***Renewable and Sustainable Energy Reviews***, Vol. 82, Part 1, (2018), 734-742. (https://doi.org/10.1016/j.rser.2017.09.031).

97. Adibfar, A., "Wind energy in Iran, Feed in tariffs, wind energy potential", Federal Ministry for Economic Affairs and Energy, Renewables Made in Germany, (2015).

98. Ackermann, T., "An overview of wind energy-status 2002", ***Renewable and Sustainable Energy Reviews***, Vol. 6, No. 1-2, (2002), 67-127. (https://doi.org/ 10.1016/S1364-0321(02)00008-4).

99. Abbasi, M.R., Monazzam, M.H., Ebrahimi, S.Y., Zakerian, M.F. and Dehghan, A., "Assessment of noise effects of wind turbine on the general health of staff at wind farm of Manjil, Iran", ***Journal of Law Frequency Noise, Vibration and Active Control***, Vol. 35, No. 1, (2016), 91-98. (https://doi.org/10.1177/0263092316628714).

JREE: Vol. 7, No. 3, (Summer 2020) 80-86

Journal of Renewable Energy and Environment

Research Article

Journal Homepage: www.jree.ir

Design and Analysis of a Combined Savonius-Darrieus Wind Turbine for Irrigation Application

Mahdi Shahmari, Payam Zarafshan*, Shahriar Kouravand, Morteza Khashehchi

Department of Agro-Technology, College of Aburaihan, University of Tehran, Pakdasht, Tehran, Iran.

PAPER INFO

Paper history:
Received 18 March 2020
Accepted in revised form 21 July 2020

Keywords:
Irrigation
Combined Savonius-Darrieus Wind Turbine
Experimental Setup
CFD
ANSYS
Q-Blade

ABSTRACT

Renewable energies as a clean replacement resource of fossil fuels have many advantages, among which wind has the potential to be the very applicable source in the world. To use wind energy, two kinds of turbines have been developed; the Vertical Axis Wind Turbine (VAWT) and Horizontal Axis Wind Turbine (HAWT). In small scale applications, using a VAWT has some advantages such as low cost and noise, simple mechanism, and the low sensitivity to the wind direction. In this paper, the design and analysis of a combined wind turbine, consist of the Savonius-Darrieus rotor, are performed to use in irrigation applications. To predict the output power, a series of experiments were conducted using the Computational Fluid Dynamics (CFD) method. For this purpose, ANSYS fluent and Q-Blade software programs are used. To design the rotor performance, NACA symmetric airfoils are considered. Next, this combined turbine was made and experimental tests were performed. Finally, the output power is computed and so, the water flow rate for irrigation purposes such as water pumping is obtained. The results indicate that the self-starting of the turbine is improved using the considered design. This could be useful in regions with low wind speed.

1. INTRODUCTION

Nowadays, finding an efficient way to use renewable energies is rapidly growing in all engineering applications. Irrigation, as an example of engineering applications, has been a central feature of agriculture and is the basis of the economy and society of numerous societies. This is the engineering of controlling and harnessing the various natural sources of water, by constructing dams, reservoirs and canals, and finally distributing the water to the agricultural fields, which these operations require a specific amount of energy. This energy can be supplied by either fossil fuels or renewable resources. The limitation of fossil fuels in terms of accessibility and environmental effects resulted in performing renewable energies. Wind as one of the most important renewable energy resources can be used instead of fossil fuels, especially in arid areas with sufficient wind power.

Wind turbines have been used for irrigation and rustic mills since the 7th century AD in the ancient Persia, [1]. So, using wind turbines for irrigation applications such as water pumping operation could be a common purpose for energy consumption. In fact, wind turbine produces the electricity or mechanical energy directly from the kinetic energy of the wind. Wind turbines are classified into two categories: Vertical Axis Wind Turbine (VAWT) and Horizontal Axis Wind Turbine (HAWT). In small scale usage, the VAWT is the most common selection, [2]. In comparison with the HAWT, the VAWT has a simple structure, lower noise, and lower maintenance, [2]. Many studies have been conducted in the case of VAWT design, among which, Eriksson et al. made a comparison between Darrius and H-Rotor (two most famous VAWT types) wind turbines, [2]. They found that the most advantageous turbine is H-Rotor. El-Samanoudy et al. focused on the influence of some design parameters of VAWTs; such as the number of blades, pitch angle and the airfoil type, [3]. They realized that using NACA 0021 airfoil, the maximum power coefficient is about 25 % under a 10-degree pitch angle. Castelli et al. converted the basic BEM theory to a CFD code and analyzed a three-bladed wind turbine (NACA 0021 type) performance, [4]. Durrani compared a set of three NACA airfoils (0012, 0015, 0018) and a thicker airfoil size NACA 0022, [5]. He concluded that the NACA 0015 has a more stable performance at the various Tip Speed Ratios (TSRs) than the others. Eleni et al. investigated the behavior of NACA 0012 in various angles of attack. They observed that the k-w modeling method is the best solving method which was fitted with the experimental data, [6]. Mohammad studied the common symmetrical and unsymmetrical airfoils using the CFD method with the aim of optimizing the power output of the H-rotor turbine, [7]. Sabaeifard et al. compared the computational and experimental results of H-rotor VAWT, [8]. They showed that parameters like the airfoil type, blade quantity, and the solidity represent the solving method. Also, the power coefficient was 0.35 in the CFD model and 0.32 in the wind tunnel experiment. Lanzafame et al. studied the comparison between the classical turbulent model and the Shear-Stress Transport (SST) turbulent model, [9]. They obtained a good agreement between the experimental and the CFD results. Jouilel et al. compared different NACA airfoil shapes and found that the NACA 00XX airfoil's manufacturing cost is less than the NACA 44XX, [10]. Mohammad et al. focused on the H-rotor performance with different airfoils at low Reynolds numbers, [11]. Two meshing models are compared by using Fluent and Gambit software programs and different solving methods. They achieved that the SST k-ω method is suitable on ANSYS software and the k-ϵ method is realizable on Gambit software. Nguyen et al. investigated the effect of the NACA 00XX thickness on the

*Corresponding Author's Email: p.zarafshan@ut.ac.ir (P. Zarafshan)

starting capability, [12]. They compared four NACA symmetric airfoils and found that the best starting capability is related to the thicker airfoil. Patil et al. considered the CFD analysis of NACA 0012 at different Reynolds numbers and different pitch angles, [13]. These results were compared with the experimental data of Sandia National Laboratory, whereas the lift and the drag coefficient increased in the higher Reynolds number. Sahin and Acir studied the NACA 0015 performance in different Reynolds numbers and different pitch angles, [14]. Extracted results of CFD were compared with the experimental data which were obtained from the wind tunnel test. They found that the best performance of the rotor occurs at the pitch angle of 8°. Hameed and Afaq designed a turbine that its blades shell had a thickness 1 to 5 mm, [15]. They found that decreasing the inner shell thickness from 5 to 2 mm resulted in decreasing distortion and stress.

An experimental study to increase the efficiency of Savonius turbines has been done by [16]. They found the best number of the blade is 2 and the turbine with 2 blades had better power output in all aspect ratios. Also, they found that the combined 2 stage Savonius turbines have more power output. Mohamad Hadi Ali studied the Savonius turbines with 2 and 3 blades, [17]. He found that the coefficient of power for 2 blades was more than 3 blades since an increasing number of blades result in an increasing drag force. The influence of the number of blades on the output power of the Savonius turbine has been investigated by [18]. Turbine with 2, 3 and 4 blades was tested and results showed that the turbine with 3 blades had the best rotation and turbine with 4 blades had the best torque. This result comes from the inverse relation between RPM and torque. Combined Darrieus-Savonius turbine was investigated by [19]. Founded results show better output power for the combined turbine. Also, increasing TSR can result in increasing output power but this increasing limited to a certain point. Gawade et al. compared single Savonius with combined Darrieus-Savonius turbines, [20]. The maximum power coefficient (Cp) is 0.19 and 0.39 for single Savonius and combined turbine, respectively. Akin et al. studied the combined turbine and found that started RPM will be increased in the combined turbine, [21]. Also, the combined turbine could start easily in comparison with a single Darrieus turbine. Chauhan et al. used statistical analysis of wind data with Weibull distribution for analyzing wind probability in Indian State Rajasthan, [22]. The investigation is done at 25 m and 65 m hub height. Most probable speed has been found 5.881 m/s and 6.775 m/s for 25 m and 65 m height correspondingly. Also, the density of mean energy was founded by about 110.006KWh/m^2.

In this paper, a combined wind turbine is designed to supply the needed power for water pumping operation. This designed turbine achieved better self-starting performance at low wind speed. To this end, the NACA 0015 symmetrical airfoil has been selected for blades of the H-rotor. Since the low wind speed, Tehran is the pilot of the investigation and so, the wind data were obtained and analyzed. In this regard, the rotor was manufactured with 3 blades and 1.5 m height. Finally, simulation analyses were performed using ANSYS, Fluent and Q-Blade software programs with the wind speed 5.6 m/s.

2. INVESTIGATING METHOD

2.1. Simulation setup

To model the turbine, an H-rotor Darrieus as shown in Fig. 1, has been chosen due to its simple structure. This is the advantage of H-rotors in comparison with the other Darrieus turbines [2]. For wind speed, collected data, since 2009, were taken from Iran Methodological Organization. Also, Tehran was selected for the investigation pilot. So, data were analyzed with Weibull distribution function, and results showed that the average wind speed is 5.6 m/s. The Weibull and Rayleigh probability density functions are the most common way of analysis of wind speed data and Rayleigh probability density is the special case of Weibull distribution, [23]. To this end, a graphical method has been chosen for the Weibull distribution function. Data of 12 stations within Tehran were studied to achieve the best situation of the wind flow which has enough flow speed during 12 months of the year to perform rotation on the turbine. Most of the studied stations had wind flow less than 3 m/s in the majority of the months. The analysis showed that the best station is located on the northeast part of Tehran (35.7° E, 52.44° N) at Firozkoh Global Atmospheric Watch (GAW). The air properties are summarized in Table 1. After data collection, airfoil type needed to be considered and so, symmetric NACA 00XX airfoils were selected. The most common airfoils among H-rotor turbines, as studied in the literature, are 0012, 0015, 0018 [6]. After airfoil selection, simulations were performed by open source Q-Blade software to ensure the airfoils compatibility (Q-Blade Website). So, all airfoil models (as shown in Fig. 2) were analyzed with Q-Blade software. All simulations were conducted with the chord length 0.18 m and the radius 0.5 m. Double-Multiple Stream-tube Model was used in Q-Blade software for numerical analysis. It should be noted that the mentioned algorithm is applicable for analysis of lift based VAWT. Fig. 3 shows the power coefficient (C_p) for the mentioned three airfoil types, whereas the airfoils NACA 0015 and NACA 0018 show a similar pattern in all TSR values. Also, the best obtained TSR is 3.5. Moreover, the NACA 0012 at TSR 3.5 has the same C_p as the two other models. But, based on the input parameters; height 1.5 m and chord length 0.18 m, it is necessary to consider a stronger rotor which in this study is the thicker one (either NACA 0015 or NACA 0018). Due to the similar behavior of NACA 0015 and NACA 0018 as shown in Fig. 3, and the fact that the thicker airfoil has more weight than the other one, NACA 0015 airfoil was selected as the best case. To validate the obtained results, the performance of NACA 0015 was compared with the existing literature [6-7]. In CFD analysis, ANSYS fluent software was used. The initial data which were obtained from Q-Blade software was set as the input data at ANSYS fluent software. In the next step, a rotor solving domain needs to be defined. For the number of blades in the rotor, the best operational configuration is related to the 3 blades rotor, [4]. Fig. 4 shows the rotor domain with 3 blades that were modeled in ANSYS software. The height and the chord length of blades were selected as 1.5 m and 0.18 m, respectively. To prevent the boundaries' influence on the study, the domain was defined as the square with length 26D, where D defined as the rotor diameter. The boundary condition was defined for the right and the left borders as the velocity inlet and the pressure outlet, respectively. Also, two symmetrical boundaries were defined in the top and the bottom borders. In the middle of the domain, a circle with 1 m diameter was defined as the rotating zone. Table 2 shows the main characteristics of the designed rotor. All measuring areas meshed with the triangular method. For the area near the blades, the meshing resolution is increased. The meshing structure is shown in Fig. 5. For accurate prediction of the

flow near the blades' wall, the structural mesh with rectangle shape was used as shown in Fig. 6. The maximum value of y+ for the blades is 60. At first, the simulation was started in fluent software with a steady-state condition. It should be noted that in the simulation, a moving frame was chosen. After 1000 iterations, the simulation was coupled with the other one. In the second simulation, the sliding mesh method was used. Also, the TSR of the rotor was set to be 3.5. So, the angular speed was found to be 40 rad/s. To achieve better quality results, the time step size is 0.00044 sec., which is related to 1 degree rotating of the rotor. Besides, 1800 time steps were selected which is equal to 5 turns of the rotor. For each time step, 50 iterations were also selected, and residuals were adjusted to 1e-5. After these 1800 time steps, the momentum coefficient, C_m, was captured for one more rotation (360 time steps), concluding the total time step 2160.

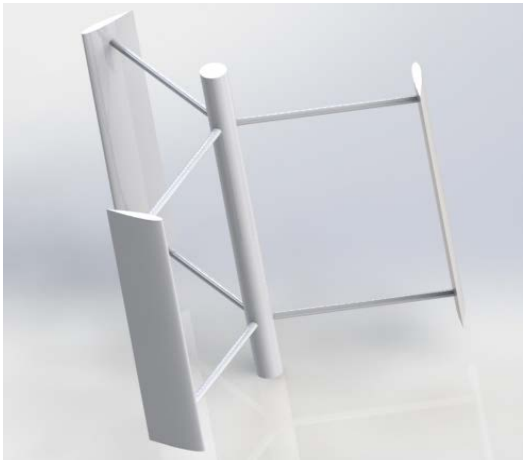

Figure 1. CAD model of H-Rotor turbine.

Table 1. Air standard properties.

Fluid type	Fluid properties		
	Density (kg/m^3)	Viscosity (kg/m-s)	Pressure (Pa)
Air	1.225	1.7894e-05	101325

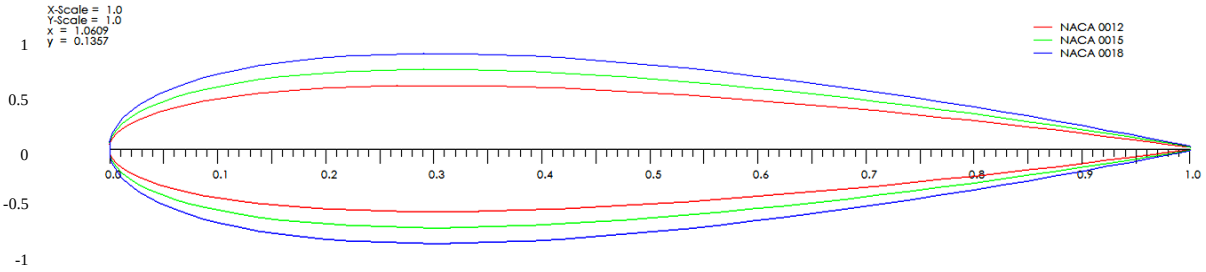

Figure 2. Three blades cross-section.

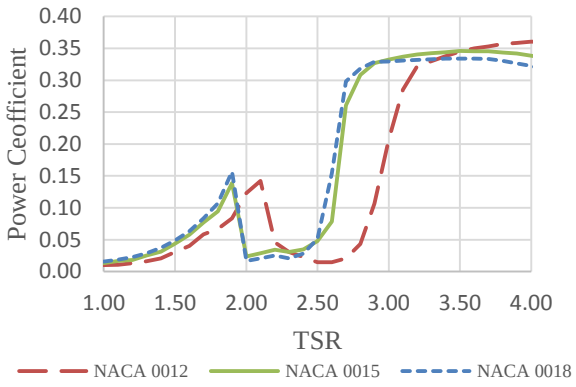

Figure 3. C_p vs TSR simulation result from Q-Blade software.

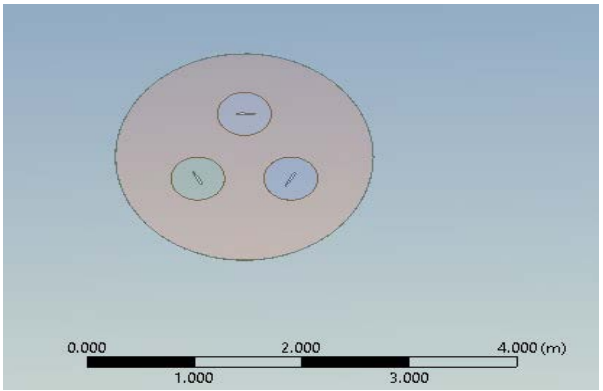

Figure 4. Model of the domain in ANSYS software.

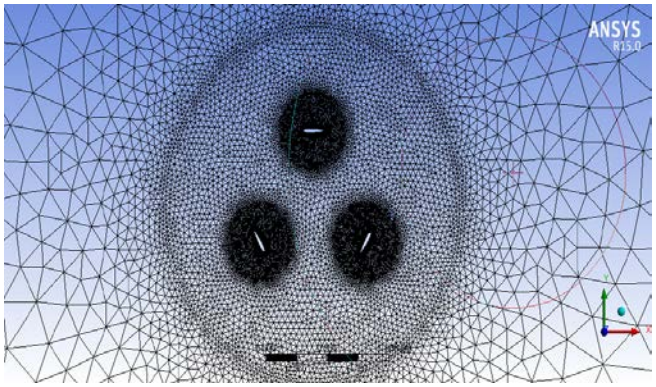

Figure 5. The meshing structure.

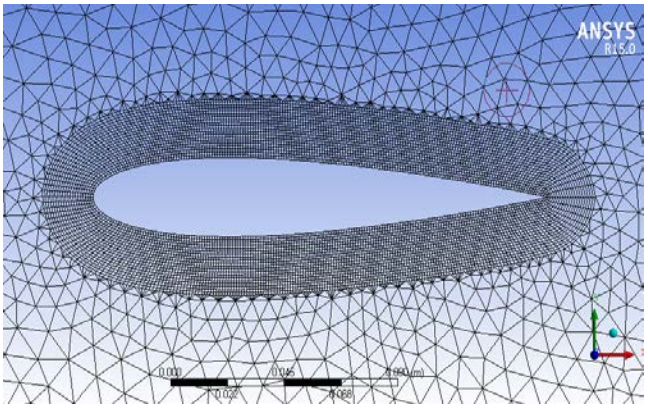

Figure 6. Structure of the mesh near the blades.

In addition, the realizable $k-\varepsilon$ solving method was selected. For the solution method, the pressure-velocity coupled was chosen. Pristo solving method was selected for the pressure and momentum. Also, the turbulent kinetic energy and turbulent dissipation rate were adjusted to the second-order upwind. So, the accuracy and the total solving time of simulation were increased. This method is the most popular for the prediction of rotating turbines, [12]. Also, the realizable $k-\varepsilon$ solving method can predict the flow near the blades in the strong pressure gradient areas better than the standard $k-\varepsilon$ method, [12]. Besides, for the Savonius turbine, simulations are done in ANSYS software, which has 50 cm diameter and 40 cm height (Fig. 7). The steady situation was selected for time and also, 2000 iterations were performed.

Table 2. Design features of simulated rotor.

Denomination	Features				
	Height	Diameter	No. of blades	Chord length	Blade section
Rotor	1.5 m	1 m	3	0.18 m	NACA0015

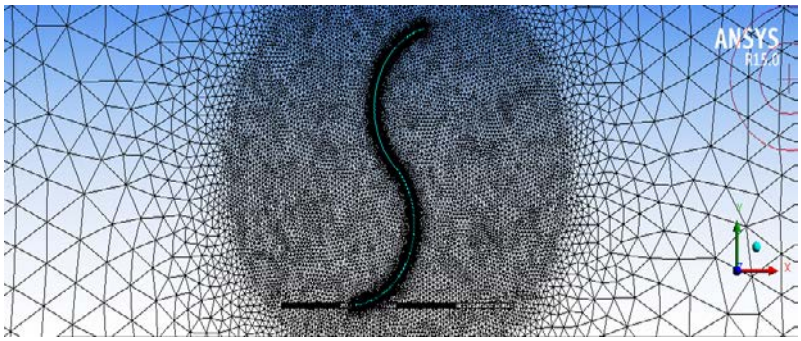

Figure 7. Meshing of Savonius turbine in ANSYS Software.

2.2. Mathemtical equations

Weibull distribution equation can be stated as:

$$F(v)=\left(\frac{k}{C}\right).\left(\frac{v}{C}\right)^{k-1}.\exp\left[-\left(\frac{v}{C}\right)^{k}\right] \quad (1)$$

where C and k are defined as the Weibull scale and shape parameters, respectively. For the graphical method, Eq. (1) is converted to the logarithmic form as:

$$\ln[-\ln(1-F(v))]=k\times\ln(v)-k\times\ln(C) \quad (2)$$

By plotting $\ln(v)$ and $[-\ln(1-F(v))]$, the Weibull scale and shape parameters are achievable, [24]. To find the power coefficient of rotor, Fluent software could give C_m. Total available power which could achieve from the wind is related to the wind speed (v_∞), the total area of passing flow from the rotor (A) and the flow density (ρ) as:

$$P_{max}=\frac{1}{2}\rho V_\infty^3 A \quad (3)$$

Power coefficient is described as the power ratio which the rotor could gain from the flow to the total available power as:

$$C_p=\frac{P}{P_{max}} \quad (4)$$

Also, the non-dimensional lift, drag and moment coefficient are, [25]:

$$C_L=\frac{L}{q_\infty S},\ C_D=\frac{D}{q_\infty S},\ C_M=\frac{M}{q_\infty Sl} \quad (5)$$

where L is the lift force, S is the reference area, q_∞ is the dynamic pressure of the flow, D and M are the drag force and pitching moment, respectively, and l is the reference length. The TSR ratio is also defined as:

$$\lambda=\frac{r\omega}{V_\infty} \quad (6)$$

where r is the rotor radius and ω is the angular velocity. Total C_p is given by C_m as, [26]:

$$C_p=C_M\lambda \quad (7)$$

2.2.1. Realizable k − ε solving method

Reynolds-averaged Navier-Stokes equation can be given as:

$$\frac{\partial}{\partial t}(\rho u_i)+\frac{\partial}{\partial x_j}(\rho u_i\rho u_j)=-\frac{\partial p}{\partial x_i}+\frac{\partial}{\partial x_i}[\mu(\frac{\partial u_i}{\partial x_j}+\frac{\partial u_j}{\partial x_i}-\frac{2}{3}\delta_{ij}\frac{\partial u_l}{\partial x_l})] +\frac{\partial}{\partial x_j}(-\rho\overline{u_i'u_j'}) \quad (8)$$

The non-linear term of equation or $(-\rho\overline{u_i'u_j'})$ described the fluctuation still appear in RANS. This influence is called the Closure problem. To solve this problem, Boussinesq introduced the concept of eddy viscosity. This theory shows that the transfer momentum is caused by turbulence. It could be modeled with the eddy viscosity. The relationship between the Reynold stress tensor and the strain tensor can be defined as:

$$\tau_{ij}=2\mu_t S_{ij}-\frac{2}{3}\rho k\delta_{ij} \quad (9)$$

where μ_t or the eddy viscosity is a scalar property and so:

$$-\rho\overline{u_i'u_j'}=\mu_t(\frac{\partial u_i}{\partial x_j}+\frac{\partial u_j}{\partial x_i})-\frac{2}{3}(\rho k+\mu_t\frac{\partial u_k}{\partial x_k})\delta_{ij} \quad (10)$$

Being of Reynolds stress tensor as the proportion of the strain tensor is the main disadvantage of Boussinesq theory.

Future model like the k-ε developed model covers this shortcoming. The transport equations can be given as:

$$\frac{\partial}{\partial t}(\rho k)+\frac{\partial}{\partial x_j}(\rho k u_j)=\frac{\partial}{\partial x_j}[(\mu+\frac{\mu_t}{\sigma_k})\frac{\partial k}{\partial x_j}]+p_k+p_b \\ +\rho\varepsilon-Y_M+S_k \quad (11)$$

and:

$$\frac{\partial}{\partial t}(\rho\varepsilon)+\frac{\partial}{\partial x_j}(\rho\varepsilon u_j)=\frac{\partial}{\partial x_j}[(\mu+\frac{\mu_t}{\sigma_\varepsilon})\frac{\partial \varepsilon}{\partial x_j}]+\rho C_1 S_\varepsilon \\ -\rho C_2\frac{\varepsilon^2}{k+\sqrt{\nu\varepsilon}}+C_{1\varepsilon}\frac{\varepsilon}{k}C_{3\varepsilon}P_b+S_\varepsilon \quad (12)$$

where:

$$S=\sqrt{2S_{ij}S_{ij}},\ C_1=\max[0.43,\frac{\eta}{\eta+5}],\eta=S\frac{k}{\varepsilon} \quad (13)$$

and the model constants are:

$$C_{1\varepsilon}=1.44, C_2=1.9, \sigma_k=1.0, \sigma_\varepsilon=1.2 \quad (14)$$

It is important to note that this model is known as the most expensive computationally model, [27].

2.3. Experimental setup

Turbines were modeled in Solidworks software as shown in Fig. 8. Each blade of the Darrieus turbine is divided into a few smaller sections. As shown in Fig. 9, balsa wood has been chosen as a blades material with the aim of low weight and good shapeable capability. Then, laser cutting CNC machine has been used to achieve good accuracy of shape sections. Also, this figure shows Balsa wood with a thickness of 1.5 mm which is used for covering sections. To improve the stability of the structure, a balsa pole with a square cross-section was selected and all sections were mounted with a distance of 10 cm. Moreover, aluminum was chosen for the main turbine shaft. For mounting blades on the mentioned shaft, 9 tubes of fiber glass with a diameter of 7.5 mm were chosen. Epoxy glue was selected for the tightening of the fiber glass tube to balsa wood blades and the main aluminum shaft. For the Savonius turbine, sheet metal with a thickness of 1 mm was used. Also, 2 circles with diameter 50 cm were mounted to the curve blades by spot welding to keep the blades. To prevent vibration, the main shaft was tightened from 3 points with the bearing system. 2 iron plates with the weight of 35 Kg were used for keeping turbine stability during its rotations. To run the experimental condition, a blower with 4 axial fans was used for the turbine test. For adjusting fans' speed, a dimmer was placed between the fans and the power source. For measurement of the wind speed, an anemometer was used. Static torque was measured by a digital torque meter. To study the influence of the Savonius turbine, the coupling system was added between two turbines. Finally, the designed experimental setup is shown in Fig. 10.

3. RESULTS AND DISCUSSION

Weibull distributions of 12 stations were investigated and it found that the best station with the most probability of wind flow at year is Firozkoh GAW. The scale and shape coefficient of Weibull distribution is 6.25 and 1.513, respectively. This Weibull distribution with the graphical method is shown in Fig. 11. The average wind speed finds as 5.6 m/s and the maximum speed is 10 m/s. So, TSR is considered as 3.5 for the selected NACA 0015 blades which are used for the simulation to achieve the best prediction of C_p. The output average value of C_m from ANSYS and Fluent software programs is 0.04. To find the C_p coefficient, Eq. 7 has been used and it is calculated as 0.14. To approve the obtained value, a simulation was done in Q-Blade software. Q-Blade software predicts the value of C_p in TSR 3.5 for the NACA 0015 about 0.34 as shown in Fig. 12. Also, the total achievable energy from the wind is calculated as 164.4 Wh. According to the Betz limit, the maximum value of C_p is 0.59. Thus, the total available power from the wind is 97 Wh. With the obtained data from the simulation, the considered H-rotor can produce 52.8 Wh. According to the torque coefficient which is found from simulation and using Eq. 5, the total achievable torque is 0.58 N.cm. After separating two turbines, experimentally maximum static torque for Darrius wind turbine is found 0.48 N.cm. Then, both turbines are coupled and the blower speed adjusted with dimmer. As shown in Fig. 13, torque coefficient was measured at different wind speed and results were compared with simulation. In the low wind speed, simulation results were less than experimental results because of the low accuracy of the simulation in low Reynolds numbers. Also, with increasing the wind speed because of the existence of the Savonius turbine in an actual situation, experimental results show lower values than the simulation. The main reason for this leakage is the fact that the Savonius turbine's behavior changed during increasing the wind speed and after increasing the wind speed this kind of turbine produced negative torque. It found that after the wind speed reaches 4 m/s, the Savonius turbine easily could start to rotate both turbines. In the simulation of the Savonius turbine, it was found that with the wind speed 3 m/s, the produced turbine torque would be enough to start the rotation according to the low weight of Darrius turbine (Fig. 14). The output power of the turbine can be used to produce a static head on the water level for irrigation purposes. To this end, it founds that with the simulation output values, the water can be pumped to 10 m height with the flow rate 1.9 m^3/h. Also, the obtained experimental results show the flow rate 0.84 m^3/h. The difference between these two values related to the simulation and the actual conditions is the fact that Savonius turbine's behavior changed during increasing the wind speed and after increasing the wind speed this kind of turbine produced negative torque.

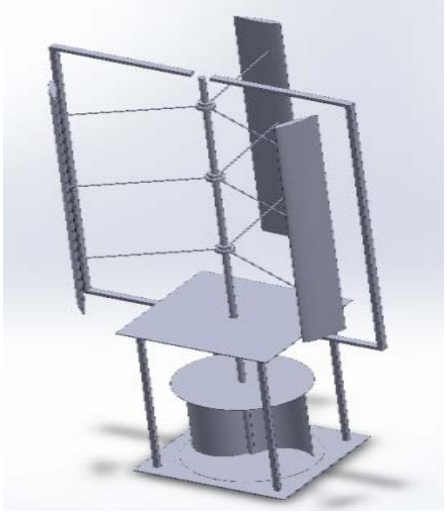

Figure 8. Modeled combined wind turbine.

Figure 9. Covered sections with Balsa wood.

Figure 10. Desigend experimental setup.

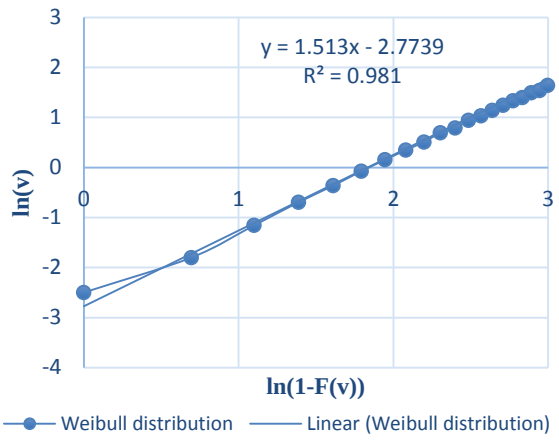

Figure 11. ln(v) vs ln(1-F(v)) scheme for scale and shape parameter of Weibull distribution.

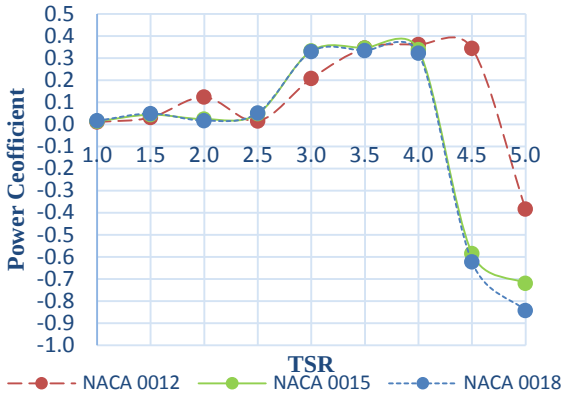

Figure 12. C_p vs TSR from Q-Blade software for 3 NACA symmetric airfoils.

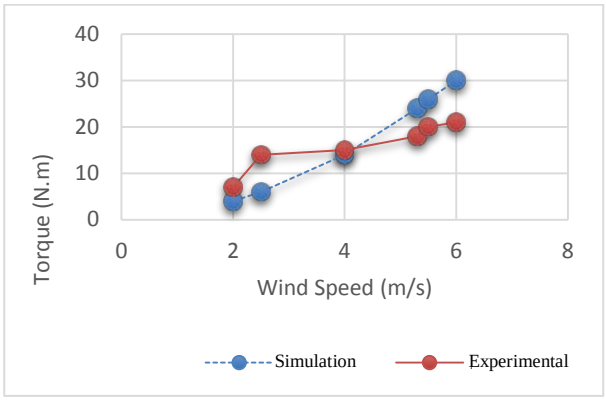

Figure 13. Comparision between produced torque in the experiment and the simulation.

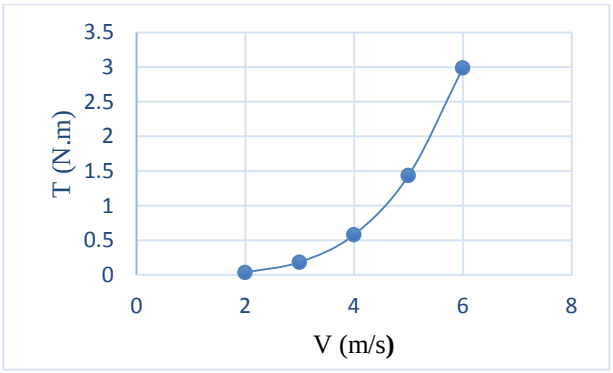

Figure 14. Produced torque in the simulation of Savonius turbine in ANSYS software.

4. CONCLUSIONS

In this paper, the design and analysis of an H-rotor wind turbine with the purpose of irrigation applications were considered. In which, Tehran was chosen as the pilot of the investigation since its low-speed wind. This wind speed required the designed combined wind turbine. Next, the simulation was performed. According to the results, the best station with the most probability of wind along one year was Firozkoh. The maximum and the mean wind speed value of this pilot were 10 m/s and 5.6 m/s, respectively. Also, the best performance of blades for the H-rotor turbine was related to the NACA 0015. As expected, the best value of TSR for NACA 0015 was considered as 3.5. Finally, the output power was computed and so, the water flow rate for irrigation

purposes such as water pumping was obtained. The results indicated that the self-starting of the turbine was improved using the considered design.

5. ACKNOWLEDGEMENT

The authors would like to thank the financial support provided by University of Tehran for accomplishing this research.

REFERENCES

1. Prasad, S. and Auradi, V., "Optimized design of rotor blade for a wind pump", ***International Journal of Renewable Energy Research (IJRER)***, Vol. 2, No. 4, (2012), 746-749.
2. Eriksson, S., Bernhoff, H. and Leijon, M., "Evaluation of different turbine concepts for wind power", ***Renewable and Sustainable Energy Reviews***, Vol. 12, No. 5, (2008), 1419-1434. (https://doi.org/10.1016/j.rser.2006.05.017).
3. El-Samanoudy, M., Ghorab, A. and Youssef, S.Z., "Effect of some design parameters on the performance of a Giromill vertical axis wind turbine", ***Ain Shams Engineering Journal***,. Vol. 1, No. 1, (2010), 85-95. (https://doi.org/10.1016/j.asej.2010.09.012).
4. Castelli, M.R., Englaro, A. and Benini, E., "The Darrieus wind turbine: Proposal for a new performance prediction model based on CFD", ***Energy***, Vol. 36, No. 8, (2011), 4919-4934. (https://doi.org/10.1016/j.energy.2011.05.036).
5. Durrani, N., "A detailed aerodynamic design and analysis of a 2D vertical axis wind turbine using sliding mesh in CFD", ***Proceedings of 49th AIAA Aerospaces Sciences Meeting and Exhibition***, (2011).
6. Eleni, D.C., Athanasios, T.I. and Dionissios, M.P., "Evaluation of the turbulence models for the simulation of the flow over a National Advisory Committee for Aeronautics (NACA) 0012 airfoil", ***Journal of Mechanical Engineering Research***, Vol. 4, No. 3, (2012), 100-111. (https://doi.org/10.5897/JMER11.074).
7. Mohamed, M., "Performance investigation of H-rotor Darrieus turbine with new airfoil shapes", ***Energy***, Vol. 47, No. 1, (2012), 522-530. (https://doi.org/10.1016/j.energy.2012.08.044).
8. Sabaeifard, P., Razzaghi, H. and Forouzandeh, A., "Determination of vertical axis wind turbines optimal configuration through CFD simulations", ***Proceedings of International Conference on Future Environment and Energy***, (2012).
9. Lanzafame, R., Mauro, S. and Messina, M., "2D CFD modeling of H-Darrieus wind turbines using a transition turbulence model", ***Energy Procedia***, Vol. 45, (2014), 131-140. (https://doi.org/10.1016/j.egypro.2014.01.015).
10. Jouilel, N., Radouani, M. and El Fahime, B., "Geometric modeling and contribution to the choice of a blade profile", ***Proceedings of Xème Conférence Internationale: Conception et Production Intégrées***, (2015).
11. Mohamed, M., Ali, A. and Hafiz, A., "CFD analysis for H-rotor Darrieus turbine as a low speed wind energy converter", ***Engineering Science and Technology, an International Journal***, Vol. 18, No. 1, (2015), 1-13. (https://doi.org/10.1016/j.jestch.2014.08.002).
12. Nguyen, C., Le, T. and Tran, P., "A numerical study of thickness effect of the symmetric NACA 4-digit airfoils on self starting capability of a 1KW H-type vertical axis wind turbine", ***International Journal of Mechanical Engineering and Applications (IJMEA)***, Vol. 3, No. 3-1, (2015), 7-16. (https://doi.org/10.11648/j.ijmea.s .2015030301.12).
13. Patil, B.S. and Thakare, H.R., "Computational fluid dynamics analysis of wind turbine blade at various angles of attack and different Reynolds number", ***Procedia Engineering***, Vol. 127, (2015), 1363-1369. (https://doi.org/10.1016/j.proeng.2015.11.495).
14. Şahin, İ. and Acir, A., "Numerical and experimental investigations of lift and drag performances of NACA 0015 wind turbine airfoil", ***International Journal of Materials, Mechanics and Manufacturing***, Vol. 3, No. 1, (2015), 22-25. (https://doi.org/10.7763/IJMMM.2015.V3.159).
15. Hameed, M.S. and Afaq, S.K., "Design and analysis of a straight bladed vertical axis wind turbine blade using analytical and numerical techniques", ***Ocean Engineering***, Vol. 57, (2013), 255-248. (https://doi.org/10.1016/j.oceaneng.2012.09.007).
16. Mahmoud, N.H., El-Haroun, A.A., Wahba, E. and Nasef, M.H., "An experimental study on improvement of Savonius rotor performance", ***Alexandria Engineering Journal***, Vol. 51, No. 1, (2012), 19-25. (https://doi.org/10.1016/j.aej.2012.07.003).
17. Ali, M.H., "Experimental comparison study for Savonius wind turbine of two & three blades at low wind speed", ***International Journal of Modern Engineering Research (IJMER)***, Vol. 3, No. 5, (2013), 2978-2986.
18. Wenehenubun, F., Saputra, A. and Sutanto, H., "An experimental study on the performance of Savonius wind turbines related with the number of blades", ***Energy Procedia***, Vol. 68, (2015), 297-304. (https://doi.org/10.1016/j.egypro.2015.03.259).
19. Sharma, K.K., Biswas, A. and Gupta, R., "Performance measurement of a three-bladed combined Darrieus-Savonius rotor", ***International Journal of Renewable Energy Research***, Vol. 3, No. 4, (2013), 885-891.
20. Gawade, S.G. and Patil, D.S., "Comparative study of a single stage Savonius with a combined Savonius-three bladed Darrieus", ***International Journal For Technological Research In Engineering (IJTRE)***, Vol. 2, No. 6, (2015), 542-545.
21. Ilhan, A., Bilgili, M. and Sahin, B., "Analysis of aerodynamic characteristics of 2 MW horizontal axis large wind turbine", ***Wind and Structures, An International Journal***, Vol. 27, No. 3, (2018), 187-197. (https://doi.org/10.12989/was.2018.26.3.187).
22. Chauhan, A. and Saini, R.P., "Statistical analysis of wind speed data using Weibull distribution parameters", ***Proceedings of IEEE 1st International Conference on Non Conventional Energy (ICONCE)***, Kalyani, India, (2014). (https://doi.org/10.1109/ICONCE.2014.6808712).
23. Celik, A.N., "Assessing the suitability of wind energy speed probability distribution functions based on wind power density", ***Renewable Energy***, Vol. 28, (2003), 1563-1574.
24. Kidmo, D., "Statistical analysis of wind speed distribution based on six Weibull methods for wind power evaluation in Garoua, Cameroon", ***Revue des Energies Renouvelables***, Vol. 18, No. 1, (2015), 105-125.
25. Anderson Jr, J.D., Fundamentals of aerodynamics, Tata McGraw-Hill Education, (2010).
26 Patel, M.B. and Kevat, V., "Performance prediction of straight bladed Darrieus wind turbine by single streamtube model", ***International Journal of Advanced Engineering Technology (IJAET)***, Vol. 14, No. 2, (2013), 86-89.
27. Marzouk, O.A. and Huckaby, E.D., "Simulation of a swirling gas-particle flow using different k-epsilon models and particle-parcel relationships", ***Engineering Letters***, Vol. 18, No. 1, (2010).

ABSTRACTS

Heat Transfer, Environmental Benefits, and Social Cost Analysis of Different Insulation Methods by Considering Insulation Disadvantages

Mohsen Fallah[a,b*], Zahra Medghalchi[b]

[a] *Department of Mechanical Engineering, Azarbaijan Shahid Madani University, Tabriz, Iran.*
[b] *Research Institute of Applied Power System Studies, Azarbaijan Shahid Madani University, Tabriz, Iran.*

P A P E R I N F O

Paper history:
Received 11 December 2019
Accepted in revised form 18 May 2020

Keywords:
Anti-Insulation
Wall Insulation Configuration
HVAC Operation Mode
Greenhouse Gas Emission
Social Cost

A B S T R A C T

In this paper, the thermal performance of four common insulators in two internal and external insulation systems is investigated for the ASHRAE setpoint range by applying detailed numerical simulation and Anti-Insulation phenomenon. Anti-Insulation phenomenon and consequent extra load on the HVAC system can occur following the thermal insulation of a building if proper temperature setpoint is not selected. In the next step, the proper setpoint is analyzed under simulated building conditions, and all related criteria are studied for this temperature. Also, continuous and intermittent operations of the air conditioning system are investigated. Moreover, the assessment of the environmental benefit of wall insulation is performed by evaluating greenhouse gasses emission payback period and social cost saving. A residential building is simulated in the EnergyPlus software for the case study. Results show that Anti-Insulation occurs approximately at 22 ºC. Both external and internal insulations lead to a significant reduction in energy consumption. Nevertheless, the external insulation shows a bit more reduction. Intermittent operation outperforms the continuous operation by 8 % on average. The insulator's production phase is considered in the analysis of the insulation environmental benefits. Results show that, in this case, the prioritization of insulators would be different from that case in which this process is not considered. According to results, in terms of social costs, applying thermal insulation to residential buildings is necessary.

چکیده

پدیده آنتی‌اینزولشن پدیده ای است که در صورت عدم انتخاب دمای آسایش سرمایش مناسب پس از عایقکاری ساختمان رخ داده و منجر به افزایش بار سرمایشی ساختمان می‌شود. برای نشان دادن این مسأله ابتدا عملکرد حرارتی چهار عایق متداول با دو روش عایقکاری داخلی و خارجی برای محدوده دمای آسایش استاندارد ASHRAE-55 مورد بررسی قرار گرفته است. سپس دمای آسایش سرمایش بهینه محاسبه شده و پس از آن تمامی معیارهای ارزیابی عملکرد حرارتی عایق ها برای این دما مورد بررسی قرار گرفته است. همچنین عملکرد سیستم تهویه مطبوع یکسره با سیستم تهویه مطبوع قطع-وصلی مقایسه شده است. فواید زیست‌محیطی عایقکاری با محاسبه دوره جبران گازهای گلخانه ای انتشار یافته طی فرآیند تولید و حمل ونقل عایق از طریق صرفه‌جویی انرژی حاصل از عایقکاری ساختمان محاسبه شده است و میزان صرفه‌جویی در هزینه‌های اجتماعی گازهای گلخانه‌ای نیز بدست آمده است. ساختمان مورد مطالعه واحد مسکونی یک مجتمع می باشد که در نرم‌افزار انرژی پلاس مدلسازی شده است. بر اساس نتایج، پدیده آنتی‌اینزولشن در دمای تقریبی ۲۲ $^{\circ}C$ اتفاق می‌افتد، لذا در ادامه کار دمای ۲۱ $^{\circ}C$ و ۲۰ $^{\circ}C$ به ترتیب برای دمای آسایش سرمایش و گرمایش انتخاب شده است. هر دو روش عایقکاری داخلی و خارجی منجر به صرفه‌جویی انرژی می‌شود که عایقکاری خارجی عملکرد نسبتاً بهتری دارد و سیستم تهویه مطبوع قطع-وصلی ۸ ٪ صرفه‌جویی بیشتری نسبت به سیستم تهویه مطبوع یکسره بدست می‌دهد. بررسی های زیست‌محیطی نشان می‌دهد اولویت انتخاب عایق در حالتی که پروسه تولید آن لحاظ شده متفاوت با زمانی خواهد بود که این پروسه در نظر گرفته نشود. همچنین از لحاظ بررسی صرفه‌جویی هزینه‌های اجتماعی به کارگیری عایق در ساختمان‌ها ضروری می‌باشد.

An Overview of Hydroelectric Power Plant: Operation, Modeling, and Control

Ghazanfar Shahgholian[a,b]

[a] *Smart Microgrid Research Center, Najafabad Branch, Islamic Azad University, Najafabad, Iran.*
[b] *Department of Electrical Engineering, Najafabad Branch, Islamic Azad University, Najafabad, Iran.*

P A P E R I N F O

Paper history:
Received 01 March 2020
Accepted in revised form 14 June 2020

Keywords:
Operation
Control
Renewable Energy
Hydropower
Hydraulic Turbine
Governing System

A B S T R A C T

Renewable energy provides twenty percent of electricity generation worldwide. Hydroelectric power is the cheapest way to generate electricity today. It is a renewable source of energy and provides almost one-fifth of electricity in the world. Also, it generates electricity using a renewable natural resource and accounting for six percent of worldwide energy supply or about fifteen percent of the world's electricity. Hydropower is produced in more than 150 countries. Hydropower plant producers provide energy due to moving or falling water. This paper presents and discusses studies on hydroelectric power plant fields, which have been carried out by different investigators. This work aims to study and provide an overview of hydroelectric power plants such as applications, control, operation, modeling and environmental impacts. Also, the hybrid power and efficiency of the hydroelectric power plants has been investigated. The applications of a flexible AC transmission system (FACTS) controller in the power system with the hydroelectric power plants are presented.

چکیده

انرژی تجدیدپذیر بیست درصد از انرژی الکتریکی در سراسر جهان را تأمین می‌کند. نیروگاه برق آبی ارزانترین روش برای تولید برق امروزی است. این یک منبع تجدیدپذیر انرژی است و تقریباً یک پنجم برق در جهان را تأمین می‌کند. همچنین، این نیروگاه با استفاده از منابع طبیعی تجدیدپذیر، شش درصد از انرژی در سراسر جهان یا حدود پانزده درصد از برق جهان را تولید می‌کند. نیروگاه برق در بیش از ۱۵۰ کشور جهان تولید می‌شود. تولیدکنندگان نیروگاه برق به دلیل حرکت یا ریزش آب انرژی را تأمین می‌کنند. در این مقاله به بررسی و بحث در مورد نیروگاه‌های برق آبی می‌پردازیم که توسط محققان مختلف انجام شده است. هدف از این کار بررسی و ارائه مروری بر نیروگاه‌های برق آبی مانند برنامه‌های کاربردی، کنترل، بهره‌برداری، مدل‌سازی و تأثیرات محیطی است. همچنین، قدرت ترکیبی و کارایی نیروگاه‌های برق آبی مورد بررسی قرار گرفته است. برنامه‌های کنترل‌کننده سیستم انتقال انعطاف‌پذیر AC (FACTS) در سیستم برق با نیروگاه برق آبی ارائه شده است.

Energy Simulation and Management of the Main Building Component Materials Using Comparative Analysis in a Mild Climate Zone

Nima Amani

Department of Civil Engineering, Chalous Branch, Islamic Azad University, Chalous, Iran.

P A P E R I N F O

Paper history:
Received 16 April 2020
Accepted in revised form 04 July 2020

Keywords:
Energy Conservation
Energy Management
Comparative Analysis
Residential Building
Materials
Case Study

A B S T R A C T

Must limited energy resources and the need for energy saving make the design of buildings more efficient in terms of energy consumption. For this reason, proper orientation of buildings, use of sunlight, natural ventilation, application of consumable materials are factors that help reduce heat and cooling loads. The objective of this study is to evaluate the energy efficiency of residential buildings using natural energy and optimizing the choice of materials for heat and cold saving with the Ecotect simulation software. According to analysis and simulation, it was found that the optimum materials of the main building components in a mild climate zone of Rasht city include (a) the Brick Conc block Plaster for a wall with the total radiation incident of 340 W/m^2 and a radiation absorption of 240 W/m^2, (b) Double Glazed-Low E for windows with the total radiation incident of 340 W/m^2 and a radiation absorption of 100 W/m^2, (c) Foam Core Ply Wood for door with the total radiation incident of 340 W/m^2 and a radiation absorption of 200 W/m^2, (d) ConcSlab- OnGround for floor with the total radiation incident of 340 W/m^2 and a radiation absorption of 220 W/m^2, and (e) Conc Roof Asphalt for roof with the total radiation incident of 340 W/m^2 and a radiation absorption of 300 W/m^2. According to an hourly temperature analysis of all stories of the building on two hot and cold days of the year and as observed by the design and material selection requirements, the building will be conditioned in an almost thermal comfort zone (below 30 degrees) in the warm season.

چکیده

هدف از این مطالعه، ارزیابی راندمان انرژی ساختمانهای مسکونی با استفاده از انرژی طبیعی و بهینه‌سازی انتخاب مواد جهت صرفه‌جویی در گرما و سرما با استفاده از نرم‌افزار Ecotect است. با توجه به تحلیل‌های انجام شده با استفاده از نرم‌افزار شبیه‌سازی، مشخص شد که ماده بهینه اجزای اصلی ساختمان در منطقه آب و هوایی معتدل شهر رشت، Brick Conc block Plaster برای دیوار با انعکاس تابش کل ۳۴۰ وات بر مترمربع و جذب تابش ۲۴۰ وات بر مترمربع است. Double Glazed-Low E برای پنجره با انعکاس تابش کل ۳۴۰ وات بر مترمربع و جذب اشعه ۱۰۰ وات بر مترمربع؛ Foam Core Ply Wood برای درب با انعکاس تابش کلی ۳۴۰ وات بر مترمربع و جذب تابش ۲۰۰ وات بر مترمربع؛ ConcSlab- OnGround برای کف با انعکاس تابش کل ۳۴۰ وات بر مترمربع و جذب تابش ۲۲۰ وات بر مترمربع و Conc Roof Asphalt برای پشت بام با کل انعکاس تابش ۳۴۰ وات بر مترمربع و جذب اشعه ۳۰۰ وات بر مترمربع می‌باشند. با توجه به تجزیه و تحلیل دمای ساعتی برای کلیه طبقه های ساختمان در دو روز گرم و سرد سال، با توجه به طراحی و الزامات انتخاب مواد، مشخص می‌شود که ساختمان در منطقه آسایش حرارتی نزدیک (زیر ۳۰ درجه) در فصل گرم واقع شده است.

Cost and Environmental Pollution Reduction Based on Scheduling of Power Plants and Plug-in Hybrid Electric Vehicles

Roya Pashangpour[a], Faramarz Faghihi[a*], Soodabeh Soleymani[a], Hassan Moradi CheshmehBeigi[b]

[a] *Faculty of Mechanics, Electrical Power and Computer, Science and Research Branch, Islamic Azad University, Tehran, Iran.*
[b] *Department of Electrical Engineering, Razi University, Kermanshah, Iran.*

PAPER INFO

Paper history:
Received 02 February 2020
Accepted in revised form 05 July 2020

Keywords:
Scheduling of Power Plants
Plug-in Hybrid Electric Vehicles
GAMS
Uncertain Behavior

ABSTRACT

There has been a global effort to reduce the amount of greenhouse gas emissions. In an electric resource scheduling, emission dispatch and load economic dispatch problems should be considered. Using renewable energy resources (RESs), especially wind and solar, can be effective in cutting back emissions associated with power system. Further, the application of electric vehicles (EV) capable of being connected to power grid reduces the pollution level in the transportation sector. This paper investigates a resource scheduling with uncertain behavior of RESs and EVs by considering the penalty factors of emission for each conventional power plant in Hormozgan province of Iran for a 10-year period from 2016 to 2026. In this study, combined-cycle and thermal units are also taken into account. The CPLEX Solver is utilized for resource scheduling problem in GAMS. For combined-cycle power plants, ramp rate constraints are also included. To investigate the impact of uncertainties, different scenarios are considered. The obtained results demonstrate that Hormozgan province has a decent potential of utilizing RESs and EVs to achieve pollution reduction and optimal cost.

چکیده

امروزه تلاش زیادی در سطح جهان برای کاهش میزان انتشار گازهای گلخانه‌ای صورت گرفته است. استفاده از منابع انرژی تجدیدپذیر، به ویژه انرژی باد و خورشیدی، می‌تواند برای کاهش انتشار گازهای گلخانه‌ای مرتبط با سیستم انرژی مؤثر باشد. از طرف دیگر، استفاده از وسایل نقلیه الکتریکی که قادر به اتصال به شبکه هستند، باعث کاهش سطح آلودگی در بخش حمل و نقل می‌شود. در این مقاله، برنامه‌ریزی منابع انرژی با عدم قطعیت منابع انرژی نو و خودروهای الکتریکی و در نظر گرفتن فاکتورهای جریمه انتشار برای هر نیروگاه مرسوم در استان هرمزگان، برای یک دوره ۱۰ ساله از سال ۲۰۱۶ تا ۲۰۲۶، بررسی شده است. در این مطالعه همچنین سیکل ترکیبی و واحدهای حرارتی در نظر گرفته شده است. مسأله برنامه‌ریزی منابع با بهره‌گیری از GAMS حل شده است. از طرفی برای نیروگاه سیکل ترکیبی، محدودیت شیب تغییرات لحاظ شده است. جهت بررسی تأثیر عدم قطعیت، سناریوهای مختلفی درنظر گرفته شده است. نتایج نشان می‌دهد استان هرمزگان از پتانسیل مناسبی برای استفاده از منابع انرژی های تجدیدپذیر و خودروهای الکتریکی در راستای رهیافت بهینه حداقل‌سازی آلایندگی و هزینه برخوردار است.

Quantification of Thermal Energy Performance Improvement for Building Integrated Photovoltaic Double-Skin Façade Using Analytical Method

Mahdi Shakouri[a], Alireza Noorpoor[a*], Hossein Ghadamian[b]

[a] *Department of Environmental Engineering, School of Environment, College of Engineering, University of Tehran, P. O. Box: 11155-4563, Tehran, Iran.*
[b] *Department of Energy, Materials and Energy Research Center (MERC), MeshkinDasht, Alborz, Iran.*

P A P E R I N F O

Paper history:
Received 25 April 2020
Accepted in revised form 13 July 2020

Keywords:
Analytical Method
Building Integrated Photovoltaic Thermal
Double Skin Façade
Energy Saving
Thermal Performance

A B S T R A C T

This study presents an analytical method for quantifying the improvement of thermal energy performance of a building integrated photovoltaic double-skin façade. The system was suggested as a retrofit measure for an existing building in Tehran. The effect of thermal performance was analyzed through computer-assisted developed codes using Engineering Equation Solver (EES) software. Three scenarios were defined and for each scenario, temperature and velocity profiles were provided through continuity, momentum, and energy equations. Given that the monocrystalline photovoltaic modules and the double-glazed windows are quite common in the current condition in Tehran, the authors considered them for analysis. A comparison of results is valuable for those cases that intend to select either glass or photovoltaic as the outer façade. The quantitative results illustrate that the proposed system would reduce the cooling demand in the summer case by 18.5 kilowatts, which is around 8.7 percent of the current cooling load. According to the results of the sensitivity analysis, both glass and photovoltaic façades were of greater efficiency in terms of energy saving in the summer. By increasing the ratio between the photovoltaic outer façade to the surface area of the glass section, the amount of energy saving due to the total cooling load reduction will increase. The results of the analysis showed that the application of the suggested system would reduce the thermal load by 2.1 percent in the winter season.

چکیده

در این تحقیق، روش تحلیلی کمّی کردن مقدار بهبود عملکرد انرژی حرارتی برای سامانه فتوولتائیک حرارتی ساختمان دو پوسته ارائه شده است. سامانه مورد مطالعه به عنوان یک راهکار اصلاحی برای یک ساختمان اداری در حال بهره‌برداری واقع در شهر تهران پیشنهاد شده است و تأثیر استفاده از آن بر عملکرد حرارتی با استفاده از برنامه رایانه‌ای کدنویسی شده در نرم‌افزار حل‌گر معادلات مهندسی تحلیل شده است. برای این منظور سه سناریو تعریف شد و برای هر سناریو، پروفایل دما و سرعت با استفاده از معادلات پیوستگی، مومنتوم و انرژی توسعه داده شده است. با توجه به این که در شرایط کنونی شهر تهران، استفاده از ماژول‌های فتوولتائیک مونوکریستالی و پنجره‌های دو جداره متداول است، محققان برای شبیه‌سازی این نوع ماژول و پنجره را مورد استفاده قرار دادند. مقایسه نتایج این تحقیق با هدف انتخاب ماژول فتوولتائیک یا شیشه برای پوسته بیرونی ارزشمند است. نتایج کمّی نشان‌دهنده آن است که سامانه پیشنهادی قابلیت کاهش بار سرمایشی فصل تابستان به میزان ۱۸/۵ کیلووات را دارا است که درحدود ۸/۷ درصد بار سرمایشی کنونی است. براساس نتایج تحلیل حساسیت، هر دو نوع مواد مورد استفاده تأثیر قابل توجهی در صرفه‌جویی انرژی فصل تابستان دارند. براساس نتایج تحلیل‌ها، با افزایش نسبت سطح ماژول فتوولتائیک به شیشه، مقدار صرفه‌جویی انرژی به‌واسطه کاهش بار سرمایشی افزایش می‌یابد. نتایج تحلیل نشان می‌دهد که کاربرد سامانه پیشنهادی در فصل زمستان، امکان کاهش تقاضای بار حرارتی به میزان ۲/۱ درصد را فراهم می‌کند.

Assessing Economic, Social, and Environmental Impacts of Wind Energy in Iran with Focus on Development of Wind Power Plants

Hasan Hekmatnia[a], Ahmad Fatahi Ardakani[b*], Armin Mashayekhan[c], Morteza Akbari[d]

[a] *Department of Geography & Urban Planning, Payam Noor University, Iran.*
[b] *Department of Agricultural Economics, Faculty of Agriculture & Natural Resources, Ardakan University, P. O. Box: 184, Ardakan, Iran.*
[c] *Shirvan Higher Education Complex, Ferdowsi University of Mashhad (FUM), Mashhad, Iran.*
[d] *Department of Desert Area Management, Faculty of Natural Resources and Environment, Ferdowsi University of Mashhad (FUM), Mashhad, Iran.*

PAPER INFO

Paper history:
Received 15 March 2020
Accepted in revised form 18 July 2020

Keywords:
Renewable Energy,
Environmental Pollution
Wind Power Plant
Global Warming
Iran

ABSTRACT

As a key economic element, energy plays an important role in the development of societies. Economic growth and its urgent need for energy highlight the need for optimal energy use. Wind energy is an energy source that has become an increasingly common source of electricity. In this study, socio-economic impacts of the cost of electricity generated by wind power plants were assessed with Iran as the focus of this study. The environmental impacts of wind energy were also considered by reviewing and analyzing research papers. Studies showed that although the use of wind energy in Iran began in Manjil in northern Iran, no significant progress has been made in this field despite all the efforts over the past years. The results indicated that the initial cost of launching wind turbines was the most important factor in the failure of this technology. The costs of purchasing turbines, construction of roads, provision of electrical infrastructure, project management, installation of turbines, insurance premiums, grid connections, and power lines were shown to affect costs of energy production. Furthermore, operation and maintenance costs, the choice of installation location, increasing production capacity, expansion of the energy market, and policies in the country can play an essential role in determining the cost of wind energy production. Given that power generation using wind turbines are economical, it is recommended that turbines be installed in suitable windy locations. In addition, considering that one of the crises facing the world and especially Iran is environmental pollution, utilizing energies such as wind energy for generating electricity is advised due to their lower pollutant emissions and lower economic and social costs.

چکیده

انرژی به عنوان یکی از عناصر کلیدی اقتصادی نقش مهّم و حیاتی در توسعه جوامع ایفا می‌کند. رشد روز افزون اقتصاد و نیـاز مبـرم آن بـه انـرژی، ضرورت استفاده بهینه انرژی را نمایان می‌سازد. انرژی باد از جمله منابع انرژی است که استفاده از آن برای تولیـد الکتریسـیته، سـرعت رو بـه رشـد بالایی را نشان می‌دهد. در این تحقیق اثرات اجتماعی- اقتصادی ناشی از هزینه‌های انرژی برق تولیدی که با استفاده از نیروگـاه‌هـای بـادی بدسـت می‌آیند با تمرکز بر کشور ایران بررسی شده است. تأثیرات زیست محیطی انرژی باد نیز با بررسی و تحلیل مقالات تحقیقاتی مورد توجه قـرار گرفتـه است. مطالعات نشان می‌دهد در طی سال‌های گذشته، استفاده از انرژی تجدیدپذیر بادی در منطقه منجیل در شمال ایران آغاز گردید ولی بـا تمـام تلاش‌های انجام شده، پیشرفت چشم‌گیری در این زمینه صورت نگرفته است. نتایج نشان دهنده آن است که هزینه‌های اوّلیه راه‌اندازی توربین بادی، مهّم‌ترین عامل در عدم موفقیّت این تکنولوژی بوده است. هزینه‌هایی از جمله هزینه خرید توربین، ساخت و ساز راه‌ها، زیربنای الکتریکـی، مـدیریت پروژه، نصب توربین‌ها، حق بیمه، هزینه اتصالات شبکه و خطوط انتقال نیرو می‌توانند بر هزینه تمام شده تولید انـرژی از بـاد نقـش اساسـی داشـته باشند. علاوه بر این، هزینه‌های بهره‌برداری و نگهداری، انتخاب محل نصب، افزایش ظرفیت تولید، گسترش بازار انـرژی و سیاسـت هـای موجـود در کشور می‌تواند در تعیین هزینه های تولید انرژی بادی نقش اساسی داشته باشد. با توجه به اینکه تولید انرژی برق از توربین‌های بـادی دارای صـرفه اقتصادی است، لذا توصیه می‌شود توربین‌های بادی در مکان‌های مستعد نصب شوند. همچنین با توجه به اینکه یکی از بحران‌های پیش‌روی جهان و بخصوص ایران، آلودگی محیط زیست است و تولید الکتریسته از توربینهای بادی باعث صرفه جویی در هزینه‌های اقتصادی و اجتماعی می‌گردد، لـذا استفاده بیشتر از انرژی‌های پاک در تولید انرژی الکتریسته نیز توصیه می‌شود.

Design and Analysis of a Combined Savonius-Darrieus Wind Turbine for Irrigation Application

Mahdi Shahmari, Payam Zarafshan*, Shahriar Kouravand, Morteza Khashehchi

Department of Agro-Technology, College of Aburaihan, University of Tehran, Pakdasht, Tehran, Iran.

P A P E R I N F O

Paper history:
Received 18 March 2020
Accepted in revised form 21 July 2020

Keywords:
Irrigation
Combined Savonius-Darrieus Wind Turbine
Experimental Setup
CFD
ANSYS
Q-Blade

A B S T R A C T

Renewable energies as a clean replacement resource of fossil fuels have many advantages, among which wind has the potential to be the very applicable source in the world. To use wind energy, two kinds of turbines have been developed; the Vertical Axis Wind Turbine (VAWT) and Horizontal Axis Wind Turbine (HAWT). In small scale applications, using a VAWT has some advantages such as low cost and noise, simple mechanism, and the low sensitivity to the wind direction. In this paper, the design and analysis of a combined wind turbine, consist of the Savonius-Darrieus rotor, are performed to use in irrigation applications. To predict the output power, a series of experiments were conducted using the Computational Fluid Dynamics (CFD) method. For this purpose, ANSYS fluent and Q-Blade software programs are used. To design the rotor performance, NACA symmetric airfoils are considered. Next, this combined turbine was made and experimental tests were performed. Finally, the output power is computed and so, the water flow rate for irrigation purposes such as water pumping is obtained. The results indicate that the self-starting of the turbine is improved using the considered design. This could be useful in regions with low wind speed.

چکیده

انرژی‌های تجدیدپذیر به عنوان یک منبع جایگزین تمیز از سوخت‌های فسیلی دارای مزایای بسیاری هستند، از جمله می‌توان به انرژی باد اشاره نمود که این پتانسیل را دارد تا منبع بسیار کاربردی در جهان باشد. برای استفاده از انرژی باد، دو نوع توربین در دسترس می‌باشد که عبارتند از: توربین بادی محور عمودی (VAWT) و توربین بادی محور افقی (HAWT). برای کاربردهایی در مقیاس کوچک، استفاده از VAWT برخی از مزایا از قبیل هزینه کمتر، سر و صدای کمتر، مکانیزم ساده و حساسیت کمتر نسبت به جهت باد را دارا می‌باشد. در این مقاله، طراحی و آنالیز یک توربین عمودی از نوع ترکیبی ساوینیوس-داریوس مورد مطالعه قرار گرفته است که می‌تواند برای کاربرد آبیاری مورد استفاده قرار گیرد. برای این منظور، یک شبیه‌سازی مبتنی بر دینامیک سیالات محاسباتی (CFD) و یک سری آزمایش‌های واقعی برای پیش‌بینی توان خروجی انجام شده است. برای شبیه‌سازی‌ها، از نرم‌افزارهای ANSYS و Q-Blade استفاده شده است. برای طراحی عملکرد روتور، پروفیل‌های متقارن NACA در نظر گرفته شده است. در مرحله بعد، این توربین ترکیبی ساخته شده و بررسی‌های آزمایشی انجام شده است. نتایج نشان می‌دهند انحراف بین شبیه‌سازی و نتایج تجربی واقعی است. سرانجام، توان خروجی توربین محاسبه می‌شود و بنابراین، سرعت جریان آب برای اهداف آبیاری مانند پمپاژ آب بدست می‌آید. نتایج نشان می‌دهد که خود شروع شوندگی توربین با توجه به طراحی انجام شده بهبود می‌یابد. این امر می‌تواند در نواحی با سرعت باد پایین مفید باشد.

CONTENTS

Mohsen Fallah **Zahra Medghalchi**	Heat Transfer, Environmental Benefits, and Social Cost Analysis of Different Insulation Methods by Considering Insulation Disadvantages	1-13
Ghazanfar Shahgholian	An Overview of Hydroelectric Power Plant: Operation, Modeling, and Control	14-28
Nima Amani	Energy Simulation and Management of the Main Building Component Materials Using Comparative Analysis in a Mild Climate Zone	29-46
Roya Pashangpour **Faramarz Faghihi** **Soodabeh Soleymani** **Hassan Moradi CheshmehBeigi**	Cost and Environmental Pollution Reduction Based on Scheduling of Power Plants and Plug-in Hybrid Electric Vehicles	47-55
Mahdi Shakouri **Alireza Noorpoor** **Hossein Ghadamian**	Quantification of Thermal Energy Performance Improvement for Building Integrated Photovoltaic Double-Skin Façade Using Analytical Method	56-66
Hasan Hekmatnia **Ahmad Fatahi Ardakani** **Armin Mashayekhan** **Morteza Akbari**	Assessing Economic, Social, and Environmental Impacts of Wind Energy in Iran with Focus on Development of Wind Power Plants	67-79
Mahdi Shahmari **Payam Zarafshan** **Shahriar Kouravand** **Morteza Khashehchi**	Design and Analysis of a Combined Savonius-Darrieus Wind Turbine for Irrigation Application	80-86

Journal Homepage: www.jree.ir